Structural Elements with Mathematically Defined Surfaces for Enhanced Structural and Acoustic Performance

by

Donald Quinn O'Sullivan

B.S., Mechanical Engineering
B.A., Russian
University of Arizona, 1995

S.M.M.E., Mechanical Engineering
S.M.T.P.P., Mechanical Engineering
Massachusetts Institute of Technology, 1998

SUBMITTED TO THE DEPARTMENT OF MECHANICAL ENGINEERING
IN PARTIAL FULFILLMENT OF THE DEGREE OF

DOCTORATE OF PHILOSOPHY

at the

MASSACHUSETTS INSTITUTE OF TECHNOLOGY

February 2001

Signature of Author .....
Department of Mechanical Engineering
September 20, 2000

Certified by .....
Professor Alexander Slocum
Thesis Supervisor

Accepted by .....
Professor Ain A. Sonin
Chairman, Department Graduate Committee

[redacted]

Structural Elements with Mathematically Defined Surfaces for Enhanced Structural and Acoustic Performance

by

Donald Quinn O'Sullivan

Submitted to the Department of Mechanical Engineering
on September 20, 2000 in Partial Fulfillment of the
Requirements for the Degree of Doctorate of Philosophy
at the Massachusetts Institute of Technology

ABSTRACT

Two design methods are explored to reduce vibration, minimize unwanted acoustic noise, and increase stiffness in structures. The first design approach is to create nearly isotropic panels with increased stiffness using two-dimensional curvature. These quasi-isotropic designs can be used in lieu of typical panel reinforcements, and can provide an inexpensive alternative to honeycomb sandwich designs. The second approach is to design panels formed into the shape of a mode shape to reduce detrimental modal dynamics. The effects of combining the two-dimensionally curved designs with constrained layer damping is also investigated. Further, it is also the goal of this research that these panels can be inexpensively manufactured with current manufacturing methods (*e.g.* stamping, rolling, thermoforming, *etc.*), resulting in a more effective structural element that does not require significant extra cost or weight.

Initial analysis was performed using geometric modeling and finite element analysis. Experimental analysis involved both static and dynamic system identification. The experimental results indicate that quasi-isotropic designs can be accomplished with two-dimensional curvature. These quasi-isotropic designs increase the stiffness of a panel and raise the natural frequency by a factor of 2 (compared to a flat panel of the same mass). Although the quasi-isotropic designs have no acoustic benefit, they were shown to be effective replacements as honeycomb cores. The mode-shaped designs demonstrated the unique quality of simultaneously reducing vibration and acoustic noise over a broad frequency range (50-10,000 Hz). The mode-shaped panels demonstrated a factor of 3 increase in the natural frequency, a ten-fold reduction in dynamic deflection displacements, and a 3 to 4 dB RMS reduction in the radiation index over a broad frequency range.

Thesis Supervisor:
Professor Alexander H. Slocum
Department of Mechanical Engineering

Committee:
Professor Alexander H. Slocum (Committee Chairman)
Professor Richard Lyon
Professor Samir Nayfeh

ACKNOWLEDGMENTS

Funding for this research was provided by in part by a National Science Foundation Fellowship awarded to Don O'Sullivan. In addition, Ford Motor Company provided funds and assistance that helped to make this research possible.

First, I want to thank my adviser, Professor Slocum, for providing guidance, motivation, humor, enthusiasm, energy, and constant encouragement. His endless optimism and mania inspired me to see this work through to its completion.

I would also like to thank the many people whose help made this research possible. Thanks to Sami Kotilainen who was a great study partner for the qualifying exams. Thanks also goes to Tim Glenn for the late night discussions and help with the laser vibrometer. Thanks to Mauro Atalla for access to the anechoic chamber and use of the equipment in the Active Material and Structures Lab. Thanks to Sean Montgomery and Kelly Harper whose last minute help made the reverberant chamber a reality. Thanks to Jason Sicotte at Associated Spring for use of the Laminated Object Manufacturing machine. Thanks to Matt Page for help with the Three-dimensional printing machine. Thanks to Harold Sears at Ford for all his help making the stereolithography molds. Thanks to Ken Fedeson and Kevin Tallio at Ford for showing interest in my work. Thanks to the gentlemen in the Papalardo Machine Shop for all their time, assistance and advice. Thanks to Leslie Regan who was always there to answer any question and offer encouragement. And of course, thank you to my committee members, Professor Lyon and Professor Nayfeh, for providing guidance.

A special thanks goes to my wife, Kim, whose understanding, patience, kindness and love kept me going through the most trying times. She, more than anyone provided support, therapy, and input for all facets of my work.

TABLE OF CONTENTS

LIST OF FIGURES

LIST OF TABLES

Chapter 1

INTRODUCTION

1.1 Problem Definition

Frequently, there is a trade-off between reducing detrimental vibration and minimizing acoustic noise in structural members with weight and space restrictions. Detrimental vibration, vibration that leads to increased wear and harmful structural coupling, often occurs at less than audible frequencies where large displacements occur. To help counteract these harmful vibrations the structure's stiffness is commonly increased (often at a significant cost), which can lead to greater acoustic noise. On the other hand, if the acoustic noise is the primary source of concern, then the best way to reduce audible noise is often by adding mass and reducing stiffness or by incorporating bulky absorption material. By increasing mass and reducing stiffness, harmful coupling between the structure and the surrounding acoustic medium can be greatly reduced, but this is undesirable for structures requiring high stiffness and low weight (*i.e.* many vehicles and low cost enclosures). This method also directly counters the methodology stated above when trying to reduce harmful vibration. Additionally, the use of acoustic absorption material is frequently limited by space restrictions, as very thick layers of absorptive material are required for lower audible frequencies. In short, it is difficult to design machine enclosure and reinforcement panels that meet structural and acoustic requirements while maintaining minimum weight, space, and cost requirements.

1.2 Desired Contributions

The research attempts to make the following contributions to address the above problem of reducing unwanted compliance, vibration and acoustic noise:

1. Demonstrate that it is beneficial to incorporate two-dimensional curvature and mathematically defined surfaces into structural panels.
2. Design two-dimensionally curved panel designs that increase stiffness and minimize unwanted modal dynamics to minimize acoustic noise.
3. Demonstrate that quasi-isotropic panels can be designed using mathematical algorithms and two-dimensional curvature.
4. Show that greater levels of damping can be achieved when constrained damping layers are combined with two-dimensionally curved panel designs.
5. Provide an inexpensive alternative to honeycomb and reinforced panel designs.

1.3 Motivation

Traditional machine and building elements rely primarily on rectilinear components. The assumption that the components must be flat or rectilinear leads to a certain amount of convenience during assembly, but also limits the performance of certain components. The basis of this work is that desirable behavioral properties can be attained simply by adding intelligently designed two-dimensional curvature to appropriate components. By rejecting the use of standard flat panels, fundamentally new designs can be developed that demonstrate unique and improved properties compared to standard panels, without the use of secondary treatments and modifications.

It is important to identify why noise reduction panels and machine enclosures are necessary. In general, industrial machine enclosures are used to restrict access to parts, reduce acoustic noise, provide structural reinforcement, and improve aesthetics. Industrial machines use noise enclosures to ensure a quiet work environment. Noise levels can exceed 100 dB in some areas where heavy machinery is used, causing safety issues for employees and disturbing neighboring areas [Lord, 1987]. Enclosures in industry also serve to protect the machines and the operators. By restricting access to a machine's inte-

rior, an enclosure acts as a barrier that keeps out harmful contaminants and debris while simultaneously protecting the operator from dangerous mechanisms. Finally, industrial machines sometimes require enclosures merely to improve aesthetics, making a product more marketable.

Vehicle enclosures are necessary for the reasons stated above but they also provide structural reinforcement and often aid in locomotion. Aircraft panels and floor elements not only serve to enclose the aircraft, but they also provide a majority of the structural reinforcement, carrying more of the load than the aircraft frame. In addition, aircraft panels are essential in forming the lifting structure of the wing, enabling the aircraft to fly. In boats the panel enclosure also provides a great deal of structural reinforcement as well as ensuring a sleek and buoyant craft. Among other reasons, automobiles use panels extensively to ensure passenger comfort, reinforce flimsy members (*e.g.* hoods and trunks), and protect passengers in the event of an accident.

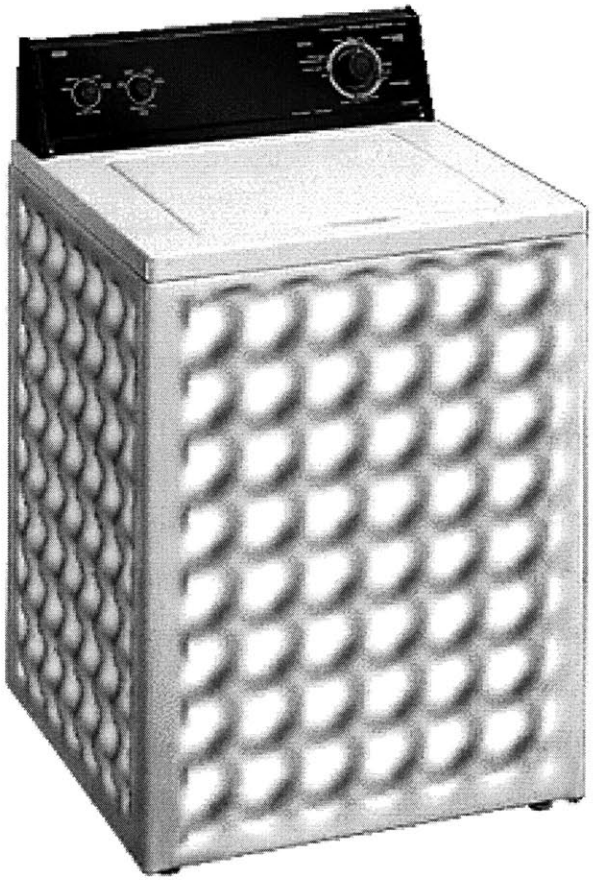

Figure 1.1 An example of an appliance with two-dimensionally curved panels to reduce vibration (amplitude exaggerated for effect).

Another application for enclosures is in home and office appliances. Computers, washing machines, refrigerators, copiers, and many other appliances require machine enclosures for many of the above reasons, but also have a much greater restriction on acoustic noise due to the environment in which they must operate. In addition to the greater restriction

on acoustic noise there is often a greater restriction on space, which makes the task of quieting more challenging. The quality of many appliances is sometimes largely determined by how quietly they operate.

A final application is as improved and inexpensive alternative to cores in sandwich type panels. Examples of this type of construction can be found in mundane objects such as cardboard, and in exotic structures like air and space-craft. The goal is to be able to replace unidirectional and honeycomb sandwich material with two-dimensionally curved panels that demonstrate better performance than typical cardboard designs, and provide a less expensive alternative to exotic honeycomb designs.

The many uses and requirements of enclosure panels is due in part to the varied ways in which noise and vibration permeates and escapes structures. Three basic categories of noise propagation that relate to enclosures can be identified: structure to structure coupling, acoustic to structure coupling, and structure to acoustic coupling. A significant challenge is developing an enclosure panel that can perform well in all three categories. The first category is very common in machine enclosures where the enclosure is used to restrict access and improve aesthetics, rather than minimize noise. Unfortunately, vibrating machines that do not have acoustic noise problems without an enclosure may demonstrate acoustic noise problems when an enclosure is applied. Further, structural coupling may cause the panels to vibrate excessively, causing exaggerated vibration of the machine, perhaps reducing performance and operating life. The second category is prevalent in vehicles, such as launch vehicles, where excess acoustic noise can couple strongly with structures leading to excess wear and severe stresses [Gerard, 1989]. The same is true for boundary layer noise in aircraft and road noise in automobiles, although wear and stress are less severe, the resulting internal acoustic noise is no less annoying. The last category is important in any enclosure where acoustic noise is a factor. An appliance, such as a washing machine, that demonstrates a large amount of vibration can lead to significant coupling from the flimsy body panels to the acoustic medium. Additionally, coupling from the structure to the acoustics is likely significant in the previous two categories.

Therefore, to design an effective enclosure it is necessary to understand the different transmission paths and to be able to mitigate the different types of coupling simultaneously.

The performance of panel designs must take into consideration the cost of production of the panels. A better performing panel that costs significantly more to manufacture will likely prove to be of little benefit. Therefore, it is necessary to consider design and manufacturing complexity when determining the overall benefit of the panel. Part of the goal of the panel designs contained herein is to minimize additional costs by using standard manufacturing methods. The panels in this thesis are intended to be manufacturable using common techniques such as stamping (used extensively in automobile manufacturing), thermoforming (*i.e.* injection molding and vacuum forming for plastic panels), and rolling (for producing large amounts of panels for generic use).

In summary, the goal of the research is to design new two-dimensionally curved panels that perform better than flat and one-dimensionally curved panels. The panel performance is gauged in terms of its structural and acoustic properties, as well as the cost to produce the panels.

1.4 Past and Current Solutions

To develop innovative designs it is important to identify research that has been conducted in the area of panel design, dynamics, and performance. It is also necessary to investigate whether curvature has been used in panel designs for the purposes previously stated. Current state of the art research for machine enclosures and panels can be divided into two main categories: passive and active. Passive designs utilize materials, geometry and damping to enhance performance and require no control system. Active designs, on the other hand, utilize a combination of actuators, sensors, and control algorithms to improve performance. Active systems generally require secondary modification and are often of much greater complexity than passive designs. The panels discussed in this thesis fall into the category of passive designs.

1.4.1 Passive Panel Design and Research

Many different passive modifications and panel designs have been developed through the years to alter and enhance panel performance. Generally the designs or modifications are intended to address either acoustic noise or vibration. Rarely are the designs intended to address both. Most state of the art passive designs that reduce acoustic noise were developed for architectural purposes, although many passive designs have been developed for automobiles and aircraft [Crocker, 1993; Lord, 1987; Crocker, 1975]. Designs developed to reduce vibration are more common for machine enclosures and vehicles where the excess vibration disturbs other aspects of system operation. In addition to reducing acoustic noise and vibration, panels have been designed to alter a structure's static mechanical properties or to change a structure's appearance and shape.

Buildings (homes, factories and offices) often require special treatment to minimize noise in environments where quiet is required. Research in architectural engineering has developed several innovations that are used to reduce transmission of noise between rooms or enclosures. Two effective designs that utilize laminar/sandwich designs are the "Shear Wall" (described in U.S. Patents 3,087,570, 3,087,574, and 3,249,178) [Watters, 1966; Watters, 1963; Watters & Kurtze, 1963], and the "Coincident Wall" (described in U.S. Patent 3,422,921) [Warnaka, 1969]. The "Shear Wall" increases transmission loss by increasing the critical frequency of the wall. By placing a constrained damping layer of material between the outer face of the wall and the inner frame of the wall, increases in the critical frequency can be achieved thereby increasing the amount of transmission loss at higher frequencies. The "Coincident Wall" also utilizes a sandwich design. The primary notion behind the design is to reduce the critical frequency of the wall or panel such that it is near its first fundamental frequency, while increasing the damping of the wall or panel. This allows for greater transmission loss at higher frequencies (frequencies above the critical frequency).

Other more common designs for reducing acoustic noise exist. An example of a portable design is a lead curtain, which minimizes stiffness and maximizes mass to increase trans-

mission loss. Perforated panels have been used to reduce some acoustic noise. The perforations cause localized wave cancellation of the fluid and thus act as a sound absorber. The most common panel design for acoustic absorption utilizes add-on material such as foam or fiberglass that has a high coefficient of absorption. The most common example of this panel design is the ubiquitous ceiling tile, often used in offices. Other designs are laminar and combine a stiff reinforcing panel covered in absorption material. Wedged shaped panels can be found in anechoic chambers and sound studios. In general, the difficulties with using sound absorption material are that it is prohibitively bulky, requiring thick material for lower frequencies, and it degrades over time.

Panel designs for vehicles and some appliances often utilize non-flat panel designs to increase or alter structural properties. Most of these designs incorporate ribs or reinforcing members to increase the stiffness of a panel. Hoods and trunks of automobiles often place reinforcing members on the underside of the panel so that it does not deflect or vibrate excessively. A significant amount of research has been performed by the automotive industry to reduce both acoustic noise and vibration, but reducing acoustic noise has proven to be the more challenging of the two problems [Mraz, 1993].

Several studies have been performed on various components to try and determine optimal rib reinforcement designs. Yikang Zhang *et. al.* performed a dynamic analysis to determine optimal rib patterns for exhaust system components [Zhang, 1991]. Kevin Zhang *et. al.* applied a similar technology to automotive floor panels to minimize acoustic noise [Zhang, 1997; Zhang, 1995]. Nachimuthu *et. al.* used finite and boundary element analysis to try and determine optimal bead patterns on automotive panels for powertrain noise reduction [Nachimuthu, 1997]. White *et. al.* also applied finite element analysis, coupled with shape optimization, to try and determine optimal reinforcing rib geometry for an air cleaner enclosure [White, 1997]. In addition to these studies on automobile components, Leheta *et. al.* performed a similar rib reinforcement design optimization for longitudinally stiffened ship bottoms [Leheta, 1997]. While the above explored the positive aspects of reinforced panel designs, VanBuskirk pointed out that merely stiffening panels may in fact

lead to increased acoustic noise, especially in regions where the ear is most sensitive [Van-Buskirk, 1993].

In addition to the optimization of reinforced panels, research has been performed to determine more optimal methods and designs for damping panels. Nagai *et. al.* researched the benefits of using constrained damping layers in steel automobile panels to minimize vibration and noise. Their design was a simple laminar structure that placed a constrained damping layer between flat sheets of steel, resulting in improved damping characteristics. More importantly, they showed that the formability, weldability and strength of the panels were not greatly inhibited by the constrained damping layer [Nagai, 1991]. Cheng *et. al.* performed a design optimization on panels treated with a variable thickness visco-elastic coating to maximize damping. Their analysis involved a cost function that penalized the additional weight of the visco-elastic coating and demonstrated the benefits of using free damping layers as opposed to constrained damping layers [Cheng, 1995]. Finally, Qian *et. al.* explored the benefits of various damping materials and methods on ribbed reinforced panels. Their work concluded that constrained damping layers provided the greatest increase in damping, especially when combined with a large number of ribs (although no rational for the better performance is provided) [Qian, 1997].

Several researchers have chosen to examine the machine enclosure design process from a macroscopic perspective, analyzing the entire enclosure and modifying various components to minimize vibration and noise. Oka *et. al.* sought to reduce "boom-noise", vibrations that strongly couple to the first several acoustic modes of an enclosure [Oka, 1991]. Iwahara *et. al.* used a least squares method coupled with finite element analysis to minimize unwanted vibrations in automobile bodies, and to determine optimal reinforcement for convertible automobiles [Iwahara, 1991]. Others have used these more global approaches to try and determine the most important sources of noise and transmission into enclosures and automobiles [Hendricx, 1997; Drozdova, 1997; Panov, 1994].

Highly relevant to this thesis is research that investigates shell and curved panel designs to reduce vibration and acoustic noise. Ng examined the use of one-dimensional curvature on a perforated panel for a close-fitting noise enclosure. The panels were studied using an analytic model. Ng examined the influence of cylindrical curvature on the panel's stiffness and transmission loss characteristics, and demonstrated that the modal dynamics shift upward with increasing curvature [Ng, 1995]. Zhang *et. al.* also investigated the influence of one-dimensional curvature on a muffler casing. The research was performed using finite element analysis. Their research demonstrated that curvature has a large influence on the structural dynamics, producing a shift in modal frequencies, and may be helpful in reducing the radiation efficiency of modal dynamics [Zhang, 1995]. Steyer, Chung, and Brassow performed research on two-dimensionally curved shells to help minimize vibration and noise for the side cover of transmission casings. To perform the analysis finite element analysis and design optimization software was utilized. An initial study analyzed a square panel with circular domed curvature and multi-lobed curvature, and showed a dramatic increase in natural frequencies [Steyer, 1997]. Another study used design optimization software to determine an even more rigid design to attain a specific first natural frequency [Chung, 1997]. Although the research did not show specific benefits to a reduction in vibration or noise, the two-dimensional curvature demonstrated a strong influence on the panel dynamics.

Historically, curvature in structures has proven to be very beneficial. The Greeks used circular columns to carry the most load with a minimum cross section and hence the least amount of material. The Romans used arches to distribute loads and minimize stresses in many of their structures. Curvature in structures has also proven to be acoustically beneficial in amphitheaters, concert halls, and sound studios and can be used to focus or disperse sound waves. Biological examples of curvature are apparent in trees, coral, a turtle's shell, and in the bones of our bodies, to name a few. Panels have used curvature much less in the past, the one exception being corrugated panels. Corrugated panels have been used extensively in architectural structures to provide light, inexpensive, but rigid walls, floors and roofs. Corrugated designs have also been used extensively in reinforced cardboard

designs. The one significant drawback of the one-dimensionally curved design of corrugated panels is their orthotropic behavior that can lead to undesirable structural and acoustic behavior (the details of this will be discussed in Chapter 2). Beyond corrugated panels, very little advancement has been made in terms of using curvature, especially two-dimensional curvature, in panel designs. However, there is a large pool of research in mechanics and dynamics that focuses on the behavior of shells.

Shells are thin-walled structures that have varying degrees of curvature. Shells with two-dimensional curvature are often referred to as doubly curved shells or panels. The majority of this research has focused on developing analytical models for these shells, some with rectangular boundary conditions [Liew, 1996; Bhimaraddi, 1991]. Others have concentrated on the dynamics of these shells exclusively when combined with composite materials [Chun, 1995; Chaudhuri, 1994; Kabir, 1991]. While a small amount of this research is focused towards an application, such as turbine blades [Hu, 1999], most of the research is pure in the sense that it does not mention a specific field of use. Unfortunately, much of this pure research of shells has limited application to this thesis because of many of the assumptions and restrictions placed on the models (*i.e.* limited degree of curvature, lack of multiple inflection points, simplified boundary conditions and panel shapes). As a result, most of the initial analysis in this thesis will rely on geometric approximation methods and finite element analysis.

1.4.2 Active Panel Research

Active control is considered the final option when trying to minimize noise and vibration. It is applied when all passive design techniques prove ineffective or infeasible due to weight, space, or other restrictions. Active control techniques are generally feedback or feed-forward based control systems that attempt to minimize or alter noise and vibration to maintain performance requirements. They utilize a variety of actuators (*e.g.* shakers, piezoceramic patches, speakers, *etc.*), sensors (*e.g.* accelerometers, optical sensors, microphones, *etc.*), amplifiers, and control boards, and vary greatly in size and complexity.

In the past fifteen years there has been a large increase in research on actively controlled panels, and they have found uses in many aircraft, space structures, and other vehicles. A majority of the structural control techniques utilize piezoceramic patches epoxied onto panels, coupled with strain sensors or accelerometers and feedback control routines, such as rate feedback [Hansen, 1998; Reza Moheimani, 1998; Berkman, 1997; Clark, 1993; Mathur, 1993]. These designs have proven effective in reducing structural vibration, but less effective in reducing acoustic noise. Some research has even been performed on panels that have imbedded actuators and sensors within a composite matrix [Bingham, 1998]. More common techniques to actively suppress acoustic noise often involve the use of speakers that can locally cancel acoustic noise that emanates from panels [Char, 1994; Rossetti, 1994].

Although active control techniques have been shown to improve performance, they are often very complex and expensive. Thus, they have found use in only the most exotic of applications. In addition, they are less robust than most passive designs due to their reliance on electronic components and multiple external systems. Part of the goal of this research is to reduce the need for these complex actively controlled panels by demonstrating that greater performance can be attained with the novel passive designs introduced in this thesis.

1.5 Research Hypotheses and Approach

This research explores the validity of three hypotheses. One, that two-dimensionally curved panels can exhibit isotropic behavior at lower frequencies, allowing for inexpensive methods of stiffening many designs. Two, especially detrimental modes of vibration can be eliminated from a panel's dynamics by forming the panel into the shape of the unwanted mode (with the amplitude being greater than the elastic deformation range). Three, increased damping over damped flat panels can be obtained by incorporating viscoelastic or constrained damping layers in the two-dimensionally curved designs. All of these hypotheses are based on the notion that two-dimensionally curved panels can pro-

vide greater performance in reducing unwanted acoustic noise and vibration than their flat and one-dimensional counterparts. These hypotheses are explored through analytic and numerical methods and experimental verification.

1.5.1 Hypotheses

The first hypothesis is that a two-dimensionally curved panel can be designed that has nearly the same bending stiffness in all directions. A quasi-isotropic design can be used in many application were orthotropic behavior is undesirable. This includes architectural members, machine components, and enclosures. Two-dimensional designs may also prove to be a better performing design than those currently used in reinforced panel designs (*e.g.* cardboard), and may provide an inexpensive alternative to honeycomb, which is very expensive. A two-dimensionally curved design can be simply manufactured out of sheet using standard techniques such as stamping, rolling, or thermoforming (very common in manufacturing processes of automobiles and other machine components), while a honeycomb sandwich design often requires more precise and less automated manufacturing techniques and is therefore more difficult and expensive to manufacture.

The second hypothesis forwards a method of minimizing the effect of particularly detrimental modes of vibration. The foundation for this hypothesis is that if a panel is formed into a particular mode shape, then any deformation of the panel similar to that shape must be in stretching, and therefore must occur at a considerably higher frequency. This can be especially beneficial when a particular mode dominates the vibration or acoustic transmission of noise, as is often the case with the first mode of vibration. The hypothesis does not claim that this method eliminates all unwanted modes, but rather it claims that a certain unwanted mode can be inhibited from occurring. Some of the resulting mode shapes will undoubtedly demonstrate undesirable characteristics, but much less so than the removed mode shape. The resulting panel will also have greatly increased stiffness, which is beneficial in reducing unwanted vibration.

The final hypothesis asserts that when the panel designs of hypothesis one and two (or any two-dimensionally curved panel) are combined with constrained or visco-elastic damping layers greater damping can be obtained than would otherwise be obtained with flat designs that also use damping layers. The reasoning behind this hypothesis is two-fold. One, the two-dimensional curvature moves the damping layers away from the neutral axis of bending, which may lead to greater deformation of the damping layer. Since the amount of damping is a positive function of the amount of deformation in the damping layer (*i.e.* more strain leads to greater damping), the two-dimensionally curved panels will demonstrate greater damping. The second reason is that the two-dimensional curvature of the panel and the constrained damping layer is subjected to multi-directional deformation when bent. Unlike a flat panel, which primarily deforms in a single direction, a two-dimensionally curved panel is subjected to deformation in many directions simultaneously, leading to an overall greater amount of strain and thus damping.

1.5.2 Research Approach

The research described in this thesis progresses through four levels of analysis. First, analytic relations between the panel geometry and its behavior are established. Unfortunately, modern analytic models are unable to characterize the complex behavior of many two-dimensionally curved panels. Thus, the second level of analysis utilized a numerical approach to gain insight into the panels' geometry and dynamic characteristics. The third level of analysis utilizes finite element analysis to determine more exact dynamic and modal characteristics of the panel. Finally, comparative experimental analysis is performed to demonstrate the panels acoustic and vibration responses and behavior.

The first level, analytic analysis, is used to gain estimates of modal frequencies, gain insight into the mechanical behavior, analyze panel geometry, and determine quasi-isotropic shapes. This stage of research relies primarily on classical mechanics and differential geometry. It became clear early that due to the complexity of the designs, analytical models are of limited use and accuracy.

The second and third levels of analysis rely on numerical methods to develop and analyze panel designs. Matlab is also used to apply some of the analytic techniques numerically so that many designs can be quickly developed and examined. In Matlab, routines are written to generate panels using Fourier based designs, statistically based designs, point by point designs, and optimization methods that utilize least square cost functions. The most promising of these designs, based on estimated performance, manufacturability, and simplicity, are then analyzed using finite element analysis when possible. The designs are exported from Matlab into PRO\Engineer and analyzed using PRO\Mechanica. Primarily, modal analysis is used to gain insight into the panels' expected behavior. The finite element analysis is also used, to some extent, as a design iteration method, whereby designs are altered once their modal behavior was determined. Once a limited set of candidate designs are determined, experimental analysis is performed.

Experiments to examine both the structural and acoustic behavior of the panels is performed on three different testbeds. The testbeds are essentially rectangular enclosures that are designed to have minimal response, acoustically and structurally, on five sides so that the side with the experimental panel dominates the transfer function response. A small enclosure is used to mimic the setting of an actual machine enclosure, rather than using a standardized testing method that may or may not correlate to machine enclosures. Both structural and acoustic excitation and sensing methods are used in conjunction with several testing configurations that emphasize various enclosure settings. In addition, static bending tests are performed to examine the static stiffness properties of the sandwich panel designs.

1.6 Overview

Chapter 2 is dedicated to reviewing some of the necessary background knowledge in vibration and acoustics. The relations and differences between structural and acoustic behavior is emphasized. In addition, some of the basic mechanics of panels are discussed as well as the theory behind visco-elastic and constrained damping.

Chapter 3 focuses on two-dimensionally curved designs with lower order isotropy. Designs are developed and analyzed with the use of differential geometry and numerical methods. Analysis of these designs are performed using both analytic and numerical models. Finite element analysis results are included that demonstrate the modal characteristics of some of the designs as well as the resulting structural properties.

Chapter 4 investigates the theory behind mode-shaped designs. It evaluates how particular modes can be eliminated and estimates projected results of these designs, including the benefits of eliminating unwanted modes. These designs are then analyzed using numerical methods, including finite element analysis. Modal results are provided to demonstrate the elimination of the unwanted mode.

Chapter 5 discusses prototype manufacturing and the experimental setup and goals. Issues such as scaling, interference, realistic complexity, and experimental weaknesses are discussed. Manufacturing of prototypes for the experiments is the primary focus of the manufacturing section, but some general discussion of manufacturing processes for commercial production are also addressed.

Chapter 6 presents the final results of the research, primarily focusing on the experimental results and how they relate to the earlier presented hypotheses. The performance of the panels are discussed, as well as means of improving performance.

Finally, Chapter 7 provides conclusions of the research. The benefits as well as the drawbacks of the designs are analyzed and recommendations are made for their use. In addition, suggestions for future work are made to maximize the benefit of this research.

Chapter 2

VIBRATION AND ACOUSTICS BACKGROUND

The purpose of this chapter is to discuss the principles of vibration and acoustics upon which the hypotheses and research were based. Basic principles that strongly affect the behavior of unwanted noise and vibration in machine enclosures are also discussed. In addition, this chapter emphasizes the principles associated with structural-acoustic coupling. The following is not meant to be an all inclusive source of information, but rather a brief background necessary to understand the current research.

2.1 Noise and Vibration Transmission Paths

Ideally when trying to control noise and vibration it is desirable to eliminate the problem at its source. Unfortunately, this is prohibitive in many situations where the source is inaccessible (*e.g.* bearings inside a mechanism), uncontrollable (*e.g.* aerodynamic noise on automobiles and aircraft), or simply unlocatable (*e.g.* shockwaves in steam pipes). In fact, in many cases it proves costly to try to mitigate noise and vibration at its source. As a result, often the best method of controlling unwanted noise or vibration is along its transmission path, preferably closest to the source of noise.

For most machines, there are three types of transmission paths through which unwanted energy (*i.e.* noise and vibration) travels. The most common (and most considered) transmission path is the solid structure out of which a machine or structure is made. The structure can transmit several different kinds of disturbances, commonly referred to as

vibrations. The vibrations in a structural transmission path can often be altered by changing the mass, stiffness and damping of the structure. The second transmission path of interest is through gas, most commonly air. The disturbances in the gas are generally referred to as acoustic noise and are usually limited to compressional waves (although some turbulent and aerodynamic disturbances can be important in several situations). These disturbances are more difficult to control because it is often impossible to change the mass, stiffness and damping of a gaseous system (especially open air environments). The third transmission path is liquid, and can be in the form of water, hydraulic fluid, and oils, to name a few. This transmission path is common for boats, pumps, lubricated bearings, and heat exchangers. The types of disturbances in liquids are similar to those in gas, with a greater emphasis on turbulent disturbances, and with similar difficulties in controlling properties. Since the focus of this thesis is machine enclosures, specifically panels, the liquid transmission path will not be emphasized.

An important aspect of controlling noise and vibration is understanding how they are transmitted through various objects, and the mechanisms of coupling between different objects. Stated another way, it is essential to determine the source of vibration and noise (even if the exact origin cannot be determined) and how to prevent it from reaching the area where its presence is detrimental. To do this it is necessary to understand the dynamics of the systems through which the noise and vibration travels, and how to change the disturbances using enclosures, damping, controls, and principles of design. The following sections provide brief overviews of the dynamics of the transmission paths of interest, particularly in relation to panels.

2.2 Structural Vibration

Vibration in structures is simply defined as oscillatory motion about a mean position. Energy enters the system at the point of excitation and a portion of the energy propagates through the structure as waves. The waves excite coupled objects, reflect off boundaries, and dissipate over time (generally the energy is changed to heat by a process referred to as

damping, which can occur in many different ways). The initial response of systems or the response of very large systems is dominated by travelling waves. The energy in a finite system at steady state is dominated by modal vibrations, which can be thought of as standing waves. The following two sections provide a brief description of these two processes.

2.2.1 Propagation of Waves and Vibration

To ensure a common understanding, some basic concepts must be introduced. The most common parameter associated with waves and vibration is frequency, denoted here by f to indicate frequency in Hertz (Hz, cycles per second) and ω to indicate frequency in radians per second. The frequency relates the temporal occurrence of waves and vibration. Another important parameter is the wavenumber, denoted here as k. The wavenumber is the spatial equivalent of frequency, as it essentially relates the wavelength by indicating the number of waves per unit distance. The wavenumber has the following associated equations

$$k = \frac{\omega}{c} = \frac{2\pi}{\lambda}, \tag{2.1}$$

where c is the speed of the wave and λ is the wavelength. The wavenumber is commonly used in acoustics and appears sporadically throughout this work.

Waves are most commonly represented by sinusoids (*i.e.* a wave being no more than a harmonic variation in time and/or space), but throughout this work the exponential representation is also used due to its mathematical ease. Often waves are represented by $fn(t) = A\sin(\omega t + \phi)$ where A represents the amplitude and ϕ represents the phase. In many texts, and in this work, it is common to see the wave also denoted as $fn(x,t) = Re\{\tilde{A}\exp[j(\omega t - kx + \phi)]\}$, where Re indicates the real portion of the equation, $\tilde{A}$ is the complex amplitude (some number $a + jb$), and j is the imaginary unit (square root of negative one). In this representation the change per unit distance is accounted for with the spatial relation of the wavenumber.

Structures can be deformed and experience stresses in shear, compression, and in tension (tension is nearly identical to compression most materials in the linear range of deformation). The energy of deformation propagates through the structure as vibrational waves that are a combination of shear waves, compressional waves, and torsional waves (although torsional waves can be considered another form of shear waves). In most structures all three types of waves are significant. For plate-like structures, such as panels, the most significant type of wave or deformation is called a bending wave, which is a combination of shear and compressional waves. Bending waves are characterized by their deflection normal to the surface and translational propagation parallel to the surface (in the case of travelling waves).

In most cases, bending waves in solids are *dispersive*, meaning they travel different speeds at different frequencies. This is important when considering coupling to *non-dispersive* objects such as fluids. In solids, the speed of a bending wave increases with increased frequency and stiffness, and decreases with increased mass. The bending wave speed for panel structures is given by,

$$c_B = \sqrt[4]{B\frac{\omega^2}{m}} \tag{2.2}$$

where m is the surface density (*i.e.* $\rho_m h$, where ρ_m is the material density and h is the material thickness), ω is the angular frequency of the wave, and B is the bending stiffness of the panel in the direction of travel of the bending wave. The bending stiffness can be represented by,

$$B = \frac{EI}{(1-\nu^2)} \tag{2.3}$$

where E is Young's modulus (sometimes referred to as flexural modulus), I is the cross-sectional second moment of inertia, and ν is Poisson's ratio. [Bies, 1996]

From the perspective of wave dynamics, which is used throughout this chapter, the propagation of a one-dimensional plane bending wave in an infinite plate is the same as in an infinite beam. The one exception being that the relationship between longitudinal strains and stresses must be accounted for, to allow for the lateral constraint that is absent in a finite width beam. The common beam bending differential equation is thus,

$$\frac{EI'}{(1-\nu^2)}\frac{\partial^4 q}{\partial x^4} = -m\frac{\partial^2 q}{\partial t^2}, \tag{2.4}$$

where I' is the second cross-sectional moment of inertia per unit width (*i.e.* $h^3/12$ for a uniform plate of thickness h), x is the coordinate direction of the travelling wave, and q is the transverse displacement at the coordinate x.

Assuming a simple harmonic wave, $q(x, t) = Re\{\tilde{A}\exp[j(\omega t - kx)]\}$, the wave equation can be written as,

$$\tilde{B}k^4 = \omega^2 m, \tag{2.5}$$

where the $\tilde{B}$ represents the bending stiffness per unit width. The general solution to this differential equation is

$$q(x, t) = C_1 e^{(j\omega t - jkx)} + C_2 e^{(j\omega t - kx)} + C_3 e^{(j\omega t + jkx)} + C_4 e^{(j\omega t + kx)}, \tag{2.6}$$

where again k is the wavenumber (perhaps more conveniently thought of as $k^4 = m\omega^2/\tilde{B}$). The $e^{(j\omega t - jkx)}$ and $e^{(j\omega t - kx)}$ terms represent the spatial rightward travelling waves and $e^{(j\omega t + jkx)}$ and $e^{(j\omega t + kx)}$ terms represent the spatial leftward travelling waves. The e^{kx} and e^{-kx} represent the evanescent waves. The constants, C_i, are determined by applying the boundary conditions and solving.

In the case of two-dimensional bending wave fields, which may propagate in both the x and y directions simultaneously, a more complex wave equation is required. Derivation of the complete classical solution is tedious and can be found in references such as Cremer *et al.* [Cremer, 1973]. For a thin plate lying in the x-y plane, where the wavelengths of the

frequencies of interest are an order of magnitude greater than the plate thickness, the bending wave equation is

$$\frac{EI'}{(1-\nu^2)}\left(\frac{\partial^4 q}{\partial x^4}+2\frac{\partial^4 q}{\partial x^2\partial y^2}+\frac{\partial^4 q}{\partial y^4}\right) = -m\frac{\partial^2 q}{\partial t^2}, \tag{2.7}$$

where the above neglects shear and rotary inertia, which for the cases considered is acceptable. Unfortunately there is, as of yet, no solution to this two-dimensional wave equation for panels with rectangular boundaries. There are solutions however to circular plates, but as this work focuses on rectangular panels it provides little insight. The best we can hope to do is use the one-dimensional version in Equation 2.4, as well as some approximations based on Equation 2.4, to help gain some insight into the problem.

For more complex systems, such as shells and orthotropic panels, there is even less hope of finding analytical solutions. However, there are some parameters related to wave propagation that can provide insight about the wave dynamics. The cross-sectional bending stiffness of a curved or corrugated panel can be estimated by

$$B = \frac{Eh}{(1-\nu^2)L}\int_0^L\left(z^2+\frac{h^2}{12}\right)dl \tag{2.8}$$

where again E is the modulus of elasticity, ν is Poisson's ratio, L is a characteristic length of the panel, and z is the height from the neutral axis to the center of the panel thickness along the distance l [Bies, 1996]. Figure 2.1 illustrates these variables in relation to a generic cross-section. Note that this parameter neglects shear, which is only valid when the thickness of the panel is much smaller than the characteristic length. This approximation of the bending stiffness can then be used in Equation 2.2 to estimate the bending wave speed in corrugated and two-dimensionally curved panels. It should be noted that in certain cases, especially two-dimensionally curved panels, this approximation over-estimates the actual bending stiffness. The over estimation is a result of the fact that when a bending wave propagates through a panel it will not necessarily travel along a straight cross-sec-

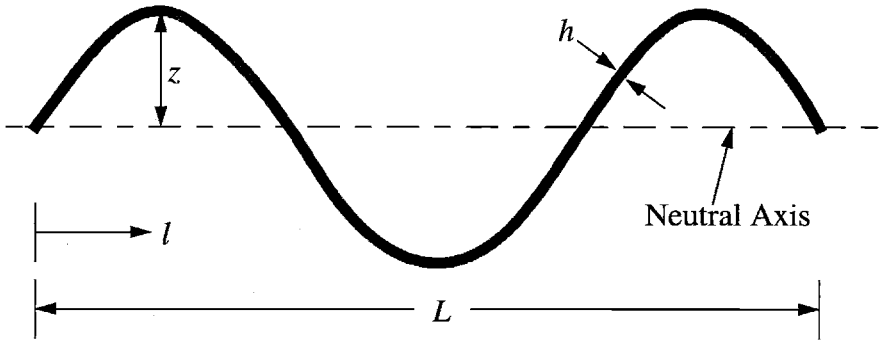

Figure 2.1 A simple sketch illustrating the variables for calculating the cross-sectional bending stiffness B.

tion, but instead the wave front may conform around obstacles such that the energy required to deform along the wave front is minimized.

2.2.2 Natural Frequencies and Modes of Vibration

The last section discussed waves without assuming anything about the boundary conditions or what happens when waves encounter obstacles or borders where waves reflect. This section uses the wave perspective to illustrate a common phenomenon where finite structures demonstrate a mathematically definable behavior when vibrating. In general, structures have certain preferred spatial and temporal deformations or modes when excited. Understanding why these preferred modes occur can be difficult. Typically, modes and vibration are taught from a mathematical perspective, where the degrees of freedom are carefully defined, and modal solutions are determined using linear algebra and eigenfunctions. Often the physicality of the vibration is lost from this perspective.

A modal analysis can also be performed from a wave perspective, and the logic is often more easily understood, especially for thin members such as beams and panels. As a wave travels through a medium it is characterized by a sinusoidal change in amplitude, but this is very different than the non-intuitive shapes often describing modes. One can understand how these shapes arise by looking at boundaries and obstacles comprising the structure. Take for example a finite beam. Assuming minimal damping, a wave reaching a

boundary must be reflected because the energy must be conserved. The reflecting wave then is superimposed upon the initial wave, creating an interference pattern. Some of these interference patterns are destructive and some are constructive. The interference patterns create standing waves and these standing waves result in mode shapes. Assuming a homogenous material, the geometry and mass of the structure or beam determines the shape and frequencies at which the standing wave patterns are created. From a spatial wave perspective on a beam, the standing wave or mode is formed when the wavenumber or wavelength coincides with the length of the beam. For a simply supported beam this would mean that the nodes (stationary parts of the standing wave) coincide with the mean harmonic values and the supports of the beam. From a temporal perspective this would theoretically occur at an infinite number of frequencies, where the wavelengths become successively smaller. These are the natural frequencies of the beam and their associated shapes are the mode shapes. The same is essentially true for more complex structures like panels, but the standing wave patterns can be highly complex, especially with two-dimensional wave interference.

Resonance of a structure occurs when the structure is excited near or at its natural frequency. This does not mean that modes cannot be excited at off resonant frequencies; it merely means that the response is greatest when excited at or near their natural frequency. The lowest natural frequency is often very important and is referred to as the *fundamental frequency.* There is a similar phenomenon to resonance that is often overlooked. If a structure is excited by a set of forces and these forces are spatially distributed to match with the standing wave pattern and occur at the same wave speed, then the structure's response is greater, regardless of the frequency. This phenomenon is generally referred to as *coincidence*, and the lowest frequency at which coincidence can occur is referred to as the *critical frequency.* Coincidence is discussed in greater detail in Section 2.4 [Fahy, 1985].

Vibration is often characterized by a superposition of preferred modes. Each mode will vibrate most strongly when it is excited at its resonant frequency. In complex structures,

such as machines, the structure as a whole has its own resonant frequencies and modes of vibration. The components of the structure, such as panels, vibrate with the structure at the entire structure's resonant frequencies. Each component influences the entire structure's resonant behavior, and depending on the degree of coupling and boundary conditions between the component and structure, the individual component's resonant behavior and modes may be significant and apparent in the overall dynamics. If a component is weakly coupled to the structure, or its boundary conditions can be categorized nearly as fixed, then the components individual behavior may be apparent. In other words, the component's behavior within the structure is more likely to resemble its individual behavior as if it were mounted with idealized boundary conditions. These are sometimes referred to as "local modes".

In the case of panels on machine enclosures, the panel's boundary conditions are often nearly rigid. Although they cannot be categorized as simply supported or clamped because their boundaries are compliant, their behavior often resembles an approximate combination of the two. For a first approximation it is reasonable to consider the boundaries either simply supported or clamped. For the case of a simply supported panel (simply supported on all sides and rectangular in shape) the natural frequencies can be estimated by,

$$f_{i,n} = \frac{\pi}{2}\sqrt{\frac{B}{m}}\left[\frac{i^2}{a^2}+\frac{n^2}{b^2}\right] \text{ (Hz)} \qquad i, n = 1,2,3,... \tag{2.9}$$

where again m is the surface density, B is the bending stiffness of the panel, a and b are the length and width of the panel, and i and n correspond to the number of nodal lines plus one in the a and b directions, or likewise the number of flexural half-waves in a particular direction. The lowest frequency mode corresponds to $i = n = 1$. The lower order mode shapes of a simply supported panel can be represented by the formula,

$$z(x,y)_{i,n} = \sin\left(\frac{\pi i}{a}x\right)\cdot\sin\left(\frac{\pi n}{b}y\right) \tag{2.10}$$

where z indicates the transverse deformation of the plate normal to the surface. The amplitude of the shape is arbitrary and meaningless as mode shapes do not have associated amplitudes. The simply supported boundary conditions allow for a nearly exact solution to be found, as in Equation 2.10, but in general an approximation is made using solutions of a series of beam modes and the Rayleigh-Ritz procedure.

For a clamped panel the natural frequencies can be approximated by,

$$f_{i,n} = \frac{\pi}{2}\sqrt{\frac{B}{m}}\left[\frac{(\alpha i)^2}{a^2} + \frac{(\varphi n)^2}{b^2}\right] \tag{2.11}$$

where α and φ are tabulated constants that are dependent on the mode order and have been experimentally determined [Blevins, 1995]. The lower order mode shapes for a clamped panel can be approximated by the formula,

$$m_{i,n} = \left(\sin\left(\frac{\pi i}{a}x\right) \cdot \sin\left(\frac{\pi n}{b}y\right)\right)^{\gamma} \tag{2.12}$$

where the coefficient γ was determined to be a value between 1.4 and 1.6 for lower order modes. This model for clamped panels was determined and verified using finite element analysis.

In most cases the actual panel dynamics are more nearly approximated by boundary conditions that lie somewhere between the values given by the clamped and simply supported conditions. This can be loosely approximated by choosing a value of γ that lies between 1.0 and 1.4, depending on whether the boundary conditions appear to resemble a clamped or simply supported condition. In addition, most actual panel boundary conditions incorporate some form of fastening and the boundaries are compliant rather than rigid. These differences between reality and the above analytical models lead to a certain degree of inaccuracy when determining the vibration characteristics of flat panels, but for a first order estimate the above models provide a quick and simple result with which to analyze designs.

Again, unfortunately, extreme difficulty is encountered when trying to analytically estimate the natural frequencies and mode shapes of two-dimensionally curved panels. Some progress has been made for simple curvature such as cylinders or spherical shells, but little of this complex analysis is applicable to many of the shapes contained herein. There are some models for orthotropic and corrugated (one-dimensionally curved panels) that may provide some additional insight. The natural frequencies of an orthotropic plate can be estimated by

$$f_{i,n} = \frac{\pi}{2}\sqrt{\frac{1}{m}}\left[\frac{(B_a i)^4}{a^4} + \frac{(B_a \nu + B_b \nu + Gh^3/3)i^2 n^2}{2a^2 b^2} + \frac{(B_b n)^4}{b^4}\right]^{1/2} \tag{2.13}$$

where $G = E/(2(1+\nu))$ is the material modulus of rigidity, B_a and B_b are the respective bending stiffnesses (as calculated in Equation 2.8) in the directions corresponding with the sides indicated by the lengths a and b *[Hearmon, 1959]*. This formula can provide slightly better estimate of two-dimensionally curved panels.

In general, the analytic models presented above give inaccurate estimates for two-dimensionally curved panels. They provide an order of magnitude estimate for the lower frequencies, but cannot be trusted to provide any information at higher frequencies. To best analyze two-dimensionally curved designs it is more reasonable to rely on numerical analysis. When possible, this work relies on finite element analysis to provide structural and dynamic information about the designs. This work does not address the details associated with the development of the finite element calculations as these are not central to the work here and can be found in a number of other sources.

2.3 Acoustics

Acoustics are an often misunderstood phenomenon. The information here is meant to provide a basic understanding of the concepts used in this thesis and to minimize confusion. Again, a wave perspective is used as the primary method to describe the dynamics of acoustic mediums.

2.3.1 Acoustic Fundamentals

Sound is perception based. This means that it is dependent on how the human body senses and translates input from the environment. Unfortunately this leads to confusion because the scientific explanation of sound does not coincide well with how humans perceive sound. This section and the next describe sound from a scientific point of view, but to help clarify, Section 2.3.3 discusses how the scientific aspects relate to perceived sound.

Sound is merely compressional waves that propagate through a fluid, air for the purposes of this work, at a speed characteristic of that fluid (although it should be noted that shear waves can also be present in viscous fluids). In this sense, sound waves are very similar to longitudinal waves in structures. In general, sound waves in fluids are *non-dispersive*, meaning that they travel at the same speed regardless of frequency. The speed of the compressional wave in a fluid can be determined by

$$c_f = \sqrt{\frac{\beta}{\rho}} \tag{2.14}$$

where β represents the bulk modulus and ρ is the fluid density. At standard temperature and pressure the speed of sound in air is approximately 344 m/sec.

Pressure disturbances lead directly to the formation of sound waves. As a result, sound waves are often described by pressure waves. One-dimensional, or plane, sound waves are sometimes represented by $p(t) = P\sin(\omega t + \phi)$ where $p(t)$ is the pressure as a function of time, P represents the pressure amplitude and ϕ represents the phase. It is sometimes simpler to denote $p(x,t) = Re\{P\exp[j(\omega t - kx + \phi)]\}$, where Re indicates the real portion of the equation, and P is the complex pressure amplitude. Again, the change per unit distance is accounted for with the spatial relation of the wavenumber.

To illustrate some other basics of acoustics, consider a spherical sound pressure wave propagating outward from a source of amplitude P_s, generated from the surface of a sphere of radius R. Assuming no reflections (*i.e.* free field) the pressure is represented by

$$p(r,t) = Re\left\{\frac{RP_s}{r}\exp[j(\omega t - k(r-R)) + \phi]\right\} \tag{2.15}$$

where r is the distance from the sphere to the point of the pressure measurement. This equation illustrates that the pressure amplitude, RP_s/r, decreases with distance from the point source. This phenomenon is more readily apparent in the far field*. In the far field sound waves are freely propagating, meaning the fluid particle velocity and wave propagation are in the same direction and their maxima and minima coincide. In the far field the pressure and particle velocity can be related by

$$\rho c_f = \frac{p(r,t)}{u(r,t)} \tag{2.16}$$

where ρ is the fluid medium density, c_f is the speed of sound waves, and u is the particle velocity. This value is often referred to as the *characteristic impedance* of the fluid medium. Note that the characteristic impedance is also valid for plane waves in the far field where the term r can be replaced by x in Equation 2.16.

An important quantity in acoustics is the intensity of a sound wave. The intensity relates the average acoustic power passing through a unit area of the medium perpendicular to the direction of sound propagation. In structural systems, power is the product of force times velocity. The power couple in fluids is the product of pressure and flow rate, but for purpose of acoustic intensity the important parameters are pressure and particle velocity (multiplying particle velocity by the unit area provides flow rate). Intensity is mathematically described by,

$$\Upsilon = \frac{1}{\tau}\int_0^\tau p(r,t)\cdot u(r,t)dt, \tag{2.17}$$

* Far field can be defined as a distance where $k^2r^2 >> 1$ and $r >> R$, where R can be generically thought of the characteristic length of the source (*i.e.* length of a panel).

where Υ denotes the intensity and τ signifies the time interval of integration. Substituting in Equation 2.16 we get

$$\Upsilon = \frac{1}{\tau}\int_0^{\tau} \frac{p^2(r,t)}{\rho c_f} dt. \tag{2.18}$$

A more common form of relating acoustic pressure is the root mean square (RMS) of the pressure. The RMS pressure is the value that most common sound meters provide and can be calculated by

$$p_{rms}^2 = \sqrt{\frac{1}{\tau}\int_0^{\tau} p^2(r,t) dt}. \tag{2.19}$$

Now the intensity can be described by

$$\Upsilon = \frac{p_{rms}^2}{\rho c_f}. \tag{2.20}$$

It should be noted that for a point source and the resulting spherical waves the intensity of sound pressure follows the *inverse square law*. In other words, the intensity is inversely proportional to the square of the distance from the point source. This is opposed to the pressure which is only inversely proportional to the distance.

It is important to understand how multiple sound sources add at a point different from the sources. Both the RMS pressure and the intensity combine in the same way. In general, for an incoherent field the pressure can be summed as follows

$$p_{total}^2 = p_1^2 + p_2^2 + p_3^2 + \ldots + p_n^2 \tag{2.21}$$

where p_i represent the sound pressure sources measured at a single point and the RMS value for pressure is assumed (as is the case from this point forward). For incoherent waves the intensity formulation is similar

$$\Upsilon_{total} = \Upsilon_1 + \Upsilon_2 + \Upsilon_3 + \ldots + \Upsilon_n = \frac{p_{total}^2}{\rho c}. \tag{2.22}$$

For tonal sources of nearly the same frequency (coherent field), the phase of the sources must be accounted for so that the superposition of waves is considered. For this calculation for tonal sources the reader is referred to the literature [Lord, 1987]. The acoustic power of the source can be determined by multiplying the intensity by an area surrounding the source.

Another fundamental acoustic concept is the decibel. The acoustic decibel is a unit of measurement based on the RMS sound pressure that scales logarithmically. The important aspect of using the decibel as a unit of measurement is that it more accurately coincides with the human sense of acoustic volume. Like most human senses, what appears like a linear change to the human senses is more nearly a logarithmic change in terms of measurable quantities. As a result, the decibel is a practical unit of measurement that adds a bit of confusion when performing calculations.

In addition, it is also important to have a reference measurement. This is necessary because there is a minimum quantity that humans can perceive. In the case of the decibel, the quantity can be described in terms of pressure, intensity, and power. The decibel measurement of acoustic volume can be measured by the following formulations

$$SL_{\wp} = \text{Sound-power Level} = 10\log_{10}\left(\frac{\wp}{\wp_{ref}}\right) \tag{2.23}$$

$$SL_I = \text{Sound-intensity Level} = 10\log_{10}\left(\frac{\Upsilon}{\Upsilon_{ref}}\right) \tag{2.24}$$

$$SL_p = \text{Sound-pressure Level} = 10\log_{10}\left(\frac{p}{p_{ref}}\right)^2 = 20\log_{10}\left(\frac{p}{p_{ref}}\right) \tag{2.25}$$

where SL denotes the "sound level" (in the case of pressure it is often referred to as sound pressure level, SPL), p_{ref} is 2×10^{-5} N/m^2, Υ_{ref} is 1×10^{-12} W/m^2, $\wp$ is the power

level and $\wp_{ref}$ is 1×10^{-12} W. The reference values are the minimum values that the average human ear can perceive at a 1000 Hz. This is sometimes referred to as the A-weighted sound level. The "A" indicates that this standard is recommended by the American National Standards Institute (ANSI). The square of the pressure is required to form the "power" relationship as indicated in Equation 2.22 [Lord, 1987].

Unfortunately, using the decibel unit of measurement can be confusing when separate sources require addition or subtraction. Because the decibel unit is on a logarithmic scale it cannot be simply added or subtracted. First, the quantity must be converted to either the power, intensity, or pressure squared, based on the reference quantity. After the quantity is converted, then the values can be added or subtracted as necessary.

2.3.2 Acoustic Waves

Like structures, fluid dynamics can be described in terms of waves. Waves in low viscosity fluids are primarily compressional waves. The wave equation can be derived from the linearized form of the continuity equation

$$\frac{\partial \rho}{\partial t} + \rho\left(\frac{\partial u}{\partial x} + \frac{\partial v}{\partial y} + \frac{\partial w}{\partial z}\right) = 0, \tag{2.26}$$

and the momentum equations

$$\begin{aligned} \frac{\partial p}{\partial x} + \rho\frac{\partial u}{\partial t} &= 0 \\ \frac{\partial p}{\partial y} + \rho\frac{\partial v}{\partial t} &= 0 \\ \frac{\partial p}{\partial z} + \rho\frac{\partial w}{\partial t} &= 0 \end{aligned} \tag{2.27}$$

where u, v, and w are the particle velocities in the x, y, and z direction respectively, and ρ implies the *mean* density of the fluid. An adiabatic process is assumed.

From these two sets of equations the wave equation governing small perturbations about the equilibrium can be derived

$$\frac{\partial^2 p}{\partial x^2}+\frac{\partial^2 p}{\partial y^2}+\frac{\partial^2 p}{\partial z^2} = \frac{1}{c_f^2}\frac{\partial^2 p}{\partial t^2}, \tag{2.28}$$

where p is the perturbation or "acoustic pressure" about the equilibrium pressure; c_f is the speed of sound from Equation 2.14; and the fluid is assumed to be inviscid, homogeneous and compressible.

Assuming the simple harmonic time dependence discussed in Section 2.3.1, and considering only the two-dimensional form (useful for fluid structure interaction), a general two-dimensional solution to Equation 2.28 can be expressed as

$$\frac{\partial^2 p}{\partial x^2}+\frac{\partial^2 p}{\partial y^2} = -\left(\frac{\omega}{c_f}\right)^2 p = -k^2 p. \tag{2.29}$$

The propagation of a plane wave in two-dimensions can be expressed as

$$p(x, y, t) = \tilde{p} \cdot \exp[-jk_x - jk_y]\exp[j\omega t], \tag{2.30}$$

where k_x and k_y indicate the wavenumber in the respective directions. The directional wavenumbers are not independent. Substitution of Equation 2.30 into Equation 2.29 yields the following wavenumber relation

$$k^2 = k_x^2 + k_y^2. \tag{2.31}$$

This demonstrates that only specific combinations of directional wavenumbers can satisfy the wave equation at any particular frequency [Fahy, 1985].

2.3.3 Perception of Noise

Knowledge of how noise is perceived is also an important aspect of effectively minimizing noise. It is important to recognize that what may scientifically or numerically appear

TABLE 2.1 Examples of sound sources and their approximate levels at close distances (*i.e.* 5 to 10 feet) [Lord, 1987].

Source of Noise	Sound Power Level (dB)	Power (W)	Sound Pressure (Pa)
Ram jet with afterburner	180	1,000,000	20,000
Near commercial jet engine	140	100	200
Rock concert	120	1	20
Car horn at 10 feet	100	0.01	2
Curb-side of busy street	80	0.0001	0.2
Inside a department store	60	0.000001	0.02
Radio at low volume	40	0.00000001	0.002
Whisper	20	0.0000000001	0.0002
Normal threshold of hearing	0	0.000000000001	0.00002

quieter may not seem quieter to the human ear. A noise mitigation solution may appear to be effective in a lab or on a graph, but in application the solution can be ineffective due to how the noise is perceived.

As mentioned in Section 2.3.1, human perception of noise and acoustic volume is more conveniently suited to a logarithmic scale. Table 2.1 is used to help demonstrate the various relationships between pressure, decibels, and power for some common sound sources. The decibel scale is not only more compatible with the human senses, but it is easier to manage as the numbers are of a limited range that correspond to many other measurements commonly used (*i.e.* temperature, length, and time scales).

One important aspect of noise control is recognizing what the human ear can discern. In general, the human ear cannot distinguish acoustic volume differences of 3 decibels or less. Therefore, to have an effective solution the change in decibel levels should be at least 5 decibels. This is not an absolute rule. The human ear is more sensitive at certain frequencies ranges than others. In general, the human ear can sense noise ranging from 50 Hz to 20,000 Hz. These values may vary from person to person. At the lower frequencies, the sound is often described as "felt" more than heard. The human ear is most sensi-

tive in the frequency range from 1,000 Hz to 10,000 Hz. Not surprisingly, this is the frequency range of most human voices. It is also the frequency range where noise control solutions must be most effective.

In addition to the above general rules on ear sensitivity, an important aspect of noise control is psychological acoustics. Much in the same way that a surface may feel unpleasant to the touch or a color hard on the eye, certain types of sounds are more annoying than others. Often, this phenomenon cannot be explained or predicted using numerically based rules. What may appear to be a good solution numerically, even considering the ear's sensitivity range, may actually turn out to be considered worse merely because the noise is "less pleasant" even though it is numerically quieter.

There are several standards and theories that describe various aspects of noise perception. It is not the goal of this section to review all these methods, rather the purpose is to make the reader aware of these issues so that accurate judgements of noise control performance can be made. For more detailed information concerning these issues the reader is referred to the literature [Lord, 1987; Kryter, 1970].

2.4 Structural-acoustic Coupling

To effectively mitigate both acoustic noise and vibration it is critical to understand the coupling process between structures and fluids. Vibration problems are often exaggerated by the influence of impinging acoustic waves, and vice-versa. Acoustic noise is prevalent where large surfaces vibrate. Unwanted sound can escape machine enclosures when the radiation and transmission loss characteristics of the enclosure panel are not properly considered. All these issues pivot on the physics of structural-acoustic coupling.

The difference between structural to acoustic coupling and acoustic-to-structure coupling is only in the direction of energy travel. The processes and dynamics that occur are essentially the same, and can be proven through the principle of reciprocity [Fahy, 1985; Smith, 1965]. To simplify the discussion, the topic of structural-acoustic coupling is described

primarily from the perspective of structure to acoustic coupling, but the reader should be aware that the principles are the same in reverse.

In machines, it is common to have quiet mechanisms that vibrate at frequencies outside the range of human perception*. These mechanisms are then attached to other components that may not be directly related to the function of the machine, such as aesthetic and enclosure components, but these components may couple and vibrate at frequencies that are within the range of human perception. To ensure quiet machines it is important to understand this phenomenon and how these structures couple to the acoustic medium. In this section the focus is on panel-like structures coupling to air.

An important concept to understand is how a vibrating structure causes an audible acoustic disturbance. In general, the mechanism of structure to acoustic coupling occurs when the surface of a structure vibrates so that it causes the acceleration of fluid particles near the structure, resulting in a density change in the fluid. The effectiveness of the coupling depends upon the amplitude of the acceleration and throw, as well as the spatial distribution of the acceleration. A fluid can accommodate a certain amount of acceleration and still behave incompressibly. When the acceleration is significant enough the fluid compresses locally, and if the acceleration is over a broad area then the density change propagates through the fluid and causes significant far-field disturbances. To properly understand the process, both spatial and temporal factors must be considered.

To demonstrate the process, simple models can be used both as illustrations of the phenomenon and as building blocks for more complex models. One such model is a volume displacement source, most often a sphere. The time variant pressure at a distance r from a radial pulsating sphere of radius a has been estimated [Kinsler, 1982] by

$$p(r,t) = \frac{1}{1+jkR}\frac{j\omega\rho Q}{4\pi r}e^{(j[\omega t - k(r-R)])} \tag{2.32}$$

* Humans can perceive sound ranging from approximately 50 to 15,000 Hz, although the range can vary from person to person.

where ρ again implies the mean fluid density, ω is the pulsation frequency, and Q is the volume flow rate of the fluid. The flow rate is important for several reasons. One, when multiplied with the collocated pressure it relates the power. In addition, the flow rate is the velocity flux of fluid through an area. As previously mentioned, the velocity is often used to describe acoustic fields. Also, if one considers the time rate of change of the flow rate, dQ/dt, then this directly relates to the particle acceleration discussed previously, and strongly influences the nature and degree of coupling. If the displacement of the normal to the sphere is described by $q = \tilde{q}e^{j\omega t}$, then the flow rate is described by

$$Q = j\omega 4\pi a^2 \tilde{q}. \tag{2.33}$$

One half of a spherical source can represent a point on a surface, and thus an elemental source of structural-acoustic coupling to form sound. For sources that are much smaller than the acoustic wavelengths considered (i.e. $ka << 1$) the pressure equation can be simplified to

$$p(r,t) = \frac{j\omega\rho Q}{4\pi r} e^{(j[\omega t - kr])}. \tag{2.34}$$

It is often helpful to write the pressure in terms of the normal velocity, $v_N = \tilde{v}_N e^{j\omega t}$

$$p(r,t) = \frac{2j\omega\rho\tilde{v}_N \delta S}{4\pi r} e^{(j[\omega t - kr])} \tag{2.35}$$

where Q has been replaced by the equivalent $2\tilde{v}_N \delta S$ and δS is the elemental surface area. Note that the above form is only applicable at distances much greater than the dimension of source features or in the case of vanishingly small sources, as is the case when integrating over a surface. Thus, the equation can be applied to planar surfaces by integration. This was first performed in the late nineteenth century by the physicist Rayleigh,

$$p(\bar{r},t) = \frac{j\omega\rho}{2\pi} e^{j\omega t} \int_S \frac{\tilde{v}_N(\bar{r}_s) e^{-jk\varsigma}}{\varsigma} dS \tag{2.36}$$

where $\bar{r}$ is the position vector of the receiving or sensing point, $\bar{r}_s$ is the position vector of the vibrating surface with velocity $\tilde{v}_N(\bar{r}_s)$, and ς is the magnitude of the vector $\bar{r} - \bar{r}_s$.

The application of the above formula to panel like structures can provide a good approximation of the acoustic field created by panels. The difficulty is encountered when one tries to determine the velocity distribution for panels of various geometries and boundary conditions. Analytic solutions are only available for the simplest of conditions. Pressure from a simply supported flat panel can be estimated because the normal velocity distribution can be represented

$$\tilde{v}_N(x, y) = \tilde{v}_{i,n} \cdot \sin\left(\frac{i\pi x}{a}\right) \cdot \sin\left(\frac{n\pi y}{b}\right) \tag{2.37}$$

where i and n relate the number of nodal lines in the x and y direction, and a and b represent the lengths of the panel (by which x and y are bounded). Combining this with Equation 2.36 the pressure created by a particular mode at an arbitrary point and frequency can be represented by

$$p(x_p, y_p, z_p, t) = \frac{j\omega\rho\tilde{v}_{i,n}e^{j\omega t}}{2\pi}\int_0^a\int_0^b \frac{\sin\left(\frac{i\pi x}{a}\right) \cdot \sin\left(\frac{n\pi y}{b}\right) \cdot e^{-jk\varsigma}}{\varsigma} dxdy \tag{2.38}$$

where x_p, y_p, z_p represent the position of the point of measurement, and ς is the distance to the point.

Since much of the above analysis is only applicable for simple systems, it is difficult to measure its worth for the complicated systems of this work. The above analysis provides essential information about how structures and fluids couple, but it is unlikely that it can provide accurate information about two-dimensionally curved systems. For this reason the detailed quantitative analysis ends here and the reader is referred to the sources Fahy [Fahy, 1985] and Wallace [Wallace, 1972]. Although the above cannot provide exact solutions, it can provide understanding that can lead to a more qualitative understanding and ability to predict the dynamics of structural acoustic coupling. The next two sections use

the above information as building blocks to describe qualitatively some of the more important aspects of structural-acoustic coupling.

2.4.1 Radiation

An important factor for a panel design is understanding how, and how well a design radiates sound. Sound radiation of panels is largely a factor of the modal dynamics of the panel. The shape of the modes and the wavenumbers can determine how well a panel radiates sound. This is especially true when the panels are structurally excited. To understand this phenomenon it is helpful to look at some mode shapes.

Figure 2.2 illustrates six different mode shapes of a flat panel. Each mode illustrates a different type of radiating mode. As a first approximation, the efficiency with which a panel mode radiates is dependent upon whether the mode shape has an equal number of positive and negative lobes. Lobes are either the peaks or the troughs of the mode shape above or below the neutral axis and are separated by nodal lines. The first mode (Figure 2.2a) generally is the most efficient at radiating noise, because there is no other lobe to cancel the volume of air it moves, and as such can be thought of as a monopole noise source. The second mode (Figure 2.2b) is an example of a mode where the two lobes cancel out the volume of air that they move and as a result there is less far-field radiation of noise. The second mode can be thought of as a dipole source with the sources 180 degrees out of phase. The fourth mode, for the configuration shown, (Figure 2.2c) is also usually an effective radiator. Although there is some cancellation, a significant area is not cancelled (*i.e.* a single lobe). In general, modes with an even number of lobes are referred to as *even* modes, and modes with an odd number of lobes are referred to as *odd* modes, with the odd modes often being more efficient noise radiators.

Higher-order modes for flat panels, as those shown in Figure 2.2d-f, demonstrate some of the same behavior as the lower order modes but the radiation behavior is a bit more complex and requires a higher level of analysis. For higher order modes the majority of radiation comes from the edges and corners of a the panel. To understand this it is necessary to

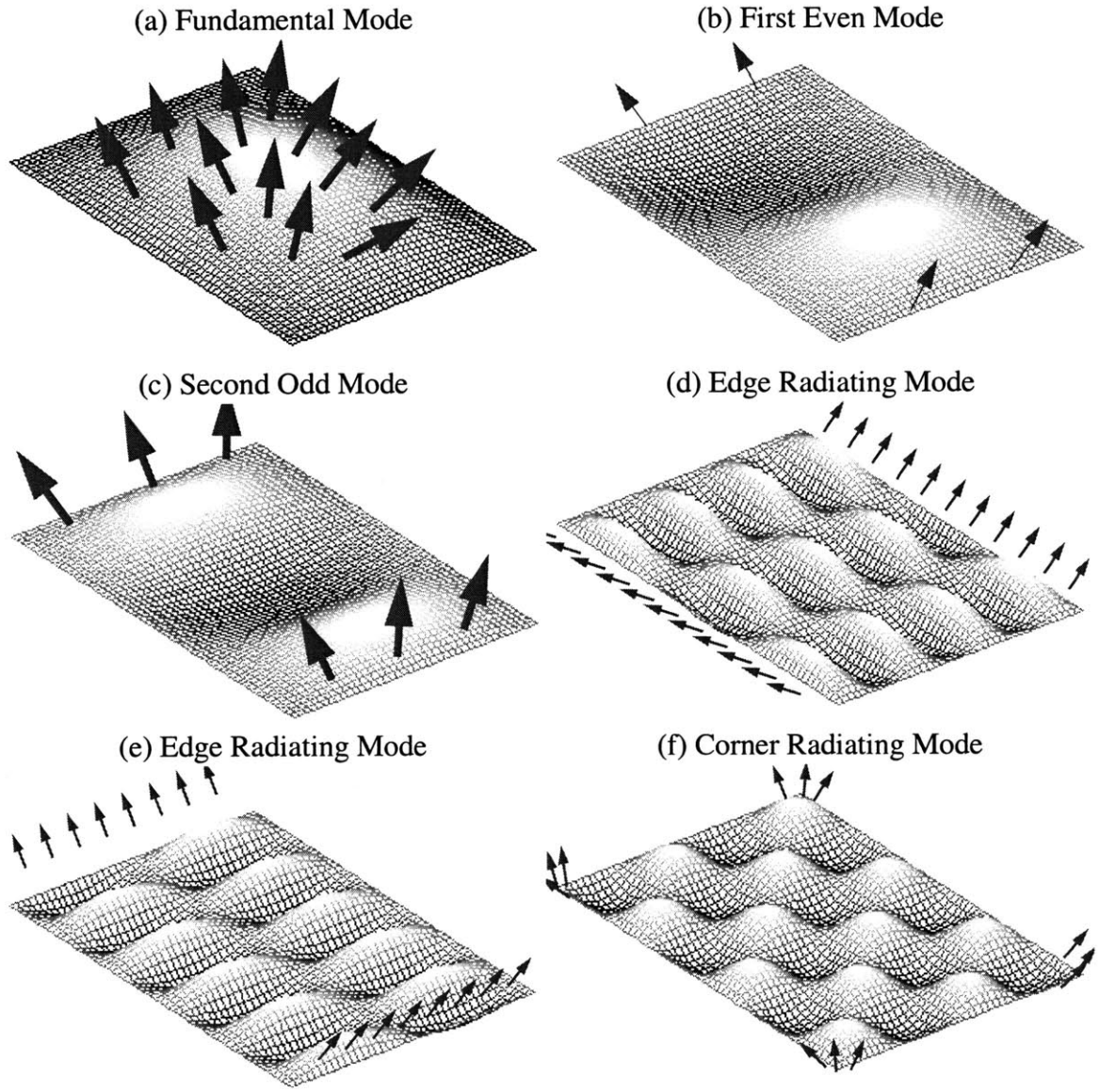

Figure 2.2 Illustrations of several mode shapes for a flat rectangular panel. The size and quantity of arrows qualitatively illustrate the radiating efficiency of the mode, and the radiation portion of the panel.

introduce the concept of the radiation index, and to examine its relationship to the critical frequency and the wavenumber.

As a measure of a panel's ability to radiate, a radiation index is defined (also referred to as radiation efficiency and radiation resistance). The radiation index is the ratio of a panel's radiated power to the power radiated by a baffled piston (assumed to be infinitely stiff) of the same area and at the same velocity. It can be represented by

$$\sigma = \frac{\wp_{panel}}{\wp_{piston}} = \frac{\wp_{panel}}{\rho c_f S \langle \overline{v_n^2} \rangle} \tag{2.39}$$

where $\wp_{panel}$ is the power radiated by the panel, $\wp_{piston}$ is the power radiated by an idealized baffled piston, S is the surface area of the panel, and $\langle \overline{v_n^2} \rangle$ is the average mean square velocity of the panel. The average mean square velocity can be calculated by

$$\langle \overline{v_n^2} \rangle = \frac{1}{S} \int_S \left[\frac{1}{\tau} \int_0^\tau v_n^2(x, y, t) dt \right] dS \tag{2.40}$$

where τ is some measure of time, and again v_n is the normal velocity of a point on the panel. The radiation index is useful in comparing the ability of a panel to radiate noise and is referred to further in this section and again in the experimental results in Chapter 6. In general, the radiation index is less than unity below the *critical frequency* and near unity above the critical frequency.

Earlier, the critical frequency was introduced as the spatial equivalent to the natural fundamental frequency; it is also the frequency at which the speed of the bending wave in the material is equal to the speed of the compressional wave in air (speed of sound in air) and is represented as

$$f_c = \frac{c_f^2}{2\pi} \sqrt{\frac{m}{B}} = \frac{\omega_c}{2\pi} \tag{2.41}$$

where c_f is the speed of sound in air. Likewise, it is the frequency at which the structural and acoustic wavenumbers are equal. The critical frequency is important because it indicates frequencies where the panel couples well with the surrounding air, regardless of the modal distribution of the panel. In physical terms, at the critical frequency the wavelength in the panel bending wave is equal to the trace wavelength at a grazing incidence, and coupling between the structure and acoustic medium is strong [Bies, 1996].

At this point one must be careful in distinguishing between structural and acoustic wavenumbers. From this point forward structural wavenumbers are subscripted with the letter b and acoustic wavenumbers are not subscripted. As in the case of acoustic two-dimensional wavenumbers (as in Equation 2.31) orthogonal structural wavenumbers can be summed in the following manner

$$k_b^2 = k_{bx}^2 + k_{by}^2 = \sqrt{\frac{\omega^2 m}{B}} \tag{2.42}$$

where k_b is the free structural wavenumber. The primary wavenumber values can be determined for each directional by

$$\begin{aligned} k_{bx} &= \pm\frac{i\pi}{a} \\ k_{by} &= \pm\frac{n\pi}{b} \end{aligned} \quad . \tag{2.43}$$

Recall that i and n indicate the number of lobes in the x and y direction respectively, and a and b represent the panel lengths in the respective directions.

Since above the critical frequency the radiation index can be assumed to be nearly unity, one must focus on what happens below the critical frequency. Three distinct regimes are apparent below the critical frequency, each corresponding to a different combination of wavenumber configurations. The first corresponds to $k > k_{bx}$, $k < k_{by}$ and is referred to as an edge radiating mode, with the edges parallel to the x axis being the primary source of radiation. The second corresponds to $k < k_{bx}$, $k > k_{by}$ and is also referred to as an edge radiating mode, with the edges parallel to the y axis being the primary source of radiation. The third regime corresponds to $k < k_{bx}$, $k < k_{by}$ and is generally referred to as a corner radiating mode because the corners are the primary sources of radiation. Figure 2.2d through Figure 2.2f provide examples of these mode shapes and their radiating portions. The above provides an introduction to some of the principles of radiation. For a more thorough treatment of the subject the reader is referred to Fahy [Fahy, 1985], and Smith and Lyon [Smith, 1965], from which the above is primarily based.

2.4.2 Transmission

Transmission of noise is an extension of the radiation phenomenon. In the above section it is assumed that the source of excitation is a structural disturbance. As such the primary source of noise is based largely on the modal dynamics (a fact that becomes important when the discussion of damping arises in a following section). Transmission of noise is essentially noise radiation that occurs due to the acoustic excitation of the panel. The acoustic excitation of the panel increases the complexity of the problem because non-modal dynamics become more significant, and as a result the radiation efficiency also increases.

In a more strict sense transmission is the relation of incident sound power to the transmitted sound power. In general, a transmission coefficient is defined to characterize the transmission loss properties of a partition. The transmission coefficient is the ratio of transmitted to incident power and is represented as

$$\tau_T = \frac{\wp_{transmitted}}{\wp_{incident}} \tag{2.44}$$

where τ_T is the transmission coefficient, and again $\wp$ is the power. The transmission loss is often used to describe the characteristics of a panel and is defined by

$$TL = -10\log(\tau_T). \tag{2.45}$$

Several predictive methods exist for determining the transmission loss analytically [Fahy, 1985; Cremer, 1973; Hearmon, 1959], but generally their application is restrictive and the results are far from accurate for non-flat structures. Therefore, transmission is treated in a more qualitative sense in this work, the goal being to understand how design changes may influence transmission.

Four significant frequency regions are evident when analyzing transmission through panels, assuming diffuse and broadband excitation. The first region is the frequency range below the fundamental frequency of the panel. In this region the transmission of sound is

primarily controlled by the stiffness of the panel, and is often referred to as the stiffness controlled region. In this region, the stiffer the panel, the lower the transmission coefficient, τ_T. An analogy for this behavior can be made with a mass-spring model. Below the fundamental frequency of the spring-mass system, the displacement and velocity of the motion of the mass for a given force is primarily dependent upon the stiffness of the spring.

The second significant region is the narrowly banded frequency near the fundamental frequency. usually, this region is where the transmission coefficient is at a maximum. For the spring-mass analogy this corresponds to the resonance of the model where the response is theoretically infinite (damping of a real system keeps the response bounded). As implied this region is a function of both the mass and stiffness (as these two factors determine the resonant frequency, $\omega = \sqrt{\frac{k}{m}}$). In addition, sometimes structural modes near the fundamental mode may also contribute to this region. Since it is controlled by the modal dynamics of the panel, the degree of transmission loss can be controlled to a limited extent by the damping of the panel.

The third region of interest lies between the fundamental frequency and the first critical frequency (*first* critical frequency is used here to imply that for non-homogeneous panels multiple critical frequencies are evident depending on the direction of incidence). This region is often referred to as the mass-law or inertia controlled region. In reference to the spring-mass model this is the region above the natural frequency where the displacement and velocity of the mass for a given force is highly dependent upon the amount of mass. This region often dominates the transmission properties of many barriers and panels for audible frequency ranges and is why, as a general rule, many transmission barriers seek to maximize mass. In this region there are often several higher order resonant modes, but these modes generally do not contribute as significantly as the fundamental mode and are minimal compared with the mass control of the transmission behavior. As a general rule the transmission loss in this region approximately increases at a rate of 6 decibels per decade above the fundamental frequency.

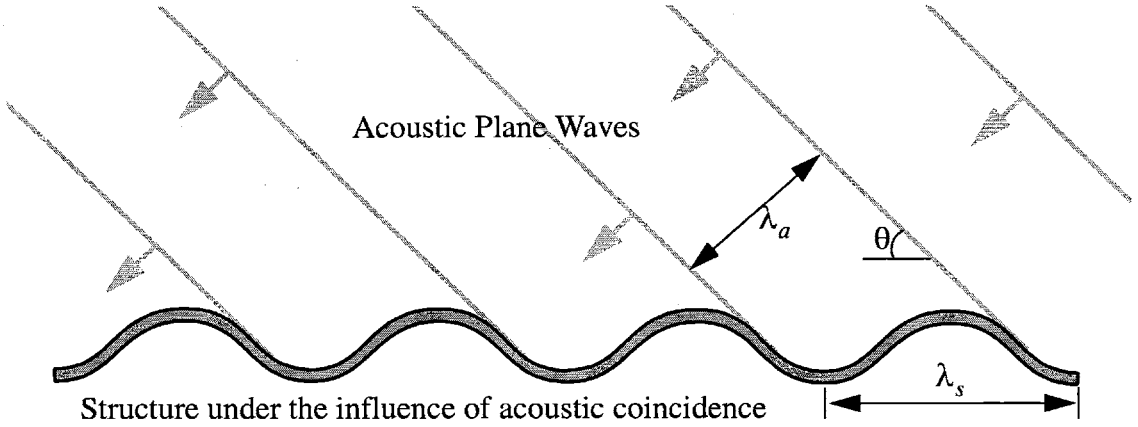

Figure 2.3 Illustration of the coincident phenomenon. If λ_a represents the acoustic wavelength, λ_s is the structural wavelength, and θ is the angle of incidence, then coincidence occurs when $\lambda_a = \lambda_s \cdot \sin\theta$.

The final region of transmission loss is referred to as the coincident region. This is the frequency range at and above the first critical frequency of the panel. The critical frequency can be thought of as the spatial equivalent of the fundamental frequency, as it is the lowest frequency where spatial separation (*i.e.* wavelength) of structural waves corresponds with the spatial separation of acoustic waves (as opposed to temporal matching during resonance). The critical frequency occurs at grazing incidence. Due to this, a great deal of structural acoustic coupling occurs at the critical frequency and leads to a decrease in transmission loss. Above the critical frequency there is a phenomenon known as coincidence between the acoustic and structural waves. Coincidence is the spatial equivalent of higher order modes and is especially important in diffuse sound environments. Coincidence is the alignment of structural and acoustic waves at angles of incidence smaller than grazing incidence. Figure 2.3 illustrate the coincidence phenomenon. Coincidence can occur at *any* frequency above the critical frequency because there is always an incident angle for which the structural and acoustic wavelengths align. In general, from the dip in the transmission loss at the critical frequency, the transmission loss increases asymptotically up to an extension of the mass controlled region at an average of 9 decibels per decade.

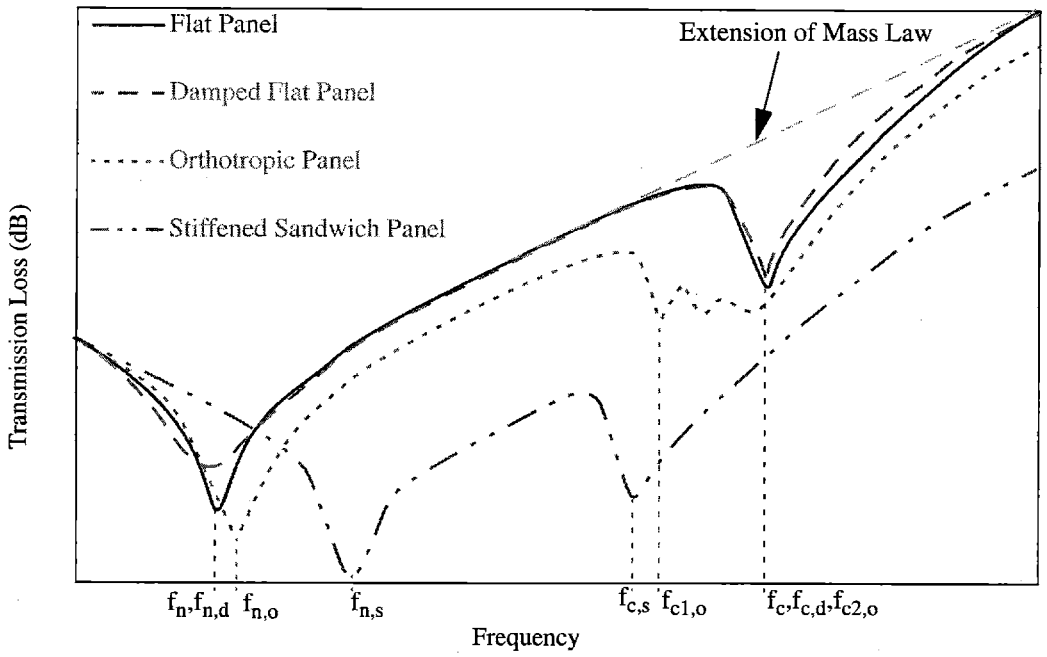

Figure 2.4 Illustration of transmission loss for four generic panels.

Illustrations of several generic transmission loss curves are depicted in Figure 2.4. It should be noted that these curves are a general representation and may not accurately depict panels in a variety of settings. Some factors that may affect the transmission loss response are size of enclosure, inclusion of absorption material, proximity of noise source to panel, and geometry of panel, to name a few. One of the more important issues in relation to this work is the effect of an orthotropic panel design. Orthotropic panels, panels that have different bending stiffness depending on the orientation of the panel, are generally undesirable for transmission loss applications. The reason for this is that the different stiffnesses lead to multiple critical frequencies, depending on the orientation of the incident waves to the panel. In addition, the stiffening of the panel also leads to a reduction in the frequency at which coincidence can occur. Figure 2.4 illustrates a simplified representation of this for the line labeled orthotropic panel. This fact is considered when the panel designs of later chapters are evaluated.

Figure 2.5 Figure illustrating the negative acoustic effect that discrete reinforcements can have on a panel design. Illustration on left shows undeformed reinforced panel. Illustration on right shows possible mode that would have undesirable acoustic radiation properties.

Again this is a cursory introduction to transmission and the reader is referred to Fahy [Fahy, 1985], and Smith and Lyon [Smith, 1965], among others [Cremer, 1973; Hearmon, 1959] for greater detail of the dynamics.

2.4.3 Notes on Stiffened Panels

Since a goal of this research is to limit vibration while minimizing the increase in acoustic noise through stiffening with two-dimensionally curved designs it is important to point out some of the factors that must be considered when discussing stiffened panels. While stiffening panels often helps to reduce vibration, it can be harmful when considering the effects on acoustic behavior. From a transmission point of view, while the fundamental frequency is increased the critical frequency is reduced. In addition, panels are most often stiffened by adding reinforcing ribs or other one-dimensional members. This leads to an orthotropic panel that will tend to demonstrate stronger coincident coupling because multiple critical frequencies are possible due to the varying panel stiffness. These factors can lead to more effective coupling between the panel and the air and greater transmission of sound [Bies, 1996]. From a radiation point of view, the ribs and cross members typically used to stiffen a panel often end up dividing a larger panel into numerous smaller panels that can radiate more efficiently than the unstiffened panel [Maidanik, 1962]. An example of this is illustrated in Figure 2.5 These issues were considered when the panels discussed in later chapters are designed.

2.4.4 Notes on Impedance

Impedance, in the most general terms, is the inherent ability of a system to accept and pass energy. A system with high impedance can have both positive and negative connotations. In most systems merely a high or low value for impedance is not enough to describe the transfer of energy. Most often a particular value (rather than a high or low value) for impedance is most effective at transferring energy; this is referred to as impedance matching.

To gain a better understanding it is helpful to think about a simple one-degree of freedom system with a spring, mass, and damper. Below the resonant frequency of the system, the stiffness is the most important aspect of a system's impedance. To best transfer energy from a second system to the one-degree of freedom system, it is best if the second system has equivalent stiffness, thereby maximizing the efficiency of the energy transfer. Above the resonant frequency of the one-degree of freedom system, the mass is the dominant factor in determining the impedance characteristics of the system, with greater mass generally leading to greater impedance. At resonance, the impedance of the system is dependent on both the mass and stiffness, but the outcome or transfer of the energy is highly dependent on the system's damping. One should notice that this closely parallels the discussion of sound transmission in the previous section.

There are several forms and mathematical definitions for impedance, and although this work tries to discuss behavior in terms of the mechanics of systems rather than the generalized impedance version, it is helpful to have an introduction to the terms. *Mechanical impedance* is the ratio of a force to the resulting velocity. This is commonly used to describe structural systems and is useful when discerning the radiation characteristics of a panel, as such it is sometimes referred to as *radiation impedance*. *Specific acoustic impedance*, sometimes referred to as *characteristic acoustic impedance*, is the ratio of acoustic pressure to the resulting particle velocity. It is useful in gauging the ability of fluid to propagate sound, and was introduced in Equation 2.16. A third type of impedance is *acoustic impedance*, which is also dependent upon pressure and particle velocity, but

also associates the acoustic wavelength and the fluid channel cross-section. This is often used when discussing mufflers and ducts. [Bies, 1996]

For further information on impedance, the reader is directed to the text by Bies and Hansen [Bies, 1996].

2.5 Sound Absorption and Mechanical Damping

First, it is important to make the distinction between acoustic absorption and mechanical damping. Acoustic absorption is the attenuation of sound waves through the use of porous, fibrous and foam-like materials whereby the acoustic energy is either acoustically cancelled or converted to mechanical energy and dissipated. Common absorption materials are mufflers, loose fiber glass, and open-cell foams. As a general rule the frequencies at which absorption material is effective is inversely proportional to the thickness of the material, and the acoustic material thickness should be greater than one quarter of the minimum acoustic wavelength of interest. This can lead to prohibitively thick layers.

Damping, unlike absorption, is the attenuation of mechanical energy. The incorporation of damping material is an effective measure for reducing vibration. Damping can also be beneficial for reducing acoustic noise, but the effectiveness is highly dependent upon the source of excitation. Damping of panels usually requires much thinner layers of visco-elastic materials that repeatedly deform visco-elastically (or flow with high viscosity) to convert the mechanical energy into heat. The effectiveness of the damping material is less a function of thickness and more a function of the degree and type of deformation the damping material undergoes. This work does not utilize or address acoustic absorption.

Several different methods of damping can be applied to panels: visco-elastic damping applied to the surface; isolation mounting applied to the boundaries and points of attachment; and constrained layer damping applied between two or more layers of material. Each method demonstrates different properties and benefits depending on the application and frequency range of interest. Visco-elastic damping applied to the surface relies on the

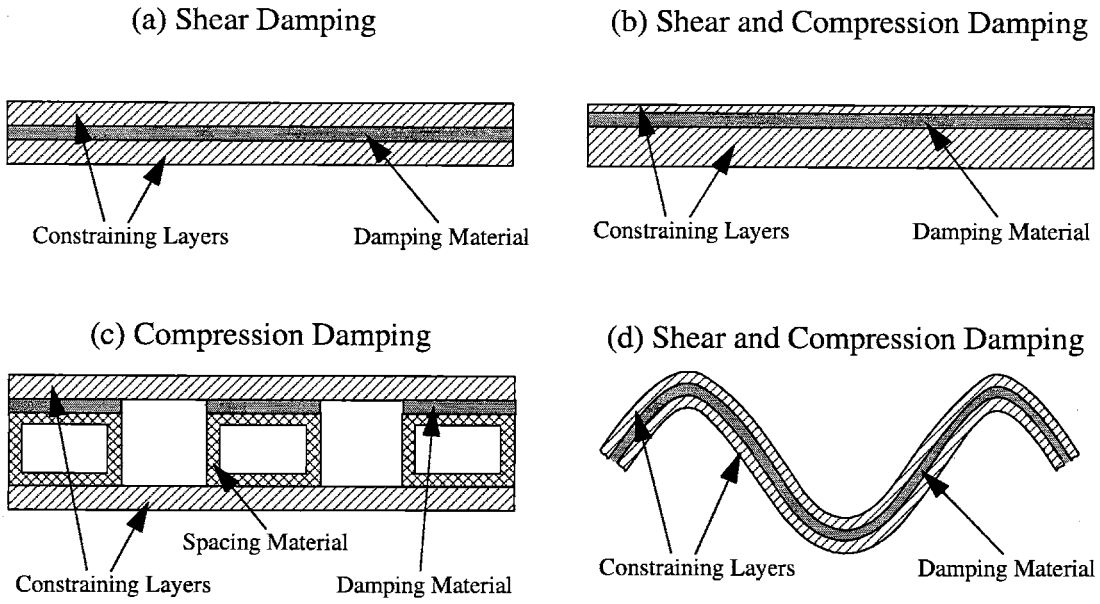

Figure 2.6 Cross-sections illustrating different constrained layer configurations. The cross-section in figure (a) primarily undergoes shearing during deformation; the cross-section in figure (b) undergoes moderate shearing and in-plane tension and compression during deformation; the cross-section in figure (c) undergoes significant in-plane tension and compression during deformation; and the cross-section in figure (d) undergoes various degrees of shearing, in-plane tension and compression, and out-of-plane tension and compression during deformation.

extensional and compressional deformation since it is placed away from the neutral axis. Damping isolation mounts are generally designed to cancel narrow band disturbances, especially rigid body motion. Constrained layer damping can be used in shear, compression, and tension, depending on where it is placed in the structure. For panels the most common approaches are to use surface and constrained layer damping. This work focuses on constrained layer damping due to its versatility, and its proven performance with both flat sheets and ribbed structures [Qian, 1997; Nagai, 1991].

Figure 2.6 demonstrates several possible constrained damping layer configurations. The different configurations utilize different properties of the damping material by subjecting it to different types of stresses and deformation processes. The effectiveness of the damping material configuration will depend on the types of loads and frequency range of interest.

The type of deformation that a panel undergoes has a strong effect on the behavior of the damping material. Although it depends on the viscosity, damping material is often most compliant in shear, and therefore shear damping is more suitably matched to lower frequency bending modes where the stiffness is more suitably impedance matched. In-plane tension and compression of the damping material can cause greater deformation with varied levels of effectiveness on frequencies depending on the material. Out-of-plane tension and compression is generally a less compliant form of deformation and is therefore often better impedance matched to address the higher frequency modes of vibration. The above statements are generalizations whose validity are greatly dependent on the situation and material, but they reasonably characterize the behavior of thin damping layers in thin panels.

Damping only strongly reduces the energy at resonance, or in modes. To understand this better it is useful to know how damping is measured. A damping factor is defined as the ratio of energy dissipated to the total energy in a system for a single cycle,

$$\eta = \frac{W_{dissipated}}{2\pi W_{total}} \tag{2.46}$$

where η is the damping factor and W represents the energy in a cycle. A majority of the energy in a system shows up as an excitation of the modes of the system (at steady state). When energy in the system is being converted to heat by viscous damping, the modal energy is reduced.

Figure 2.7 illustrates a single mode of a transfer function. The damping factor for a particular mode of a system can be determined by

$$\eta = \frac{\zeta_d}{2} = \frac{\omega_2^2 - \omega_1^2}{\omega_r^2} \cong \frac{\omega_2 - \omega_1}{\omega_r} \tag{2.47}$$

where the frequencies are those indicated in Figure 2.7, and ζ_d is the damping ratio seen in most second order systems. Equation 2.47 is useful when determining the damping fac-

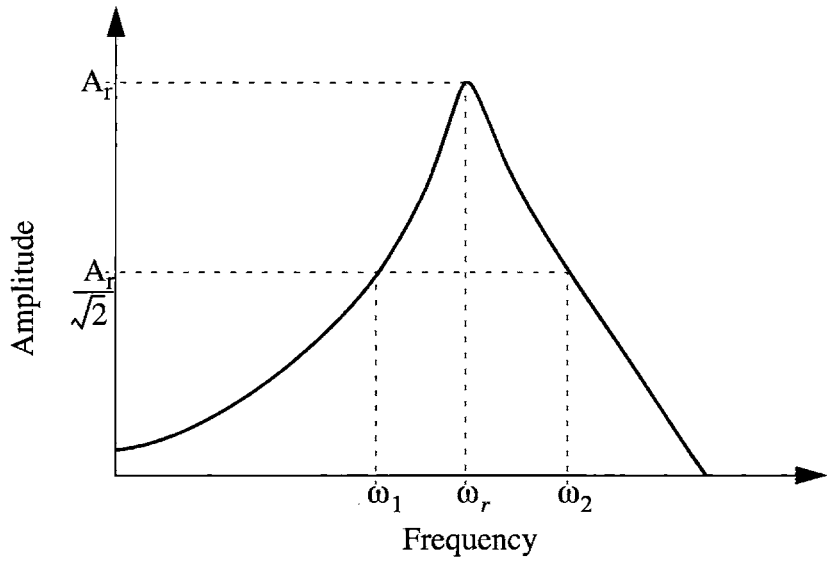

Figure 2.7 Depiction of a mode and the associated parameters that determine the degree of damping.

tors for experimental systems. It should be noted that the damping factor can vary greatly from mode to mode in the same system. This is because one mode will deform in an entirely different manner than another, and depending on the damping properties and the geometry of the system the damping material may be more or less effective based on the deformation.

To gain insight into the variables that affect damping, one can look at a simple model for a constrained damping layer in a beam with a configuration as shown in Figure 2.6a. Through the Navier-Stokes equation and the solution to a simply supported Euler beam, one can arrive at an equation for the damping factor of a beam

$$\eta = \frac{\mu k_b^2 H}{2\rho h \omega_n} \tag{2.48}$$

where μ is the damping material viscosity, k_b is the wavenumber of the beam, H is the thickness of one layer of the beam, ρ is the beam material density, h is the damping material thickness, and ω_n is the natural frequency of the beam. For a simply supported beam the natural frequencies are

$$\omega_n = k_b^2 \sqrt{\frac{EI}{\rho A}} \tag{2.49}$$

where E is Young's modulus, I is the bending inertia, and A is the cross-sectional area of the beam. This leads to

$$\eta = \frac{\sqrt{3}\mu}{h\sqrt{E\rho}}. \tag{2.50}$$

From this it appears that damping, for the configuration shown in Figure 2.6a, is dependent on the damping material's viscosity and thickness, and the beam's material properties. The reader should be reminded that the above is only reasonable for the configuration shown in Figure 2.6a [Marsh, 1994].

As an important final note, it is necessary to realize the effect of damping on acoustics versus vibrations. It was noted above that damping only has a strong affect on the structural modes of a system. As a result, damping is not always an effective means of acoustic noise reduction. Damping can significantly reduce structurally actuated radiation, but it may not have a significant effect on acoustically excited transmission. This is because transmission often occurs due to coincidence which can be an off-resonance form of structural excitation. This fact must be considered when designing and evaluating panel designs.

Chapter 3

DESIGN OF QUASI-ISOTROPIC PANELS USING CURVATURE

Rather than using one-dimensional corrugations or laminated honeycomb designs to alter and improve stiffness properties of panels, it is the goal of this chapter to explore methods of increasing stiffness by using two-dimensionally curved panels. It was proposed in the hypotheses of Chapter 1 that improved performance over one-dimensionally corrugated designs, and comparable performance to that of honeycomb sandwich designs could be achieved by incorporating two-dimensional curvature into panels. In addition, it was asserted that greater damping may be achieved when using a constrained damping layer with the two-dimensionally curved panel designs, over typical flat constrained damping layer designs. This chapter seeks to discuss the design issues of these panels by developing analytical theory, and modeling the systems.

The rationale for trying to alter the stiffness with two-dimensional curvature is four-fold. One, it is desirable to have the ability to change a panel's stiffness properties so that control can be exerted over the structure's static and dynamic behavior. Two, it may be desirable to reduce the critical frequencies near to that of the fundamental frequency such that greater transmission loss may be attained over a narrow frequency range (note, to accomplish this, significant damping must be attained within the structure). Three, increased damping may be attained by combining a constrained damping layer with the two-dimensionally curved design (*i.e.* due to the greater degree of deformation required during bending). Finally, it is desirable from a manufacturing and economic standpoint to be able to

use a single layered design that can be stamped, injection molded, or thermoformed into shape, rather than using multiple layers and materials in a honeycomb sandwich design. It should also be noted that using a two-dimensionally curved design may be an inexpensive alternative to honeycomb when the curved design is used in a sandwich design.

3.1 Altering Stiffness with Two-dimensional Curvature

For several decades it has been accepted that curved panels and shells can demonstrate increased stiffness over flat panels [Hu, 1999; Steyer, 1997; Ng, 1995; Zhang, 1995; Bhimaraddi, 1991]. This knowledge has been used to create many structures with greater stiffness and stability. Aside from spherical designs these designs were generally limited to one-dimensionally curved panels such as cylindrical designs and corrugated or ribbed designs. For structural purposes these designs can be beneficial, but due to their orthotropic bending stiffness the application of these designs is limited. In acoustic applications it can be detrimental to have a highly orthotropic panel design due to the increased frequency range over which one encounters critical frequencies (see Chapter 2). The increased range of critical frequencies can lead to a reduction in transmission loss and thus noisier enclosures and components. In addition, orthotropic corrugated panels rely on specific boundary conditions to ensure their structural functionality. To increase the isotropy of panels and alleviate the dependence on boundary conditions two-dimensionally curved designs are investigated.

In many structural and acoustic applications one would like to attain an isotropic design that exhibits a constant bending stiffness in all directions along the panel. Unfortunately, it is not possible to achieve this over all frequencies due to the fact that at small scales any curvature in a panel will lead to some variation in stiffness. The best one can hope to accomplish is isotropic behavior over the lower order modes, resulting in a narrowly banded range of critical frequencies, where the global bending stiffness properties are maintained within a desired window to maximize stiffness and minimize structural acoustic coupling.

An important obstacle in determining optimal two-dimensional designs is defining metrics by which the designs are evaluated. Since a goal of this chapter's research is to be able to compete with light and stiff sandwich designs, some primary metrics are maximum and minimum stiffness (preferably narrowly banded), weight, and cost. The metrics of weight and cost are relatively easy to determine, but trying to evaluate the isotropy of a two-dimensionally curved panel can be quite complex. Even common geometric definitions that relate to a panel's stiffness can be misleading.

The most common measure of a panel's stiffness, assuming a homogeneous material, is the cross-sectional second moment of inertia for bending,

$$I = \frac{h}{L}\int_0^L \left(z^2 + \frac{h^2}{12}\right) dl \tag{3.1}$$

where h is the thickness (assumed to be nearly constant for this research), L is the length of the cross-section being analyzed, and z describes the surface topography of the panel. Refer to Equation 2.3, Equation 2.8, and Figure 2.1 in Chapter 2 for further details concerning the relation of this term to bending stiffness. With this definition of stiffness one can evaluate various designs. Ideally the value for I should be constant regardless of the length and orientation of the cross-section along L. Equation 3.1 leads us to the conclusion that the goal of the designs should be to move the material away from the neutral axis. Although not directly captured in Equation 3.1, it should be obvious that the distribution of material should be even and uniform above and below the neutral axis.

A primary weakness of the definition in Equation 3.1 is that it assumes that bending occurs along straight lines. This is likely a poor assumption for many two-dimensionally curved designs. Although convenient for flat panels and beams, the typical definition for bending stiffness fails to capture the physical possibility that bending may conform to a panel's shape, minimizing energy during bending. Thus, the bending "line" does not occur along a straight line. Bending waves typically conform around obstacles such that the energy of deformation is minimized. This phenomenon is difficult to characterize and

is not directly addressed by this work. It is left as a responsibility to the designer to be aware of this phenomenon when evaluating designs. Further discussion of this phenomenon occurs in the following sections.

Like many design studies, this research does not assume that a single optimal design exists for all situations or applications. Rather, multiple design approaches may yield several well performing designs. Some designs may perform well in certain applications where others do not. Using this philosophy, several different and promising panel designs were achieved using distinctly different approaches. The approaches can be classified into four separate categories: mathematical or parametric definition; statistical design; computer generated designs; and designs based on experience, iterations, and a human understanding that cannot otherwise be quantified. The following sections discuss these design approaches.

3.2 Parametrically Defined Surfaces

The most logical method by which to define a two-dimensionally curved surface that demonstrates isotropy is through mathematical definition. By developing differential equations that characterize the stiffness regardless of orientation one should be able to determine solutions that satisfy the specified requirements. The difficulty in this approach is that it is highly dependent on the criteria that is used to define the desired characteristics.

As a first approach, formulas were developed to try and determine a surface with constant isotropy, regardless of orientation (maintaining boundaries parallel to the x and y axes), noting that a constant panel thickness and homogeneous material properties are assumed. To do this, parametric definitions of the surface using differential geometry were used.

The class of surfaces that this thesis is concerned with are referred to as *graphs**. A general representation for a panel surface described by $\bar{r}$ is,

$$\bar{r}(u, v) = x(u, v)\hat{i} + y(u, v)\hat{j} + z(u, v)\hat{k} \tag{3.2}$$

where x, y and z are simply the cartesian coordinates; u and v are variables describing mappings of lines or curves on the surface and are functions of the parametric variable t; and $\hat{i}$, $\hat{j}$ and $\hat{k}$ are the unit directional vectors. In the case of a graph, the surface description can be simplified because $x = u$ and $y = v$,

$$\bar{r}(u, v) = u\hat{i} + v\hat{j} + z(u, v)\hat{k}. \tag{3.3}$$

Since our definition for the second moment of inertia in Equation 3.1 is only valid along straight lines, the mappings of u and v must also be straight lines represented by,

$$u = a_1 + tb_1 \tag{3.4}$$

$$v = a_2 + tb_2 \tag{3.5}$$

where a_1 and a_2 convey the distance from the origin to the line, b_1 and b_2 convey the direction of the line, and t represent the parametric variable. In defining the surface or graph we must also consider that the height of the surface must be bounded, *i.e.* $-c \le z \le c$, where c is a preset limit.

Combining the parametric definition for a surface with the desired requirements, a differential equation can be formed that should lead to a class of surfaces that satisfy the predetermined requirements. The first goal is to see if a constant bending inertia can be attained. Combining the surface definition with a generalized formula for the second moment of inertia,

* This means that a line perpendicular to the x-y plane (defined as the plane parallel to the panel) can only intersect the surface once. This restriction is necessary to ensure that the panels can be easily manufactured by thermoforming or stamping.

$$\widehat{I} = \frac{1}{L}\int_0^L g[(a_1 + tb_1), (a_2 + tb_2)]dt \tag{3.6}$$

where $\widehat{I}$ is a generalized representation for the second moment of inertia, and $g = z^2$, which is a function of u and v. To achieve constant stiffness the derivative of Equation 3.6 must be zero for all values of a_1, a_2, b_1 and b_2. Therefore,

$$\frac{d}{dt}\widehat{I} = \frac{\partial}{\partial u}\widehat{I}\frac{\partial u}{\partial t} + \frac{\partial}{\partial v}\widehat{I}\frac{\partial v}{\partial t} = 0 \tag{3.7}$$

or equivalently,

$$0 = \frac{1}{L}\int_0^L \left(\frac{\partial g}{\partial u}\cdot\frac{\partial u}{\partial t} + \frac{\partial g}{\partial v}\cdot\frac{\partial v}{\partial t}\right)dt, \tag{3.8}$$

$$0 = \frac{1}{L}\int_0^L \left(\frac{\partial g}{\partial u}\cdot b_1 + \frac{\partial g}{\partial v}\cdot b_2\right)dt. \tag{3.9}$$

noting that $\frac{\partial u}{\partial t} = b_1$ and $\frac{\partial v}{\partial t} = b_2$. The above is referred to as an integrodifferential equation. Unfortunately, it is only solved when g is zero at all locations (*i.e.* a flat surface)! This can also be arrived at intuitively by realizing that any surface with curvature cannot have identical distribution of material at all scales, especially at scales smaller than the surface features.

To arrive at a non-trivial solution it is necessary to relax some of the constraints on the differential equation. Instead of requiring that the stiffness be constant at all cross-sections over all lengths, it may be more reasonable to require that the stiffness be constant over some fixed length, rather than a variable length. Another approach may be to merely find a surface where the minimum stiffness, in any direction over a certain length, is greater than some prescribed minimum and where a maximum surface height is maintained. In addition, it is also very important to determine a more accurate definition for bending stiffness. Unfortunately, to perform all the above may be considered a thesis unto itself, and

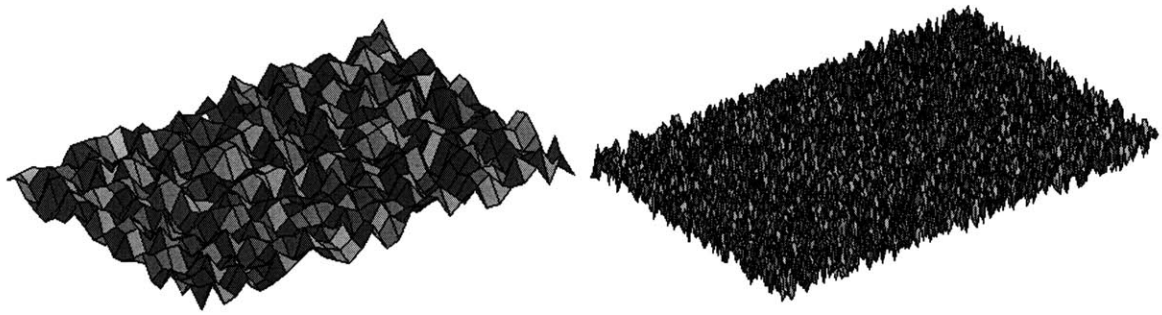

Figure 3.1 An example of a random graph surfaces defined by white noise with banded amplitudes. The two panels illustrate different resolutions that lead to different feature size.

thus further development of this technique is left for future work so that other techniques can explored.

3.3 Statistically Defined Surfaces

A second approach to designing the panels is to use a statistically varied surface. In other words, use some method of random material distribution to ensure a varied and dispersed surface. Over a large surface, randomly distributing the material at an upper and lower extreme should lead to a design that has a nearly constant stiffness in all directions. The key to coming up with designs that demonstrate a useful potential is again recognizing the weakness of the definition for stiffness, and to be aware of the manufacturing restrictions placed on panel shapes.

If the panel were simply defined by a white noise distribution of material (noting that it still must be classifiable as a graph), then it is likely that the surface features would be too small to be able to be manufactured. In addition, this approach to a panel design would not likely demonstrate a great deal of increased stiffness because the bending would merely conform around the random jagged features. Figure 3.1 illustrates two examples of panels defined by white noise. The designs appear crinkled or folded, and the sharp corners are part of the reason that these designs are less desirable, as they lead to stress concentrations, provide paths for bending, and are difficult to manufacture. Another option may be to use load-limited noise to limit the maximum curvature.

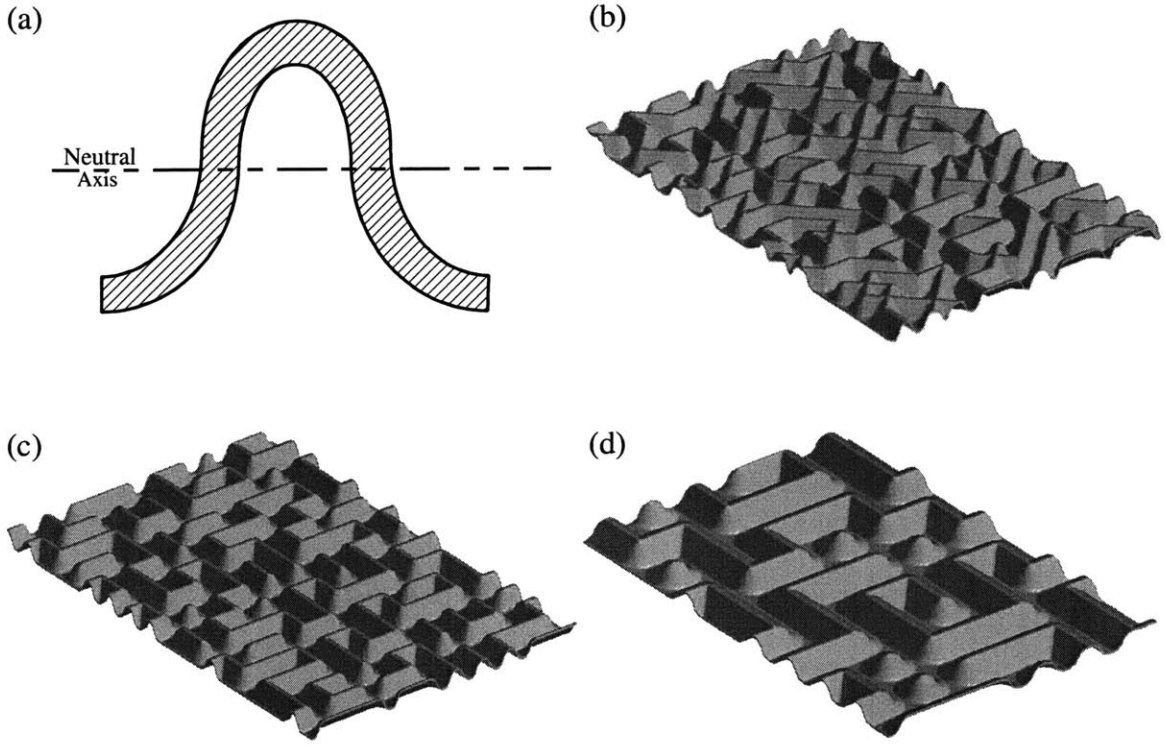

Figure 3.2 Illustrations of various aspects and designs of random maze defined panels. The top left figure depicts the cross-sectional shape of the maze's rib. The other three figures depict different levels of detail and varied numbers of allowed walking directions.

Another method that utilizes a random distribution of material is to dimple the surface at random locations. If rounded dimples are used then the folds and creases encountered in the first random design can be avoided. The problem with a dimpled surface is that the bending can conform around the dimples to some extent, thereby lessening the ability to increase stiffness. In addition, the discrete shape of the dimple can be more difficult to manufacture. In processes like vacuum forming and stamping, a great deal of thinning can occur when forming dimple-like shapes because a great deal of deformation occurs on all sides of the feature.

A third random based design that addresses some of the shortfalls of the previous two is referred to as the maze design. The maze design is based on a random non-intersecting walk pattern. Figure 3.2 shows several illustrations of different panel designs defined by

the random maze and the cross section of the maze's rib. Essentially a stepped rib pattern is formed that has a random distribution of material. Unlike other rib-type patterns, the maze design's ribs intertwine to ensure a more isotropic bending stiffness. The cross-section of the rib is in the shape of a domed dimple that has even distribution above and below the neutral axis. The algorithm that defines the shape also ensures that every portion of the panel is defined by the maze shape. As shown in the figure, the maze rib can be of different sizes, and the number of directions in which the maze is formed can be set to create more complex shapes. The size of the rib and the number of directions indicated is ultimately determined by the application and the manufacturing restrictions. Ideally one would prefer a finely detailed maze as this generally leads to a more isotropic surface, but the more detailed surfaces are difficult to make. This rule is generally applicable to all the two-dimensionally curved designs.

3.4 Computer Generated Designs

A third method of designing two-dimensionally curved panels with isotropic behavior is to use computer-based optimization algorithms. The most important aspect of designing the panels with this method is in setting up the problem. Computer-based algorithms can only produce results as good as the programmer's ability to pose the problem.

Many different variables exist in designing a two-dimensionally curved panel, and it is necessary to give the computer a starting point. Several different approaches were attempted when providing the computer with starting geometries and methods of evaluating the geometry. The three primary approaches were based on: two-dimensional Fourier based shapes, simple tile based designs, and specific geometric design optimization. In addition to providing the computer with a good starting point, the optimization method used must properly account for the desired qualities in a manner that allows for convergence in a reasonable amount of time.

The optimization routine used herein primarily relied upon a least squares method of optimization. Whereby a cost function is defined and minimized. The cost function takes on the following form,

$$C = \sqrt{\sum_{1}^{n} W \cdot \xi_i^2} \tag{3.10}$$

where C represents the cost function, ξ_i is a quantifiable parameter intended to be minimized, W is a weighting factor (the greater value of W the more important the parameter), n is an integer representing the number of parameters to be considered. Setting up the cost function is the most important aspect of the optimization problem. The cost function lets the user define what parameters are important by their relative weightings. In addition, by including, or not including, various parameters different outcomes are possible. Further, one must carefully consider how many parameters and variables to include. Complex optimizations require complex parameters and many variables, but the more complex the optimization the more likely it is that undesirable local minimas will be found, thereby leading to sub-optimal results.

An important aspect of setting up the cost function is determining what parameters are to be included. Since the goal of these designs are to achieve a lower-order bending isotropy it is necessary to include parameters related to the bending stiffness. This becomes extremely complex in the wake of the fact that a two-dimensionally curved panel has an infinite number of cross-sections to evaluate. To define a workable parameter only a limited subset of these cross-sections can be evaluated. The analysis is first limited by the resolution of the matrix defining the surface. A typical resolution for this work varied between 0.1 and 0.01 inches for an 8 by 12 inch panel. This leads to a maximum range of 92,150,400 to 921,599,040,000 as a total possible number of cross-sections to evaluate (not very computationally feasible). As a first cut at simplification only those cross-sections that go from boundary to boundary can be evaluated, thus leading to a range of 159,600 to 15,996,000 possible cross-sections (more computationally feasible). To reduce

this further, the evaluation may be set to skip a certain number of cross-sections, realizing that this may lead to detrimental results. A further level of simplification can be achieved by only looking at those cross-sections that are parallel to the boundaries (these often are important because nodal lines often form parallel to the boundaries). This simplification leads to a possible range of 200 to 2,000 cross-sections to evaluate. It must be pointed out that there are many other reasonable approaches to simplify the cross-sectional analysis; the above are a few of the methods investigated. It should also be noted that with each level of simplification it is more and more unlikely that a global optimum can be attained, but it ensures that the computation can be performed in a single lifetime. Further, the aforementioned problem of not being able to exactly characterize the bending cross-section (*i.e.* merely assuming bending occurs along straight lines) leads to an even greater likelihood that a sub-optimal design will be reached.

Some other parameters that need to be considered may characterize the size of the features, the sharpness of the transitions, and the level of detail. Features that are too small will be difficult to manufacture, while features that are too large may lead to unwanted local compliance and degraded isotropy. The sharpness of feature transitions can also strongly affect the manufacturability of the panel, especially when stamping and thermoforming at sharp corners may lead to stress concentrations and tears. Finally, detailed features in the panel may further hamper the manufacturability of the designs as increased complexity will lead to greater requirements in the manufacturing process.

Another important aspect when defining the cost function is the complexity of the relationship between the variable that can be altered and the parameter included in the cost function. The more complex the parameter, such as some measure of total bending stiffness, the more difficult it is to establish a relationship between the cost and the initial variable. If the initial variable is imbedded in several layers of functions the causality will be more difficult to establish, often leading to suboptimal results.

Two-dimensional Fourier based shapes were the first explored. The computer was provided with a modified two-dimensional Fourier series with a limited number of elements in the series. The variables that the computer could manipulate were the amplitude, wavelength, and phase of each Fourier element. A modified form of the "Fourier" series that allows products between the x and y direction terms can be represented by

$$z = \sum_{0}^{k}\left(\prod_{0}^{n_k}\left(A_{n_k}\cdot\sin\left(\frac{\pi}{T_{n_k}}\cdot x+\phi_{n_k}\right)\right)\cdot\prod_{0}^{m_k}\left(A_{m_k}\cdot\sin\left(\frac{\pi}{T_{m_k}}\cdot y+\phi_{m_k}\right)\right)\right) \tag{3.11}$$

$$x = a\rightarrow b,\ y = c\rightarrow d,\ z = g\rightarrow h,$$

where x, y, z represent the spatial coordinates, A represents the amplitude, T represents the period, ϕ represents the phase, n represents the number of products in the x direction, m represents the number of products in the y direction, and k represents the length of the series. The terms a, b, c, d, g, and h represent the boundaries of the surface or profile in each respective direction.

The idea of using a Fourier based surface came from the realization that any shape can be represented by a Fourier series. The formula allows for a common set of variables (*i.e.* amplitude, wavelength, and phase) in a simple and expandable form that is simple to alter merely by adding or removing elements. Even with this simple starting point many optimization obstacles were encountered. If greater than six elements were included in a series, then convergence errors were encountered. In general, plausible designs were obtained only when fewer than three elements were included. Some of the resulting surfaces are shown in Figure 3.3.

A second optimization approach was to provide the computer with a more definitive shape and allow the computer to alter the scale of various features. The shape used in this design was based on a series of ellipses of which the computer could alter the minor and major radii. The basic shape of the feature was pre-defined but the exact proportions depend on

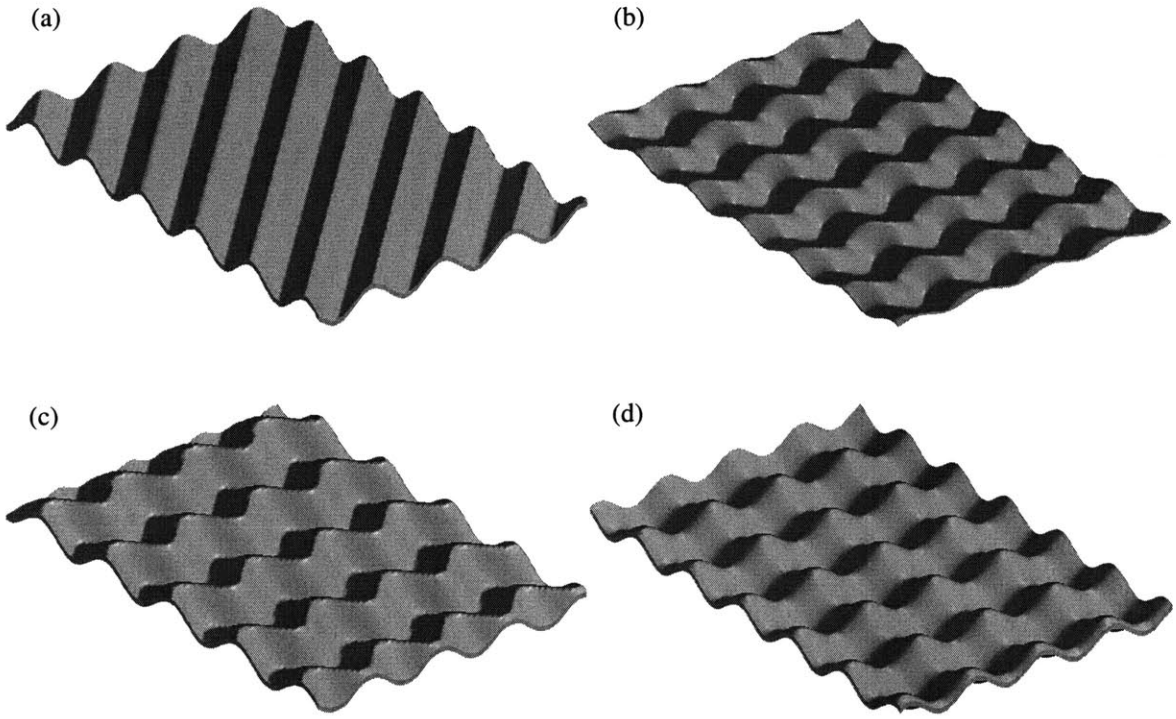

Figure 3.3 Examples of Fourier based optimized designs. Designs (a) and (d) used only the stiffness measurements parallel to the boundaries to arrive at a design, while designs (b) and (c) took into account diagonal bending cross-sections. Note that while the result in design (a) used multiple dimensions in its definition, a one-dimensional surface resulted. The resulting surface appears effective according to the computer algorithm but it is obviously very orthotropic.

the optimization routine. Figure 3.4 illustrates the basic shape of which the surface is made and the configuration of the panel once the shape is repeated on the panel surface.

By altering the major and minor radii of the ellipses, significantly different bending stiffness can be obtained. In addition, the reduced number of variables in the optimization allows for better convergence. The major drawback of this approach is the limitation of the initial design. The initial design essentially pre-defines the basic surface and therefore the optimized version of this design is unlikely to be a global optimum.

The third and final computer optimized design approach uses a tile based approach. The basic approach is to provide a square area that is some fraction of the panel (preferably an order of magnitude smaller than the smallest panel length) defined by a pre-determined

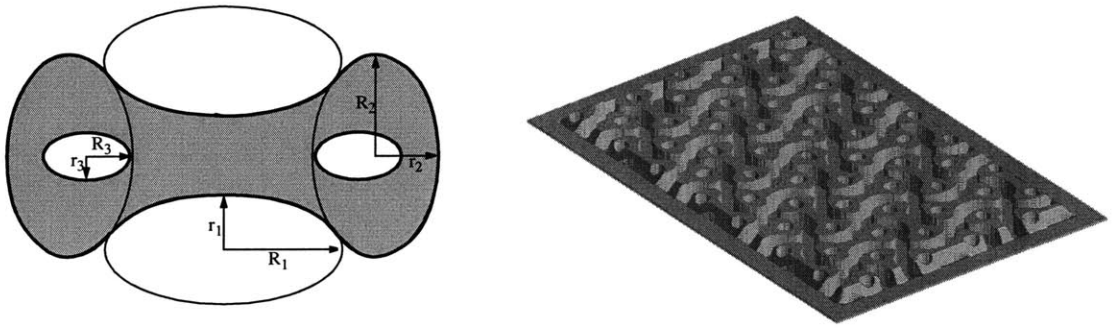

Figure 3.4 Illustration of a panel defined by elliptical arches. The figure on the left illustrates the basic geometry, where the shaded area indicates the raised portion; the small *r* indicates the minor radius and the large *R* indicates the major radius and are the variables of the design. The figure on the right is a panel formed with this basic geometry.

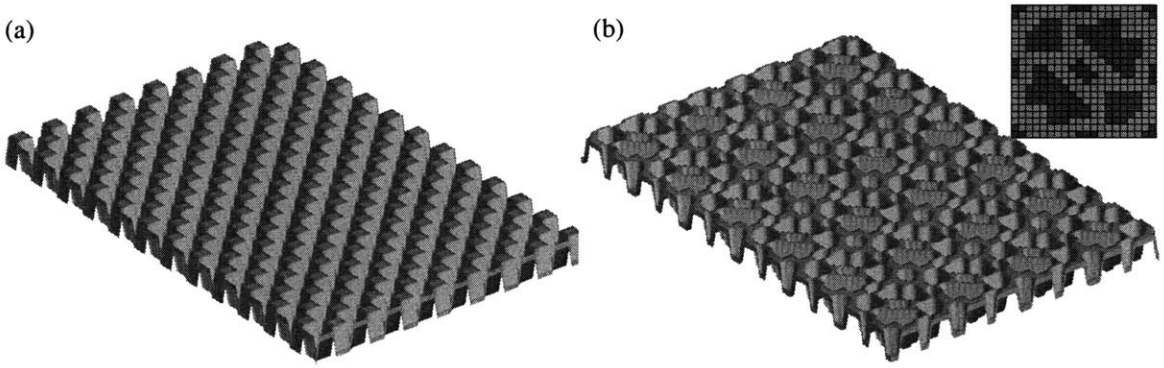

Figure 3.5 Tile optimized panel designs. The panel on the left only accounts for stiffness parallel to the boundaries while the panel on the right accounts for diagonal stiffness as well. The right panel shows the single tile of which the panel is comprised.

resolution of points. The height of each point then becomes the variable that the optimization algorithm can alter. The resulting design is a tiling of the identical squares.

The complexity of the optimization can be controlled both by the size of the square and the resolution of the square. The larger the square and the greater the resolution of points defining the square, the more complex the optimization becomes, and the less likely the algorithm can converge. Some of this complexity can be reduced by limiting the height increments of the points in the tile. The simplest case being when the point is only allowed to be zero or the maximum height. Figure 3.5 illustrates an example of a tile and the associated panel formed from the tile.

3.5 Intelligently Optimized Designs

Unfortunately, the previous designs are based primarily upon algorithms and methods that cannot consider some of the intangible and mathematically undefined characteristics of a panel's design. To account for these types of characteristics the best method is often to utilize the human ability to design and recognize these often unquantifiable intangibles. The previously discussed methods provide a starting point on which to build new intelligently optimized designs.

The analysis results may indicate a stiff, quasi-isotropic design, but experimentally it may fail because the mathematical analysis fails to capture some important aspect of the structure. Experience and understanding of the difficult to quantify issues are essential when developing a quasi-isotropic panel design. Some of the issues that must be considered include the fact that bending does not always occur along straight lines, the manufacturability of the design, the aesthetics or appeal, and other limitations of the mathematical parameters.

As mentioned before, it is important to realize that bending in a two-dimensionally curved panel is unlikely to follow the straight cross-sections usually assumed in bending stiffness analysis. Armed with this knowledge a designer can qualitatively analyze designs to determine how easily bending can conform around various panel features and then make modifications to improve the design. In doing this it is often helpful to look at contour plots of the panels to determine how much a bending line must conform as it propagates through a panel. Figure 3.6 depicts some of the earlier discussed designs as contour plots. The designer can build on these previous designs, making modifications to improve them without dramatically altering the design.

A second consideration that a designer must make is the manufacturability of the design. This includes issues such as the sharpness of transitions, the size and detail of the features, and the repeatability of the shape. Transitions that are too sharp are likely to lead to stress concentrations and tears. Features that are too small or detailed are more difficult to man-

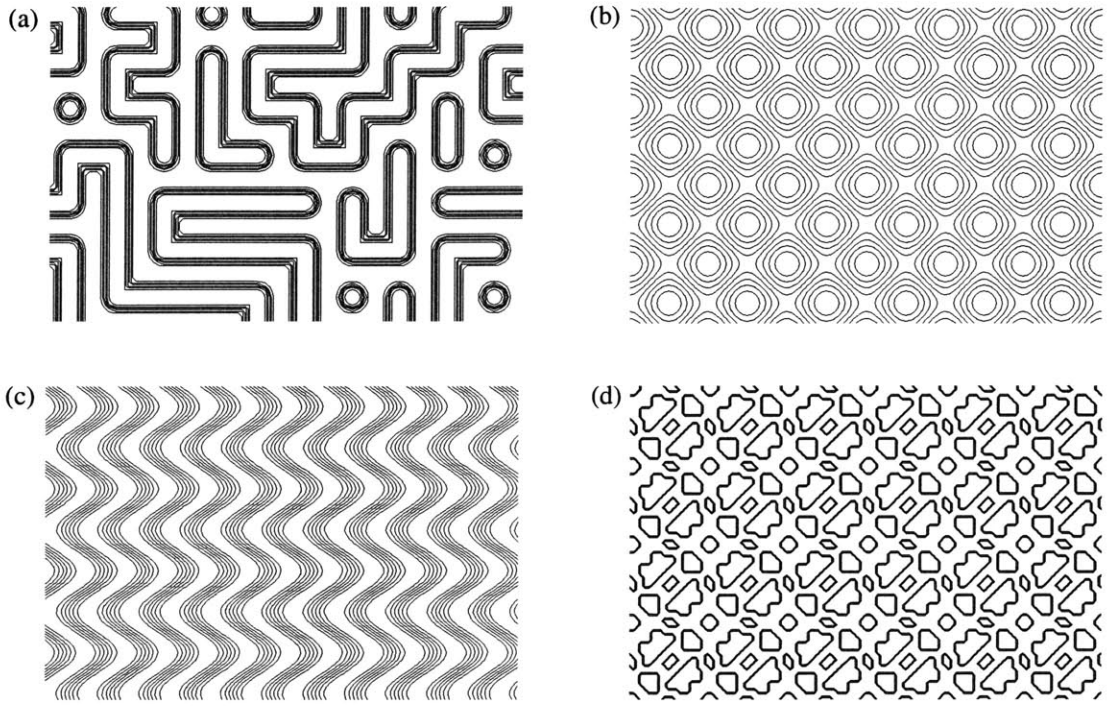

Figure 3.6 Illustrations of some of the previous designs depicted by contour plots. Long continuous straight lines (or blank areas) indicate weak bending areas. Closely spaced lines indicate steep transitions.

ufacture with standard manufacturing processes. Finally, it is often beneficial to use shapes that are repeatable. Repeatable shapes that can be tiled or stacked are desirable so that panels of different sizes can be manufactured without creating entirely new tooling. For repeatability, the tile and Fourier based designs are generally more desirable than the statistically based maze designs (although it should be noted that it is possible to modify a maze design to make it repeatable).

In recognizing these and other limitations of the mathematical parameters estimating the performance of the panels the designer can modify the designs and come up with entirely new designs that show improved characteristics. One design method that was pursued was based on the two-dimensionally curved ribbed design based on a combination of the maze and Fourier approach. It was recognized that two-dimensionally curved rib-like structures could possibly lead to lower-order isotropic designs. One manner in which to

create these two-dimensionally ribbed patterns is by imbedding the two-dimensionally curved shape within a sinusoid as follows

$$z = \sin(fn(x, y)) \tag{3.12}$$

where the function of x and y essentially contains a formula for a shape. If one wanted to create concentric circular ribs then the panel surface would be defined by

$$z = A \cdot \sin((x - c_x)^2 + (y - c_y)^2 - r^2) \tag{3.13}$$

where A is the amplitude of the ribs, r represents the radius of the initial repeated circle, and c_x and c_y determine where the center of the concentric circles lie. An illustration of a panel with this shape is shown in Figure 3.7a. The concentric circle design does very little to stiffen the first mode of vibration because the bending lines during the first mode are often nearly circular. To address this one can add sinusoidal variations in the azimuthal direction to create a sort of flower petal design. Mathematically this shape is represented by

$$z = A \cdot \sin\left\{(x - c_x)^2 + (y - c_y)^2 - \left(\sin\left(n_l \cdot \operatorname{atan}\left(\frac{(y - c_y)^2}{(x - c_x)^2}\right)\right)\right)^2 - 2r \cdot \sin\left(\left(n_l \cdot \operatorname{atan}\left(\frac{(y - c_y)^2}{(x - c_x)^2}\right)\right) - r^2\right)\right\} \tag{3.14}$$

where n_l represents the number of lobes or petals in the flower shape. An example of this type of panel is illustrated in Figure 3.7b. Although this panel eliminates the circular bending lines of the previous design, there still exists several areas where the design exhibits bending compliance, especially near the corners and edges. In addition, this shape is quite complex and would likely be difficult to manufacture.

Another approach is to use more exaggerated "zig-zag" patterns like those created with the Fourier based approach. A zig-zag design can be defined by

$$z = A_z \cdot \sin\left(y - \left(A_z \cdot \sin\left(\frac{\pi}{T_z} \cdot x\right)\right)\right) \tag{3.15}$$

where A_z is the amplitude of the sinusoidal zig-zag pattern in the x-y plane, and T_z is the wavelength of the zig-zag design. The effectiveness of this design is based primarily on the ratio of the amplitude, A_z, to the wavelength, T_z. The quality of being highly repeatable is also very desirable as this leads to greater manufacturability. Unfortunately, the repeatability of the zig-zag shape also seems to limit its effectiveness as an isotropic shape. The repeated troughs and valleys line up along diagonals and lead to much more compliant regions.

To address the above problem another design was developed. The design used the basic premise of the zig-zag design with periodically altering amplitudes and an offset progression. It is described by

$$z = A_z \cdot \sin\left\{\Lambda_x \cdot \sin\left(\frac{\pi}{T_x} \cdot x\right) - \lambda_y y - \Lambda_y \cdot \sin\left(\frac{\pi}{T_y} \cdot y\right) - \lambda_x x\right\} \tag{3.16}$$

where A_z again relates the height of the panel, and the other variables are various weightings controlling the relative lengths and amplitudes of the alternating zig-zag pattern. The altering amplitudes ensure that the peaks and troughs do not line up and thus should lead to a more isotropic design than the simple zig-zag design. This design is illustrated in Figure 3.7c.

Several other design methods were explored that tried to utilize old and new geometric knowledge. One design included Penrose based tiling patterns. Another investigated fractal based designs. A third sought to combine repeated geometric patterns that intertwined in an almost "Escheresque" manner. There are as many possibilities as there are shapes in the world. Due to the difficulty of analytically and numerically defining a "good" design ("good" here meaning stiff and quasi-isotropic) it is difficult to determine which designs will turn out to be superior. The fact that the problem is non-deterministic

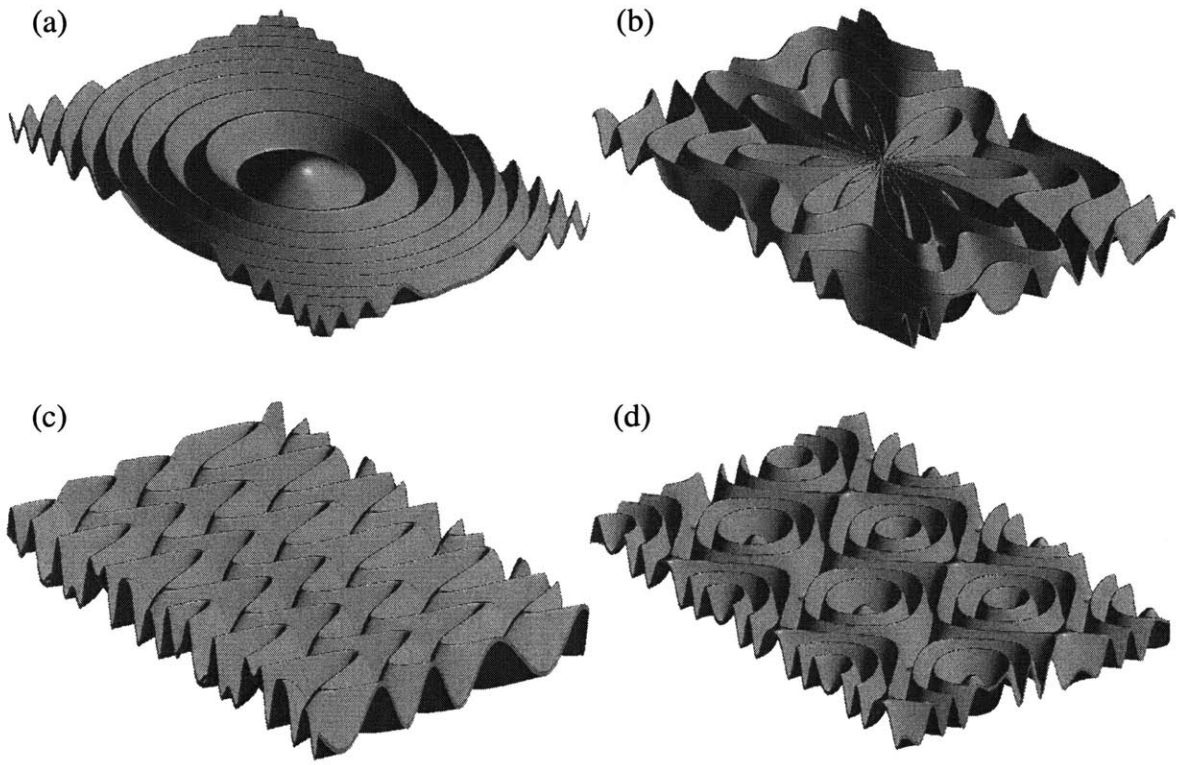

Figure 3.7 Illustrations of manually designed panels that use two-dimensional sinusoidal rib patterns.

makes it both an ideal and difficult design problem. All that can be done is to use a designer's instinct combined with crude analysis tools.

3.6 Comparative Analysis of Designs

Some of the previously discussed methods can be used to analyze basic properties of the designs. Estimates of the cross-sectional bending stiffness can be calculated along various directions. Additionally, the natural frequencies of the panel can also be estimated by using the estimated bending stiffness. To further estimate the behavior of the different panel designs, some of the less complex shapes can be analyzed using finite element analysis.

Although most of the results are presented in a dimensionless manner it is important to note that the boundary conditions for these initial analyses are clamped on all sides (noting

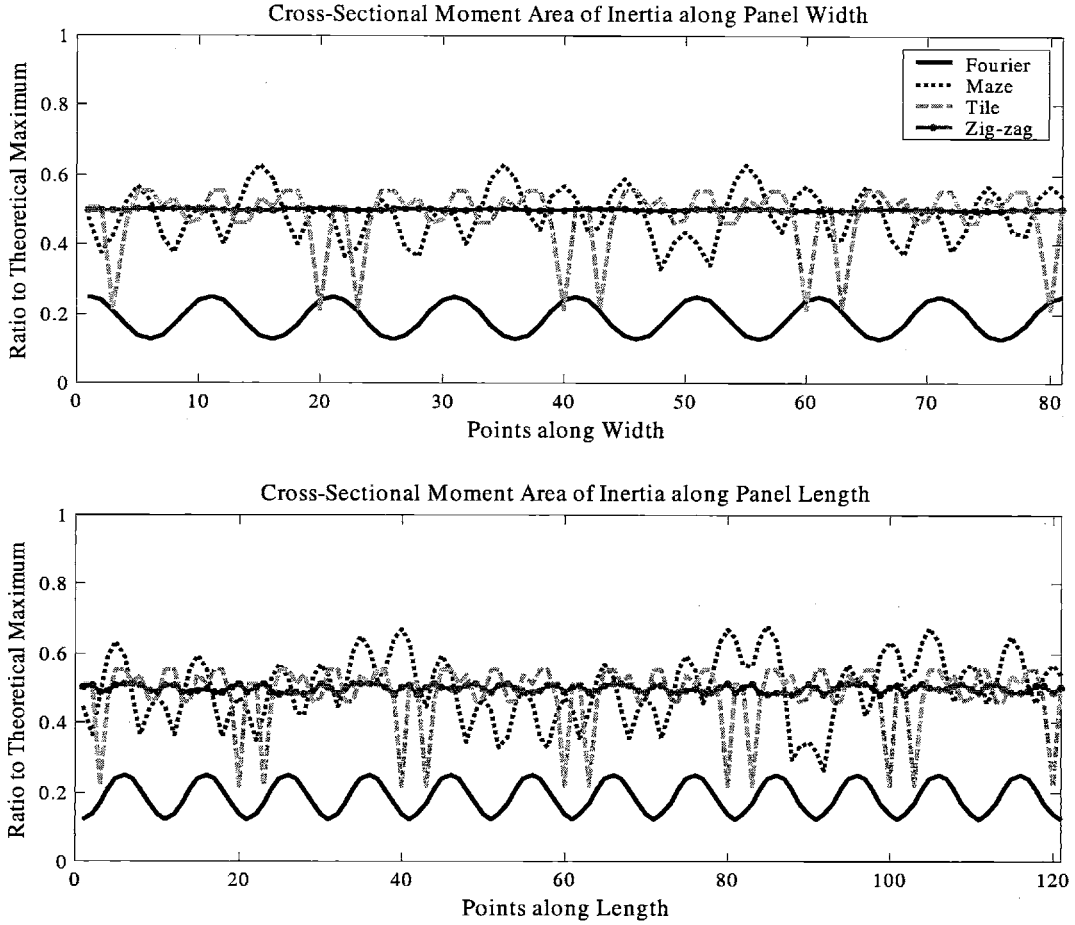

Figure 3.8 Estimated cross-sectional bending stiffness, parallel to panel boundaries, of several panel designs. Each point along the *horizontal* axis represents the cross-sectional bending stiffness, as defined in Equation 3.1, for a point along the respective panel axis. The *vertical* axis values are normalized by the theoretical maximum. The Fourier design is shown in Figure 3.3b; the Maze design is shown in Figure 3.2c; the Tile design is shown in Figure 3.5b; and the Zig-zag design is shown in Figure 3.7c.

that a clamped panel will have increased stiffness, and that most machine enclosures have boundary conditions that lie somewhere between a clamped and simple support). In general, frequencies are normalized by the fundamental (first natural) frequency results of a flat panel with the equivalent thickness, size, material, and boundary conditions.

As a first comparison the cross-sectional bending stiffness can be analyzed at all cross-sections parallel to the boundaries. This will provide a comparative first look at the stiffness along the cross-sections that are often most critical for rectangular panels (as nodal lines generally form parallel to the boundaries). Figure 3.8 shows a comparison of several

of the previously discussed panel designs. In general these values over estimate the stiffness because they do not take into account the true bending path and they do not consider non-parallel cross-sections.

To account for the bending stiffness along non-parallel cross-sections one can look at the bending stiffness of a much broader array of cross-sections. One method is to look at cross-sections extending from every boundary point to every other boundary point. The result is an array of points that form a surface describing a global estimate of the bending stiffness. A desirable result would be a nearly flat surface (small standard deviation) with a large average value. Figure 3.9 shows several stiffness surfaces for different panel designs.

From the above plots it appears that the Maze design provides the greatest overall average stiffness, while the Zig-zag design provides a more uniform and isotropic design. It should also be noted that a correction factor was included in the tile design such that rounding at the corners was assumed for manufacturing purposes. This leads to a greater reduction in the stiffness than would otherwise be obtained by the exact design in Figure 3.5b, with the extreme transitions and sharp corners.

Since the above are merely analytical estimates based on straight cross-sections, it is likely that there is a significant amount of error in the results. To try and account for some of this error one can take the analysis a step further and perform finite element analysis. This will lead to more accurate estimates of the designs' stiffness, and more importantly can provide some insight into the mode shapes. In addition, the finite element analysis can be used as a comparison to the analytical results and provide some information about the effect of altering amplitude of the panel features. Unfortunately, the complexity of many of these shapes makes it extremely difficult to represent them in a drafted form, and even more difficult to be able to represent them in a form that allows for finite element analysis. As a result only limited designs can be analyzed with finite element analysis, but the designs that can be analyzed provide insight into how well the simple analytic estimates

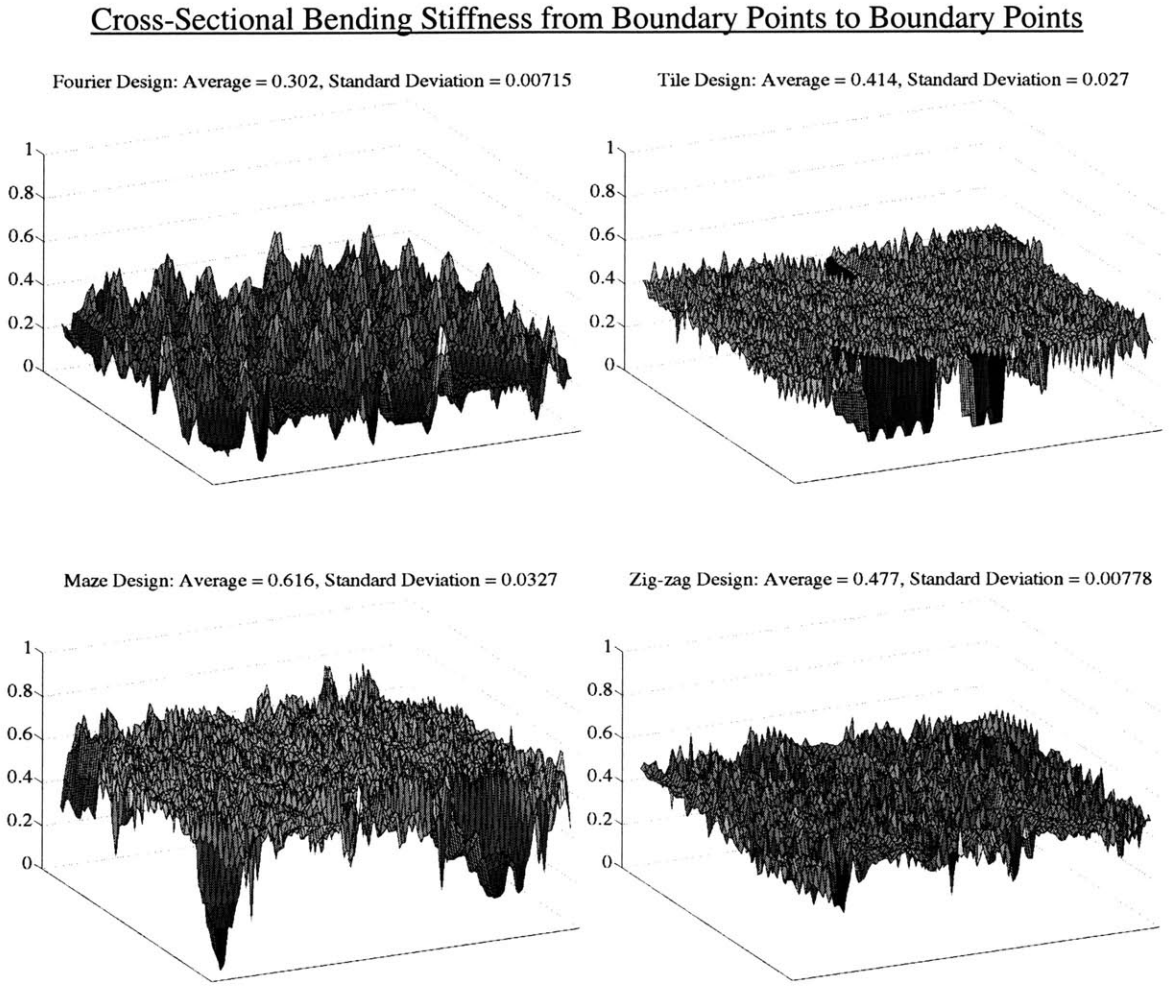

Figure 3.9 Plots of two-dimensional arrays describing the bending stiffness of several panel designs. Each point in the array describes the bending stiffness along a line from one point on the panel boundary to another point on the boundary. The values are normalized by the theoretical maximum. Once again, the Fourier design is shown in Figure 3.3b; the Maze design is shown in Figure 3.2c; the Tile design is shown in Figure 3.5b; and the Zig-zag design is shown in Figure 3.7c.

work and can provide information about how amplitude of the design affects performance. Further discussion of this is provided in Chapter 5.

Two of the designs that were analyzed with the finite element analysis are the "Simple Fourier" design and the "Course Maze" design. The finite element analysis assumed constant thickness and used shell elements (the assumption of constant thickness is not very realistic for vacuum formed and stamped designs, but provides insight into the general behavior of the design). Some of the resulting mode shapes and associated natural fre-

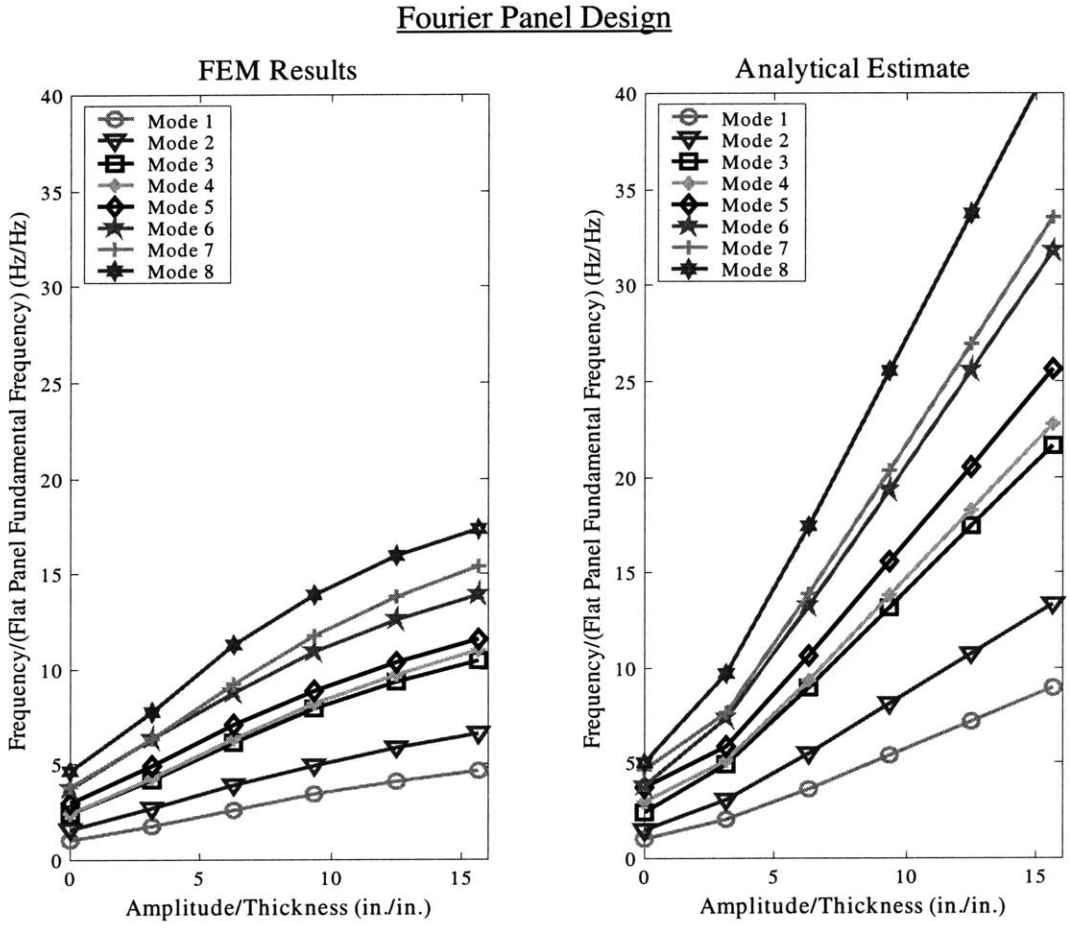

Figure 3.10 Plots of first natural frequency versus amplitude the indicating the effect of increased amplitude. Results are presented for both analytical and finite element analysis.

quencies are depicted in Appendix A. From these results it is clear that some lower-order isotropy exists because the first few mode shapes have the same basic shape as a flat panel. A truly isotropic design should have the same mode shapes as an isotropic panel. It can be inferred that the designs that indicated better performance in the analytic analysis should also demonstrate better modal performance.

Another use of the finite element analysis is to study how the amplitude of the curvature may effect the designs' behavior. By altering the amplitude in successive finite element runs, the effect on stiffness can be estimated, and a relationship can be established between amplitude and stiffness for a particular design. This can then be compared to the trend indicated by the analytic analysis, as is shown in Figure 3.10. The analytical esti-

mate is based upon Equations 2.8, and 2.13, where the bending stiffness was assumed to be the minimums given by cross-sections parallel to the boundaries (see Figure 3.8). As expected the analytic results overestimate the natural frequencies. It should be noted that if the amplitude becomes too great then lateral movement of the features will dominate the dynamics and the natural frequencies may decrease with increasing amplitude.

3.7 Multi-layered Panel Designs

Rather than using the panels as a single layer, alternative designs can be accomplished by attaching flat members to the raised surfaces of the two-dimensionally curved panels. These multi-layered designs will have greater rigidity and may prove to be an inexpensive alternative to honeycomb designs. The advantage of the two-dimensionally curved designs to honeycomb is that they can be manufactured for far less cost. The manufacturing methods of rolling, stamping, vacuum forming, and injection molding can all be used to manufacture two-dimensional panels at significantly smaller variable cost than the typical extrusion methods used for honeycomb designs.

The primary requirements of the two-dimensionally curved portion of the multi-layer design are to maintain a nearly constant overall thickness, minimize shear, and to maintain some degree of isotropy. The single layer designs discussed above should provide the necessary qualities. In fact, some of the issues, such as bending conforming around curved features, should be less of an issue because the multi-layer design should help to maintain the neutral axis at the center of the system.

Unfortunately, these designs are far too complex to model analytically, or even numerically. Therefore, analysis of these designs are performed experimentally and the results are presented in Chapter 6. Both static and some dynamic results are presented with comparisons to honeycomb designs.

If successful, these inexpensive alternatives to honeycomb and other multi-layered designs could prove to be a powerful advance for many structures (aircraft, space vehicles,

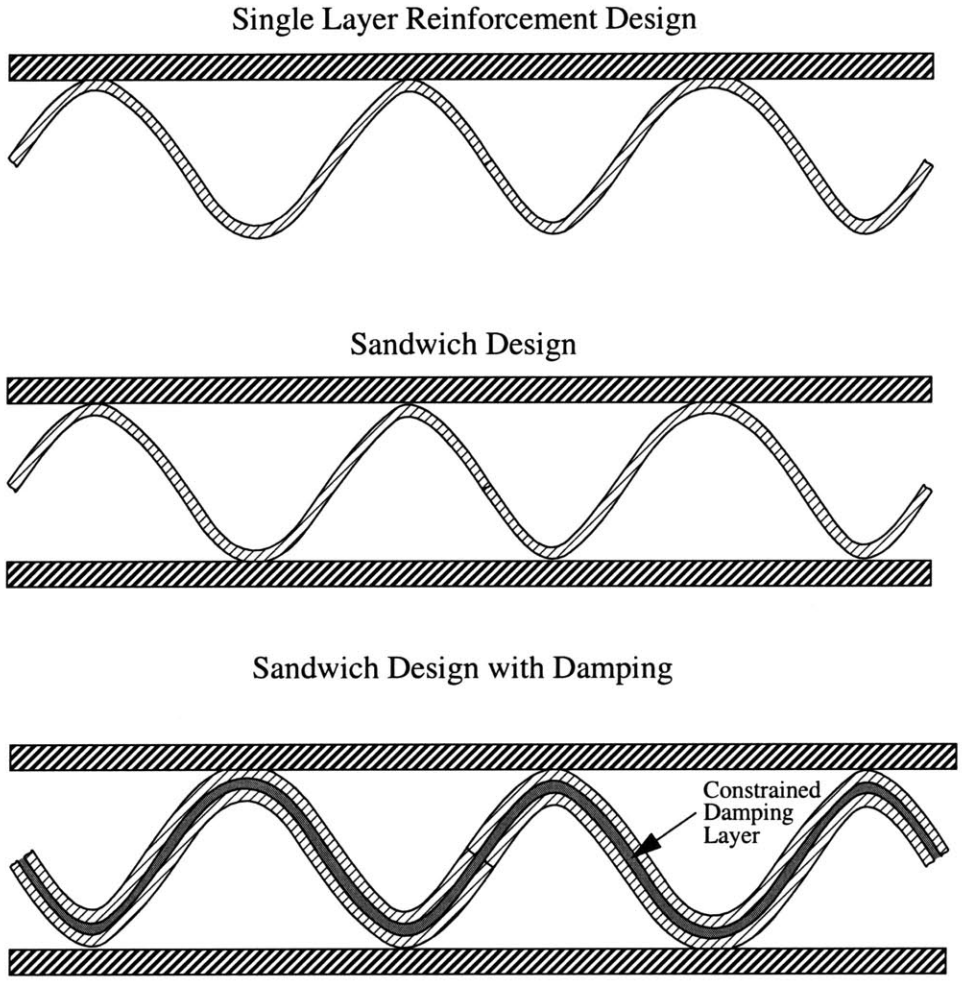

Figure 3.11 Three different configurations for multi-layer designs with two-dimensional curvature.

even cardboard) that require light but stiff components. Figure 3.11 illustrates some possible configurations.

3.8 Damping and Two-dimensional Curvature

Another important aspect of the two-dimensionally curved pseudo-isotropic designs is their behavior when they are used in conjunction with constrained damping layers. Constrained damping has been shown to be very effective for controlling vibration [Hale, 1994; Marsh, 1994]. It is believed that when the constrained damping layer is combined with these curved panels greater damping can be achieved.

The rationale for increased damping with curved surfaces is two-fold. One, some of the damping material is moved away from the neutral axis where it will undergo greater extensional and compressional deformation. If the majority of this deformation is in the plane of the damping material, then a greater degree of deformation, may occur than if the material is in shear at the neutral axis. Two, the curvature of the surface will lead to multi-directional deformation. Again, the multi-directional flow or deformation may lead to greater damping.

One possible drawback of the curved surface is out-of-plane deformation in the constrained damping layer. The effectiveness of the damping layer is likely to be less when deformed in the out-of-plane direction. Near the neutral axis during bending, the curvature may cause the constraining layers to move in opposite directions normal to their surface causing a transverse compression or extension of the damping layer. A simple illustration of this concept is depicted in Figure 3.12. This type of deformation may inhibit the damping performance. Several different types of damping material configurations may be required to determine an ideal design.

Due to the complexity of the dynamics of the curved surfaces combined with the constrained damping layer, relevant models are difficult to develop. Instead, this phenomenon is studied only through experimental analysis and will be discussed further in Chapter 6 and Chapter 7.

3.9 Summary

Several design approaches were introduced to create two-dimensionally curved, quasi-isotropic panels. Simple analytic and numerical tools were used to analyze and compare the resulting designs. Several key issues such as multi-layered designs, damped designs, and dynamic behavior were also addressed. Although some important issues were raised and some significant design criteria were established, a great deal of knowledge remains undiscovered concerning two-dimensionally curved designs and their dynamic and static behavior. Significant academic effort in dynamics, mathematics and physics will be

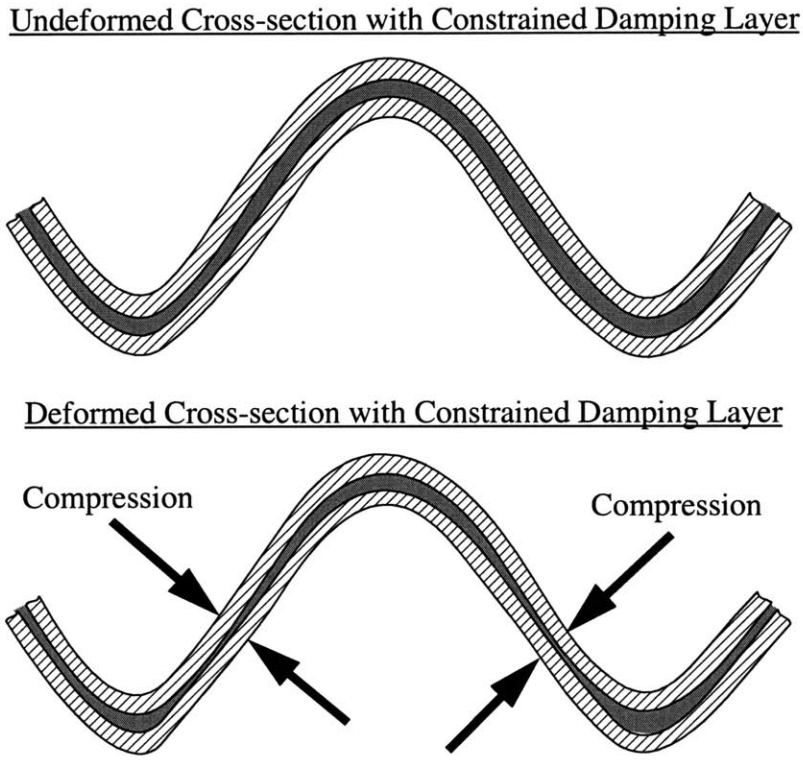

Figure 3.12 Illustration of possible transverse compression that may occur in the constrained damping layer, which may inhibit damping at lower frequencies.

required to establish more effective means of designing and analyzing two-dimensionally curved panels with near isotropic behavior.

The next step in this area of the work is to examine some of the designs further with experimental analysis. Since it is prohibitive to examine a great number of designs, only a few are to be examined with the hopes of learning more about the behavior of these two-dimensionally curved panels. Due to the results of the numerical analysis it was determined that designs that can provide the greatest insight into the behavior of quasi-isotropic shapes were the Fourier design in Figure 3.3b, the Maze design in Figure 3.2d, and the Zig-zag design in Figure 3.7c. These designs represent designs with both subtle and extreme curvature and each has various degrees of repeatability. In addition, the designs represent a broad spectrum of predicted performance. These designs are experimentally

examined in Chapter 6. Their static and dynamic behavior is investigated, as well as their performance when combined with constrained damping layers and multi-layer designs.

Chapter 4

DESIGN OF MODE-SHAPED PANELS

As was discussed in Chapter 2, the shape of the modes of vibration have a significant effect on the vibration and radiation characteristics of panels. Some modes are more detrimental than others. For many vibration problems, the first few modes of a panel tend to be the most detrimental because of their large displacements and shape. This is often why vibration problems are addressed with stiffening members. Acoustically, the first odd modes also tend to be the most undesirable because of their ability to radiate noise. It would be of great benefit if panels could be designed to have greater stiffness *and* the resulting mode shapes be less affective at radiating acoustic noise. Unfortunately, however, current methods of stiffening result in reduced vibration, but increased audible acoustic noise [VanBuskirk, 1993].

4.1 Rationale for Mode-shaped Panels

The approach used here to increase stiffness and minimize unwanted acoustic noise is quite simple; design the panel such that it has the geometry of the most undesired mode. If the amplitude of the modal design is great enough then that mode shape should not appear in the lower frequency modal dynamics because the mode shape can only occur due to nearly pure stretching, which requires greater energy for plate like structures. This is not to say that it is impossible for a similar mode shape to appear, but since the deformation

would be primarily due to stretching, it would occur at a much higher frequency and with smaller displacement and velocity amplitudes.

The resulting panel design should have greater stiffness because it will posses the properties of a doubly curved shell. Shells have been shown to demonstrate much greater stiffness, especially at lower frequencies, because of the coupling between transverse and longitudinal displacements. Increased stiffness is primarily due to the shell's ability to support a greater portion of the load parallel to the surface, rather than in the transverse direction [Blevins, 1995; Dym, 1974; Gol'Denveizer, 1961]. In addition, the resulting mode shapes are less likely to demonstrate the unwanted mode shape in which the panel is formed, thus leading to a stiffer *and* quieter panel. Further, the subtle curvature of the panel design should not lower the critical frequency of the panel. At the higher frequencies where the critical frequency is encountered the bending deformation wavelengths that coincide with the acoustic waves are small enough that the strain energy of the mode shapes are dominated by bending deformation, and strains due to stretching is less significant.

The use of a mode-shaped design cannot guarantee that the resulting mode shapes are significantly less detrimental or less efficient at radiating noise. The design can only reduce the likelihood of one particular mode shape from occurring. Fortunately, the fundamental mode of a flat panel often dominates both the structural and acoustic performance of a panel, making it the predominant shape in which to form the panels. The resulting mode shapes of this mode-shaped panel should not resemble the modes of a flat panel, at least the lower-order modes. The design goal is to ensure that the resulting lower order modes resemble even modes more than odd modes, and to increase the fundamental frequency (indicating an increase in stiffness).

An important point is that there is a minimum amplitude of the shape of the panel that must be obtained for the design to function properly. The mode-shaped design must have an amplitude that is much greater, preferably an order of magnitude, than the elastic bend-

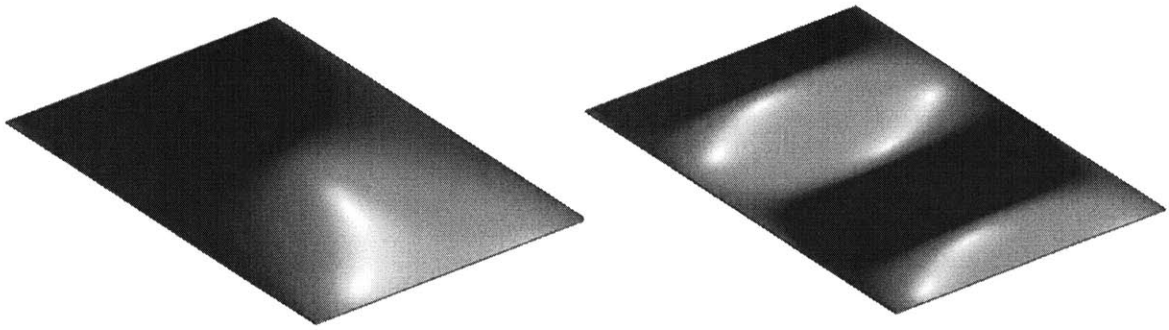

Figure 4.1 Illustrations of two mode-shaped panels assuming simply supported boundary conditions. The fundamental mode is on the left and the next lowest odd mode shape is on the right.

ing range of a flat panel deforming in that shape*. Otherwise the panel may still bend in that shape and the dynamics will not be greatly affected. The reason for this is discussed in greater detail in the next section. Figure 4.1 depicts two mode-shaped panels.

4.2 Mechanics of Curved Structures

To understand the rationale behind the above assertions it is helpful to look at the mechanics of several thin curved systems. First, thin beams are discussed and analyzed to demonstrate how curvature and mode-shaped designs affect the mechanics of the system. Next, two-dimensionally curved (*i.e.* doubly curved) panels are discussed and analyzed.

4.2.1 Curved Beams

Since, many approximate solutions for differential equations describing panels are based on the solutions of beam equations, it is useful to first discuss the dynamics of curved beams. The study of beams not only provides insight into the mechanics of panels, but it also allows for a more complete analysis due to the relative simplicity of the beam equations compared to that of panel equations.

* A comparable metric for most materials would be to say that the amplitude of the shape must be an order of magnitude greater than the thickness of the panel.

The most commonly analyzed curved beams are those with circular curvature (also referred to as circular arcs). Although circular curvature does not accurately describe the geometry of a mode-shaped design, it is similar and provides a useful starting point for the discussion. It is noted that the thickness of these beams is assumed to be much smaller than the radius of curvature of the arc so that shear deformation and rotary inertia can be neglected (a valid assumption for all the systems in this chapter). Further, the beams are assumed to be of rectangular cross-section, essentially a slice of a shell, so that the flexural and torsional dynamics are not internally coupled. Also, only longitudinal and in-plane flexural vibrations are considered (as out of plane flexural vibrations are not a relevant factor in panels).

The two primary classifications of interest here for the modal dynamics of circular arcs are longitudinal modes and in-plane flexural modes. Longitudinal modes are those where the primary deflections are due to extension and/or compression of the beam along the axis of the beam. Flexural modes are dominated by the transverse displacement of the beam. It has been shown that longitudinal modes have much higher natural frequencies than flexural modes for the circular arcs discussed [Blevins, 1995]. This fact is critical to the design of mode-shaped panels. The curvature of the arc couples the bending and longitudinal modes such that the first in-plane flexural mode is influenced considerably. If the boundaries of the arc are fixed (*e.g.* pinned or clamped), then the beam cannot support the first in-plane flexural mode. Further, lower order odd mode shapes are strongly affected by the curvature due to the fixed boundaries, while even mode shapes can form in the presence of fixed boundaries [Blevins, 1995]. This phenomenon has important acoustic ramifications. It can be inferred that the odd shaped modes will be shifted to significantly higher frequencies due to the greater degree of longitudinal coupling that must occur. This shifting of the odd modes to significantly higher frequencies is likely to lead to a reduction of the radiation index over the frequency range of interest, although material and geometric parameters must be considered for each case.

It is possible to delve deeper into the specific dynamics of a mode shaped beam, one can adapt and analyze the non-linear coupled equations for a beam where longitudinal and flexural deflections are considered. In addition, one-dimensional shell equations can also be used to analyze the dynamics of mode-shaped beams. These developments are left for later work as the purpose here is to explore several aspects of the design rather than focussing on a single related phenomenon.

4.2.2 Discussion of Shells and Stiffness

By plastically deforming a flat panel into one of its mode shapes, one creates a curved shell. If the boundaries are fixed (either pinned, clamped or somewhere in between), then the resulting shape is a doubly curved shell, similar to those shown in Figure 4.1. A significant amount of research has been devoted to the study of doubly curved shells because of their structural properties. They tend to have high rigidity-to-weight ratios and thus are ideal for many vehicle applications [Hu, 1999; Steyer, 1997; Chun, 1995; Zhang, 1995].

The detailed development of shell theory is beyond the scope of this work. It is a mathematically complex field that has occupied a great deal of effort on the part mathematicians, physicists and engineers. Even in its most complete form, the field can only weakly characterize the dynamic phenomenon of some of the designs contained in this thesis. To that end the details of shell theory are not included in this work and the reader is referred to the literature [Liew, 1996; Bhimaraddi, 1991; Dym, 1974; Leissa, 1973; Gol'Denveizer, 1961]. This section merely illustrates some of the beneficial results that can be realized by shell and mode-shaped designs.

As one of the goals of this work is to increase stiffness to reduce vibration, it is important to recognize how this can be accomplished with shell and mode-shaped designs. A result of having a mode-shaped panel is that it ensures an increase in stiffness due to the shifting of deformation from flexural bending to longitudinal extension and/or compression deformation (as was described in the previous section on beams). In fact, shells cannot support bending deformation alone, unlike flat panels. The shift from bending to stretching leads

to an increase in transverse stiffness because the compression or tension of a thin object requires greater energy than bending [Blevins, 1995; Dym, 1974].

A simple example of the above phenomenon is apparent in structural arches. The arched doorway is able to support greater loads because the forces are supported primarily in compression, where the stiffness can be approximated by $k_c \cong \frac{EA}{L}$. A flat-topped doorway can support less of a force because the load is supported in bending, where the stiffness (at the center) can be approximated by $k_b \cong \frac{384EI}{5L^3}$. For most situations where the length to thickness ratio is great, the stiffness of the arch is much greater.

Looking more specifically at panel and shell structures, it is possible to make a comparison between the natural frequencies of a panel in bending and a panel in pure stretching. As was discussed previously, to have a mode-shaped panel deform further into the mode shape in which it is designed, it must primarily deform in stretching (assuming fixed boundaries and a panel shape amplitude much greater than its thickness). In this case the panel deforms much like a membrane, for which there is accurate theory and equations of motion. A membrane is a plate-like structure that can only resist deformation in tension or compression. The natural frequencies for a rectangular membrane are approximated by

$$f_{i,n} = \frac{1}{2}\sqrt{\frac{Eh}{mA}\left[\frac{i^2}{a^2}+\frac{n^2}{b^2}\right]} \text{ (Hz)} \qquad i,n = 1,2,3,... \tag{4.1}$$

where m is the surface density, E is the modulus of elasticity, h is the panel thickness, a and b are the length and width of the panel, A is the panel area (*i.e.* $A = a \cdot b$), and i and n correspond to the number of nodal lines plus one in the a and b directions, or likewise the number of flexural half-waves in a particular direction [Blevins, 1995; Gol'Denveizer, 1961]. The lowest frequency mode corresponds to $i = n = 1$. Armed with this formulation and Equation 2.9, which describes the natural frequencies of a flat plate in bending, a comparison can be made for the natural frequencies of a panel in bending versus a panel in pure stretching for the same approximate mode shape. If the comparison factor, χ, is defined as follows,

$$f_{bending} = \chi \cdot f_{stretching} \tag{4.2}$$

then χ can be determined to be

$$\chi = \frac{\pi h}{a}\sqrt{\frac{\left(i^2 + n^2\left(\frac{a}{b}\right)^2\right)}{12(1-\nu^2)}} \tag{4.3}$$

where ν represents Poisson's ratio. From this it is evident that a panel in pure stretching occurs at much higher frequencies than a panel in bending for the panel geometries considered (*i.e.* $h << a$). For the fundamental mode shape, the natural frequency of a panel in stretching is at least two orders of magnitude greater than that of the natural frequency of a panel in bending, and this increases as the thickness of the panel decreases or the area of the panel increases. Therefore, although the mode-shaped panel can deform further into the shape in which it is designed, it occurs at significantly higher frequencies with reduced displacement and velocity.

One can gain further insight and develop a simple model for the fundamental-mode-shaped panel by analyzing a spherical section. First, there is a distinction between "shallow" sections and "deep" sections. Deep sections have greater curvature to length ratios (length here refers to a characteristic length of a panel). Typically a deep section has a maximum height that is no less than an order of magnitude greater than the smallest characteristic length, while a shallow section has a height less than an order of magnitude of the smallest characteristic length. The designs in this work typically have a height that is near the transition between these two distinctions, but since the two extremes should converge at their intersection the use of either should suffice for a very approximate solution. A shallow spherical shell is illustrated in Figure 4.2.

It has been shown that for shallow spherical shells there is a strong relation between the natural frequencies of a flat panel and a spherically shaped panel with the same thickness, boundary conditions, geometry, and material properties. The natural frequencies have been shown to be related by the following formula

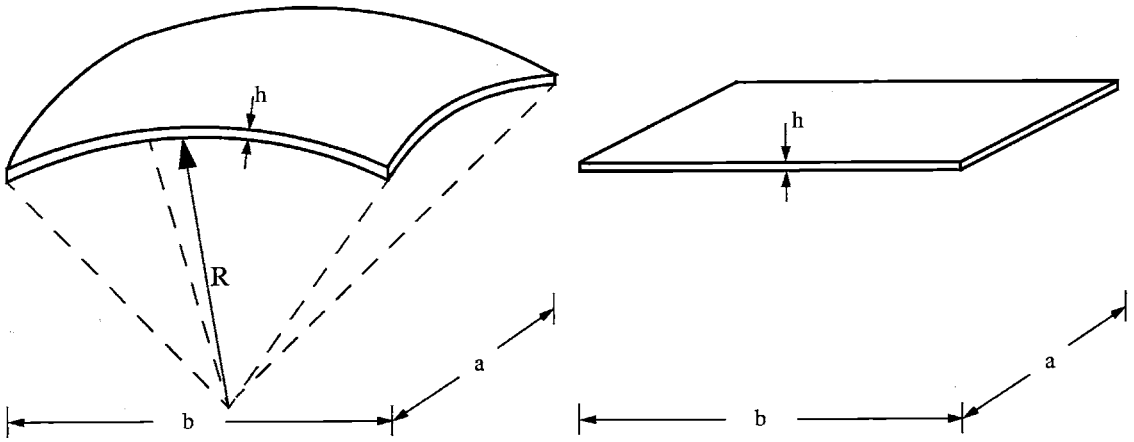

Figure 4.2 Illustration of a shallow spherical shell with rectangular plan-form, with lengths *a* and *b*.

$$\omega_{shell} \cong \sqrt{\omega_{plate}^2 + \frac{E}{\rho R^2}} \tag{4.4}$$

where ω_{shell} is the natural frequency of the spherical shell (in radians), ω_{plate} is the natural frequency of the flat plate, E is the elastic modulus, ρ is the material density, and R is the radius of curvature of the spherical shell [Blevins, 1995]. It is evident that the curved panel has a higher natural frequency than the flat panel and thus a higher stiffness. It is also a strong function of the curvature of the panel. This equation can be combined with Equation 2.9, for example, to provide an estimate for the natural frequencies of simply supported shells. In addition, it can be used with other panels with any boundary condition, by using previously solved values. It should be noted that shallow spherical sections with rectangular boundaries have similar mode shapes to that of a *flat* panels, an undesirable result. Therefore, spherical shells are *not* likely to provide the same beneficial acoustic results as a mode-shaped panel [Blevins, 1995]. This is further emphasized in later sections using finite element analysis.

The above formula can be used as an initial approximation for the natural frequencies of a mode shape design. As a first approximation, one can assume that the mode shape design has a spherical cross-section whose curvature is determined by

$$\kappa = \frac{1}{R} = \frac{2H}{\left(\frac{b}{2}\right)^2 + H^2} \tag{4.5}$$

where κ denotes curvature, H is the height or amplitude of the panel curvature, and b is the length of the longest side of the panel. Unfortunately, this approximation is only valid for the first mode of a rectangular panel, as shown in the left portion of Figure 4.1. Like most shell theory, it cannot account for multiple points of inflection in a curved panel, as shown by the next odd mode in the right portion of Figure 4.1.

Another important issue for the acoustic performance of these panels is the critical frequency and coincidence. In general, when the stiffness of a panel is increased the critical frequency decreases and the frequency range of coincidence increases, often causing greater audible structural acoustic coupling. One of the benefits of the fundamental-mode-shaped design is that the critical frequency is nearly the same as a flat panel of the same thickness and material. The reason for this is because at the higher frequencies and shorter wavelengths where coincidence is an issue the stiffness increase due to the subtle curvature of the design is much less significant. When one reaches the sort of scales where coincidence is encountered, the bending wave behavior of the mode-shaped designs is very near that of a flat panel (assuming $L >> h$, where L is the characteristic length of a wave and h is the panel thickness) [Bies, 1996].

To further illustrate this, one can analyze a differential element of a shell as shown in Figure 4.3. By looking at the strain contributions from bending and longitudinal deformation one can gain a qualitative understanding of the mechanics of shells for various vibration conditions. By analyzing the elements in Figure 4.3 the strain contributions can be shown to be

$$\varepsilon_{b_x} = -\frac{z}{1-\frac{z}{r_x}}\left(\frac{1}{\bar{r}_x} - \frac{1}{r_x}\right), \quad \varepsilon_{b_y} = -\frac{z}{1-\frac{z}{r_y}}\left(\frac{1}{\bar{r}_y} - \frac{1}{r_y}\right) \tag{4.6}$$

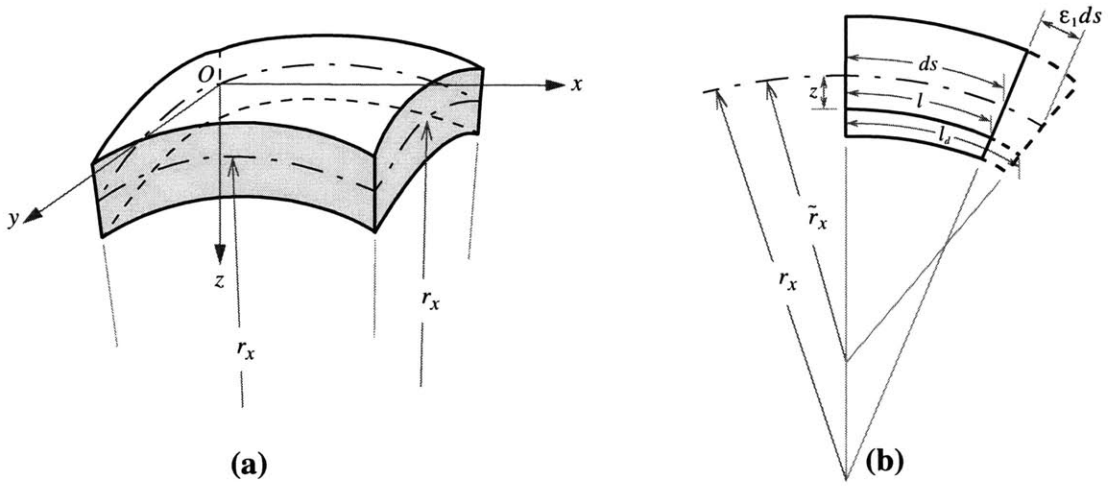

Figure 4.3 Illustrations of a differential shell element. Figure (a) shows the two-dimensionally curved differential element, and figure (b) demonstrates the combination of longitudinal and bending strains for one direction of the differential element.

$$\varepsilon_{s_x} = \varepsilon_1, \varepsilon_{s_y} = \varepsilon_2 \tag{4.7}$$

where ε_{b_x} and ε_{b_y} are the strains due to bending in the x and y directions respectively, ε_{s_x} and ε_{s_y} are the strains due to longitudinal deformation at the mid-surface in the x and y directions respectively, z is the distance from the mid-surface of the shell element, r_x and r_y are the undeformed radii of curvature of the shell, and $\tilde{r}_x$ and $\tilde{r}_y$ are the radii of the shell element after deformation. The total strain is thus

$$\begin{aligned}
\varepsilon_x &= \frac{l_{d_x} - l_x}{l_x} = \frac{\varepsilon_1}{1 - \frac{z}{r_x}} - \frac{z}{1 - \frac{z}{r_x}}\left(\frac{1}{\tilde{r}_x(1-\varepsilon_1)} - \frac{1}{r_x}\right), \\
\varepsilon_y &= \frac{l_{d_y} - l_y}{l_y} = \frac{\varepsilon_2}{1 - \frac{z}{r_y}} - \frac{z}{1 - \frac{z}{r_y}}\left(\frac{1}{\tilde{r}_y(1-\varepsilon_2)} - \frac{1}{r_y}\right)
\end{aligned} \tag{4.8}$$

where l_x and l_y are the undeformed length of the shell element at a distance z from the mid-surface, and l_{d_x} and l_{d_y} are the deformed length of the shell element at a distance z from the mid-surface. Some simplifications can be made since the shell is assumed be

thin (*i.e.* $h << r_x, r_y$), namely $1 - \frac{z}{r_x} \cong 1 - \frac{z}{r_y} \cong 1$. It can be further assumed that the longitudinal deformation has a negligible effect on the curvature of the element (*i.e.* $1 - \varepsilon_1 \cong 1 - \varepsilon_2 \cong 1$). Thus, the equations simplify to

$$\varepsilon_x = \varepsilon_1 - z\left(\frac{1}{\tilde{r}_x} - \frac{1}{r_x}\right) = \varepsilon_1 - z(\Delta\kappa_x),$$
$$\varepsilon_y = \varepsilon_2 - z\left(\frac{1}{\tilde{r}_y} - \frac{1}{r_y}\right) = \varepsilon_2 - z(\Delta\kappa_y) \tag{4.9}$$

where $\Delta\kappa_x$ and $\Delta\kappa_y$ represent the changes in curvature due to bending [Timoshenko, 1940].

From these equations several qualitative statements can be made concerning the strain energy contribution due to bending or longitudinal deformation. At lower order bending modes (*i.e.* modes with bending curvature on the order of the curvature of the shell) the change in curvature, $\Delta\kappa_x$ and $\Delta\kappa_y$, is less significant and the total strain energy is more likely to be dominated by longitudinal strains, whereas at higher order bending modes (*i.e.* modes with bending curvature much greater than the curvature of the shell) the change in curvature becomes significant and the total strain energy is more likely to be dominated by strains due to bending. This phenomenon implies that the higher order bending of subtly curved panels, such as the mod- shaped panels discussed here, are not significantly altered by the subtle curvature inherent in the panel. Thus, the critical frequency, which occurs due to higher order bending, is not significantly effected (*i.e.* reduced) for these panel designs.

Another method of illustrating this phenomenon is to discuss what is referred to in acoustics as the *ring frequency*. The ring frequency is generally associated with cylinders or pipes and is used to describe the deformation characteristics of the system. Below the ring frequency the bending wave response is dominated by the curvature of the shell, and

above the ring frequency the shell behaves more like a flat panel, with little increase in stiffness due the curvature of the shell [Bies, 1996]. Although the formula for ring frequency is based on a cylinder, it can be generalized to any thin curved shell as follows

$$f_r = \frac{c_L}{2\pi r} = \frac{\sqrt{\frac{E}{\rho(1-\nu^2)}}}{2\pi r} \tag{4.10}$$

where c_L represents the longitudinal bending wave speed which is determined from the material modulus, E, density, ρ, and Poisson's ratio, ν, and r represents the radius of curvature of the shell. To ensure a good design the ring frequency should be as high as possible but well below the critical frequency of the panel. By ensuring that the ring frequency is below the critical frequency, one can ensure that the range of coincidence is not increased by the curvature of the panel.

4.3 Finite Element Analysis of Mode-shaped Panels

To illustrate some of the above principles this section demonstrates the behavior of mode-shaped panels for various boundary conditions using numerical analysis. Panels with three different boundary conditions were analyzed using finite element analysis and some of the results are compared with the analytical approximations given. In addition, the process of determining and defining the designs is also discussed.

4.3.1 Determining the Mode Shape

To design a panel in the shape of a mode one must know the shape of the mode for the boundary conditions in which the panel is set. Unfortunately, a good approximation only exists for the mode shapes of a simply supported boundary panel (as shown in Equation 2.10), and most panels on machine enclosures cannot be described well by simply supported boundaries.

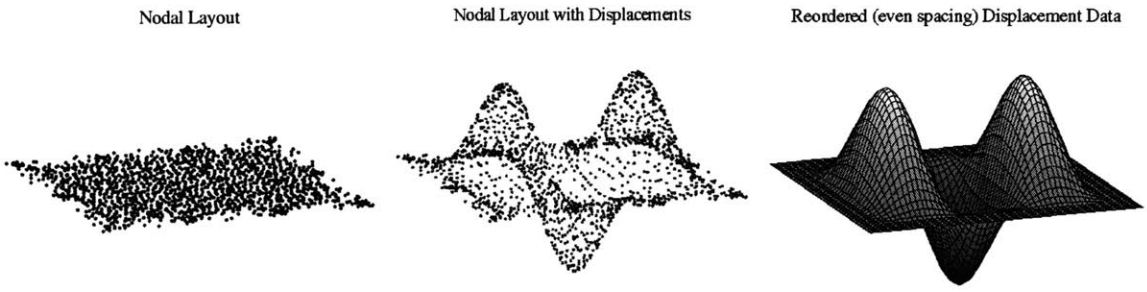

Figure 4.4 A clamped panel described by its nodes and a resulting mode shape showing the nodal displacements and the data ordered in rectilinear grid.

To describe the shapes of panels with more complex boundaries it is necessary to use finite element analysis (FEA). One can acquire an accurate representation of the mode shape by performing FEA on a computer drafted version of the panel and the accompanying members that are deemed necessary to describe the panel's dynamics. The FEA model is set up such that the nodal spacing is sufficient to accurately define the modal geometry and then the modal data is exported to an external subroutine that allows the interpretation, ordering and analysis of the resulting mode shapes. The panels were created in PRO\Engineer; FEA was performed in PRO\Mechanica; and the data was ordered and analyzed with subroutines written in Matlab.

Figure 4.4 illustrates the nodal positions on a rectangular panel with clamped boundary conditions. The figure also shows the nodal displacements and the results when the data is ordered onto a rectilinear grid. The data must be ordered so that it can be put in a format that can be read by a computer aided drafting program (*i.e.* PRO\Engineer). This process is discussed in greater detail in Chapter 5.

4.3.2 Analysis

To gain a better understanding of the dynamics of mode-shaped panels one can look at the results of a finite element modal analysis. The modal analysis can provide information about the panel design's stiffness and radiation characteristics. Three different boundary conditions were analyzed using finite elements analysis: simply supported, clamped, and

an approximation of bolting down the panel. The boundary conditions were applied to all four sides of the panel.

To broaden the study two different mode shapes were analyzed. In addition to the fundamental mode, the next "odd" mode shape was analyzed. This was the fourth mode for the aspect ratio of the panel chosen. Although it was previously determined that the fundamental-mode-shaped panel should be the superior design, it is useful to see how other mode-shaped panels behave. The next "odd" mode was chosen due to its often negative acoustic effects.

Simply Supported Boundaries

The first boundary conditions analyzed were the simply supported boundary conditions. As a first analysis, the effect of amplitude on the mode-shaped panel's behavior was examined. Essentially the finite element analysis was run several times with the same shape but with successively larger amplitudes. The results of this can be seen in Figure 4.5. It is evident that a larger height in the panel's shape leads to greater natural frequencies. This is only true to a point; once the height of the panel's shape becomes near the order of the panel length, then lateral displacement modes will begin to dominate the dynamics and the frequencies will be decreased by increased amplitudes. Although the frequencies increase with increased amplitude, the mode shapes do not change dramatically until the amplitude of the panel is well into the plastic deformation range (of the corresponding flat panel). Evidence of this can be seen in Appendix B, where the progression of mode shapes are shown with increasing amplitude.

The mode shapes for a simply supported panel with the shape of the fundamental and fourth mode are illustrated in Figure 4.6. The significance of these results is not only the dramatic increase in the natural frequencies, especially the fundamental frequency, but the alteration of the mode shapes of the panel. Unlike a flat panel, the resulting shapes appear to have a much more symmetric form, resembling more of the "even" rather than the "odd" mode shapes. This should lead to a reduction in the radiation efficiency of the panel

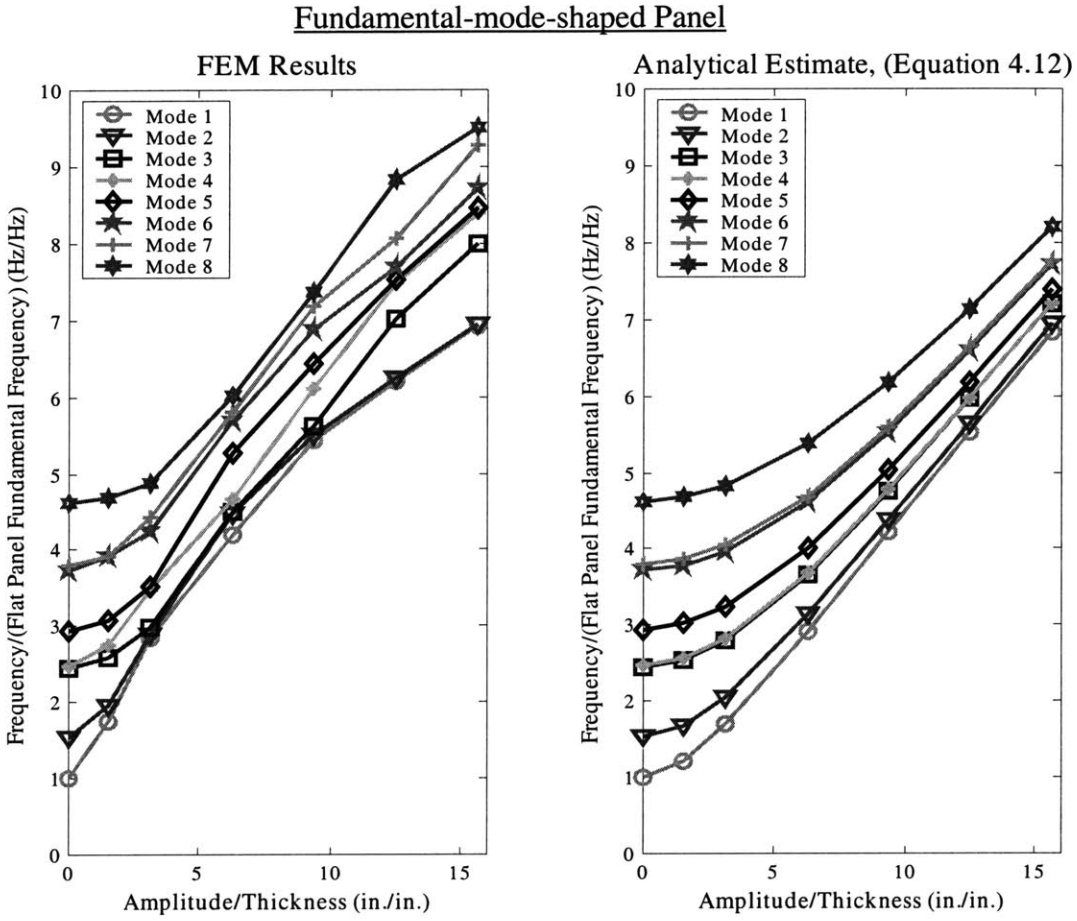

Figure 4.5 Effect of the height of the fundamental-mode-shaped panel with pinned boundary conditions. Results are presented for both analytical and finite element analysis.

at these lower frequencies. Although some of the modes are not perfectly symmetric, there is much greater volume cancellation than in the corresponding modes of a flat panel. This result supports the statements in Section 4.2.1 concerning the behavior of curved beams.

In addition, it is worthy to note that the increase in frequency seems dependent on the degree of curvature of the panel shape in relation to the curvature of the mode. The panel with the lower-order curvature (the panel shaped like the fundamental mode of a flat plate) seems to have a more significant effect on the lower-order modes, while the panel with the higher-order curvature appears to have a greater effect on the correspondingly higher-order modes with similar degrees of curvature. This trend is apparent for other boundary

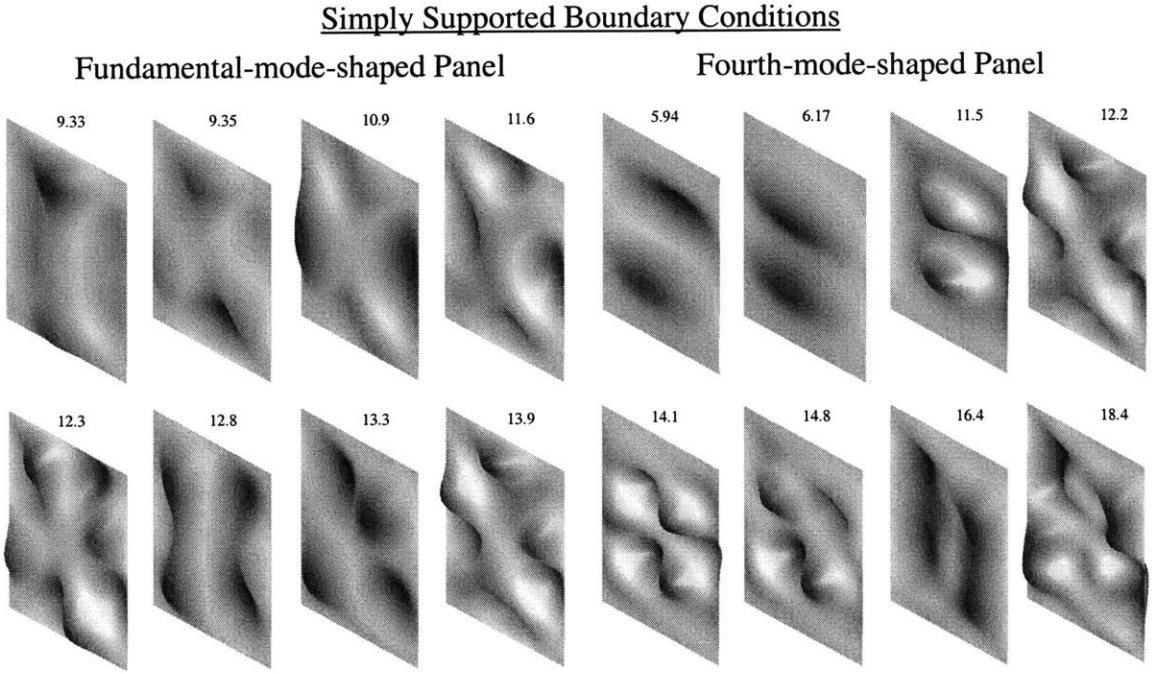

Figure 4.6 The first eight mode shapes for a panel formed in the fundamental and fourth mode shape of a flat panel with simply supported boundary conditions. Note the symmetric deformation characteristics of the modes for the fundamental-mode-shaped panel, thereby leading to greater localized acoustic cancellation. Amplitude to thickness ratio is approximately 10. The numbers indicate the frequency of the mode with the value normalized by the fundamental frequency of a flat panel with the same boundary conditions.

conditions (see next section) and for the panel designs of Chapter 3, and is also supported by the discussion and theory presented in Section 4.2.1 and Section 4.2.2.

Clamped Boundary Conditions

The next set of boundary conditions analyzed were those for clamped boundary conditions. The shape of the panel is similar to that for simply supported boundaries, namely a lobe structure, but the slope is zero near the boundaries as dictated by the boundary conditions. The results for this panel are shown in Figure 4.7. Unlike the simply supported shape, the clamped shape has less volume cancellation, especially in the first and fourth modes. This may lead to greater noise radiation, but the increase in natural frequencies should still help to reduce detrimental vibration.

Once again note that the panels' degree of curvature has a strong effect on the modes over which the shape demonstrates its greatest stiffening effect. This trend would seem to indi-

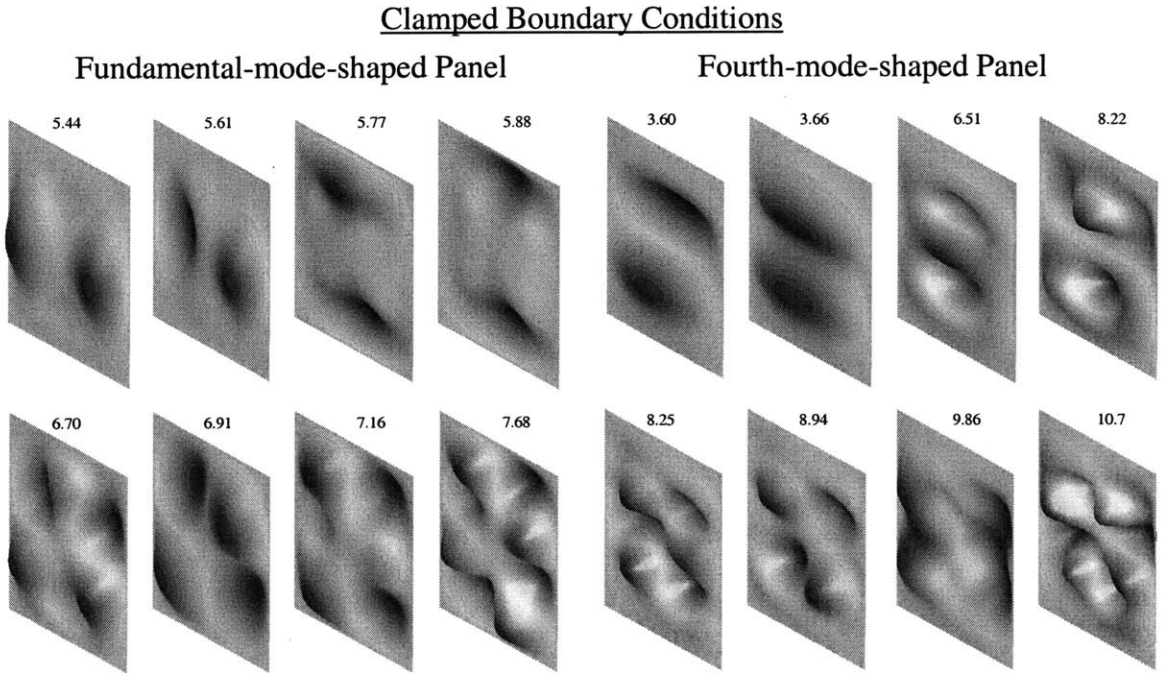

Figure 4.7 The first eight mode shapes for a panel formed in the fundamental and fourth mode shape of a flat panel with clamped boundary conditions. Amplitude to thickness ratio is approximately 10. The numbers indicate the frequency of the mode with the value normalized by the fundamental frequency of a flat panel with the same boundary conditions.

cate that if one desired to increase the stiffness in relation to particular modes then one would design the panel to have curvature similar to that of the mode over which one desires the greatest influence.

Bolted Boundary Conditions

As another example of possible boundary conditions, bolted boundary conditions were considered. Many machine enclosures attach panels by bolting or screwing down the edges at discrete points. This results in a boundary condition unlike either clamped or simply supported boundaries, but with some similarity to both. Unfortunately, to perform finite element analysis on this geometry requires complex contact analysis. Without performing contact analysis the mode shapes end up resulting like those in Figure 4.8, where significant transverse displacement can occur into the plane of support. In reality the panel would only be allowed to transversely displace in one direction (away from the bolted plane). Since contact analysis is complex and not always reliable, it was deter-

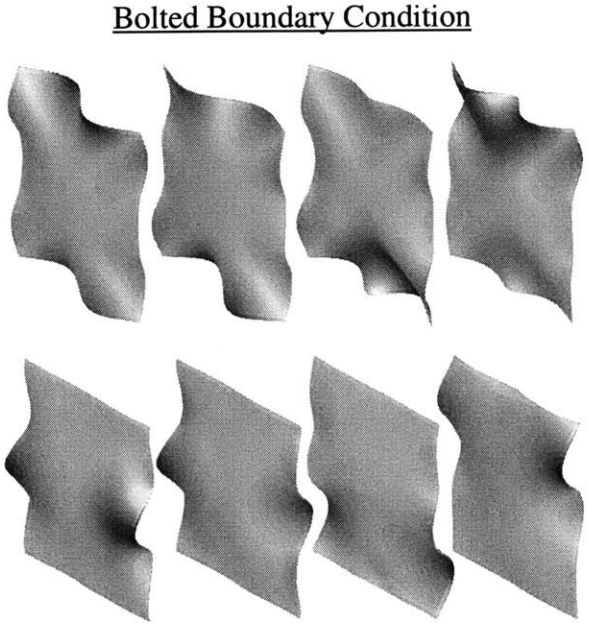

Figure 4.8 Illustration of the first eight mode shapes for a panel bolted at 10 discrete points. Note the displacement in both transverse directions. This is unlikely to occur where a panel is bolted down to a surface or rigid frame.

mined that performing experimental analysis would be more time efficient and informative. These results are presented in Chapter 6.

Chapter 5

PROTOTYPE MANUFACTURING AND EXPERIMENTAL SETUP

To be able to perform experiments and adequately analyze the two-dimensionally curved designs it is first necessary to determine how to manufacture prototypes and design the experiments. Manufacturing the prototypes first requires that the designs be represented in a form that is conducive to manufacture, whether it is an engineering drawing or otherwise. Once this is accomplished it is necessary to determine a cost effective and flexible manner in which to manufacture the prototypes. Once the prototypes are made the experiments can be designed to evaluate the relevant characteristics of the prototypes.

5.1 Data and Shape Transfer

The initial designs were created in Matlab due to its ability to represent and manipulate formulaic shapes. A graphical user interface (GUI) was created in Matlab that allowed the quick creation and manipulation of many of the aforementioned designs. The GUI was designed to accommodate many different designs and many different features including the ability to add flanges, the selection of material properties, the analysis of the designs, output options, and an array of design variables. A version of the GUI is shown in Figure 5.1. An advantage of being able to create the geometry in Matlab is that several key part properties can be manipulated. One such property is panel thickness, which can be defined as a variable rather than a constant, thus allowing panel thickness to vary as it may in reality when the part is stamped or vacuum formed.

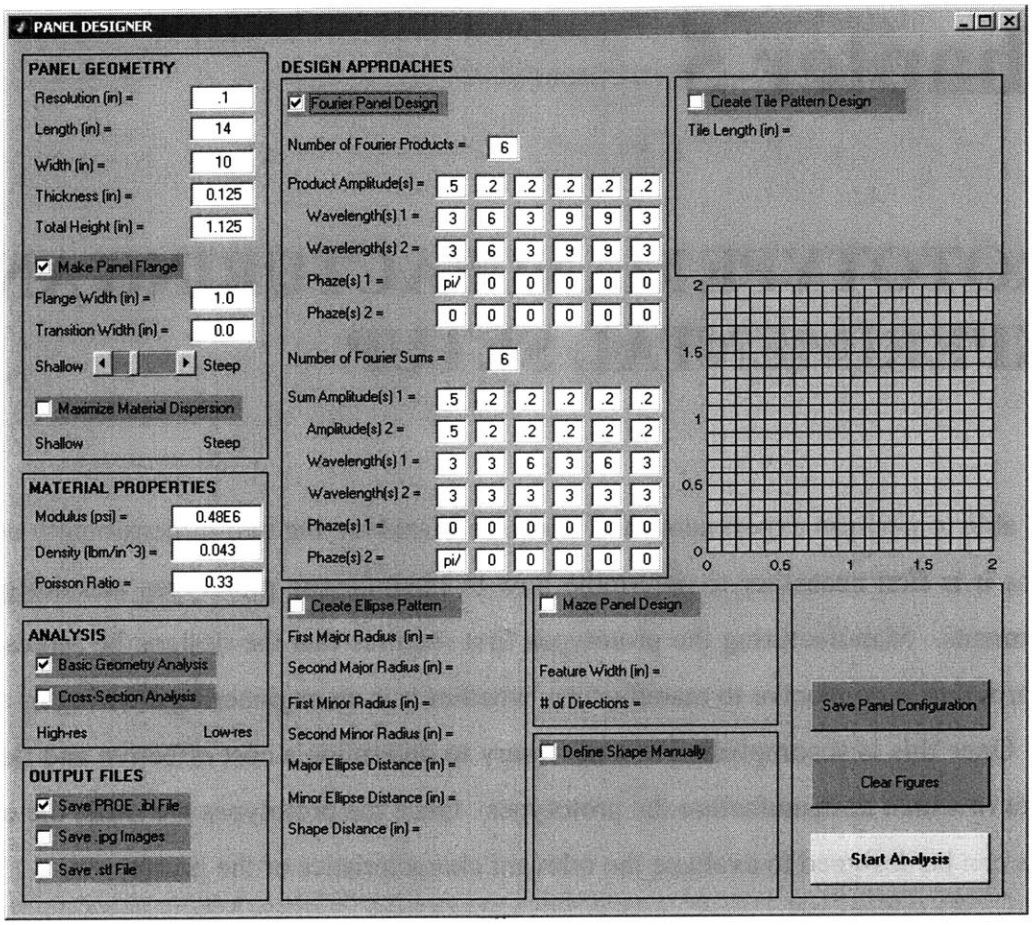

Figure 5.1 A version of the graphical user interface created in Matlab to design and manipulate two-dimensionally curved panels.

One of the more challenging aspects of the project was determining how to represent the designs in a form that could be easily manufactured and analyzed using finite element analysis. This is no small task considering the complexity of many of the shapes. It would be prohibitively difficult to try and represent many of the shapes in a CAD package by using the typical approach of building a part from standard features, primarily because there is little that can be considered standard about many of the designs.

Several options were considered. The designs were exported from Matlab in several different formats including *.stl*, a triangulation of data points in Cartesian coordinates; *.ibl,* a format recognized by Pro\ENGINEER; other ASCII formats recognized by Solidworks;

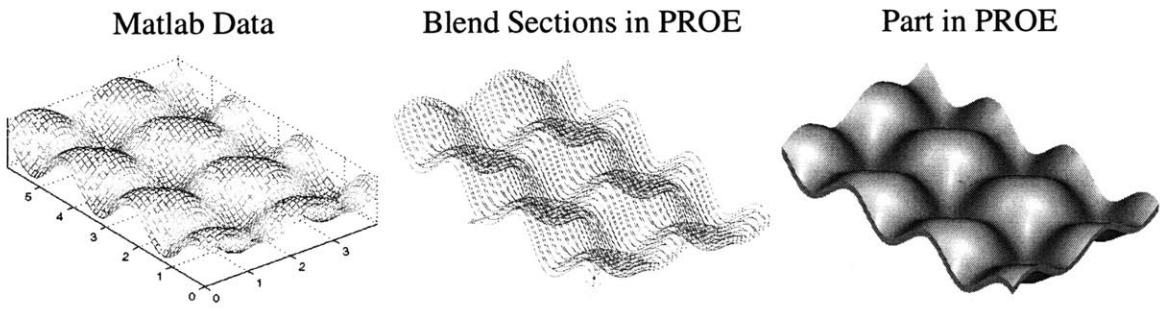

Figure 5.2 Snapshots from Matlab and Pro\ENGINEER illustrating the process of creating a part using *.ibl* files.

and an attempt was even made to export the files as VRML files. The *.stl* format would allow for manufacturing, but would not easily allow the shapes to be analyzed using finite element analysis. The advantage of the formats recognized by Pro\ENGINEER and Solidworks was that the designs could be further manipulated in a CAD package. Also, they could be represented with engineering drawings and in a greater number of exportable formats, plus they could be easily converted and analyzed using finite element analysis. After considering several options and experimenting with several third party software packages it was determined that the most efficient method was to export the designs from Matlab to Pro\ENGINEER.

The Matlab designs were converted to a series of cross-sections and these cross-sections were imported into Pro\ENGINEER as an *.ibl* file. The *.ibl* file is an ASCII file that contains points in Cartesian coordinates. The points are arranged and formatted such that the points describe a series of cross-sections in one of the Cartesian planes. Pro\ENGINEER blends a surface across the cross-sections to create a solid part. A simple example of this is shown in Figure 5.2. Once the designs were represented in Pro\ENGINEER, then they could be further manipulated, exported for manufacture, and studied using finite element analysis. It should be noted that there are limitations on the number of cross-sections that can be imported and thus the complexity of the designs are limited in this way. In addition, although some parts could be imported into Pro\ENGINEER, many of the designs still could not be analyzed with the finite element package (Pro\MECHANICA in this case) due to geometric limitations.

5.2 Prototyping Options

The next challenge was determining how to best prototype the designs in a manner that accurately represented their geometry and allowed for dynamic and static analyses. Initially, it was assumed that the panels should be made of metal, and a majority of the initial analysis was performed assuming a metal composition. Making the prototypes out of metal was seen as particularly important because some of the desired results could only be obtained using a metal composition (the flexural modulus to density ratio was seen as necessary to exercise the desired control over the natural and critical frequencies).

To this end several prototyping options were considered. One option was to machine each panel from a billet of Aluminum. Clearly this process would require a great deal of time and could only lead to a limited number of prototypes due to constraints on resources. Another option was to try and stamp the designs using a cast or rapid prototyped mold. Again, the cost, equipment restrictions, and unknowns were seen as too great to allow this process to be considered a viable option. Finally, more exotic methods were considered such as using sheets of low melting temperature alloys (such as Bismuth alloys) and then compressing these sheets in a raised temperature compression mold. This method could use inexpensive molds, materials, and would not require a great deal of capital investment. The major drawbacks to this method was that *sheets* of the low melting temperature alloy are not commercially available, and the process is untried thereby leaving many unknowns.

After careful consideration, it was decided that making the prototypes out of metal was impractical and it was determined that it would be simpler to vacuum form the designs using thermoplastics. Although the flexural bending stiffness-to-density ratio for most plastics is at least an order of magnitude less than steel or Aluminum, the flexibility and ease of manufacturing with plastics outweighed the drawbacks. In addition, thermoforming provides for a similar manufacturing process to that of stamping and rolling in metal, thereby providing some insight into characteristics such as thinning of the sheet.

5.3 Manufacturing

The next obstacles were determining how to manufacture the molds for vacuum forming and the actual thermoforming process. Several options were considered for the mold manufacture, including: CNC machining, manual forming, and casting. It was decided that the most efficient and cost effective method would be to use rapid prototyping technology. The molds could then be formed quickly and flexibly by exporting the files from Pro\ENGINEER to a *.stl* file, and then feeding the file to a rapid prototyping machine. The molds would then be created automatically with minimal effort. Again, the mold parts were initially created in Matlab, taking into consideration the thickness of the panel, and the data was imported into Pro\ENGINEER for final manipulation and export to a *.stl* file.

5.3.1 Mold Manufacturing

Several different rapid prototyping methods were considered. The three main methods examined were laminated object manufacturing (LOM), three-dimensional printing, and stereo-lithography. These three methods were considered because of the resulting parts' resistance to degradation due to temperature increases during the thermoforming process. Prototype molds were created using the three different techniques. Examples of the three different rapid prototyping processes are shown in Figure 5.3.

Each of the three different processes demonstrated various benefits and drawbacks. The laminated object manufacturing process builds up parts with layers of laser cut paper adhered with heat activated glue in a topographical manner. The result is an accurate part (tolerances of ~0.02 inches) with similar properties to wood. The part is mechanically robust and shows no negative effects during the vacuum forming process, and additionally can be altered with typical machining processes. The drawback of the LOM mold is that the building process takes a significant amount of time (~ 24 hours for a 1" by 9" by 13" part) and the LOM machine requires a fair amount of supervision to ensure quality parts. The three dimensional printing process uses built up layers of a powder (starch or plaster)

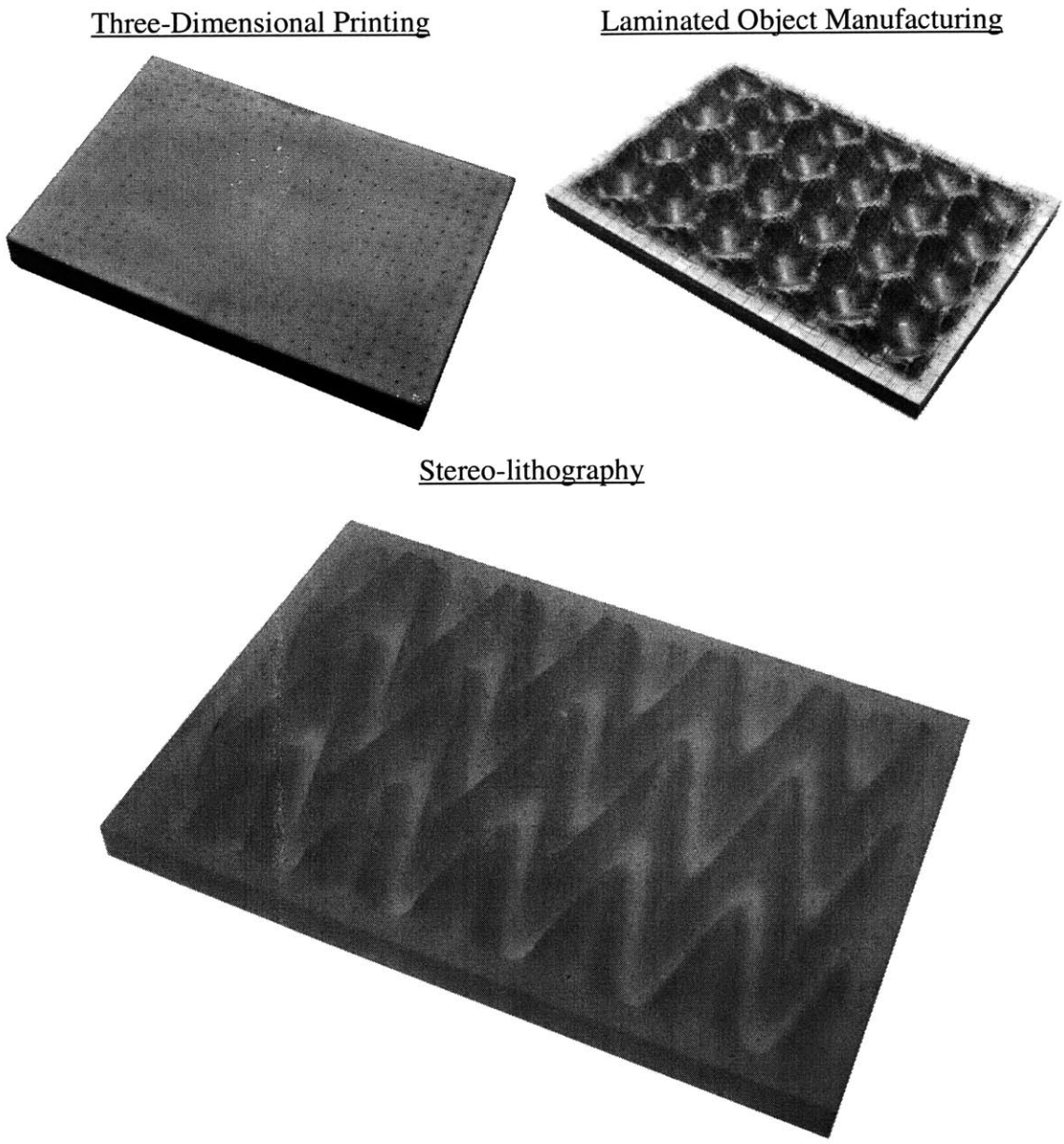

Figure 5.3 Pictures of three different vacuum forming molds, each created using a different rapid prototyping process.

bound together with an adhesive sprayed from a print head. It is the quickest of the prototyping processes (~ 2 hours for a 1" by 9" by 13" part). Unfortunately, the resulting part is not very mechanically robust and therefore requires a great deal of secondary reinforcement using epoxy, thereby negating any time saved using the process. Additionally, larger

parts tended to warp significantly, leading to tolerances greater than a tenth of an inch. Finally, the stereo-lithography process uses an epoxy slurry that is cured in layers using laser or photo exposure. The process is relatively quick and produces the most accurate parts of the three processes (tolerances ~ 0.003 inches). The resulting molds are mechanically robust and can be machined. The one slight drawback was that the molds tended to warp slightly when heated and cooled, but this does not appear to affect the vacuum formed parts because the warping was removed during the forming process due to the pressure forces. For these reasons the panel molds were made primarily using the stereo-lithography process.

5.3.2 Vacuum Forming

Vacuum forming is a simple process but several issues must be addressed before acceptable parts can be formed. The first issue is the material that must be used. The plastic must be a thermoplastic, preferably with a broad glass transition temperature range. Since a high flexural modulus-to-density ratio was desired, fiber reinforced plastics were considered, but it was determined that the cost, and the orthotropic behavior of the material would ultimately cause too many problems. Instead, Acrylic was chosen as the primary material because of its flexural modulus-to-density ratio, cost, and availability. Acrylic comes in several brands and compositions, the two most common being Plexiglas and Lucite. Lucite was used because of its availability in a variety of thin sheets. One drawback to using Acrylic is that it has a relatively narrow forming temperature range and therefore requires extra attentiveness during forming. In addition, Acrylic tends to be more difficult to form in complicated molds than most thermoplastics, such as ABS and polystyrene. This fact limited the panel designs that were able to be manufactured. The vacuum forming machine used is shown in Figure 5.4.

To aid in the pulling process (the process of applying vacuum to the heated plastic and causing it to conform to the mold shape), the hole configuration was carefully considered. Holes must be placed throughout the mold to allow a pressure vacuum to be formed

Figure 5.4 Picture of the vacuum forming machine used to make the prototypes, and close-up of mold and vacuum formed part in machine.

between the mold and the heated plastic sheet. This is especially important in fine details or deep features of the mold. To aid in this process it was determined that the number of holes should be significant, and that the holes should have a tapered design to ensure minimal flow resistance. To manually machine or drill each hole would require a significant time. To circumvent this process, holes were included in the Pro\ENGINEER model and were formed directly during the rapid prototyping process. To further enhance the process, some of the molds incorporated pyramid shaped holes to minimize air flow. Square hole cross-sections were used rather than circular to help minimize part file sizes. As *.stl* files are a series of triangles describing the surface an object, it is much less computationally cumbersome to represent linear shapes, such as pyramids, rather than curved shapes with small radii, such as cones. A close-up of a pyramid shaped vacuum hole is shown in Figure 5.5. In general, holes were spaced every quarter to half inch on the molds.

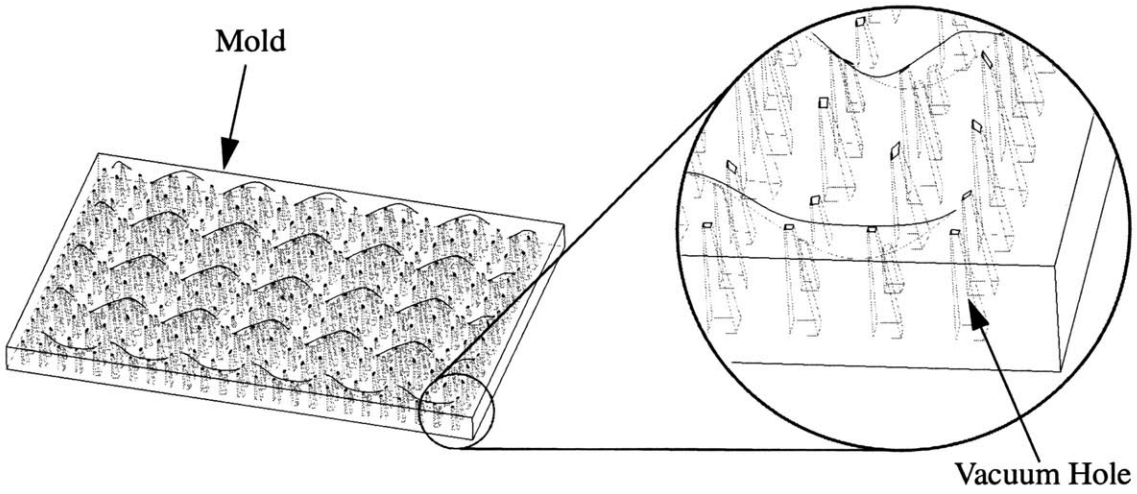

Figure 5.5 Detail of a vacuum hole in a mold design.

Even with these considerations, problems were still encountered when prototypes were manufactured. The two primary problems encountered were incomplete pulls, where the plastic sheet did not fully conform to the shape of the mold, and delamination of the sheets that included a constrained damping layer. In molds that had particularly small features, such as that shown in Figure 3.7c, the plastic sheet was unable to fully pull into the narrow gaps. For the sheets with the constrained damping layers, the adhesive and the constrained damping layer would melt during the heating process thereby making it difficult to maintain lamination during the forming process. In general, the greater the curvature in the design, the greater the likelihood of delamination. The delamination can reduce the effectiveness of the constrained damping layer.

Other problems that were encountered included excessive thinning of the parts, bubbling of the plastic due to overheating, and folding of the plastic if pre-stretching of the heated plastic was excessive. In general, most of these latter problems could be controlled. The only part that demonstrated excessive thinning was the Maze design, which thinned by as much as 95 percent in one small area of the part where the feature required excessive pulling in all lateral directions. For the other parts, the final part thickness was at least 70 percent of their original thickness, a fact that was accounted for in some of the part modeling.

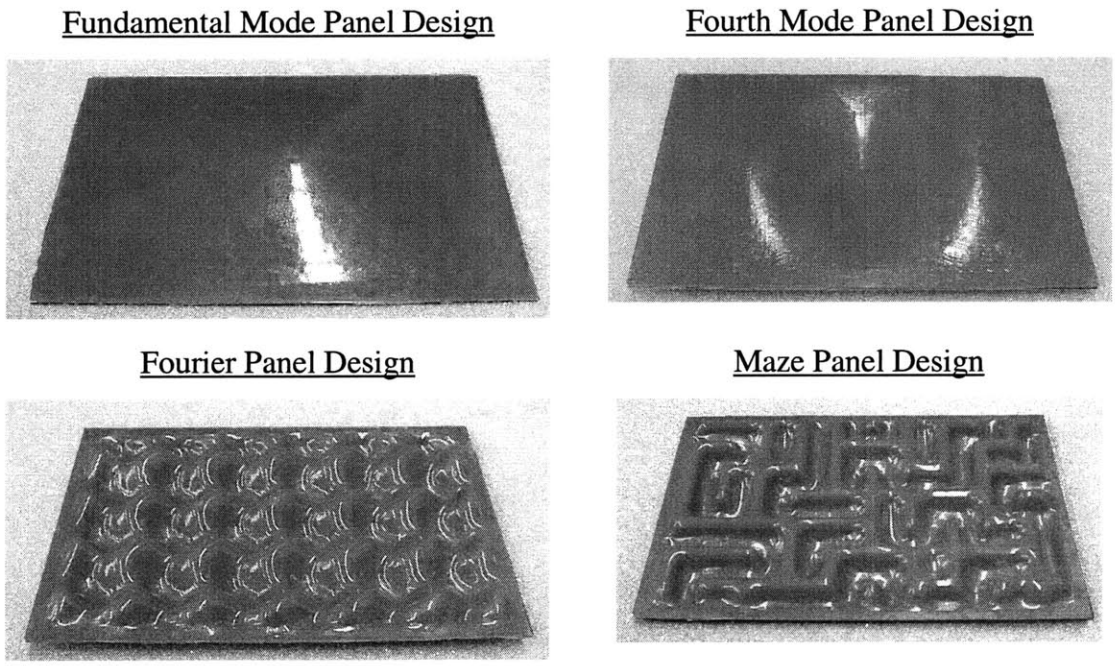

Figure 5.6 Photographs of several vacuum formed prototypes. All prototypes shown have a constrained damping layer.

Aside from the multi-layer designs, the part geometries were 9 inches by 13 inches in area with a 1.0 inch amplitude. This included a half inch flange on the entire perimeter to allow for mounting of the panels. The effective area of the panels was 8 inches by 12 inches. The initial thickness of the acrylic sheet was 0.117 inches, except for the constrained damping layer designs which sandwiched a 0.015 inch damping layer between two 0.060 inch sheets of acrylic. Also, a constrained damping layer design that utilized a 0.03 inch thick damping layer was manufactured. The damping material for both designs was Isodamp C-1000 manufactured by E-A-R. In addition, a core layer for a multi-layer panel design was created that had a nominal amplitude of 3/8 of an inch, such that the total thickness was approximately 0.5 inches. Photographs of several prototypes are shown in Figure 5.6 and Figure 5.7.

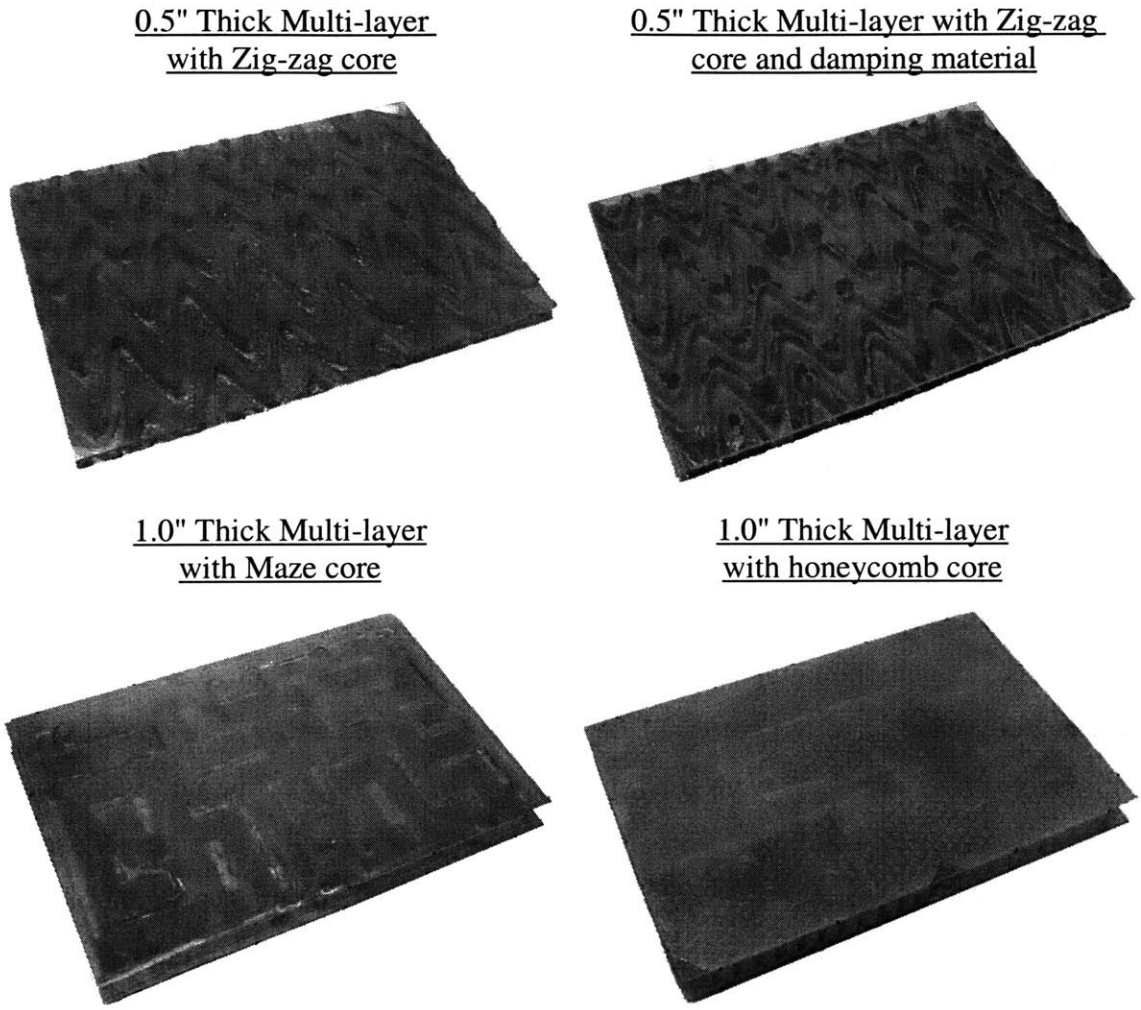

Figure 5.7 Photographs of multi-layer designs.

5.4 Experimental Setup

The experiments were designed to examine static stiffness, vibration, and acoustic properties of the panel designs. Special testbeds were designed and constructed to analyze the panel properties under various conditions. The experiments were setup in a controlled environment to ensure repeatable and reliable results. Rather than performing experiments based on previous defined standards, which require specific and often difficult to attain requirements, the experiments were performed on a comparison basis. The curved panel designs' results were compared with the results of flat panels with varying thickness

and composition. With the flat panels as a baseline, performance comparisons could be reliably made for the specific materials and setups used.

5.4.1 Experimental Testbeds

It was determined that three general test setups were required to analyze all the different properties of the panels. To test the static behavior of the multi-layer panels, a three and four point bending experiment was created. To analyze mode shapes, directional transmission, and vibration a small enclosure with a small amount of absorption material was created. Finally, to analyze diffuse transmission, radiation, and to further analyze vibration, a larger reverberant testbed was created.

The static stiffness of the panels was determined using simple three and four point bending tests. A sketch and photographs of the test setup are shown in Figure 5.8. Weight was incrementally added and the corresponding deflections, measured with a dial indicator, were recorded. These tests were used to compare the stiffness of the multi-layer two-dimensionally curved isotropic designs (with the two-dimensionally curved panel used as the core) to the honeycomb sandwich designs. Ideally, the experiments should be done using beam rather than plate structures to minimize Poisson effects, but the two-dimensional nature of the designs requires that the experiments be performed on the full panels. Since force was applied along the entire length of the panel (simulating a one-dimensional system), the panels were of the same approximate dimensions, and the tests were performed consistently, thus the results are sufficient for a comparison based analysis.

To examine directional transmission, mode shapes, and vibration a small cubicle testbed was created. The testbed was constructed from a stiff aluminum frame that used extruded members manufactured by Star-Linear. Attached to the frame on five sides were sand filled, medium density fiber board (MDFB) panels. The construction of these side panels incorporated a 1.5 inch thick layer of loose sand contained between two 0.75 inch thick MDFB boards. The choice of MDFB and sand was to ensure maximum transmission loss. At all structural interfaces neoprene foam rubber was used to ensure the sealing of all gaps

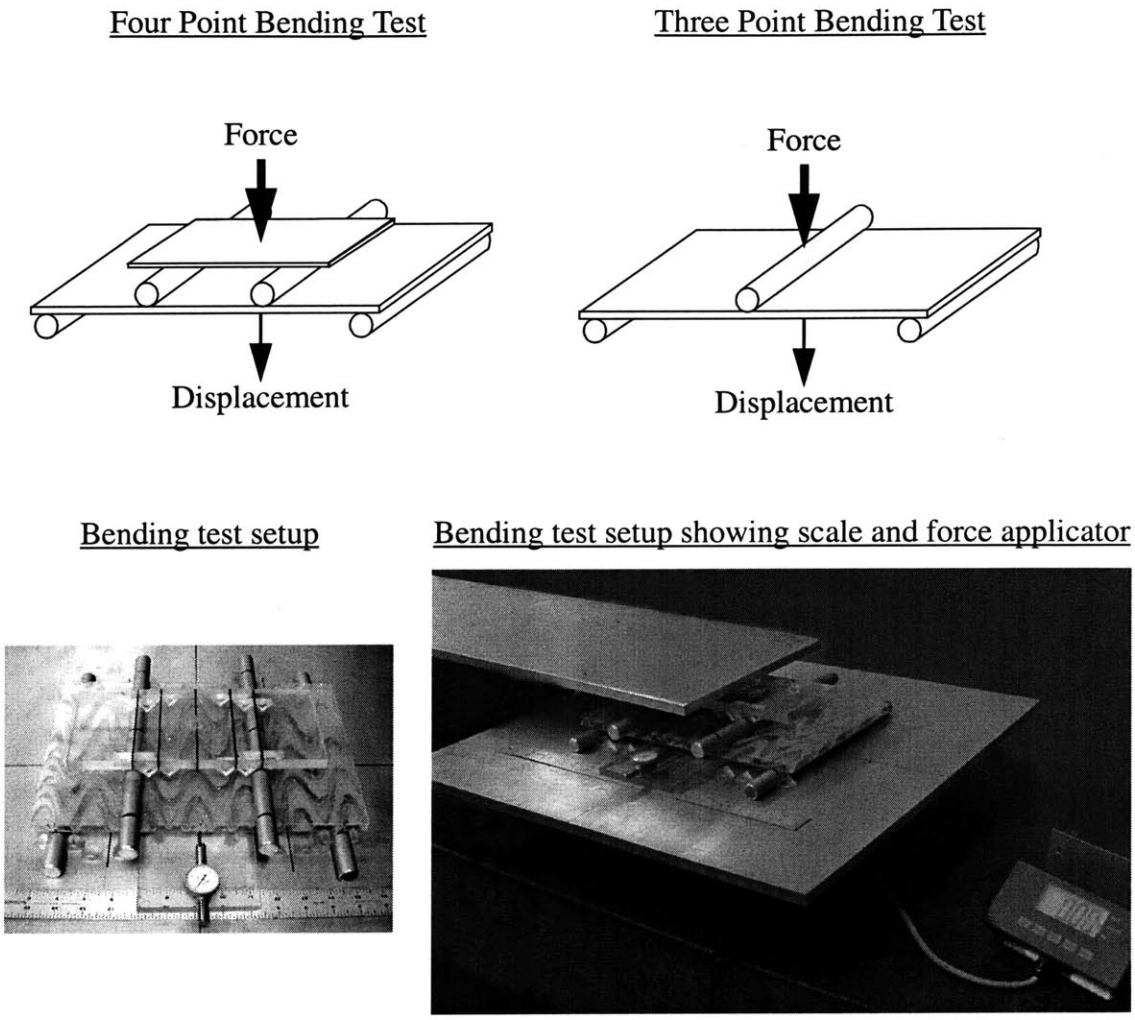

Figure 5.8 Sketches and photographs of the static bending test setup. Force was applied by placing weight on the force applicator (a long plate balanced in the middle) with one end of the applicator in contact at the center point of a plate on the top 2 cylinders; the force was measured with a scale upon which the setup was placed. Displacement was measured with a dial indicator.

and minimize component interaction. A 1.5 inch layer of acoustic absorption material was also placed on the interior wall of the testbed. These design considerations ensured that the majority of energy leaving the testbed would be through the test panel. A broad spectrum (100 - 12,000 Hz) actuation speaker was placed inside the testbed facing the test panel at a distance of approximately 9 inches. The size of the enclosure and the speaker configuration was chosen to mimic a close fitting industrial or automobile enclosure where the noise source is in close proximity to the enclosure panel. In addition, the test-

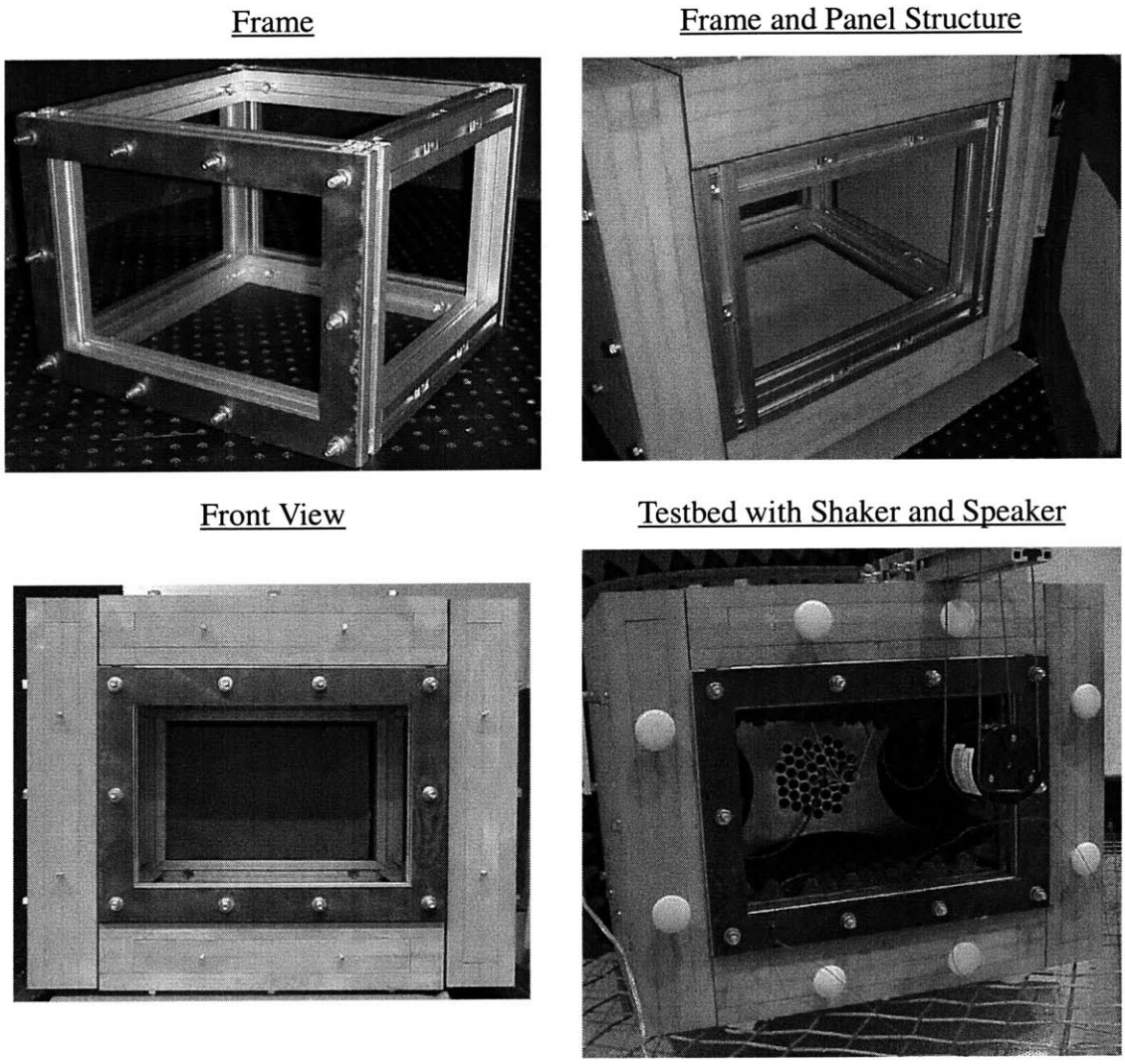

Figure 5.9 Photographs of the small enclosure testbed highlighting various aspects of the design.

bed had mounts to accommodate a shaker both inside and outside the enclosure. A shaker on the inside of the testbed was used to perform initial radiation experiments. Photos of the small testbed and some of its components are shown in Figure 5.9. The exterior dimensions of the testbed are 18 inches by 18 inches by 24 inches, and the interior volume is 11 inches by 11 inches by 15 inches. Although the testbed weighs over 150 pounds, it is meant to be a portable testbed that can be used in many different environments. A plot of the testbed response at a single interior microphone location to the speaker is shown in Figure 5.10.

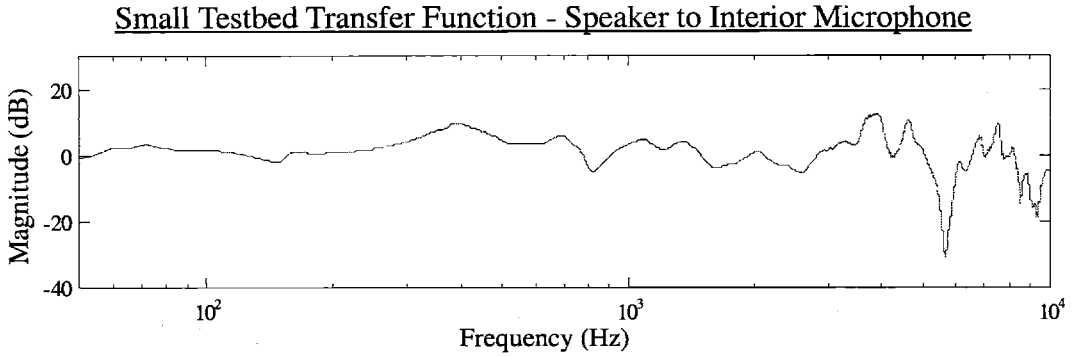

Figure 5.10 A plot of the acoustic response of the small testbed. The response represents a transfer function (voltage/voltage) from a single microphone, located in the center of the testbed, to the speaker.

In addition to the small enclosure testbed, a larger, more reverberant testbed was designed and built to examine more diffuse transmission characteristics and structural radiation. The larger testbed was designed to resemble more of a reverberation chamber than the small testbed, but still maintain some of the characteristics of a machine enclosure. The need for a more diffuse sound field was required so that the coincident characteristics of the panels could be examined. Unlike the small enclosure, which only allowed for directional incidence (*i.e.* non-diffuse), the larger enclosure allows for multi-directional incidence. This includes grazing incidence which is necessary for a study of the critical frequency. Photographs of the installed reverberant testbed are shown in Figure 5.11.

The larger testbed was constructed of many of the same components as the smaller testbed. It also used an extruded Aluminum frame with MDFB covering the sides of the enclosure. Unlike the small enclosure, the larger enclosure was mounted to an anechoic chamber (discussed in Section 5.4.2). The side facing the anechoic chamber used a sand filled panel and a significant amount of absorption material to ensure that the only significant transmission from the large enclosure would be through the test panel. The other sides of the enclosure did not need to be highly absorptive so only a single layer of MDFB was used to ensure a high degree of reflection.

One interesting aspect of the larger enclosure was determining the appropriate size of the enclosure. A compromise between cutoff frequency and maintaining a resemblance to a

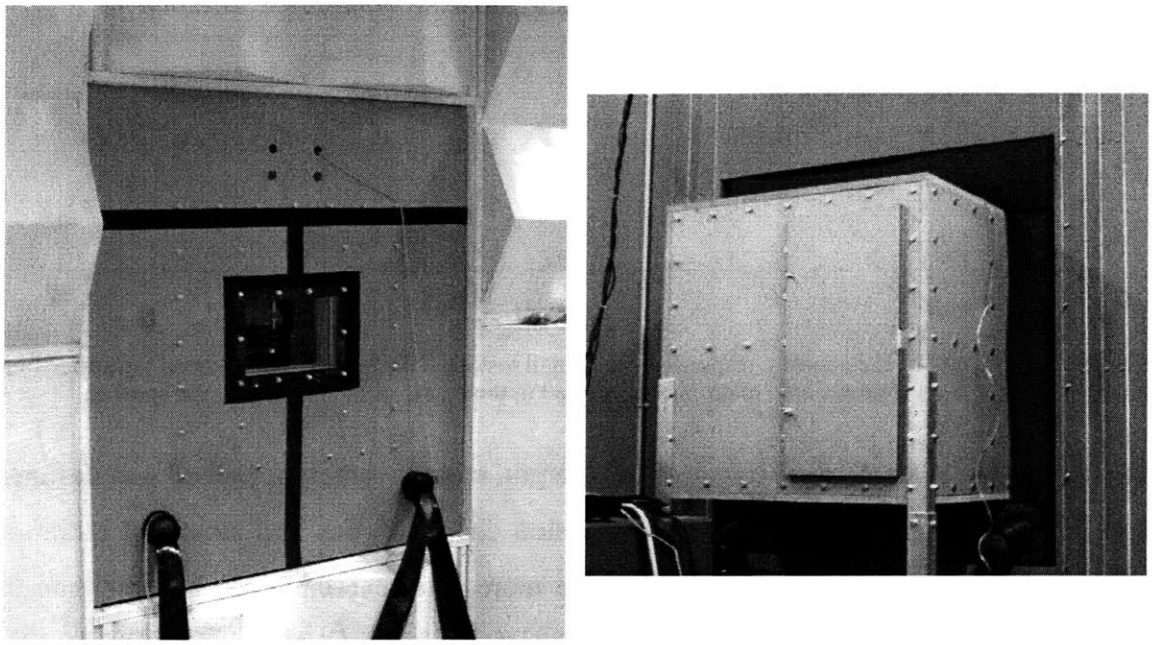

Figure 5.11 Photographs of the reverberant testbed. The photograph on the left is the testbed from inside the anechoic chamber, while the photograph on the right is the rear of the testbed from outside the anechoic chamber.

machine enclosure had to be made. In general, reverberant chambers are designed to have a cutoff frequency below the lowest frequency of interest. The cutoff frequency is the frequency below which the chamber no longer demonstrates uniform modal overlap, and is primarily based on the acoustic return time, chamber geometry, and chamber composition. Here, the cutoff frequency is defined as

$$f_c = 0.932\sqrt{\frac{\Re c^2}{-S\ln(1-\vartheta)}} \tag{5.1}$$

where c is the speed of sound, S is the surface area of the chamber, ϑ is the Sabine coefficient of absorption for the room surface, $\Re$ is a coefficient describing the modal overlap (most often chosen to be 3), and the coefficient value of 0.932 is an experimentally defined value relating to the return time.

Most reverberant chambers have a large volume and surface area and incorporate many angles to ensure as low a cutoff frequency as possible, with the intended application most

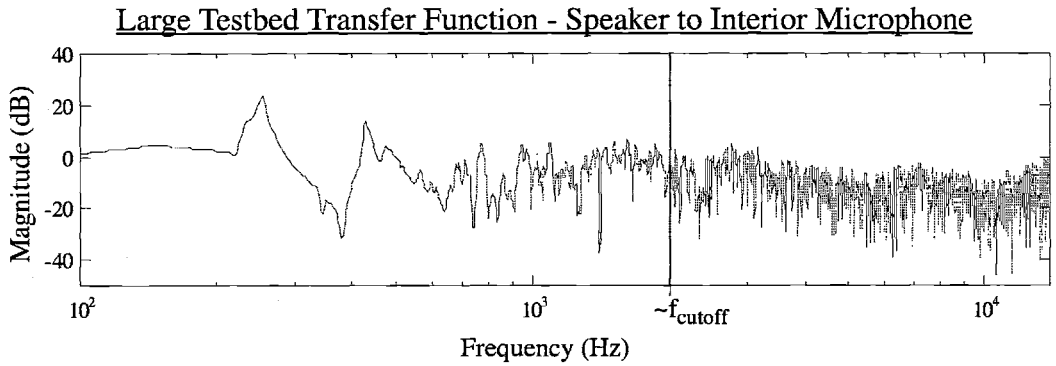

Figure 5.12 A plot of the acoustic response of the large reverberant testbed. The response represents a transfer function (voltage/voltage) from a single microphone, located near the panel, to the speaker. The apparent "noise" of the response indicates the degree of modal overlap.

often being architectural analysis [Crocker, 1975]. In the case of machine enclosures, the enclosure volumes are usually much smaller than in architectural applications and as a result experiments performed in an architecturally based system may not be highly applicable to machine enclosures. To account for these conflicting requirements, the large enclosure testbed was designed to be an order of magnitude larger than the small testbed volume, but not so large as to not resemble a machine enclosure (when compared to the experimental panels size). Although the resulting cutoff frequency of the testbed is in the lower kilo-Hertz range, it still provides for a diffuse environment with a low enough cutoff frequency to analyze coincident behavior. The interior dimensions of the reverberant testbed are approximately 30 inches by 30 inches by 30 inches and includes several additional reflective elements to increase surface area and thus the reverberant qualities. A plot of the testbed response from the speaker to a single interior microphone is shown in Figure 5.12.

5.4.2 Experimental Environment

To ensure repeatable, reliable and accurate data, the majority of experiments were performed inside an anechoic chamber. The anechoic chamber emulates an acoustic free field and is also useful for isolating the experiments during vibration analysis. The chamber measures approximately 15 feet by 12 feet by 9 feet, and has an effective operating

Figure 5.13 Photographs of the anechoic chamber where a majority of the experiments were performed.

frequency of 80 to 12,000 Hz. Photographs of the anechoic chamber are shown in Figure 5.13.

The small testbed was placed inside the anechoic chamber during experiments. The small testbed was designed such that the transmission loss on all sides, save the experimental panel side, is high enough not to have a significant effect on any of the radiation or transmission data. Acoustic data was taken for the interior, near field (~12 inches from the panel) and far field (~6 feet from the panel) for the directional transmission experiments with the small enclosure testbed. Radiation data was taken at a distance of approximately 3 feet.

As previously stated, the larger, reverberant testbed was attached to the outside of the anechoic chamber with one side coincident with the interior of the anechoic chamber. Diffuse transmission tests were performed to determine the degree of noise/power transmis-

sion from the reverberant to the anechoic chamber. An actuation speaker was placed inside the reverberant chamber and sound pressure measurements were take inside and at near and far field distances from the panel.

5.4.3 Equipment

Some of the experimental equipment used included a variety of actuators, sensors and signal conditioners as well as an amplifier and signal processor. Two primary actuators were used during the experiments, an electromagnetic shaker and a full range speaker. The electromagnetic shaker was a Bruel & Kjaer (B&K) model 4810 with a mass of approximately 1.0 kilogram. The shaker was attached to the panel using a threaded steel rod and a nylon nut epoxied to the surface of the panel. Rather than using the input to the shaker as the input signal in the transfer function, a force transducer was used to measure the force magnitude under which the panel was actually subjected. This ensured that the transfer function accurately represented the actuation of the system. The speakers used were full range speakers with an indicated frequency range of 50 to 20,000 Hz. Transfer functions of the speakers indicated that they had acceptable response over the frequency range of interest (100 to 14,000 Hz).

The sensors used included several microphones, several accelerometers, and the aforementioned force transducer. The microphones were B&K model 2669 and were used in combination with a B&K model 5935L signal conditioner. The microphones were typically mounted rigidly outside the testbeds or were suspended within the testbed. The accelerometers were Piezotronics (PCB) model 352B22, weighing approximately 0.5 grams. The accelerometers were used in conjunction with a PCB model 481 signal conditioner. Typically, the accelerometers were mounted to the panels using a wax based adhesive. Comparison tests were run to ensure that the wax adhesive provided a sufficient and rigid interface between the accelerometer and panel (comparisons were made between the wax and Super Glue, with the results showing no significant difference). In addition, accelerometer measurements were made of the testbeds to ensure that the dynamics of the

panels and the testbeds were sufficiently decoupled. The force transducer was a PCB model 208A02.

Both the shaker and speaker actuators were powered with an Audio Pro model 3400 amplifier. The amplifier was used in conjunction with a low pass, passive filter with a high pass cutoff frequency of approximately 20 Hz. The high pass filter was used to ensure that the speaker and shaker were not damaged with low frequency signals.

The digital signal processor (DSP) was a SigLab model 20-42. The actuation signal used for all experiments was a full range frequency chirp/sweep. A Hewlitt Packard oscilloscope was used to ensure that the signals generated were of uniform amplitude. The SigLab processor used in combination with a PC recorded all output and input signals and the data was saved in the form of transfer functions. The data was later imported to Matlab for further examination, reduction and analysis.

5.5 Experiments

Finally, it is necessary to determine some of the final experimental details and exactly what experiments are necessary to accurately characterize the panels. Some of the final details that need to be addressed are: panel boundary conditions, panel thickness, panel designs used in the experiments and baseline panels.

5.5.1 Experimental Boundary Conditions

According to the finite element analysis of Chapter 3, Chapter 4, Appendix A, and Appendix B, panels with clamped boundary conditions perform less desirably than panels with simply supported boundary conditions. The finite element analysis indicates that the mode shapes and natural frequencies of clamped panels are less dramatically improved by the two-dimensionally curved shapes than that of simply supported panels. For this reason, clamped boundary conditions were chosen for the experiments. The logic being that if improvement can be shown for clamped boundary conditions, then it is very likely that

equal if not better improvement can also be shown for simply supported boundary conditions, whereas the opposite is less likely to be true. In essence, the experiments try to simulate a worst case scenario. Another reason clamped boundary conditions were chosen, as opposed to a more realistic boundary condition (as purely clamped or simply supported conditions are rare in applications), was that it was necessary to experiment with boundary conditions that could be simply modeled for comparison. The ability to model nearly the exact boundary condition allows for comparison of modal spacing and density to help ensure that the experimental results are reasonable and believable. To help diversify the analysis, some experiments were also performed on panels with bolted boundary conditions, where the boundary was bolted down at several finite locations. Not only does this comparison provide a more realistic comparison with actual applications, but it also provides verification for the improvement of performance for panels with boundary conditions that more closely resemble simple supports.

The panels were clamped down using a solid one-piece frame. The clamping frame was composed of 0.25 inch thick steel, and was approximately 1.5 inches wide along the perimeter. The steel frame is visible in the photographs of Figure 5.9. To help ensure repeatability of the boundary conditions the 10 bolts attaching the steel clamping frame to the testbed frame were tightened using a torque wrench, with the torque of each bolt tightened to 75 inch-pounds (bolt diameter was 8mm with 1.25 threads per mm).

5.5.2 Baseline Panels and Panel Designs Used in the Experiments

As was previously stated, the experiments were comparison based with flat panels being used as baselines. The use of comparison based analysis helped to eliminate some of the difficulties and unknowns often associated with standardized testing procedures. By comparing the curved designs with flat panels, it could be reasonably assured that performance improvements (or lack thereof) were accurate, and that the results of the curved panel designs could be analyzed with comparable quantities for each experiment.

Five baseline flat panel designs were used as comparisons to the curved panel designs. The first and most important baseline panel was the thin flat design that had the same nominal thickness as the curved designs (0.117 inch thickness), and same material composition (*i.e.* Acrylic). This panel is the most important because it allows for comparisons based on a panel with approximately the same material mass per unit area. In addition to the thin flat panel baseline, a thicker baseline panel was also examined (0.375 inch thickness). The thicker baseline panel was used to match the approximate first frequency of some of the curved designs to demonstrate the savings in mass gained by using curved designs over merely adding material thickness. The thicker panel was also used to compare radiation efficiency. In addition to the thicker panel, honeycomb sandwich designs were also used as baseline comparisons. The honeycomb sandwich panels were used as a comparison with the multi-layer two-dimensionally curved designs, both on a structural and cost based performance metric. The honeycomb baselines used two 0.060 inch thick pieces of acrylic sandwiching a polypropylene honeycomb core. Two different core thicknesses were used, 0.375 inch and 0.875 inch, for a total panel thickness of 0.5 and 1.0 inch respectively. In all baseline cases an undamped and a damped design were experimentally analyzed, where the damped case utilized the exact same constrained damping material as the two-dimensionally curved designs.

Six types of two-dimensionally curved panel designs were experimentally examined. The following lists the panel designs that were experimentally examined and their configurations.

1. Fundamental-mode-shaped panel for clamped boundary conditions. Configurations:
   - *0.117 inch thick acrylic with 1.0 inch amplitude.*
   - *Two pieces of 0.060 inch thick acrylic with 0.015 inch thick constrained damping material with 1.0 inch amplitude.*
2. Fundamental-mode-shaped panel for bolted boundary conditions. Configurations:
   - *0.117 inch thick acrylic with 1.0 inch amplitude.*

- *Two pieces of 0.060 inch thick acrylic with 0.015 inch thick constrained damping material with 1.0 inch amplitude.*

3. Fourth-mode-shaped panel for clamped boundary conditions. Configurations:
   - *0.117 inch thick acrylic with 1.0 inch amplitude.*
   - *Two pieces of 0.060 inch thick acrylic with 0.015 inch thick constrained damping material with 1.0 inch amplitude.*
4. Fourier panel design. Configurations:
   - *0.117 inch thick acrylic with 1.0 inch amplitude.*
   - *Two pieces of 0.060 inch thick acrylic with 0.015 inch thick constrained damping material with 1.0 inch amplitude.*
   - *Two 0.060 inch thick acrylic with 0.030 inch thick constrained damping material with 1.0 inch amplitude.*
   - *0.117 inch thick acrylic and 0.030 inch thick copolyester (PETG), with 0.015 inch thick constrained damping material with 1.0 inch amplitude.*
   - *0.060 inch thick acrylic with 0.875 inch amplitude sandwiched with two 0.060 inch thick pieces of acrylic.*
5. Maze panel design. Configurations:
   - *0.117 inch thick acrylic with 1.0 inch amplitude.*
   - *Two pieces of 0.060 inch thick acrylic with 0.015 inch thick constrained damping material with 1.0 inch amplitude.*
   - *0.060 inch thick acrylic with 0.875 inch amplitude sandwiched with two 0.060 inch thick pieces of acrylic.*
6. Zig-zag panel design. Configurations (multi-layer only, 0.5 inch total thickness):
   - *0.060 inch thick acrylic with 0.375 inch amplitude sandwiched with two 0.060 inch thick pieces of acrylic.*
   - *0.060 inch thick acrylic, with 0.015 inch damping material, with 0.375 inch amplitude sandwiched with two 0.060 inch thick pieces of acrylic.*
   - *0.030 inch thick copolyester (PETG) with 0.375 inch amplitude sandwiched with two 0.060 inch thick pieces of acrylic.*
   - *Two 0.030 inch thick pieces of copolyester (PETG) sandwiching 0.015 inch thick damping material with 0.375 inch amplitude sandwiched with two 0.060 inch thick pieces of acrylic.*

5.5.3 Static Stiffness Experiments

To characterize the bending stiffness of several of the panel designs the three and four point bending analysis described in Section 5.4.1 was performed. The four point bending experiment determines the static stiffness of the designs in a minimized shear condition, while the three point bending test determines the static stiffness when the design is under a greater degree of shear. As previously stated, these experiments were performed on the multi-layer designs that incorporate a two-dimensionally curved panel core and the baseline honeycomb core panels. The experiments were performed along both lengths of the panels. In addition, the results were normalized by ideal sandwich theoretical results with the same material mass, overall panel thickness, and idealized spacing of the sandwiching layers.

5.5.4 Dynamic Vibration Experiments

The dynamic vibration characteristics of the panels were analyzed using accelerometers placed at different locations on the panel. Up to six accelerometer locations were used to ensure observability of all pertinent modes and to determine the average surface velocity. Both structural and acoustic actuation were used to ensure complete controllability of all pertinent modes. Figure 5.14 shows the locations of the accelerometers and shaker. The locations of the actuators and sensors were loosely based on the results of the finite element analysis to try and maximize controllability and observability.

The vibration analysis was performed on all of the two-dimensionally curved panels, both damped and undamped designs. Vibration analysis was also performed on the 0.5 inch thick multi-layer design. In addition, vibration analysis was performed on the flat baseline panels, save the 1.0 inch thick honeycomb panel, and it was performed for both damped and undamped designs. Vibration experiments were performed on the small and large testbed inside the anechoic chamber.

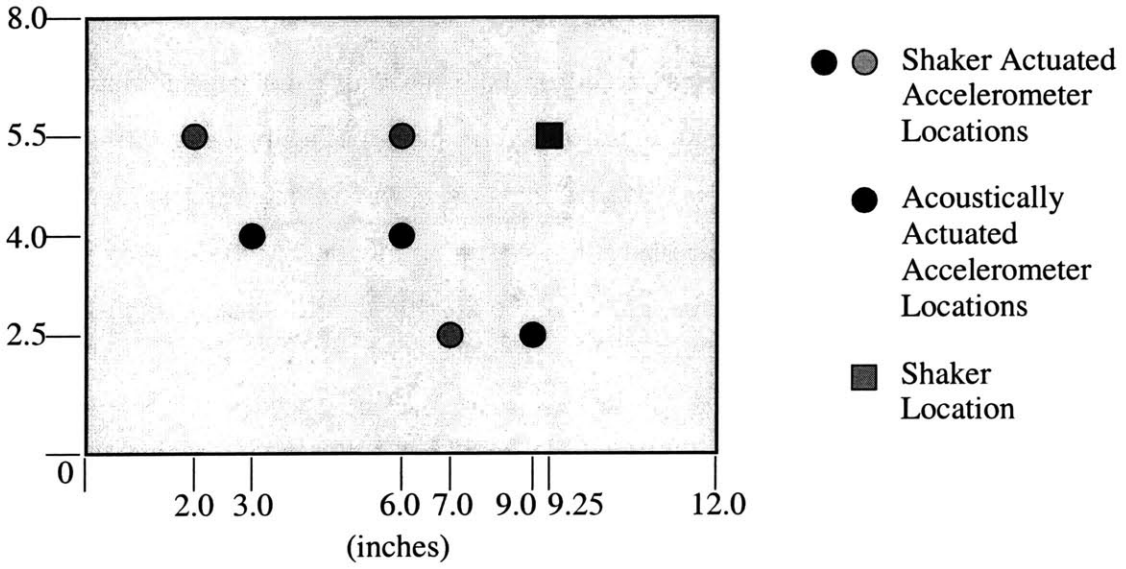

Figure 5.14 Illustration showing the locations of the accelerometers and shaker for the vibration and radiation experiments. More accelerometers were required to accurately perform the radiation experiments, and they were performed using a shaker actuator.

5.5.5 Dynamic Radiation Experiments

To determine the radiation index of the various panels, radiation experiments were performed on each of the curved and baseline panels. Particular emphasis was placed upon the mode-shaped panels because performance benefits were expected only for these designs. Six accelerometers were used to determine the average mean square velocity of the panels. The average mean square velocity was then used to determine the theoretical radiation power of an infinitely stiff cylinder of the same area as the panel designs. The actual power radiated from the panels was determined by calculating the average mean square of the pressure (as was discussed in Section 2.4.1). The pressure was measured at a radius of approximately 3 feet at four separate locations. The distance was chosen to maximize data coherence while still trying to maintain far-field measurements.

The radiation experiments were performed on the large testbed with the shaker actuator placed inside the testbed and the microphones placed outside the testbed. The radiation experiments were performed in the anechoic chamber. Again, the radiation experiments were performed on both the damped and undamped panel designs.

5.5.6 Dynamic Transmission Experiments

Transmission experiments were performed on both the small and large testbed. Directional transmission experiments were performed on the small testbed and diffuse experiments were performed on the larger reverberant testbed. A full range speaker was used as the actuator and was placed inside the testbeds. A microphone was also placed inside the testbeds, in addition to microphones placed at the near field (~12 inches), "mid-field" (~3 feet) and far field (~6 feet).

Again, the transmission experiments were performed inside the anechoic chamber. Transmission experiments were performed on all panel designs except for the multi-layer designs and the honeycomb baseline panels.

5.5.7 Laser Vibrometer Experiments

A scanning laser vibrometer, model PSV3, manufactured by Polytec was used to determine the exact mode shapes of the fundamental-mode-shaped panel. The laser vibrometer allowed the exact mode shapes to be determined so that the results could be compared to the finite element analysis results. This procedure was seen as necessary due to the importance of the mode-shaped panel design's dependence on the mode shapes in relation to acoustic radiation. This experiment was performed on the small testbed with acoustic actuation on the undamped panels only. Acoustic actuation was used to ensure that the acoustically coupling odd modes were excited. The experiments were performed on a flat panel with clamped boundary conditions and bolted boundary conditions, as well as a mode-shaped panel with clamped boundary conditions and bolted boundary conditions. Photographs of the experimental setup are shown in Figure 5.15.

Finally, it should be noted that all dynamic data was taken in the form of transfer functions and all calculations were performed in the frequency domain.

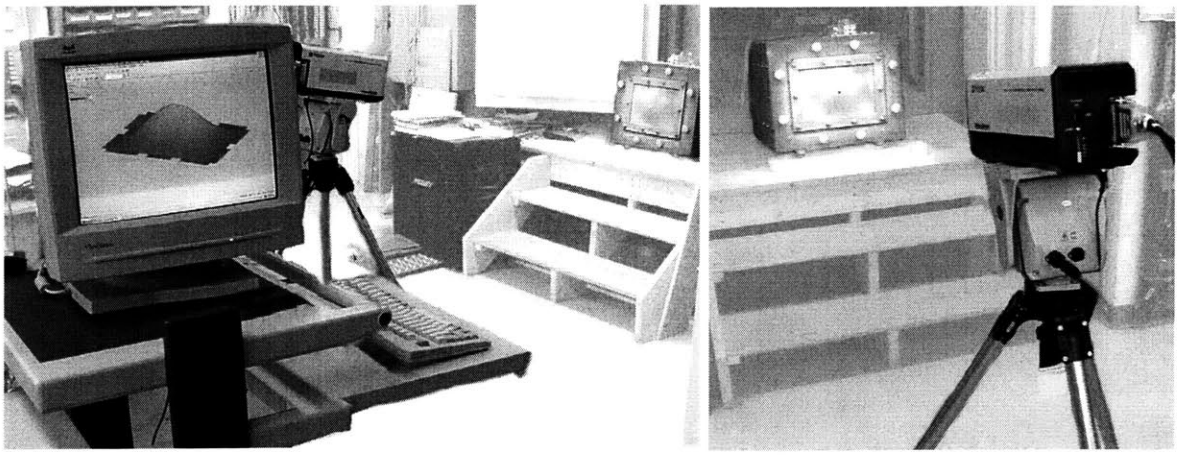

Figure 5.15 Photographs of the experimental setup for the laser vibrometer.

Chapter 6

EXPERIMENTAL RESULTS AND DISCUSSION

6.1 Experimental Summary and Data Reduction

To minimize confusion and maximize the digestibility of the data, only the most relevant data is presented in this chapter. Most of the dynamic data is presented in an octave average format so that the broadband data can be more easily understood and so that comparisons are more easily made. As was stated in Chapter 5, transfer functions or some derivative of transfer functions are presented for the dynamic data. Where appropriate the data is normalized by the equivalent flat panel experimental data, and sometimes averages are presented rather than showing all curves for every actuator sensor pair. All raw data can be found in Appendix C.

6.2 Static Stiffness Experiments

As stated in Chapter 5, static bending tests were performed on the multi-layer sandwich designs and equivalent honeycomb designs. The purpose of these experiments was to determine whether using a two-dimensionally curved panel as a core material, rather than honeycomb, provides similar static stiffness. The advantage being that forming two-dimensionally curved panels is simpler and far less expensive than manufacturing honeycomb. In addition, the two-dimensionally curved core designs are more easily manufactured into sandwich designs because they can be more easily made of a wider variety of

materials and the flat top and bottom surfaces of the two-dimensionally curved cores can be more easily fastened or adhered to the sandwiching layers.

To help understand the relative performance of the designs, and to more easily compare the data, the results were normalized by theoretical results assuming an idealized sandwich design. The idealized sandwich design assumes the same outer material and overall dimensions for each panel as well as ideal core properties (i.e. assumes a zero mass core that provides infinite compressive stiffness but zero bending stiffness). The normalization also made it possible to accurately compare designs of slightly varying thickness and dimensions. In addition, shear was assumed to be non-negligible, and the shear calculation was based on a box section with a web thickness equal to that of the core material if it were compressed into a web. The shear calculation likely introduces some minor error for the thicker designs but provides a reasonable estimate of the actual deflection.

The material properties of the flat panels used in the experiment were determined by analyzing thick sheets of the material in the exact same bending test setup used for the experiments. The results of these calibration experiments agreed well with the material properties given in the literature [Avallone, 1996]. In all cases the epoxy was assumed to provide negligible effect on the results.

Between 7 and 15 points were taken for each experiment, and multiple experiments were performed for each panel to ensure repeatability. Lines were then fit to the data to determine the stiffness (related to the slope). The data is reliable as "R-Squared" (Pearson product correlation coefficient) values greater than 0.99 were obtained. In general, "R-Squared" values greater than 0.95 indicate reliable data. Tests were performed in directions parallel to both boundaries (*i.e.* along the length and width).

6.2.1 Multi-layer Sandwich Design Results

The first multi-layer sandwich panels that were analyzed utilized a 3/8 inch thick core. Three panel configurations were analyzed: polypropylene honeycomb core baseline, 0.06

Four Point Bending Results

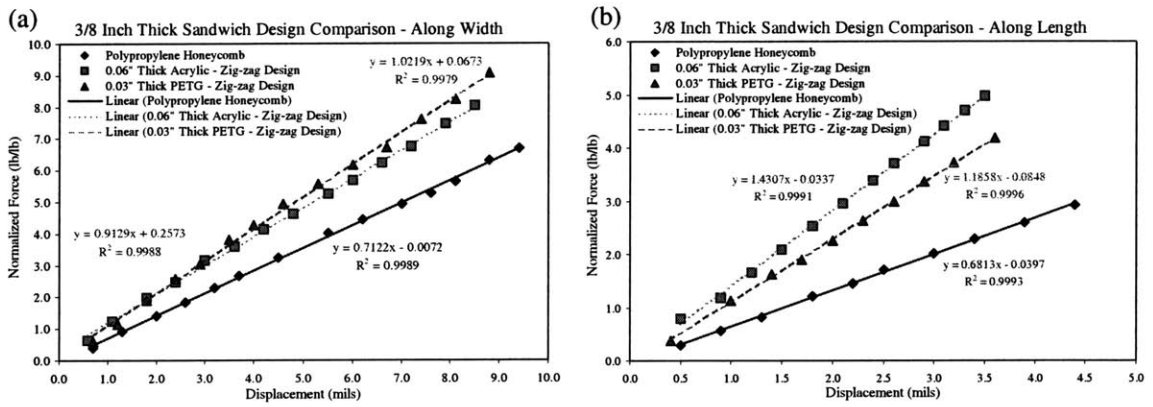

Figure 6.1 Graphs of the stiffness data for the four point bending tests performed on the sandwich panels with 3/8 inch thick cores.

Three Point Bending Results

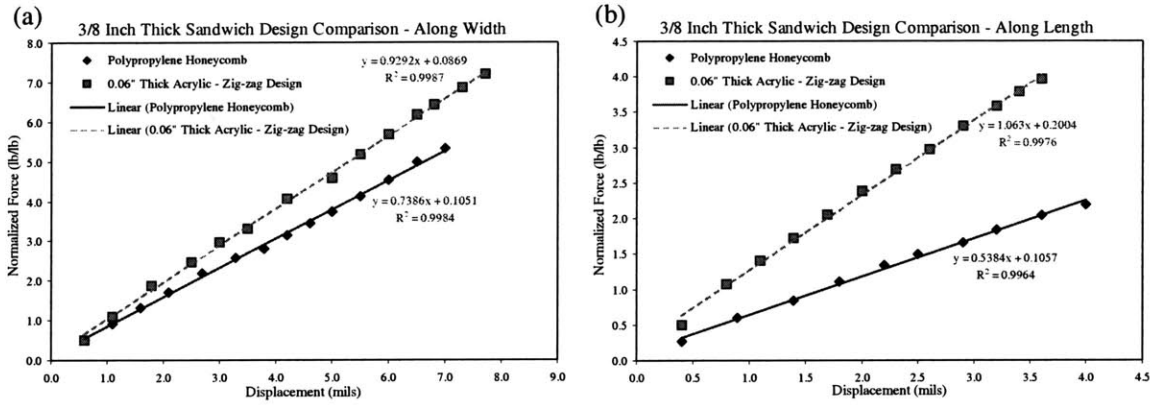

Figure 6.2 Graphs of the stiffness data for the three point bending tests performed on the two of the sandwich panels with 3/8 inch thick cores.

inch thick two-dimensionally curved Zig-zag acrylic core, and 0.03 inch thick two-dimensionally curved Zig-zag PETG (copolyester) core. The results for these tests are shown in Figure 6.1.

In addition to the four point bending tests a three point bending test was performed on the 3/8 inch thick core materials for the polypropylene honeycomb core baseline and the 0.06 inch thick two-dimensionally curved Zig-zag acrylic core. This test was performed to

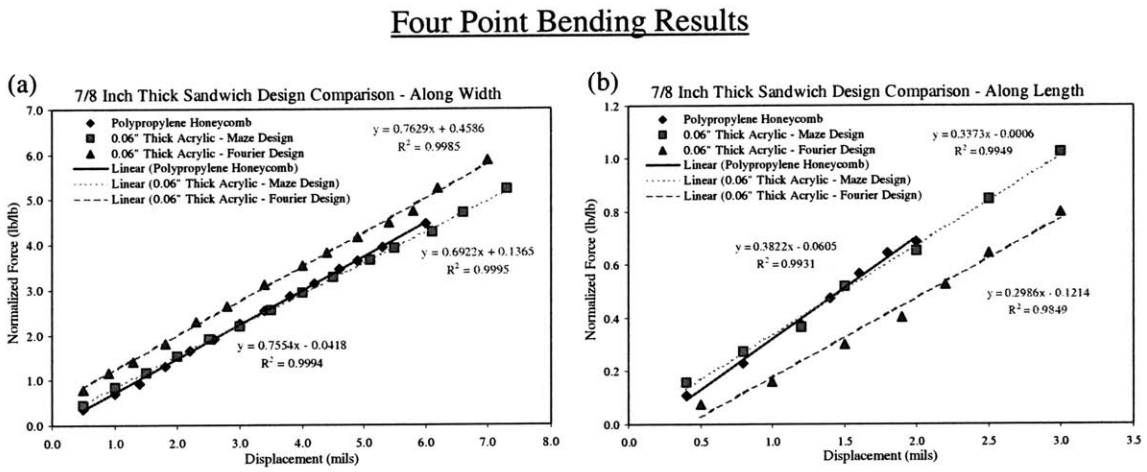

Figure 6.3 Graphs of the stiffness data for the four point bending tests performed on the sandwich panels with 7/8 inch thick cores.

determine if there was a significant difference in performance when the designs were placed in a higher shear force type of loading. The results for these tests are shown in Figure 6.2.

To gain a more complete understanding of using the two-dimensionally curved panels as a sandwich core, four point bending experiments were also performed on panels with 7/8 inch thick cores. The two-dimensionally curved cores are merely the panels used for the other experiments epoxied between two sandwiching layers. In other words, they were not designed specifically to act as a core, unlike the 3/8 inch thick core. Again, a sandwich panel with a honeycomb core was used as a comparison baseline. Also, the results are again normalized by the theoretical bending stiffness of an idealized sandwich design. The results for these tests are shown in Figure 6.3.

6.2.2 Summary and Discussion

The results for the bending experiments are summarized in Table 6.1. The most important result from these experiments is that the two-dimensionally curved core designs provide comparable performance to that of the honeycomb core designs. In fact, the two-dimensionally curved cores appear to exceed the performance of the honeycomb for the 3/8

TABLE 6.1 Summary of the static bending experiments.

Sandwich Design (Core Material)	**Normalized Stiffness** 1.0 Represents Ideal	**% Deflection Due to Shear** (Estimated)	**Weight** (lbs)	R^2	**Data Points**
4 POINT BENDING EXPERIMENTS WITH 3/8 INCH CORE (W = along width, L = along length)					
Honeycomb	0.71 (W)	4.6	0.85	0.999	14
(Polypropylene)	0.68 (L)	10.7		0.999	10
Zig-zag	1.02 (W)	4.3	0.80	0.998	14
(PETG)	1.19 (L)	10.0		0.999	10
Zig-zag	0.91 (W)	2.7	0.90	0.999	14
(Acrylic)	1.43 (L)	6.4		0.999	10
3 POINT BENDING EXPERIMENTS WITH 3/8 INCH CORE					
Honeycomb	0.74 (W)	6.1	0.85	0.998	14
(Polypropylene)	0.54 (L)	13.7		0.996	10
Zig-zag	0.93 (W)	3.6	0.90	0.999	14
(Acrylic)	1.06 (L)	8.4		0.998	12
4 POINT BENDING EXPERIMENTS WITH 7/8 INCH CORE					
Honeycomb	0.76 (W)	12.0	1.00	0.999	14
(Polypropylene)	0.38 (L)	25.4		0.993	7
Maze	0.69 (W)	13.4	0.90	0.999	14
(Acrylic)	0.35 (L)	27.8		0.995	7
Fourier	0.76 (W)	13.4	0.90	0.998	14
(Acrylic)	0.30 (L)	27.8		0.985	7

thick core comparison, and in certain cases exceed the ideal calculated stiffness. This is possible because the core of the two-dimensionally curved designs provide additional bending stiffness, where the ideal calculations assume that the cores provide no additional bending stiffness. A likely reason why the two-dimensionally curved cores can provide increased stiffness over a honeycomb core is because the two-dimensionally curved cores distribute a significant amount of its material towards the outer sandwich layers, thereby adding appreciably to the second bending moment of inertia of the system. This was especially true of the Zig-zag design because it was designed specifically to be a core and had a higher ratio of material distributed to the outer extremes. Note that the unusually low

values for the 7/8 inch thick cores along the length is likely because of a greater degree of deflection due to shear than is accounted for with the shear deflection factor.

Another important result of the static bending tests is that the orthotropy of a core is likely to lead to a more orthotropic sandwich design. This is evident because the Zig-zag panel independently demonstrates very orthotropic behavior. It is much more compliant when bending along the width, than when bending along the length, by at least an order of magnitude.* This is also true when it is used as a sandwich core, although to a much lesser extent. This is important because it indicates the necessity to have a nearly isotropic two-dimensionally curved core in order to achieve an isotropic sandwich design. A properly designed maze-like pattern could likely achieve this goal.

Other important factors not considered directly in the results of Table 6.1 are the cost and weight of the sandwich structure. By definition a sandwich design should be as light as possible. One can see that the designs that utilize the two-dimensionally curved cores have comparable weight to that of the honeycomb design. More importantly, when considering the cost of the core material, the significance of the two-dimensionally curved designs become more evident. Due to the fact that the curved designs are made of a single sheet of material formed with inexpensive and easy to mass produce manufacturing processes, the two-dimensionally curved sandwich designs can lead to much more affordable structures. The weight and cost of the designs can be accounted for by including weight and cost factors in the performance metric

$$P_w = \frac{\text{Normalized Bending Stiffness}}{\text{Panel Weight}} \tag{6.1}$$

$$P_{wc} = \frac{\text{Normalized Bending Stiffness}}{\text{Panel Weight} \times \text{Panel Cost}} \tag{6.2}$$

* The fact that the Zig-zag panel is highly orthotropic was not predicted by the simple analytic models discussed in Chapter 3 and indicates the inadequacy of these models. The folds of the Zig-zag design led to bending at the peaks and a highly compliant panel along the width, even though the design used altering amplitudes in the periodic design to keep the troughs and peaks from aligning.

TABLE 6.2 Performance metrics considering cost and weight of core material.

Sandwich Design (Core Material)	Normalized Stiffness 1.0 Represents Ideal	Weight (lbs)	P_w (1/lbs)	Estimated Cost ($)*	P_{wc} (1/($lbs)
4 POINT BENDING EXPERIMENTS WITH 3/8 INCH CORE (W = along width, L = along length)					
Honeycomb	0.71 (W)	0.85	0.86	8.0	0.11
(Polypropylene)	0.68 (L)		0.8		0.10
Zig-zag	1.02 (W)	0.80	1.28	3.5	0.37
(PETG)	1.19 (L)		1.49		0.43
Zig-zag	0.91 (W)	0.90	1.01	3.5	0.29
(Acrylic)	1.43 (L)		1.59		0.45
3 POINT BENDING EXPERIMENTS WITH 3/8 INCH CORE					
Honeycomb	0.74 (W)	0.85	0.87	8.0	0.11
(Polypropylene)	0.54 (L)		0.64		0.08
Zig-zag	0.93 (W)	0.90	1.03	3.5	0.29
(Acrylic)	1.06 (L)		1.18		0.34
4 POINT BENDING EXPERIMENTS WITH 7/8 INCH CORE					
Honeycomb	0.76 (W)	1.00	0.76	10.0	0.08
(Polypropylene)	0.38 (L)		0.38		0.04
Maze	0.69 (W)	0.90	0.77	3.5	0.22
(Acrylic)	0.35 (L)		0.39		0.11
Fourier	0.76 (W)	0.90	0.84	3.5	0.24
(Acrylic)	0.30 (L)		0.33		0.09

* Cost estimates are for 0.5 inch by 12 inch by 12 inch polycarbonate sandwich panel, based on production of 10,000 square feet of assembled sandwich panel. Price difference will generally increase with increasing thickness. Price difference for Aluminum is approximately three-quarters to half of that for plastic [Cerat, 2000; Tanis, 2000; Walsh, 2000].

The results with the cost and weight factors are shown in Table 6.2. As one can see the performance of the two-dimensionally curved sandwich panels increases significantly once cost is considered. Not only does this mean that otherwise very expensive structures that utilize honeycomb, such as air and spacecraft, can be produced for less cost, but it also means that the amount of material that is used to create a quasi-isotropic sandwich structure can be greatly reduced in applications such as corrugated cardboard.

6.3 Vibration Experiments

To analyze the vibration characteristics of the panels, accelerometers were placed on the panels at several locations and the panels were actuated. In one scenario the panels were actuated with a shaker, located to maximize the number modes excited. Another set of experiments were performed with the use of a speaker as the actuator. Using a speaker as the actuator leads to a greater likelihood that lower order odd modes dominate the lower frequency response. This is helpful in determining the radiation and transmission characteristics of a panel, as they relate to vibration. All vibration experiments were performed on the small testbed.

6.3.1 Mode-shaped Designs

The mode-shaped designs were actuated with both the speaker and shaker. Both damped and undamped panels were studied. The boundary conditions for all the panels in these experiments were clamped.

Undamped Panels

First, undamped panels were analyzed. To help minimize the amount of data presented in this chapter only the transfer functions for the shaker actuated panel are presented. The results for both the shaker actuated and speaker actuated panels are summarized in a table in Section 6.3.4. Both the acceleration and displacement data is provided. The acceleration provides information about the relative forces the panel undergoes, while the displacement data provides information about the relative strains and stresses. Both are valuable in terms of vibration. The results of the average undamped shaker actuated mode-shaped panels are shown in Figure 6.4. The raw data and the data for the speaker actuated panels are located in Appendix C.

Damped Panels

Next, damped panels were analyzed. Again, to minimize the amount of data presented in this chapter only the transfer functions for the shaker actuated panel are presented. The

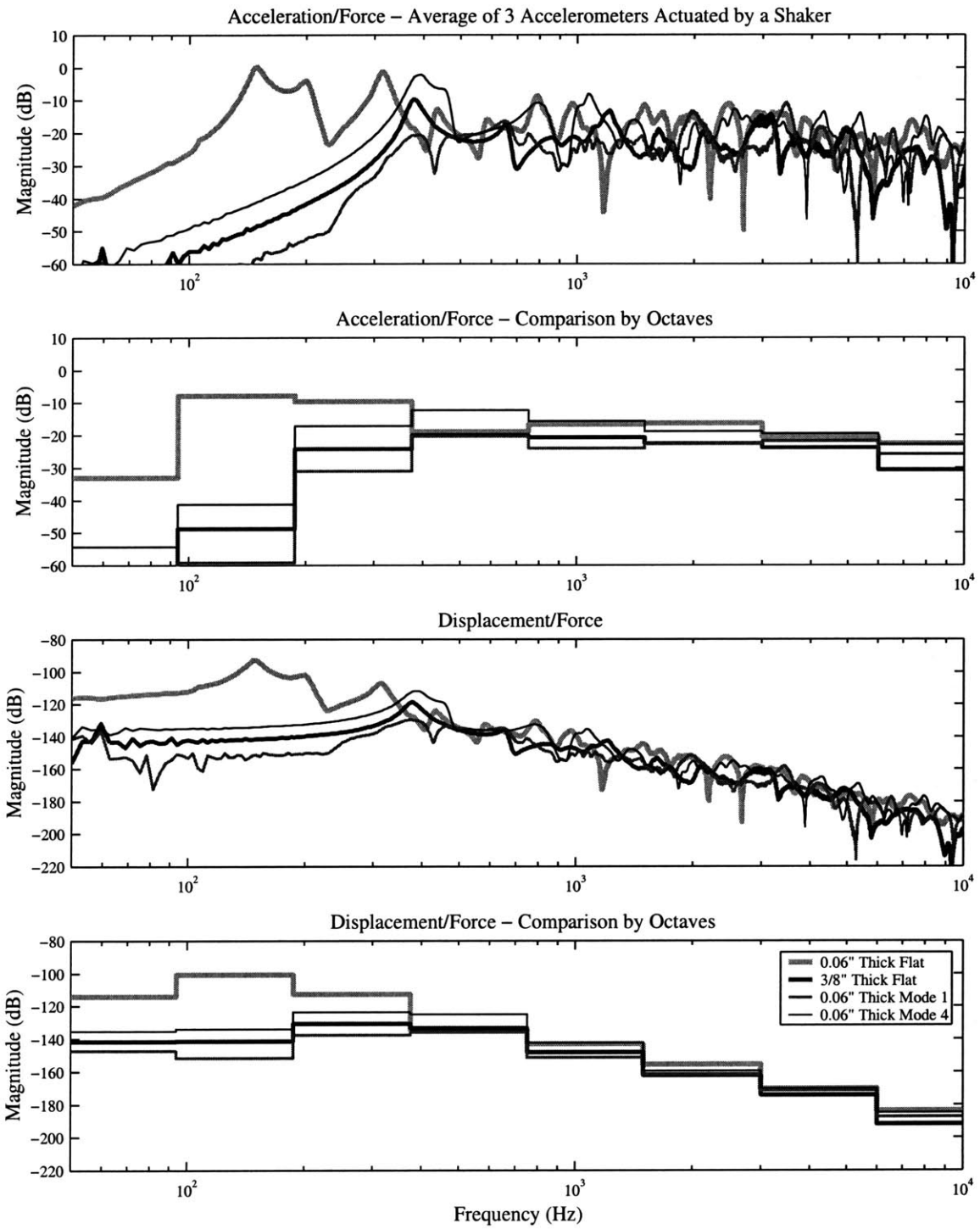

Figure 6.4 Graphs of the transfer functions for the undamped mode-shaped panels and the baseline flat panels for acceleration and displacement with shaker actuation. The plots are presented as averages over octaves to allow for easy comparison.

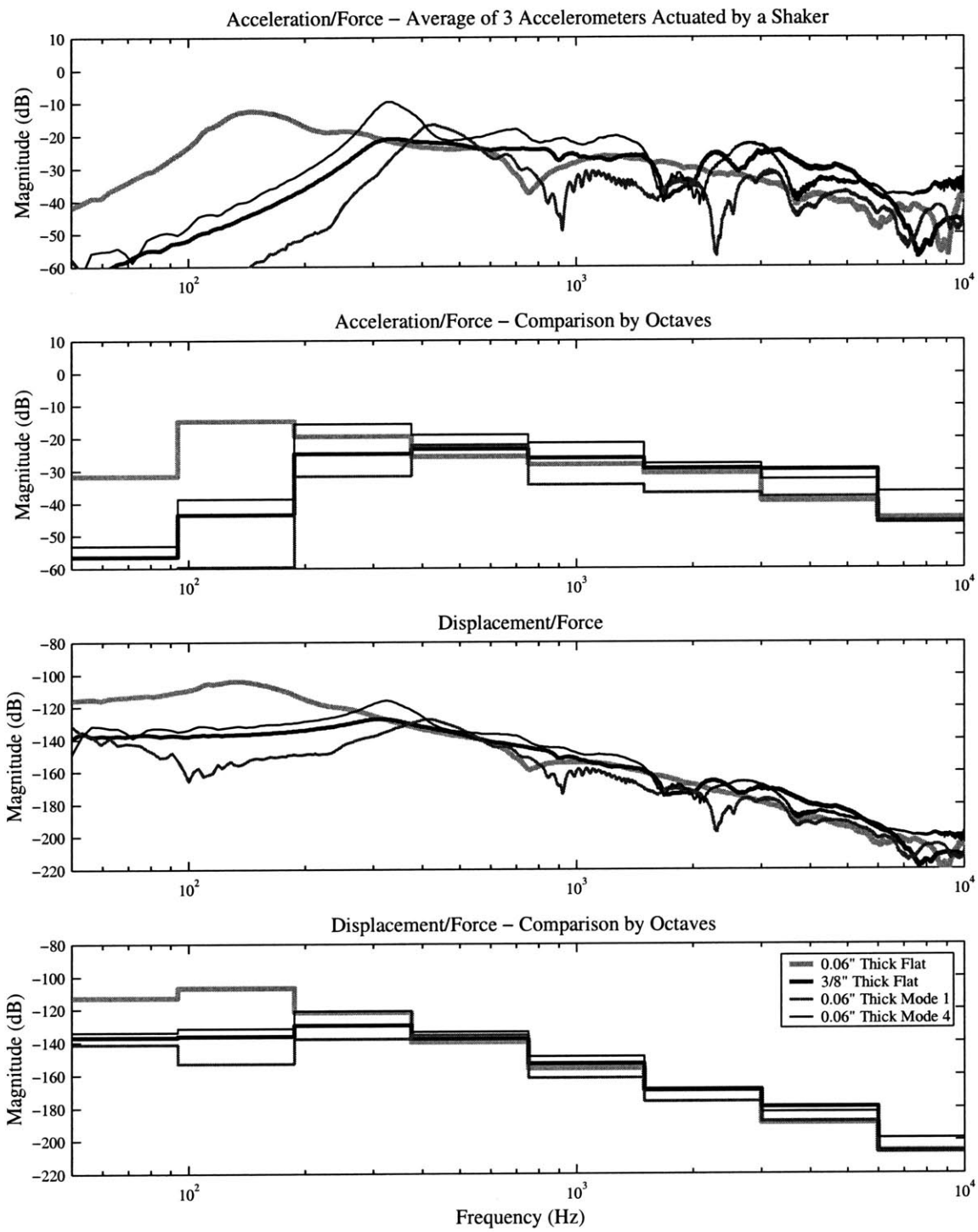

Figure 6.5 Graphs of the transfer functions for the damped mode-shaped panels and the baseline flat panels for acceleration and displacement with shaker actuation. The plots are presented as averages over octaves to allow for easy comparison.

results for both the shaker actuated and speaker actuated panels are summarized in a table in Section 6.3.4. Again, the acceleration and displacement data is provided. The results of the average damped shaker actuated mode-shaped panels are shown in Figure 6.5. The raw data and the data for the speaker actuated panels are located in Appendix C.

6.3.2 Quasi-isotropic Designs

The quasi-isotropic designs were also actuated with both the speaker and shaker. Again, both damped and undamped panels were studied. The boundary conditions for all the panels in these experiments were also clamped.

Undamped Panels

First, undamped panels were analyzed. To help minimize the amount of data presented in this chapter only the transfer functions for the shaker actuated panel are presented. The results for both the shaker actuated and speaker actuated panels are summarized in a table in Section 6.3.4. Again, both the acceleration and displacement data is provided. The results of the average undamped shaker actuated mode-shaped panels are shown in Figure 6.4. The raw data and the data for the speaker actuated panels are located in Appendix C.

Damped Panels

Next, damped panels were analyzed. Again, to minimize the amount of data presented in this chapter only the transfer functions for the shaker actuated panel are presented. The results for both the shaker actuated and speaker actuated panels are summarized in a table in Section 6.3.4. Again, the acceleration and displacement data is provided. The results of the average damped shaker actuated mode-shaped panels are shown in Figure 6.5. The raw data and the data for the speaker actuated panels are located in Appendix C.

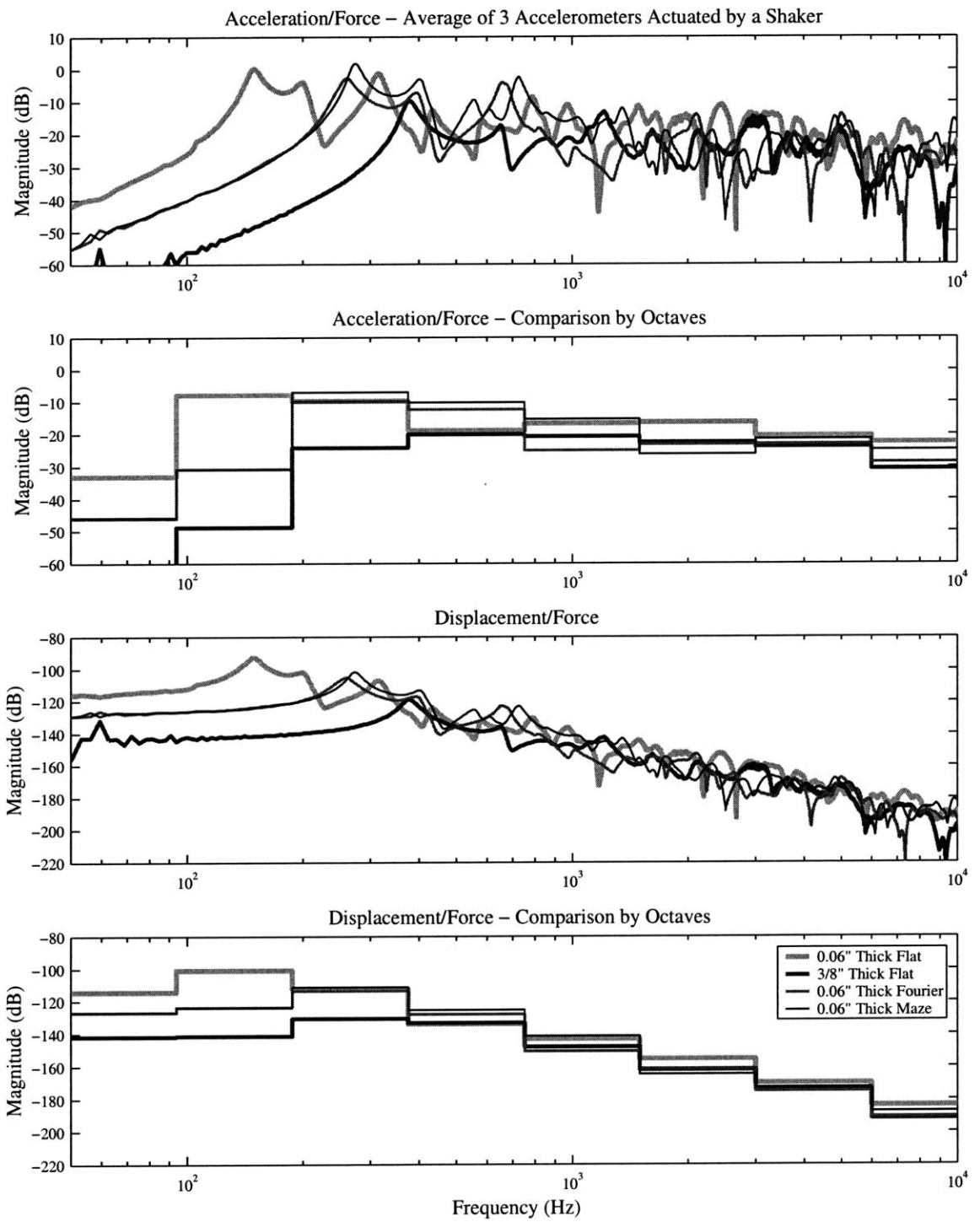

Figure 6.6 Graphs of the transfer functions for the undamped quasi-isotropic panels and the baseline flat panels for acceleration and displacement with shaker actuation. The plots are presented as averages over octaves to allow for easy comparison.

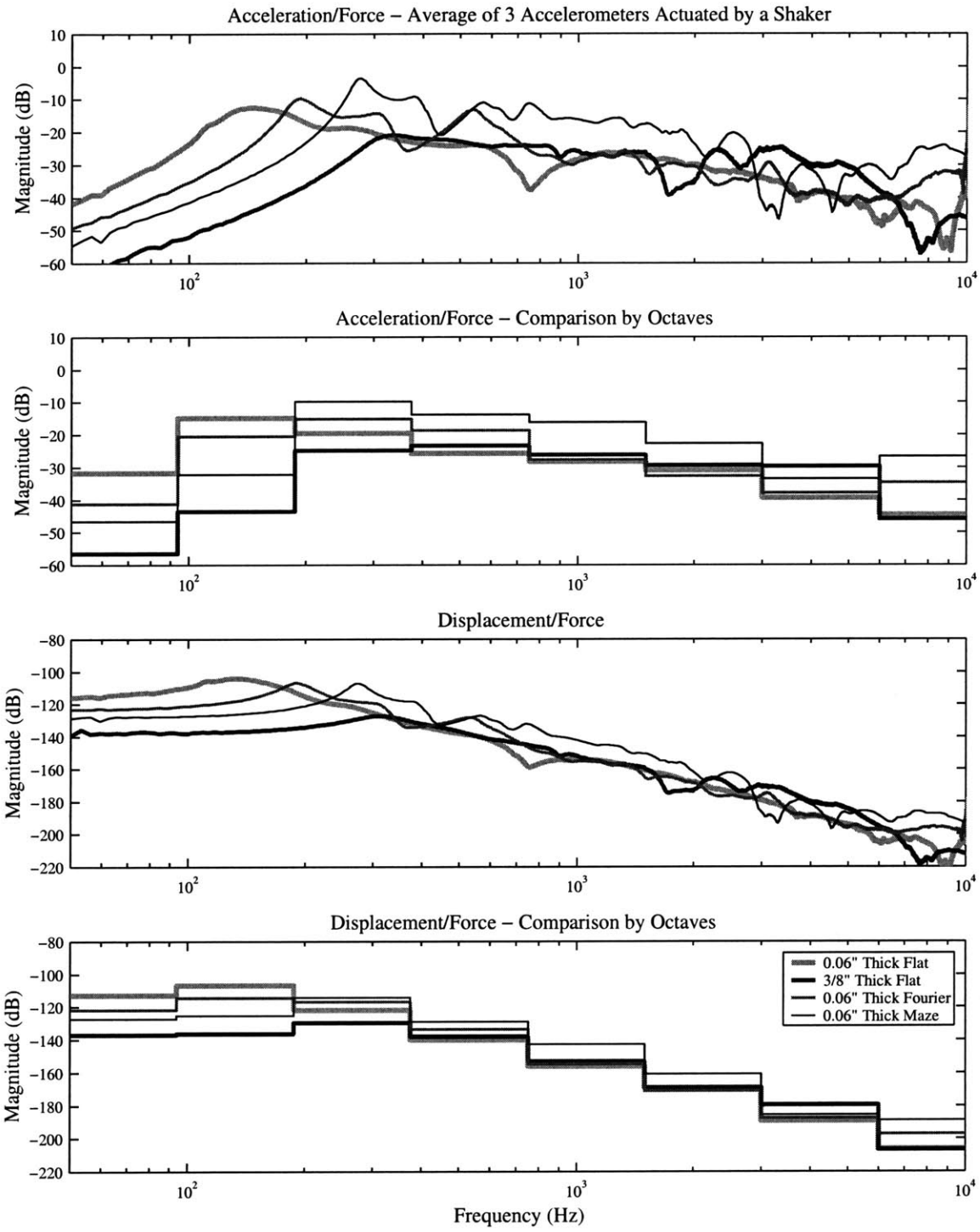

Figure 6.7 Graphs of the transfer functions for the damped quasi-isotropic panels and the baseline flat panels for acceleration and displacement with shaker actuation. The plots are presented as averages over octaves to allow for easy comparison.

6.3.3 Multi-layer Designs

To analyze the dynamic characteristics of the multi-layer sandwich designs, shaker experiments were performed on the designs. These experiments allow for a comparison of the modal content of the designs, and of the fundamental frequency. It should be noted that the Zig-zag design is slightly thinner than the honeycomb panel. In the static tests this could be accounted for by normalizing by the ideal static stiffness. To normalize the dynamic data would likely lead to greater confusion, therefore the data is presented as tested and the reader should be aware of the fact that the Zig-zag design is about 0.05 inches thinner than the honeycomb panel.

Undamped Panels

These experiments were performed on the undamped panels only. The results are presented in Figure 6.8. Although damped designs were manufactured and some preliminary experiments were performed, it was determined that the damped data provided little extra insight into the behavior of the designs. This data can be found in Appendix C. It should also be noted that the sandwich panels were tested on a different occasion with different gains than the above panels. The flat panels were retested with the same gains as the sandwich panels to provide a comparison and this is why the flat panel designs have different DC values than in the previous tables.

6.3.4 Summary and Discussion

The results for the vibration experiments are summarized in Table 6.3, Table 6.4, and Table 6.5. The shaker actuated data for the single layer panels (non-sandwich) is shown in Table 6.3, and the speaker actuated data is shown in Table 6.4. Included in these two tables are the RMS average over the broadband range (50 - 10,000 Hz), the maximum value, the difference between the flat panel and the curved panels for the RMS and maximum value, and the estimated loss factor. The sandwich panel data is located in Table 6.5.

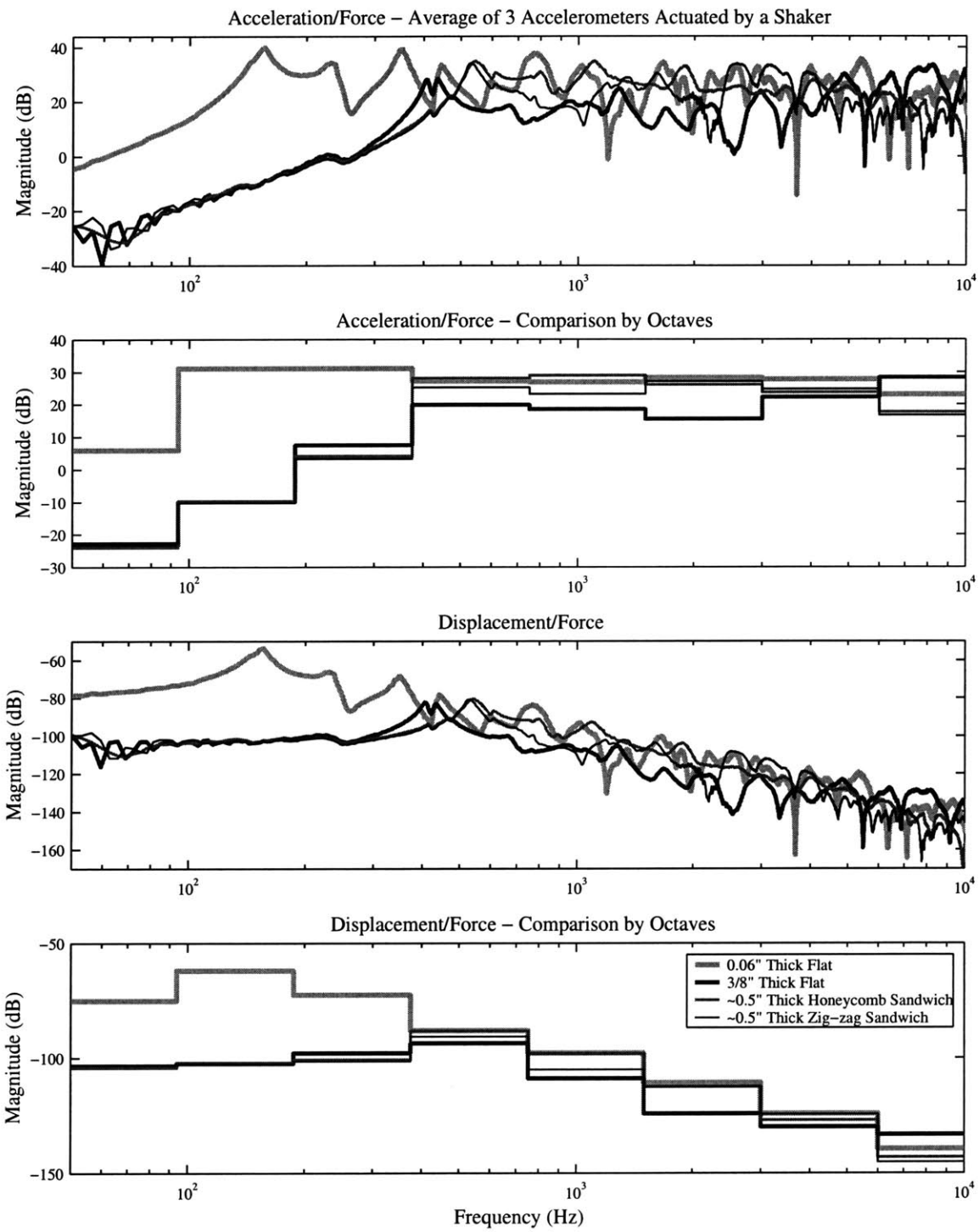

Figure 6.8 Graphs of the transfer functions for the undamped multi-layer sandwich panels and the baseline flat panels for acceleration and displacement with shaker actuation. The plots are presented as averages over octaves to allow for easy comparison.

TABLE 6.3 Summary of results for the *shaker* actuated data. Numbers in parentheses indicate a negative difference in performance (*i.e.* a worse performance). Difference numbers indicate the 0.06 inch thick flat panel performance minus the other panels' performance. Loss factors are calculated from experimental measurements and are based on at least 5 modes.

Panel Design	RMS (dB)	Difference (dB)	Max (dB)	Difference (dB)	Loss Factor
ACCELERATION DATA - UNDAMPED PANELS					
0.06" Flat	22.6	NA	0.3	NA	0.068
3/8" Flat	16.6	**6.0**	-9.6	**9.9**	0.070
0.06" Mode 1 Shaped	17.9	**4.7**	-10.7	**11.0**	0.10
0.06" Mode 4 Shaped	22.2	**0.4**	-2.1	**2.4**	0.092
0.06" Fourier Design	20.0	**2.6**	-2.7	**3.0**	0.078
0.06" Maze Design	22.6	**0.0**	1.9	**(1.6)**	0.078
DISPLACEMENT DATA - UNDAMPED PANELS					
0.06" Flat	-79.0	NA	-92.8	NA	0.068
3/8" Flat	-101.7	**22.7**	-118.7	**25.9**	0.070
0.06" Mode 1 Shaped	-107.7	**28.7**	-129.6	**36.8**	0.10
0.06" Mode 4 Shaped	-93.5	**14.5**	-111.7	**18.9**	0.092
0.06" Fourier Design	-88.8	**9.8**	-105.3	**12.5**	0.078
0.06" Maze Design	-86.2	**7.2**	-101.7	**8.9**	0.078
ACCELERATION DATA - DAMPED PANELS					
0.06" Flat	9.8	NA	-12.5	NA	0.48
3/8" Flat	10.1	**(0.3)**	-20.1	**7.6**	0.36
0.06" Mode 1 Shaped	6.5	**3.3**	-16.6	**4.1**	0.28
0.06" Mode 4 Shaped	13.8	**(4.0)**	-9.5	**(3.0)**	0.22
0.06" Fourier Design	12.7	**(2.9)**	-9.7	**(2.8)**	0.16
0.06" Maze Design	19.1	**(9.3)**	-3.6	**(7.9)**	0.14
DISPLACEMENT DATA - DAMPED PANELS					
0.06" Flat	-86.1	NA	-104.1	NA	0.48
3/8" Flat	-105.0	**18.9**	-127.2	**23.1**	0.36
0.06" Mode 1 Shaped	-106.6	**20.5**	-127.6	**23.5**	0.28
0.06" Mode 4 Shaped	-96.8	**10.7**	-116.1	**12.0**	0.22
0.06" Fourier Design	-89.8	**3.7**	-106.9	**2.8**	0.16
0.06" Maze Design	-89.9	**3.8**	-107.2	**3.1**	0.14

The vibration results indicate that the fundamental-mode-shaped panel demonstrates the best performance of the curved panels for vibration reduction. This is true for broadband as well as peak reduction. The performance improvement is less dramatic when the fundamental-mode-shaped panel is acoustically actuated, compared to the flat acoustically actuated panel. There are many possible reasons for this phenomenon. Two plausible possibilities are: that the flat panel is less excited by the acoustic actuation because a more significant portion of the modes of the flat panel are even modes; the curved panels may lead to some multiple incidence of the impinging acoustic waves.

The panel shaped as the next odd mode, the fourth mode, did not perform nearly as well as the fundamental-mode-shaped panel. This was not an unexpected result. The amount of influence the fundamental mode has over a panel's dynamics is often far greater than any of the higher modes. There are two main reasons for this phenomenon. One, the greatest gains in reducing vibration can often be made at the lower frequencies and therefore increasing the fundamental frequency is likely to lead a reduction in vibration. By design, the fundamental-mode-shaped panel raises the fundamental frequency much greater than the fourth-mode-shaped panel. Two, the ability to inhibit the fundamental mode from forming in its most detrimental form is likely to reduce the amount of vibration significantly. This is because the fundamental mode of a flat panel almost always demonstrates the greatest displacement and acceleration, often much more so than any of the higher-order modes.

The quasi-isotropic mode designs with the higher order curvature were successful in raising the natural frequencies, but were much less effective at reducing the acceleration and displacement when compared to the fundamental-mode-shaped panel. In several cases the performance was actually worse than the flat panel. This is not unexpected since the designs were not meant to change the mode shapes of the system. In fact, a truly isotropic design should have the same mode shapes as a flat panel. The poorer performance when actuated by a speaker could again be due to the multiple incidence of the impinging acoustic waves.

TABLE 6.4 Summary of results for the *speaker* actuated data. Numbers in parentheses indicate a negative difference in performance (*i.e.* a worse performance). Difference numbers indicate the 0.06 inch thick flat panel performance minus the other panels' performance. Loss factors are calculated from experimental measurements and are based on at least 5 modes.

Panel Design	RMS (dB)	Difference (dB)	Max (dB)	Difference (dB)	Loss Factor
ACCELERATION DATA - UNDAMPED PANELS					
0.06" Flat	17.0	**NA**	-7.6	**NA**	0.067
3/8" Flat	10.4	**6.6**	-8.2	**0.6**	0.091
0.06" Mode 1 Shaped	15.7	**1.3**	-12.2	**4.6**	0.10
0.06" Mode 4 Shaped	17.7	**(0.7)**	-2.7	**(4.9)**	0.082
0.06" Fourier Design	17.2	**(0.2)**	-8.0	**0.4**	0.068
0.06" Maze Design	18.7	**(1.7)**	-5.0	**(2.6)**	0.074
DISPLACEMENT DATA - UNDAMPED PANELS					
0.06" Flat	-87.7	**NA**	-101.1	**NA**	0.067
3/8" Flat	-101.2	**13.5**	-117.8	**16.7**	0.091
0.06" Mode 1 Shaped	-101.2	**13.5**	-121.1	**20.0**	0.10
0.06" Mode 4 Shaped	-96.4	**8.7**	-114.3	**13.2**	0.082
0.06" Fourier Design	-94.7	**7.0**	-111.4	**10.3**	0.068
0.06" Maze Design	-93.5	**5.8**	-109.5	**8.4**	0.074
ACCELERATION DATA - DAMPED PANELS					
0.06" Flat	11.3	**NA**	-18.5	**NA**	0.31
3/8" Flat	5.9	**5.4**	-21.4	**2.9**	0.23
0.06" Mode 1 Shaped	12.6	**1.3**	-17.1	**(1.4)**	0.24
0.06" Mode 4 Shaped	12.4	**(1.1)**	-10.0	**(8.5)**	0.16
0.06" Fourier Design	12.5	**(1.2)**	-16.3	**(2.2)**	0.16
0.06" Maze Design	15.2	**(3.9)**	-9.8	**(8.7)**	0.12
DISPLACEMENT DATA - DAMPED PANELS					
0.06" Flat	-92.6	**NA**	-112.2	**NA**	0.31
3/8" Flat	-106.8	**14.2**	-125.0	**12.8**	0.23
0.06" Mode 1 Shaped	-105.8	**13.2**	-127.1	**14.9**	0.24
0.06" Mode 4 Shaped	-98.6	**6.0**	-118.2	**6.0**	0.16
0.06" Fourier Design	-96.6	**4.0**	-114.6	**2.4**	0.16
0.06" Maze Design	-96.6	**4.0**	-114.4	**2.2**	0.12

TABLE 6.5 Summary of results for the *shaker* actuated data for the baseline and sandwich panels. The sandwich panels have a 3/8 inch core with two 0.06 inch sandwiching layers.

Panel Design	RMS Acceleration (dB)	RMS Displacement (dB)	Max Acceleration (dB)	Max Displacement (dB)
UNDAMPED PANELS ONLY				
0.06" Flat	67.8	-40.0	40.1	-53.7
3/8" Flat	64.2	-64.6	33.6	-82.3
0.5" Honeycomb Sandwich	64.4	-60.4	35.0	-80.4
0.06" Zig-zag Sandwich	64.9	-62.6	34.2	-80.8

The curvature combined with the constrained damping proved insignificant, if not detrimental. The damping of the flat panels was significantly increased by the constrained damping layer. The damping of the mode-shaped designs appear also to be significantly increased, if not as much as the flat panel. But the more dramatically curved panels were not significantly altered by the constrained damping layer. Several possible reasons may explain why this is so. The more dramatically curved panels appeared to delaminate during the forming process, thereby possibly inhibiting the constrained damping mechanism. The forming may have also redistributed the constrained damping layer (the vacuum forming process caused the constrained damping material to melt) and lessened its effectiveness. It is also possible that the shape may have led to some of the damping inhibiting deformation discussed in Section 3.8. Many other possible reasons may explain why the combination of extreme curvature and constrained damping did not have the desired effect. It can be concluded that extreme curvature and constrained layer damping is ineffective for the vacuum formed Maze and Fourier shapes. The loss factors for the panels were determined by using Equation 2.47 applied to several modes of several transfer functions and averaging.

The sandwich vibration results demonstrate that the two-dimensionally curved core and the honeycomb core provide nearly identical dynamic performance. The modal placement and content for the two designs is very similar. The data indicates that the acceleration and displacement of the two-dimensionally curved panel slightly outperforms that of the

honeycomb core. This agrees with the results of the static tests. The dynamic analysis of the sandwich panels further proves that the two-dimensionally curved core can serve as a replacement for honeycomb cores.

6.4 Radiation Experiments

Next, radiation experiments were performed to compare the radiation index of the panel designs. The radiation experiments were performed on the large testbed by placing a shaker inside the large testbed, in contact with the panel, and measuring the radiated sound power with microphones at the far field inside the anechoic chamber. The velocity of the panel was determined by measuring the acceleration at six unique locations (the acceleration signal was integrated to determine velocity). The pressure was measured at four unique locations at a constant radius. Both the radiation index and the radiated acoustic power are presented. Again the raw data is contained in Appendix C.

6.4.1 Mode-shaped Designs

Again, the experiments were performed on the fundamental-mode-shaped panel and the fourth-mode-shaped panel. The experiments were performed on both the damped and undamped panels. The boundary conditions for all the panels in these experiments were clamped. To ensure repeatability and accuracy of the data, the shaker was placed normal to the surface of the mode-shaped panels.

Undamped Panels

The radiation experimental results for the undamped panels are located in Figure 6.9. For the undamped mode designs the coherence of the data was acceptable, but the pressure measurements demonstrated minor degradation of the coherence at higher frequencies. The radiated acoustic power shown in the plots is the numerator in the radiation index calculations, and is merely the pressure to force transfer function squared times a constant.

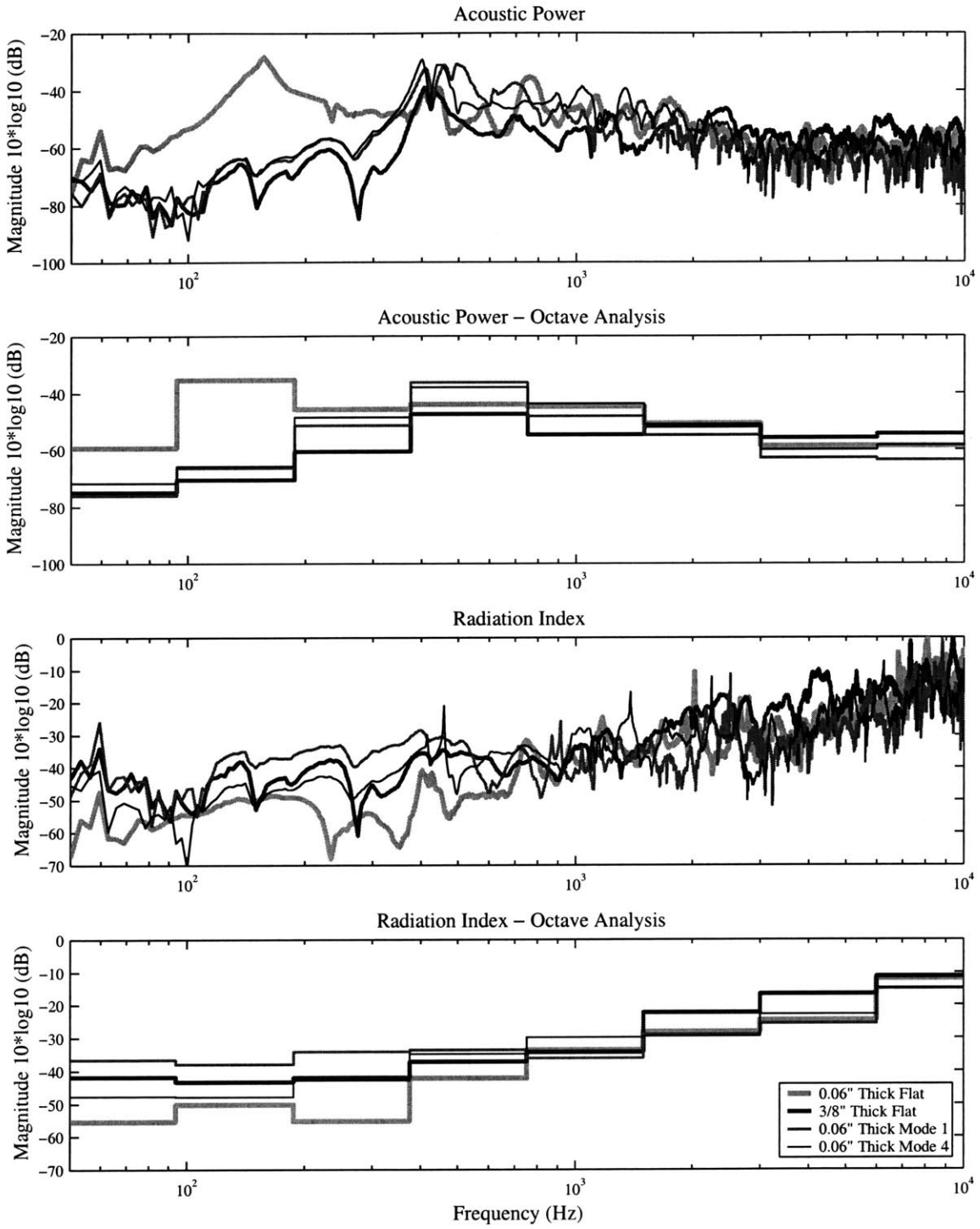

Figure 6.9 Plots of the acoustic power transfer function ((pressure/force)^2) and radiation index for the undamped mode-shaped panels and the undamped baseline flat panels. The plots are presented as averages over octaves to allow for easy comparison.

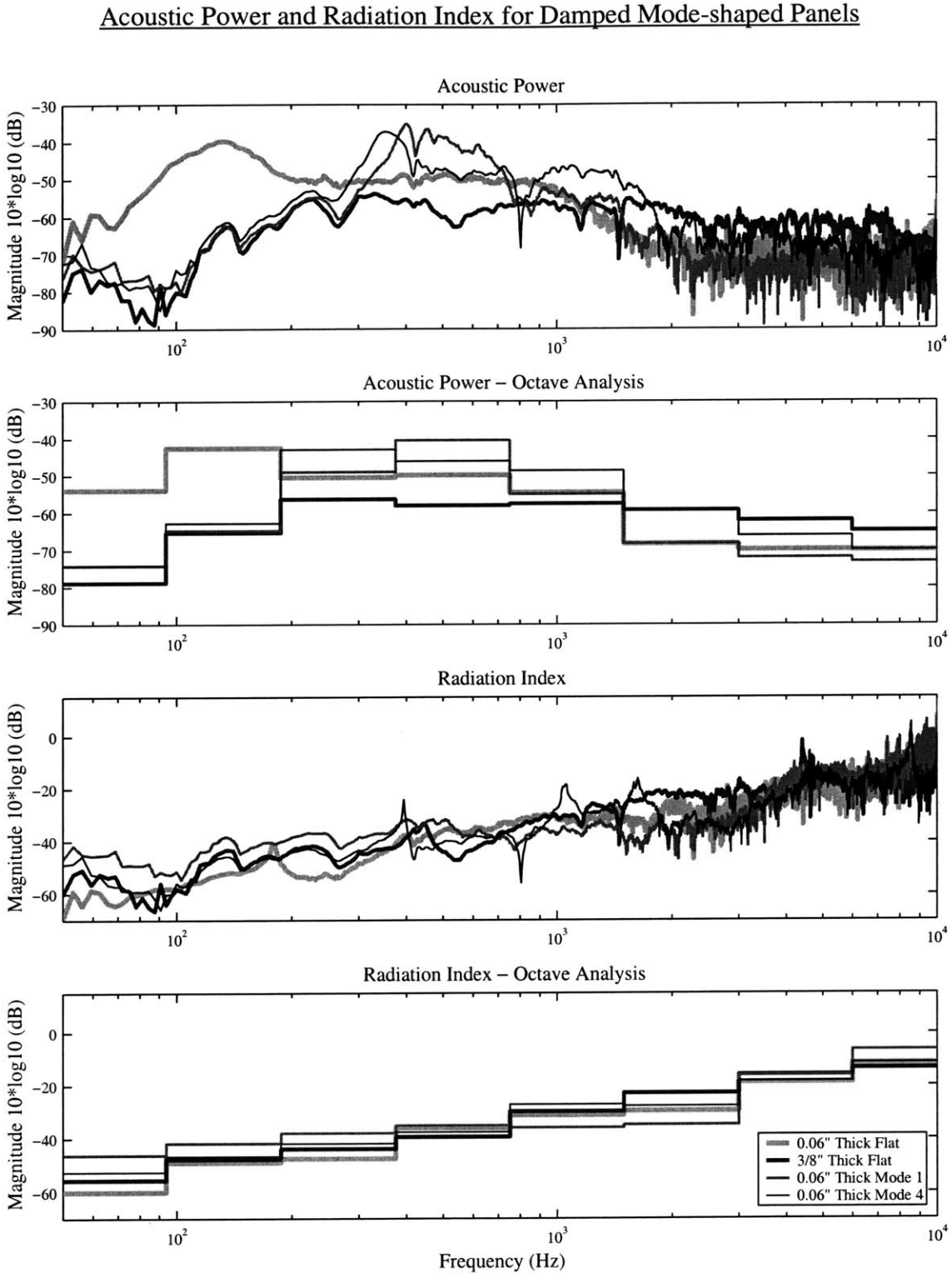

Figure 6.10 Plots of the acoustic power transfer function ((pressure/force)^2) and radiation index for the damped mode-shaped panels and the baseline flat panels. The plots are presented as averages over octaves to allow for easy comparison.

Damped Panels

The radiation experimental results for the undamped panels are located in Figure 6.10. Due to the lower radiation levels of the damped designs greater pressure coherence degradation was encountered at the higher frequencies, but the data still provides very accurate data below 4,000 Hz, and reasonable above 4,000 Hz. Again, the radiated acoustic power shown in the plots is the numerator in the radiation index calculations, and is the pressure to force transfer function squared times a constant.

6.4.2 Quasi-isotropic Designs

Again, the experiments were performed on the fundamental-mode-shaped panel and the fourth-mode-shaped panel. The experiments were performed on both the damped and undamped panels. The boundary conditions for all the panels in these experiments were clamped. To ensure repeatability and accuracy of the data, the shaker was placed normal to the surface of the mode-shaped panels.

Undamped Panels

The radiation experimental results for the undamped panels are located in Figure 6.10. For the undamped mode designs the coherence of the data was acceptable, but the pressure measurements demonstrated minor degradation of the coherence at higher frequencies. The radiated acoustic power shown in the plots is the numerator in the radiation index calculations, and is the pressure to force transfer function squared times a constant.

Damped Panels

The radiation experimental results for the undamped panels are located in Figure 6.11. Again, due to the lower radiation levels of the damped designs greater pressure coherence degradation was encountered at the higher frequencies, and again the data still provides very accurate data below 4,000 Hz, and reasonable above 4,000 Hz. Also, the radiated acoustic power shown in the plots is the numerator in the radiation index calculations, and is the pressure to force transfer function squared times a constant.

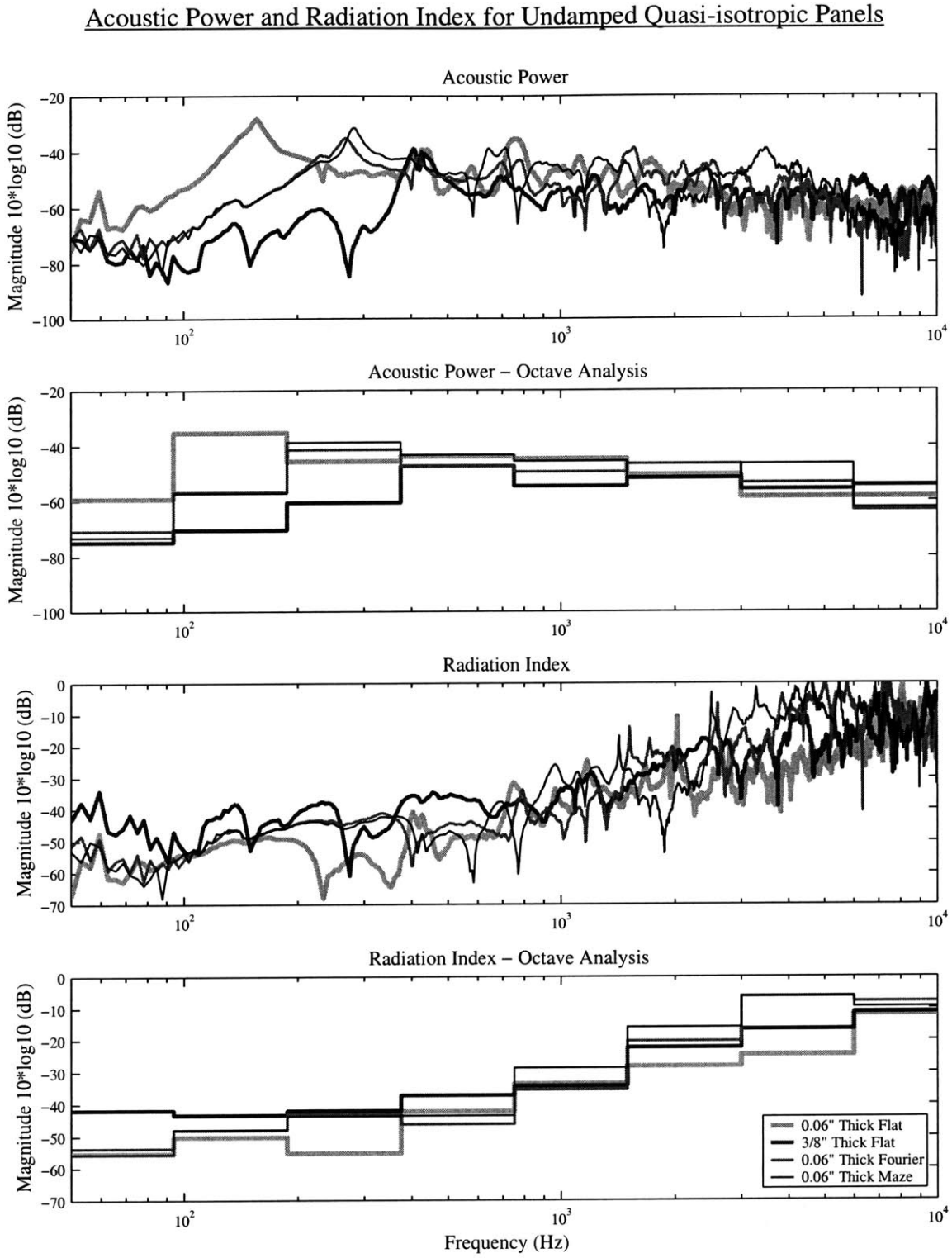

Figure 6.11 Plots of the acoustic power transfer function ((pressure/force)^2) and radiation index for the undamped quasi-isotropic panels and the baseline flat panels. The plots are presented as averages over octaves to allow for easy comparison.

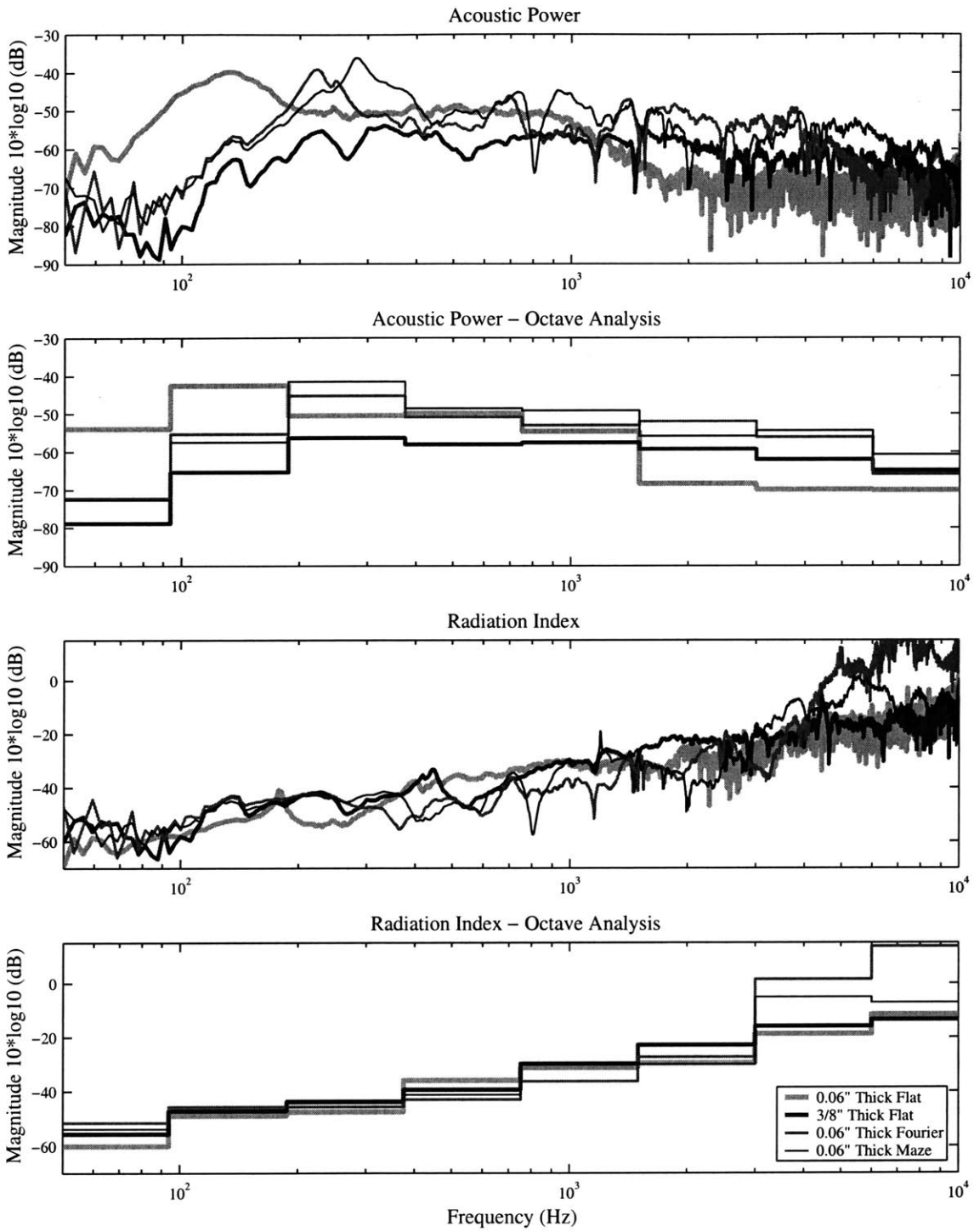

Figure 6.12 Plots of the acoustic power transfer function ((pressure/force)^2) and radiation index for the damped quasi-isotropic panels and the damped baseline flat panels. The plots are presented as averages over octaves to allow for easy comparison.

6.4.3 Discussion

A summary of the panels' radiation performance is located in Table 6.6. Once again the data indicates that the mode-shaped panel, especially the fundamental-mode-shaped panel, provided the best performance. The fundamental-mode-shaped panel did not perform as well as expected at lower frequencies. One theory for this is that the degree of curvature around the boundaries was too small to provide ample stiffening of the panel, thereby leading to some plunging. The shape of the mode-shaped panel for clamped boundaries has relatively little curvature near the boundaries and therefore the amount of shaped curvature in this range may still be within the elastic deformation range, thereby leading to some similar motion as a flat panel. This can only be speculation from the radiation data, therefore to investigate it further, the mode shapes of this panel were analyzed using a laser vibrometer in Section 6.7. In general, the mode-shaped panel performs better because the modes of the panel are less efficient radiators than that of a flat panel. The more even mode shapes lead to a greater degree of acoustic cancellation.

As expected, the thicker flat panel had a higher radiation index than the thin flat panel. This result agrees with the results given in the literature [Fahy, 1985; Maidanik, 1962]. The velocity of the panel may decrease due to stiffening, but the acoustic power does not decrease proportionately (perhaps in part due to fluidic damping on the panel, which is less significant for stiffer panels). The two-dimensionally curved quasi-isotropic panels also appear to radiate more efficiently than the flat panel. Again this is likely a result of the increased stiffness of the panel, and this also agrees with the literature.

One interesting phenomenon is the increase in radiation efficiency of the damped panels. Although the radiated power decreased for the damped panels, the radiation index increased (except for the 3/8 inch thick flat panel). The increase in the radiation index indicates that the radiated pressure is not as strongly affected as the panel velocity by the damping.

TABLE 6.6 Summary of results for the radiation data. The RMS value indicates the RMS average over 50 to 10,000 Hz. Numbers in parentheses indicate a negative difference in performance (*i.e.* a worse performance). Difference numbers indicate the 0.06 inch thick flat panel performance minus the other panels' performance.

Panel Design	Radiation Index		Radiated Acoustic Power	
	RMS (dB)	Difference (dB)	RMS (dB)	Difference (dB)
UNDAMPED PANELS				
0.06" Flat	9.0	NA	-22.8	NA
3/8" Flat	9.8	**(0.8)**	-31.0	**8.2**
0.06" Mode 1 Shaped	6.2	**2.8**	-26.9	**4.1**
0.06" Mode 4 Shaped	5.3	**3.7**	-24.2	**1.4**
0.06" Fourier Design	14.3	**(5.3)**	-22.0	**(0.8)**
0.06" Maze Design	13.5	**(4.5)**	-22.1	**(0.7)**
DAMPED PANELS				
0.06" Flat	12.5	NA	-31.8	NA
3/8" Flat	7.4	**5.1**	-40.0	**8.2**
0.06" Mode 1 Shaped	11.5	**1.0**	-31.2	**(0.8)**
0.06" Mode 4 Shaped	13.6	**(1.1)**	-28.5	**(3.3)**
0.06" Fourier Design	34.5	**(22.0)**	-28.5	**(3.3)**
0.06" Maze Design	14.8	**(2.3)**	-26.6	**(5.2)**

Finally, it is worth noting that the radiation index of a panel should approach zero near its critical frequency. Also, there is often a dramatic spike in the radiation index at the critical frequency. From the data, it appears that the two quasi-isotropic designs have critical frequencies (they are somewhat orthotropic and can therefore have multiple critical frequencies) in the 4,000 to 8,000 Hz range. The critical frequency of the 3/8 inch thick flat panel appears at about 4,000 Hz, theory predicts the critical frequency to occur at about 3,850 Hz. The mode-shaped panels and the thin flat panel do not appear to have their critical frequency in the range for the experiments taken. Theory predicts that the flat panel should have a critical frequency at about 11,500 Hz. Recall that it was predicted that the mode-shaped panels, with their subtle curvature, should have a similar critical frequency to that of the flat panel. This is discussed further in the diffuse transmission experiments of Section 6.6.

6.5 Directional Transmission Experiments

Directional transmission experiments were performed on the mode-shaped and quasi-isotropic panels. These experiments were performed in the small testbed, with a speaker placed in close proximity to and aimed directly at the panel of interest. The purpose of these experiments was to gain an understanding of the panels' performance under a directional noise load, as is often the case in machine enclosures, as opposed to a diffuse noise environment. The pressure was measured inside the testbed at two locations, and outside the testbed at two locations. The relatively few number of measurement locations will lead to a small degree of uncertainty, but the results should provide valuable insight into the various panel dynamics. All of these experiments were performed inside the anechoic chamber. Again, the boundary conditions for all of these panels were clamped.

6.5.1 Mode-shaped Designs

Again, the two mode-shaped panels were experimentally examined. Both damped and undamped panels were tested.

Undamped

The results of the undamped mode-shaped panel experiments for directional transmission are located in Figure 6.13. Both actual and octave average results are presented. The data was relatively clean for the entire frequency range of interest.

Damped

The results of the undamped mode-shaped panel experiments for directional transmission are located in Figure 6.14. Both actual and octave average results are presented. Again for the damped panels, the data coherence showed signs of degradation at the higher frequencies. Although the data was not as clean as the undamped panels, it is acceptable for the sort of comparative analysis presented here.

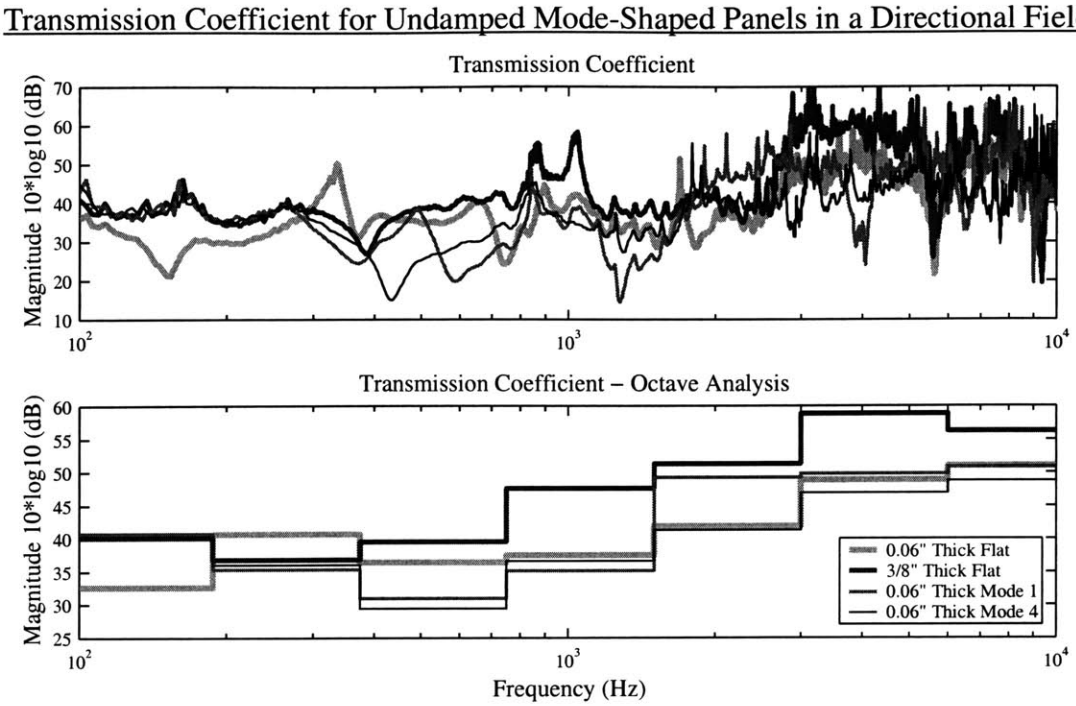

Figure 6.13 Plots of the transmission coefficient ((pressure inside/pressure outside)^2) for the undamped mode-shaped panels and baseline flat panels. Additionally, the plots are presented as octave averages.

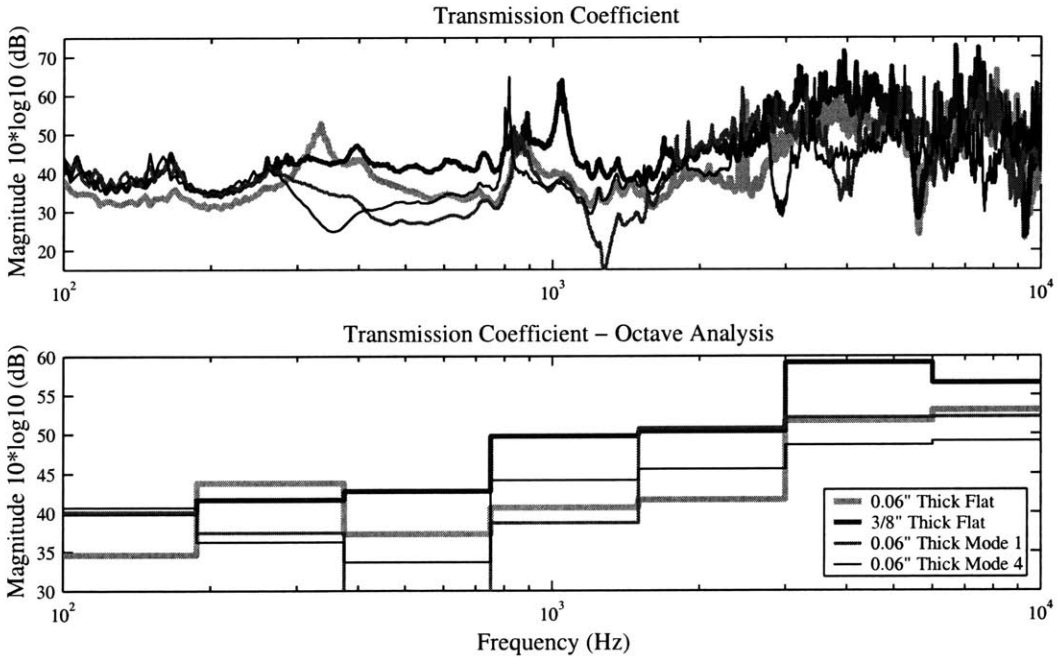

Figure 6.14 Plots of the transmission coefficient ((pressure inside/pressure outside)^2) for the damped mode-shaped panels and baseline flat panels. Additionally, the plots are presented as octave averages.

6.5.2 Quasi-isotropic Designs

Again the two quasi-isotropic panels were the Fourier and Maze panels. Both damped and undamped panels were tested.

Undamped

The results of the undamped Fourier and Maze panel experiments for directional transmission are located in Figure 6.15. Both actual and octave average results are presented. Again, the undamped panels provided relatively clean data for the entire frequency range of interest.

Damped

The results of the damped Fourier and Maze panel experiments for directional transmission are located in Figure 6.16. Both actual and octave average results are presented. Again for the damped panels, the data coherence showed signs of degradation at the higher frequencies. Although the data was not as clean as the undamped panels, it is acceptable for the sort of comparative analysis presented here.

6.5.3 Discussion

The directional transmission experiments demonstrated that the fundamental-mode-shaped panel provides increased acoustic performance, although the performance improvement in this experiment proved to be quite small. Aside from the expected higher performing 3/8 inch thick panel, all the other designs performed worse than the thin flat panel. This was true for the damped as well as the undamped panels. The data is summarized in Table 6.7.

As expected it is difficult to point out the critical frequency for these experiments. This is because the directional nature of the impinging sound (sound waves primarily parallel to the panel surface) does not significantly excite the critical frequency. To see significant excitation at this frequency, the sound environment needs to be diffuse so that grazing

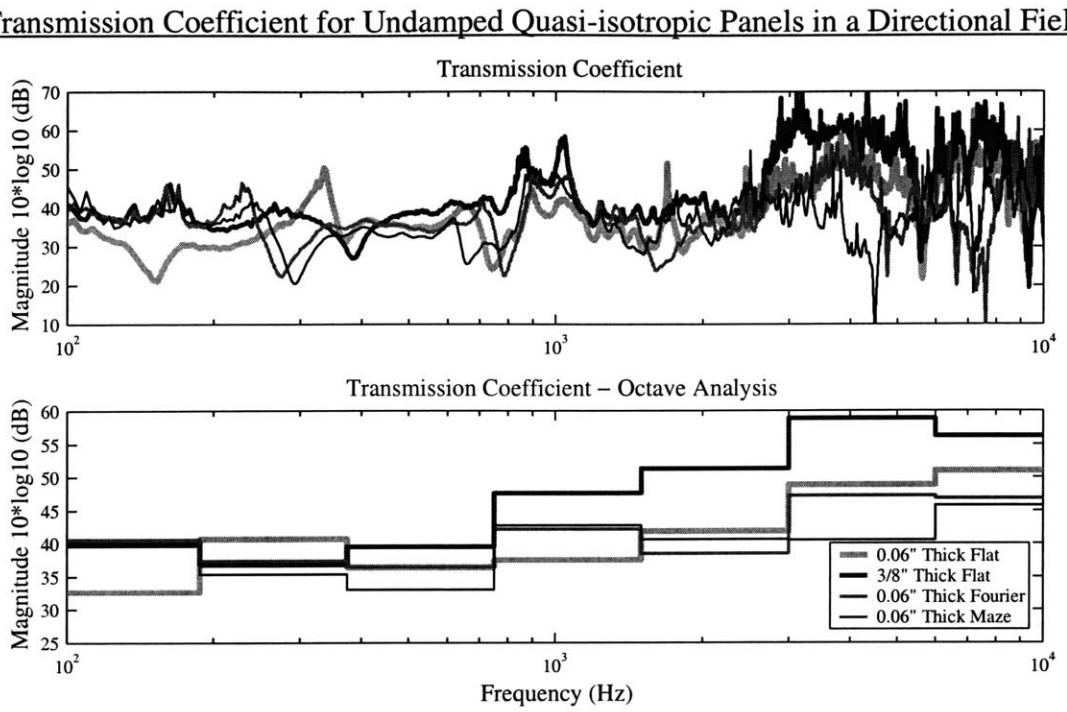

Figure 6.15 Plots of the transmission coefficient ((pressure inside/pressure outside)^2) for the undamped quasi-isotropic panels and baseline flat panels. Additionally, the plots are presented as octave averages.

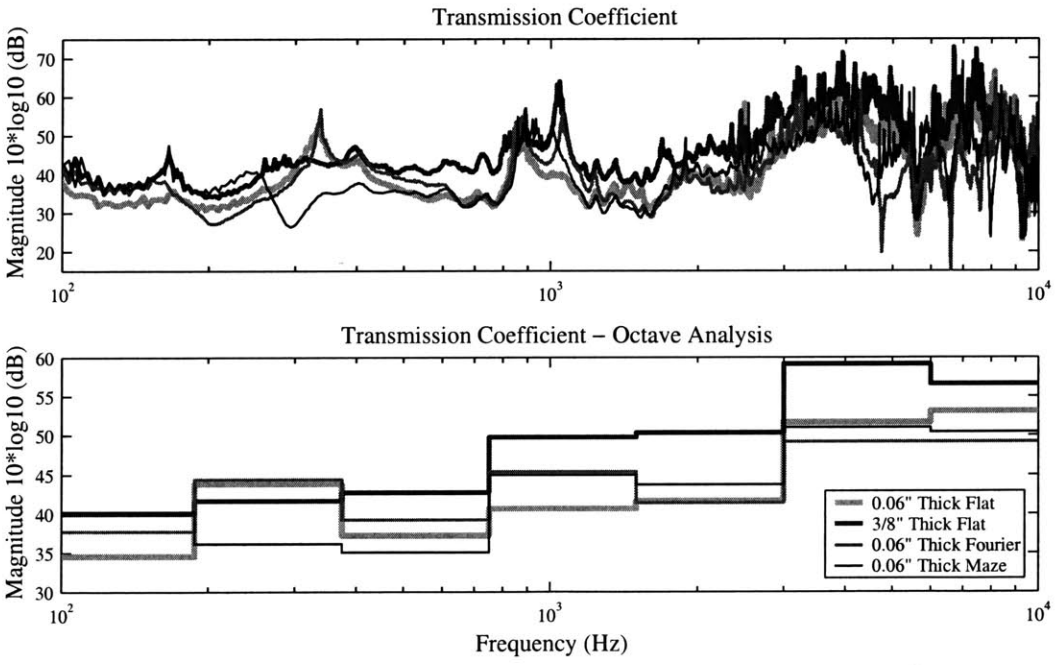

Figure 6.16 Plots of the transmission coefficient ((pressure inside/pressure outside)^2) for the damped quasi-isotropic panels and baseline flat panels. Additionally, the plots are presented as octave averages.

TABLE 6.7 Summary of results for the directional transmission data. Numbers in parentheses indicate a negative difference in performance (*i.e.* a worse performance). Difference numbers indicate the 0.06 inch thick flat panel performance minus the other panels' performance.

Panel Design	Undamped Panels		Damped Panels	
	RMS (dB)	Difference (dB)	RMS (dB)	Difference (dB)
ALL DATA IS FOR THE TRANSMISSION COEFFICIENTS FOR 50 TO 10,000 Hz				
0.06" Flat	72.4	**NA**	74.2	**NA**
3/8" Flat	79.1	**6.7**	80.4	**6.2**
0.06" Mode 1 Shaped	73.1	**0.7**	75.2	**1.0**
0.06" Mode 4 Shaped	70.9	**(1.5)**	72.6	**(1.6)**
0.06" Fourier Design	69.5	**(2.9)**	71.6	**(2.6)**
0.06" Maze Design	67.2	**(5.2)**	74.1	**(0.1)**

incidence occurs. This is presented in the following section. Regardless of the lack of coincident excitation data, the directional transmission experiment provides practical insight into many applications.

6.6 Diffuse Transmission Experiments

To address the panels' behavior in a more diffuse acoustic environment, transmission experiments were performed on the larger reverberant testbed. These experiments were performed over a larger frequency range to try and capture the critical frequency and coincident behavior of all the panels. The basic setup of the experiments was similar to the directional transmission experiments except that a diffuse sound environment was created within the larger testbed by including multiple reflective devices and orienting the speaker to maximize the diffusiveness of the reverberant chamber. Three microphone measurements were taken inside and outside the chamber. The diffuse environment transmission experiments are often utilized as a standard acoustic test for panels, and often finds greatest application in architectural fields. Again, the boundary conditions for all the panels was clamped.

6.6.1 Mode-shaped Designs

The diffuse transmission experiments were first performed on the mode-shaped panels. Again, both the fundamental-mode-shaped panel and the fourth-mode-shaped panel were tested with damped and undamped configurations.

Undamped

The results of the undamped mode-shaped panel experiments for diffuse transmission are located in Figure 6.17. Both actual and octave average results are presented.

Damped

The results of the undamped mode-shaped panel experiments for diffuse transmission are located in Figure 6.18. Both actual and octave average results are presented. Again for the damped panels, the data coherence showed signs of degradation at the higher frequencies.

6.6.2 Quasi-isotropic Designs

Again the two quasi-isotropic panels were the Fourier and Maze panels. Both damped and undamped panels were tested.

Undamped

The results of the undamped Fourier and Maze panel experiments for diffuse transmission are located in Figure 6.19. Both actual and octave average results are presented.

Damped

The results of the damped Fourier and Maze panel experiments for diffuse transmission are located in Figure 6.20. Both actual and octave average results are presented.

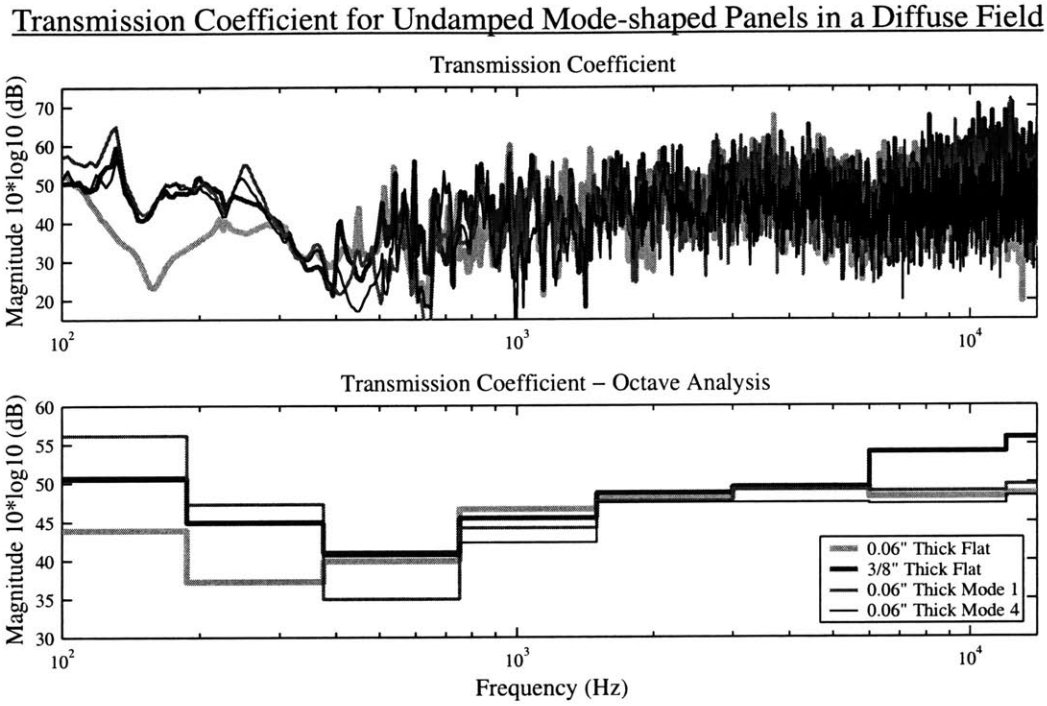

Figure 6.17 Plots of the transmission coefficient ((pressure inside/pressure outside)^2) for the undamped mode-shaped panels and baseline flat panels. Additionally, the plots are presented as octave averages.

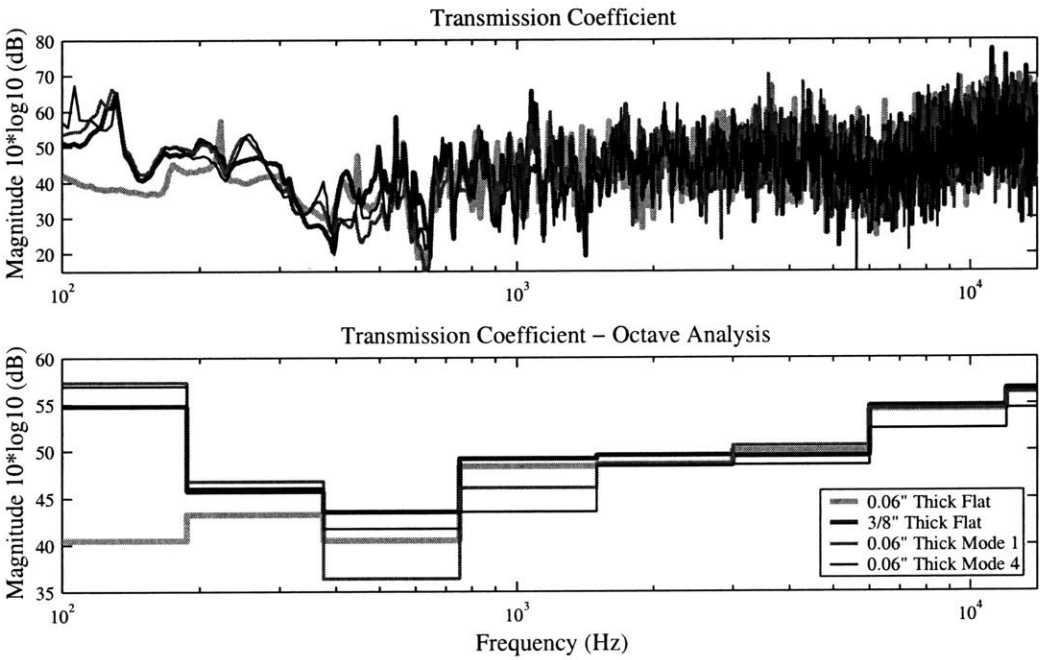

Figure 6.18 Plots of the transmission coefficient ((pressure inside/pressure outside)^2) for the damped mode-shaped panels and baseline flat panels. Additionally, the plots are presented as octave averages.

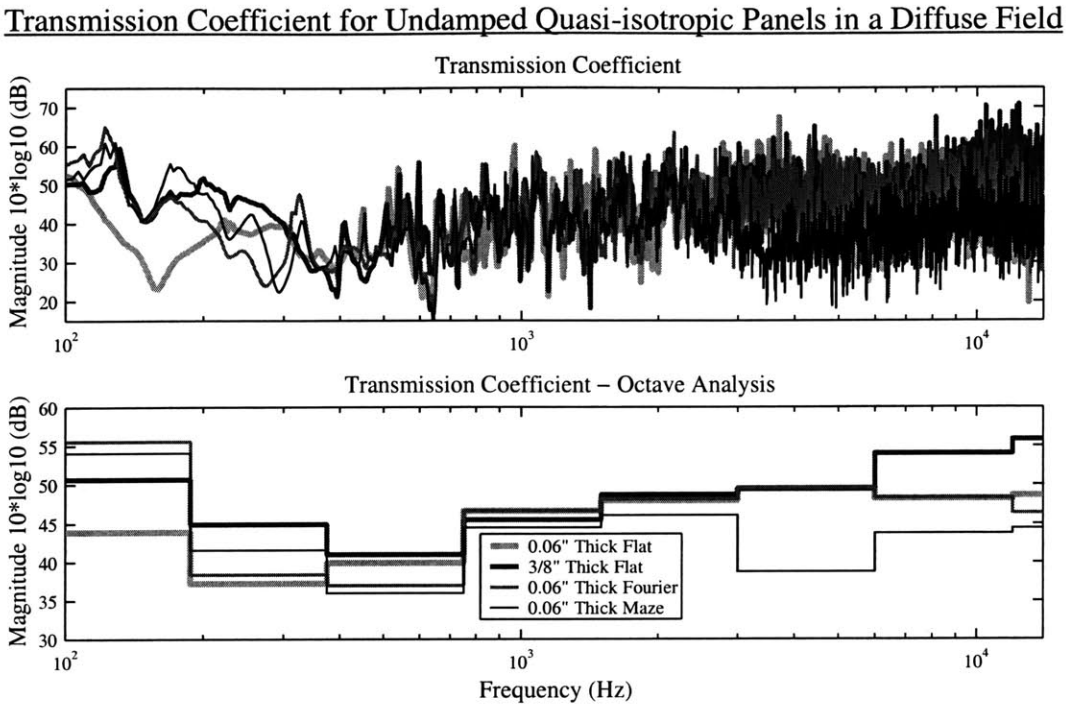

Figure 6.19 Plots of the transmission coefficient ((pressure inside/pressure outside)^2) for the undamped quasi-isotropic panels and baseline flat panels. Additionally, the plots are presented as octave averages.

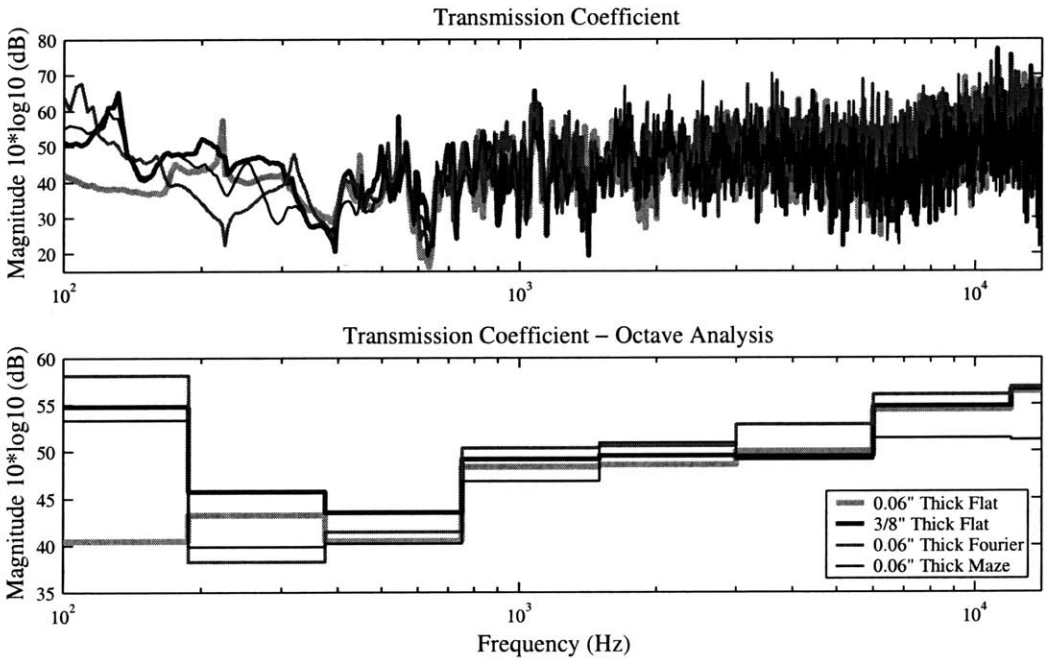

Figure 6.20 Plots of the transmission coefficient ((pressure inside/pressure outside)^2) for the damped quasi-isotropic panels and baseline flat panels. Additionally, the plots are presented as octave averages.

TABLE 6.8 Summary of results for the diffuse transmission data. Numbers in parentheses indicate a negative difference in performance (*i.e.* a worse performance). Difference numbers indicate the 0.06 inch thick flat panel performance minus the other panels' performance.

Panel Design	Undamped Panels		Damped Panels	
	RMS (dB)	Difference (dB)	RMS (dB)	Difference (dB)
RMS TRANSMISSION COEFFICIENTS FOR 50 TO 14,050 Hz				
0.06" Flat	73.0	**NA**	78.9	**NA**
3/8" Flat	78.1	**5.1**	81.2	**2.3**
0.06" Mode 1 Shaped	74.8	**1.8**	79.5	**0.6**
0.06" Mode 4 Shaped	71.8	**(1.2)**	76.9	**(2.0)**
0.06" Fourier Design	72.6	**(2.9)**	78.7	**(0.2)**
0.06" Maze Design	69.0	**(4.0)**	76.2	**(2.7)**

6.6.3 Discussion

The data for the diffuse transmission experiments is summarized in Table 6.7. It should be noted that the apparent noisiness of the data is primarily due to the reverberant nature of the testbed. The high density of modal overlap in the reverberant chamber gives the illusion of noisy data, when in fact the coherence for the data is high.

Although the experiments were performed carefully, it is difficult to obtain accurate transmission loss data. The task was made more complex due to the similarity between panels. Transmission loss data is more easily applied when the panels tested are of significantly different composition, thereby allowing easier comparison. This seems to have been further hampered by some of the characteristics of the experimental setup. Certain frequency ranges appear to have behavior that is independent of the panel. Between approximately 6,000 and 7,000 Hz the transmission loss plots appear to have a common dip. This would indicate that something in the setup, rather than the panels, is affecting the results. There may be some sound leakage, or perhaps the microphone spacing was such that a node was encountered for this frequency range. It is important to be aware of these trends before conclusions are drawn. Regardless, the experimental results substantiate the results found for the directional transmission experiments. Although all the panels perform similarly,

the fundamental-mode-shaped panel provides slightly better transmission loss over a broad frequency.

One of the goals of the diffuse transmission loss experiments was to try and identify the critical frequencies of the panels. When performing the experiments and zooming in on various frequency ranges, one could loosely identify the critical frequencies. Usually a characteristic peak was seen in the transfer function. For the flat panels the peaks coincided with theory (~ 12,000 Hz for the thin panel, and ~4,000 Hz for the thick panel). The fundamental-mode-shaped panel did not demonstrate significant peaks, but otherwise resembled the thin flat panel response at higher frequencies (>7,000 Hz). The quasi-isotropic panels on the other hand, displayed various peaks at which multiple critical frequencies could occur (between 3,000 and 10,000 Hz). Although the critical frequencies are not readily apparent in the above plots, the data does suggest that there values are within the expected ranges.

6.7 Laser Vibrometer Results

To gain a more complete understanding of the dynamic behavior of the fundamental-mode-shaped panel, a laser vibrometer was used to analyze the mode shapes of the panel. The laser vibrometer scans the surface of the panel as it is actuated and is then able to compile the data and discern the actual vibration of the surface. Using the laser vibrometer allows for the visualization of the actual mode shapes. As was discussed earlier, the benefit of the mode-shaped design is that its mode shapes are less efficient radiators. To some extent this has been established, but to further bolster the argument it is helpful to image the actual mode shapes of the panel. Also, as was stated earlier, it is believed that the limited degree of curvature near the boundaries of the clamped mode shape design leads to a degradation in performance due to some plunging in this region. The laser vibrometer can help confirm this theory.

In addition to testing the fundamental-mode-shaped panel with clamped boundary conditions, a mode-shaped panel with bolted boundary conditions was also analyzed. This was

done to see if the benefits of the mode-shaped design translate to more complex and realistic boundary conditions. Flat panels with the same boundary conditions were also analyzed so that a baseline comparison could be made. Only undamped panels were analyzed.

The panels were tested on the small testbed and were actuated by a speaker. A speaker was chosen for two reasons. One the speaker can actuate the panel without having to be in contact with the panel and interfere with the laser vibrometer. Two, and more importantly, a speaker is more likely to actuate odd modes. These are the modes that are most relevant to the radiation characteristics of a panel, especially the fundamental mode. The speaker was driven with a function generator within the laser vibrometer using a chirp, or swept sine. Transfer functions were taken with the measurement of 25 points on the panel, and the modes of the panels were determined with a 30 by 45 point grid (for a total of 1,350 measurement points).

Clamped Boundary Conditions

The average acceleration and displacement of the 25 points measured is contained in Figure 6.21. The plots also indicate the frequencies at which mode shapes were determined. Note that the magnitude is given in units of meters per second squared for acceleration and meters for displacement. These values represent the actual acceleration and displacement of the panels.

The mode shapes for the flat and mode-shaped panel are contained in Figure 6.22 and Figure 6.23, respectively. These illustrations help to demonstrate that the resulting mode shapes of a flat panel when actuated by a speaker are primarily of the odd variety. One even mode shape is shown at 250 Hz, but as can be seen from the transfer function in Figure 6.21, the corresponding amplitude of this mode shape is considerably less than the other odd mode shapes.

Conversely, the fundamental-mode-shaped panel has several modes that appear similar to even modes. As demonstrated by the finite element analysis, and as predicted, the funda-

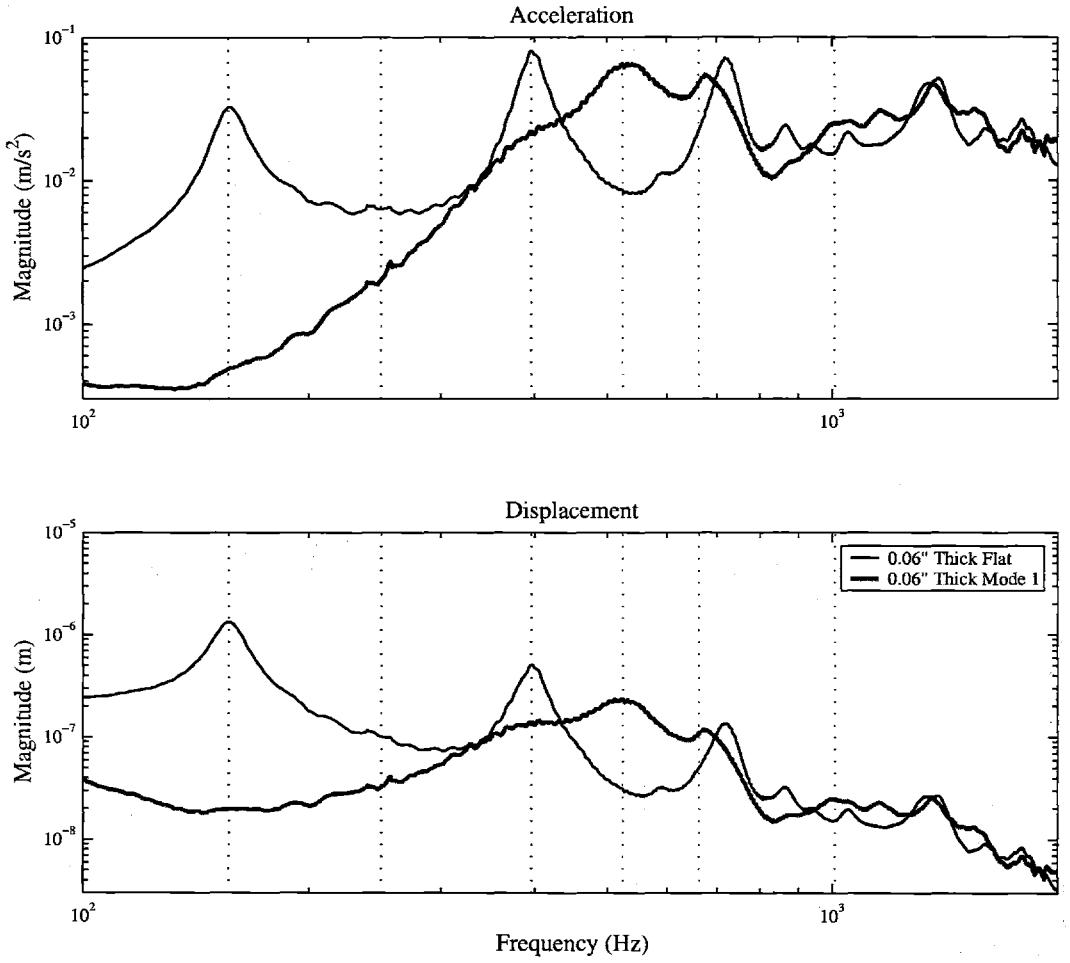

Figure 6.21 Plots of the acceleration and displacement for a flat and fundamental-mode-shaped panel with clamped boundaries measured with the laser vibrometer. The plots represent the average values measured at 25 points. The vertical lines represent the points at which a mode shape is shown.

mental-mode-shaped panel inhibits the odd mode shapes. An obvious exception to this is the first mode of the flat panel. This was not totally unexpected due to the small degree of curvature near the boundaries. In fact, this mode appears coupled and slightly out of phase with the higher order modes as well. This is more apparent when the modes are animated. The first mode coupling with the higher order modes is most likely the reason why these even modes appear when acoustically actuated.

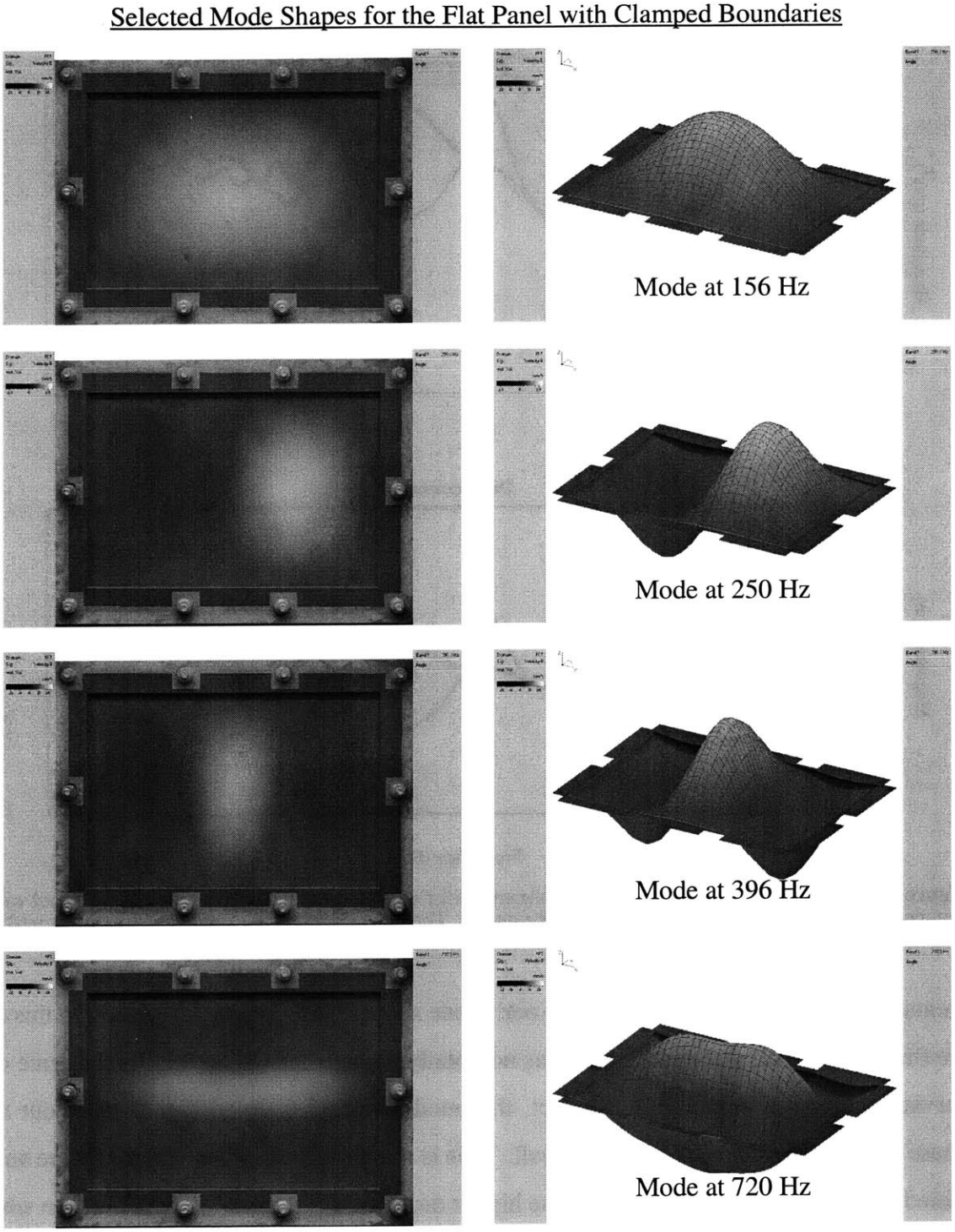

Figure 6.22 Illustrations of the actual mode shapes for the flat panel with clamped boundary conditions. The illustrations on the left represent a top view of the mode shape superimposed on the panel, while the illustrations on the right represent the three-dimensional plots of the mode shape. The grid shown represents the points at which the panel was measured.

Selected Mode Shapes for Fundamental-Mode-shaped Panel with Clamped Boundaries

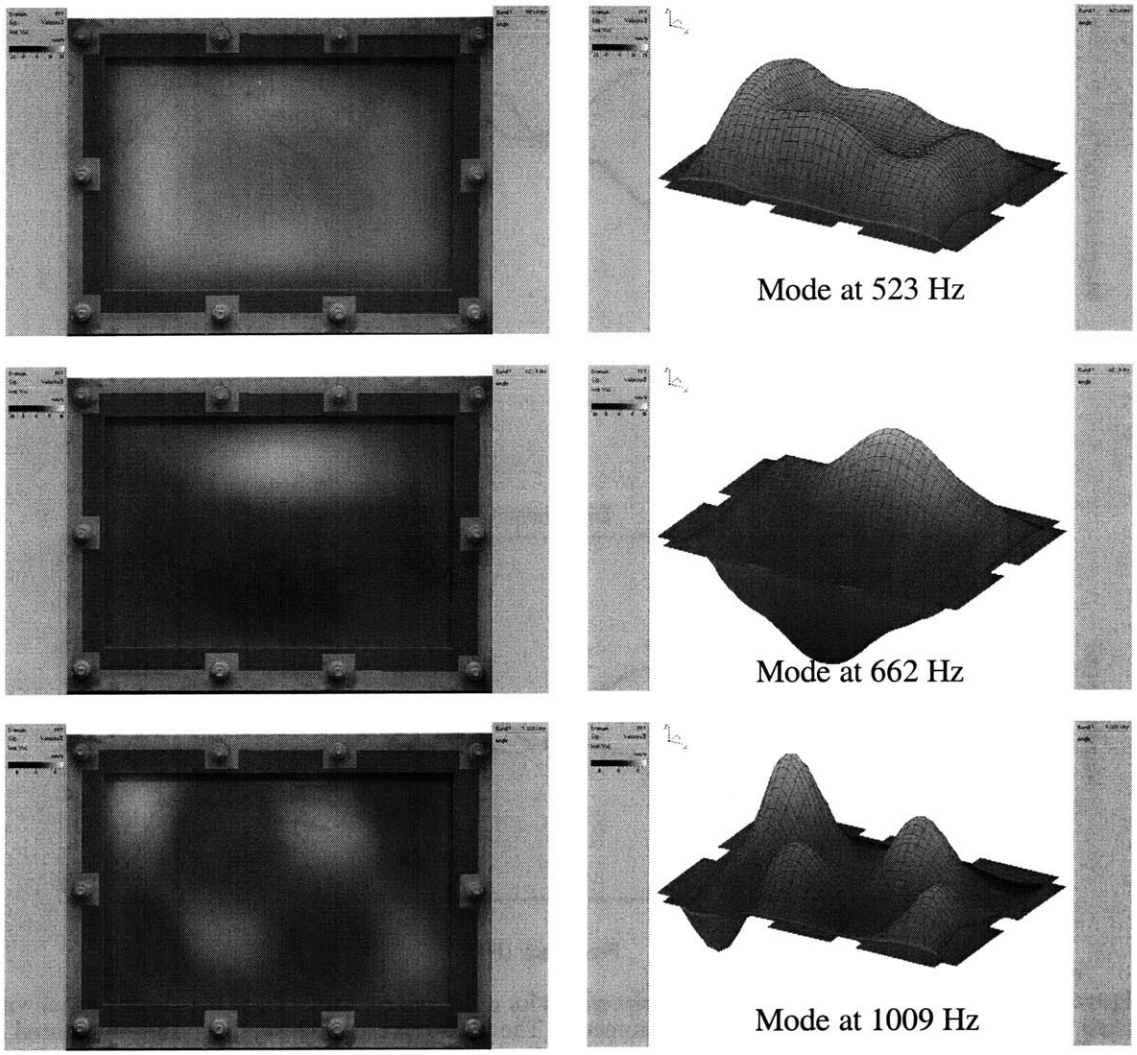

Figure 6.23 Illustrations of the actual mode shapes for the fundamental-mode-shaped panel with clamped boundary conditions. The illustrations on the left represent a top view of the mode shape superimposed on the panel, while the illustrations on the right represent the three-dimensional plots of the mode shape. The grid shown represents the points at which the panel was measured.

It is further supposed that improved performance can be achieved if greater curvature near the boundaries is incorporated in the fundamental-mode-shaped panel. This can be accomplished by either using greater amplitude in the panel design, or by using the mode shape from the simply supported case. The improved performance from these modifications is merely speculation, but the finite element analysis would seem to indicate that this should be the case. This is left for future work.

Acceleration and Displacement Transfer Functions for Panels with Bolted Boundaries

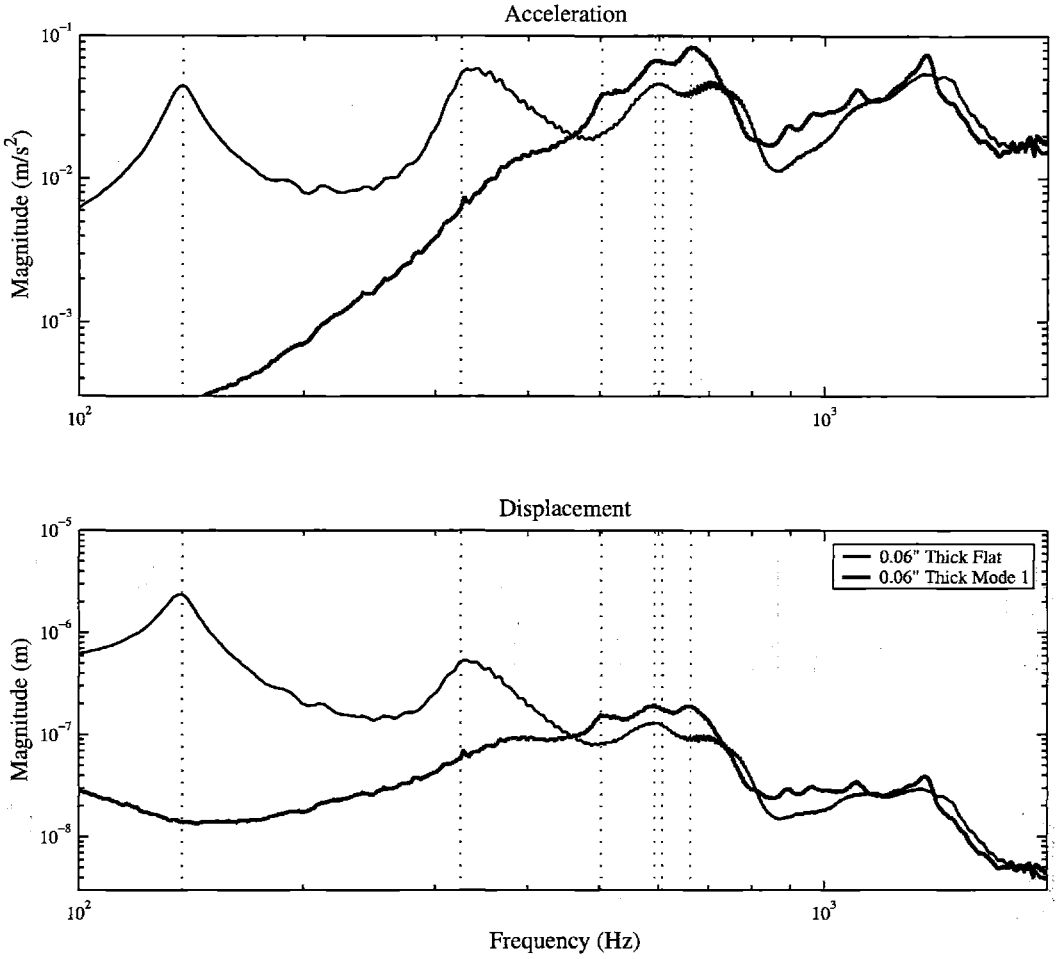

Figure 6.24 Plots of the acceleration and displacement for a flat and fundamental-mode-shaped panel with bolted boundaries measured with the laser vibrometer. The plots represent the average values measured at 25 points. The vertical lines represent the points at which a mode shape is shown.

Bolted Boundary Conditions

To determine the behavior of a panel with more common boundary conditions a panel with bolted boundary conditions was analyzed. The average acceleration and displacement of the 25 points measured is contained in Figure 6.24. The plots also indicate the frequencies at which mode shapes were determined. Again, note that the magnitude is given in units of meters per second squared for acceleration and meters for displacement. These values represent the actual acceleration and displacement of the panels. Although the maximum

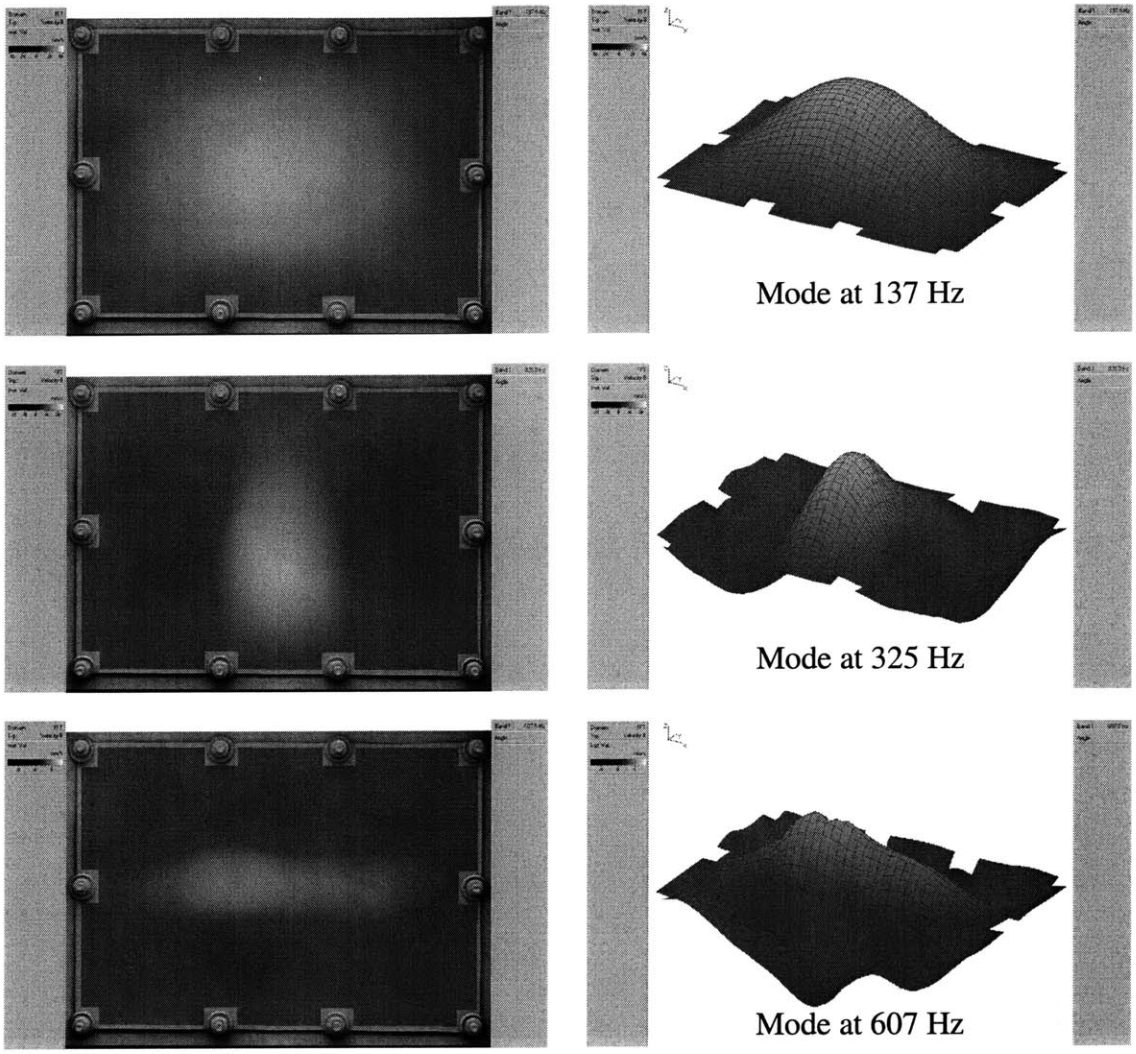

Figure 6.25 Illustrations of the actual mode shapes for the flat panel with bolted boundary conditions. The illustrations on the left represent a top view of the mode shape superimposed on the panel, while the illustrations on the right represent the three-dimensional plots of the mode shape. The grid shown represents the points at which the panel was measured.

acceleration of the mode-shaped panel is slightly higher than the flat panel, the displacement is much lower due to the significant increase in natural frequencies.

The mode shapes for the flat and mode-shaped panel are contained in Figure 6.25 and Figure 6.26, respectively. Again, the mode shapes for the flat panel are most accurately described as odd modes. Like the clamped flat panel the first three modes with the largest amplitude are the 0-0 mode, 0-2 mode, and 2-0 mode (recall the numbers describe the

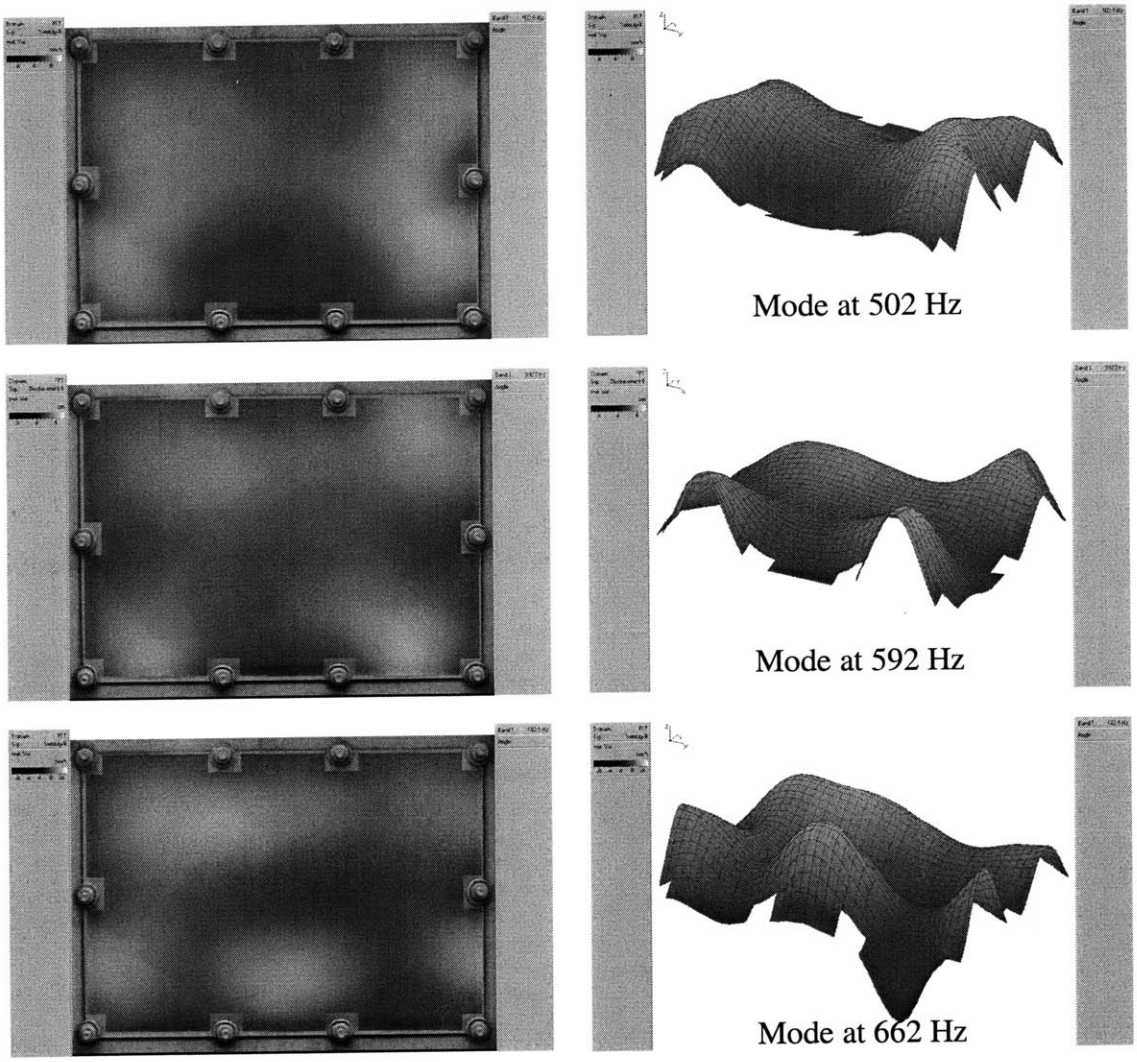

Figure 6.26 Illustrations of the actual mode shapes for the fundamental-mode-shaped panel with bolted boundary conditions. The illustrations on the left represent a top view of the mode shape superimposed on the panel, while the illustrations on the right represent the three-dimensional plots of the mode shape. The grid shown represents the points at which the panel was measured.

number of mode lines parallel to the boundaries). The mode shapes of the mode-shaped panel are considerably more complex and cannot easily be described by nodal lines. Most of the deflection in the modes appears to occur near the spacing between the bolts. The curvature of the panel inhibits the deflection near the center of the panel. More importantly, the resulting mode shapes do not appear to displace as much volume as the corresponding flat panel. This is partly explained by the reduced deflection, but also by the

volume cancellation that occurs due to the panels displacement into and out of the plane simultaneously (similar to even modes). The bolted mode-shaped panel still demonstrates many of the beneficial properties illustrated by the clamped mode-shaped panel. The plunging mode of the flat panel does not appear in the mode shapes, and it appears that the occurring mode shapes have some degree of volume cancellation. Although the bolted boundaries lead to complex dynamics, the fundamental-mode-shaped panel appears to provide a great deal of stiffening and possible acoustic radiation reduction.

The above two analyses of the mode-shaped panels further implies the benefit of incorporating the fundamental mode shape into panels. The mode-shaped panels' appear able to provide the desired combination of vibration reduction and acoustic attenuation. Other studies have shown that this result has been difficult to attain over broad frequencies, and therefore this design may lead to substantial gains in noise and vibration control

6.8 Summary

Three basic types of panels were experimentally investigated in this chapter. First, multi-layer sandwich panels were tested to determine if two-dimensionally curved cores could be used as an inexpensive alternative to honeycomb. Second, quasi-isotropic panels were investigated that utilized two-dimensional curvature to increase stiffness. Finally, mode-shaped panels were examined to try and increase stiffness while minimizing acoustic radiation. All the above panels were also investigated in combination with constrained damping material.

The results of the experiments examining the multi-layer sandwich designs indicate that two-dimensionally curved cores provide compatible performance to that of honeycomb cores. The static bending tests indicate that the two-dimensionally curved cores have similar, and in some cases superior, static stiffness to that of honeycomb cores. It was also determined that the orthotropic behavior of a core is also evidenced in the sandwich panel, but to a far lesser extent. This indicates that an isotropic core design is still vital to creating an isotropic sandwich panel. In addition, the dynamic behavior of the two-dimension-

ally curved core sandwich design and the honeycomb core design proved to be very similar, further ensuring the two-dimensionally curved core's suitability as a honeycomb replacement.

The quasi-isotropic panel designs were shown to have increased stiffness as evidenced by the increase in natural frequencies. The designs demonstrated some structural potential in applications where more isotropic behavior is required than can be provided by corrugated panels. The study of the quasi-isotropic panels will also help to further the performance of the multi-layer sandwich designs. It is speculated that a finer feature maze design would lead to beneficial properties as a sandwich core. Acoustically the quasi-isotropic designs did not provide any increased performance, and in most cases the acoustic performance was worse than that of a flat panel. This was not totally unexpected considering the reduction in critical frequency and the broadening of the critical frequency range. Although the quasi-isotropic designs studied demonstrated limited dynamic performance, further design development could lead to much greater dynamic improvement and further optimization of the two-dimensionally curved sandwich cores.

The mode-shaped panels proved to be the most beneficial designs for dynamic excitation. Much greater performance was obtained with the fundamental-mode-shaped design over the fourth-mode-shaped design, as was expected. The mode-shaped design demonstrated the ability to significantly reduce vibration while simultaneously reducing noise (often only a small amount) over a broad frequency range. The increase in stiffness is a result of the panel's curvature that provides global reinforcement similar to other shell structures. The reduction in acoustic noise is due in part to the elimination of mode shapes that have a high degree of radiation efficiency. The mode shapes of the fundamental-mode-shaped panel are more likely to resemble even modes that radiate noise less efficiently at lower frequencies. At higher frequencies, the shape of the panel allows for local compliance and thus does not lead to a significant reduction in the critical frequency. At the shorter wavelengths where the critical frequency occurs the panel's curvature is small enough that it does not reduce the critical frequency compared to the flat panel of the same thickness.

Finally, the combination of two-dimensional curvature and constrained damping material demonstrated no appreciable benefit in damping performance. For the subtly curved designs of the mode-shaped panels, the degree of damping was similar to that of a flat panel. For the more dramatically curved quasi-isotropic panels, the degree of damping appeared to be significantly less than that of a flat panel. The reason for this result can be many fold: the damping material properties altered when vacuum formed; the extreme curvature led to primarily compression instead of shearing in the damping layer; the layers delaminate during the forming process; the damping material was not properly matched to the designs; *etc.* The possibilities are numerous and most likely several combine to provide an accurate explanation. Although the results were not as desired, further development and study may prove the concept valuable.

Chapter 7

CONCLUSIONS

7.1 Summary

Four *hypotheses* were investigated in this thesis. One, unwanted mode shapes of a panel's dynamics can be greatly altered using a two-dimensionally curved design, thus leading to a stiffer panel that simultaneously reduces acoustic noise. Two, quasi-isotropic panel designs with increased stiffness can be achieved using mathematical algorithms and two dimensional curvature. Three, increased damping can be achieved when two-dimensional curvature is combined with constrained damping. Four, two-dimensionally curved panel cores can serve as inexpensive alternatives to honeycomb cores in sandwich panels with little or no degradation in performance. These four hypotheses were based on the notion that intelligently designed two-dimensionally curved panels can demonstrate improved performance over their flat and one-dimensional counterparts.

Background information on current state-of-the-art panel design was provided, in addition to the basic physics that describe a panel's dynamic and acoustic behavior. Simple analytical models were provided that loosely describe the behavior of two-dimensionally curved panels. Although the models provide for a qualitative understanding of panel behavior, their application to two-dimensionally curved panels is quite limited, thus demonstrating the need for further dynamic analysis. Although current state of the art dynamics can account for some of the behavior of doubly curved shells with no inflection points, these models can only weakly describe the dynamics of the systems studied in this work.

Several design methods were introduced to develop quasi-isotropic panels using two-dimensional curvature and mathematical algorithms. These designs have uses as both individual panels and as inexpensive cores in sandwich panels. These methods include: a parametric approach; a statistical approach; designs using computer optimization routines; and the above combined with the human ability to design. The resulting designs all demonstrated various levels of success as quasi-isotropic panels. Admittedly, the development of an optimal design was not accomplished to the degree desired. The methods introduced were effective at developing unique potential designs, but the methods of evaluating designs proved to be inadequate, thus limiting the development of optimal designs. Regardless, several potential designs were developed further for experimental analysis.

Next, panels formed in the shape of a mode of the corresponding flat panel were introduced and developed. The rationale for developing panels with modal shaping was introduced, namely to alter unwanted modal dynamics. The idea being that if a panel is formed into the shape of a mode then the unwanted mode shape is moved to a significantly higher frequency and lower order odd modes are beneficially altered. The fundamental-mode-shaped panel was the primary design because the fundamental mode of flat panels often cause the greatest disturbance, both mechanically and acoustically.

Methods of manufacturing the panels were discussed, primarily for prototyping but also for production. Vacuum forming was chosen as the method of manufacturing the prototypes because of the simplicity of the process and the ability to make prototypes and molds inexpensively. Various methods of manufacturing the molds was also discussed and stereo-lithography was chosen as the final mold production method. To create actual production parts, proven manufacturing methods such as stamping, thermoforming, and rolling can all be used.

Finally, the experimental setup, testbeds, and experimental results were developed and discussed. Three primary testbeds were developed and built: a static bending test, a small testbed enclosure, and a larger reverberant testbed enclosure. The static tests were per-

formed on the multi-layer sandwich panels. Baseline honeycomb designs and designs with two-dimensionally curved cores were both experimentally tested. All dynamic experiments were performed in an anechoic chamber. Vibration, radiation, and transmission experiments were performed on the curved panels as well as flat baseline panels, and both damped and undamped panels were investigated. In addition, laser vibrometer experiments were performed on fundamental-mode-shaped panels with clamped and bolted boundary conditions, as well as on the corresponding flat panels. These tests were used to investigate the exact lower-order modal and deformation dynamics of the fundamental-mode-shaped panels, to determine if the panels deformed in a manner consistent with the expected desired results.

7.2 Results and Contributions

At the beginning of this thesis, five desired contributions were introduced.

1. Demonstrate that it is beneficial to incorporate two-dimensional curvature and mathematically defined surfaces into structural panels.

   This general contribution essentially summarizes the entire work. The results of the research indicate that this was accomplished. While not all the design elements proved beneficial it was demonstrated that two-dimensional curved and mathematically defined panels can demonstrate improved performance characteristics over one-dimensional and flat panels, both structurally and acoustically.

2. Design two-dimensionally curved panel designs that increase stiffness and minimize unwanted modal dynamics to minimize acoustic noise.

   Mode-shaped panels were designed that sought to increase the natural frequency of the panels and simultaneously reduce the radiation efficiency of the panels. It was demonstrated that by incorporating the fundamental mode shape in the panel design, ensuring that the height of the design corresponds to plastic deformation of the panel at nearly all points, the resulting lower order mode shapes of the panel do not resemble the undesirable mode shapes of the flat panel. The resulting dynamics include a 300 percent increase in the first natural frequency, approximately a ten fold decrease in the maximum deflection, reduced radiation efficiency (corresponding to a 3 to 4 dB reduction over 10,000 Hz), and a slight reduction in acoustic transmission

(approximately 1 dB over 10,000 Hz). Visualization of the mode-shaped panel's dynamics with the laser vibrometer demonstrated that the mode shapes did not resemble the unwanted plunging mode of a flat panel. Although, better performance can likely be attained by increasing the degree of curvature such that the area near the boundaries is stiffened (or perhaps by using the simply supported fundamental mode shape).

3. Demonstrate that quasi-isotropic panels can be designed using mathematical algorithms and two-dimensional curvature.

   Several methods for designing quasi-isotropic curved panels were introduced and several were manufactured. The prototypes demonstrated approximately a 170 percent increase in the first natural frequency and a corresponding reduction in the dynamic deflection. In addition, the lower order behavior of the quasi-isotropic panels demonstrates a degree of isotropy as evidenced by the similar modal ordering and spacing at lower frequencies, but admittedly, better designs could be accomplished with finer features or larger panels. The maze-shaped design is considered the design form with the greatest potential for isotropic behavior, but further design work is needed. A basic feature that seems necessary for an isotropic shape is intertwining ribs or features with non-repeating patterns. Acoustically, the quasi-isotropic panels consistently performed worse than the flat panels. This result was undesired, but not unexpected due to the higher-order anisotropy that lead to greater coincident coupling. In addition, the increased stiffness, without the increased mass of a thicker panel, often leads to increased acoustic noise as evidenced by other studies (with the mode-shaped panel being a notable exception).

4. Show that greater levels of damping can be achieved when constrained damping layers are combined with two-dimensionally curved panel designs.

   The curved panels combined with the chosen constrained damping material demonstrated no additional damping performance over the flat panels. The subtly curved panels (*i.e.* mode-shaped panels) demonstrated similar damping characteristics to that of the flat panels, with some minor degradation in damping performance. On the other hand, the more dramatically curved quasi-isotropic panels demonstrated a large degradation in damping performance. No single reason can be identified for this reduction in performance.

5. Provide an inexpensive alternative to honeycomb and reinforced panel designs.

   The quasi-isotropic designs demonstrate the ability to serve as inexpensive replacements for honeycomb core material. The static experiments demonstrated that the quasi-isotropic core designs perform very similarly to the

> honeycomb sandwich panels. In fact, for most of the tests the quasi-isotropic core design appeared to be slightly stiffer than the honeycomb core panel, due to the quasi-isotropic design's distribution of material away from the neutral axis, without significantly adding to the sandwich panel's mass. The experiment also demonstrated that an orthotropic core is likely to lead to an orthotropic sandwich panel, although to a much lesser degree, thus further emphasizing the need for a nearly isotropic two-dimensionally curved design. The dynamic tests also demonstrated that the two-dimensionally curved core has similar properties to that of a honeycomb core. The dynamic tests also demonstrated that the two-dimensionally curved core has similar properties to that of a honeycomb core. The ability to use a single layer and easily manufactured quasi-isotropic panel as a core not only provides design alternatives, but can also reduce cost and possibly material for designs that require extremely light and stiff members, such as cardboard, architectural members, and aerospace structures.

Overall, the designs proved to be a useful alternative to the standard one-dimensional and flat panels. Not all of the hypotheses were proven to be successful, but several important benefits were demonstrated. Significant improvement can be made in the area of developing and analyzing quasi-isotropic designs. Developing more accurate models and methods for determining the actual stiffness of these two-dimensionally curved panels will lead to much improved designs. Minor changes in the mode-shaped panels may lead to further improved performance. Designing the panels such that the curvature is great enough near the boundaries will help to ensure a reduction in the plunging behavior of the modes. This is a greater problem for boundary conditions that resemble clamped rather than simply supported boundaries. Although the damping of the curved designs did not prove successful it is still possible that combining the curved shapes with other damping methods may lead to improved performance. Finally, using the quasi-isotropic designs as cores in sandwich panels was shown to be successful. The two-dimensionally curved core designs not only proved to be as stiff and lightweight as honeycomb, but the cores and the resulting sandwich panels can be manufactured for significantly less cost.

7.3 Recommendations for Future Work

Improvements in the designs can be made in several areas. In addition to design improvements, this work has also highlighted the need for improved characterization of two-dimensionally curved panels, especially with multiple inflection points. This includes determining the bending stiffness and deformation, the dynamic properties, and the acoustic properties of these panels. Also, this work has also helped to demonstrate the lack of ease with which these shapes can be defined, modeled and modified within common computer drafting and analysis programs.

With the increase in complexity of shapes and designs for products and mechanical elements it is more important than ever that the tools engineers use to design have the ability to create and manipulate complex shapes. This work was continually hampered by not being able to define the shapes and details desired in common computer aided drafting programs. In addition, many of the analysis tools used, such as finite element programs, could not handle the geometries that required analysis. Also, the conversion from one piece of software to another often encountered insurmountable difficulties. To be able to design in the future, these obstacles must be overcome to allow for constant improvement.

Although several beneficial methods of designing quasi-isotropic designs were developed, room for improvement still exists. A majority of this improvement can come from more accurate methods of determining the bending stiffness for these complex shapes. Until more accurate analytic models for the bending stiffness of these shapes is developed it will be difficult to determine ideal designs. Once more accurate models are developed, then future work can focus on parametrically defining more optimal solutions. In addition, further experimental analysis of more shapes can also lead to a greater understanding of which shapes are beneficial and why.

The next steps in understanding and developing mode-shaped designs include analysis of other boundary conditions and implementation in applications. The designs should be further analyzed with simply supported boundary conditions as well as other boundary condi-

tions. Small changes to the current designs should also be made. A more thorough study of the effect of amplitude and small changes in geometry may prove beneficial in optimizing designs for different environments. The mode-shaped designs can also be implemented in applications. Applications such as machine enclosures and vehicle component enclosures can benefit from the properties of these designs, thus further detailed analysis can determine how best to incorporate these designs.

Although the results of the experiments combining constrained damping material and two-dimensional curvature proved ineffective, other damping configurations may prove to be more beneficial. Future studies should look at using other types of damping materials, more closely matching the damping material properties with the structure. Also, other damping configurations might demonstrate greater performance. One possible suggestion is to investigate visco-elastic damping on the panels surface, rather than constraining the material. Another approach is to use damping material with variable thickness to match the deformation characteristics of the panel. An increase in structural damping is often beneficial, and utilizing the unique deformation properties of two-dimensionally curved panels may still lead to improvements.

Finally, future work involving the sandwich designs that utilize two-dimensionally curved cores should primarily be in the field of manufacturing and applications. Obviously, part of the success of these designs will depend on the development of better performing quasi-isotropic curved panels, but even with the current technology many designs can be improved. Although these designs can be made easily with current manufacturing processes, methods of manufacturing and assembling the designs should be explored to ensure their benefit. Some possible areas include rolling sandwich core material while simultaneously attaching (through welding or other process) the outer sandwiching layers, or developing designs that simplify the fastening of the outer layers. Many applications can benefit from these designs. It is likely that cardboard can be manufactured to have much greater strength and more isotropic materials while using significantly less material. This would not only be cost effective but it is also environmentally necessary as millions

of acres of forest are lost each year to the production of paper products. As stated before, exotic structures such as aerospace vehicles and platforms, that require extremely light and stiff designs, can be manufactured for significantly less cost if these two-dimensionally curved cores are used rather than honeycomb. In fact any application that requires low mass and high stiffness can benefit from these designs (*i.e.* components of boats, cars, buildings, machines, *etc.*).

Although this work has demonstrated the benefit of utilizing two-dimensional curvature in panels, other building components can also be improved through the use of two-dimensional curvature. Although examples of curvature in structures exist, the use of rectangular and flat components is widely accepted and rarely questioned. Like seeing in color for the first time, incorporating curvature into components can lead to a fundamental new way of designing structures with improved characteristics. The next time you see a structure, ask... Why is it flat? ... and remember, the earth was once thought flat.

REFERENCES

[Avallone, 1996] Avallone, Eugene A., and Theodore Baumeister, *Marks' Standard Handbook for Mechanical Engineers*, 10th Edition, McGraw Hill, Boston, MA, 1996.

[Berkman, 1997] Berkman, E.F. and E.K. Bender, "Perspectives on Active Noise and Vibration Control," *SV. Sound and Vibration*, Vol. 31, No. 1, 1997.

[Betts, 1944] Betts, Edwin Morris, ed., *Thomas Jefferson's Garden Book 1766-1824*, The American Philosophical Society, Philadelphia, Pennsylvania, 1944.

[Bhimaraddi, 1991] Bhimaraddi, Alavandi, "Free Vibration Analysis of Doubly Curved Shallow Shells on Rectilinear Planform Using Three-Dimensional Elasticity Theory," *International Journal of Solids and Structures*, Vol. 27, No. 7, Great Britain, 1991.

[Bies, 1996] Bies, David, and Colin Hansen, *Engineering Noise Control*, E & FN SPON Publishing, New York, p. 273-305, 1996.

[Bingham, 1998] Bingham, Brian S., *Structural-acoustic Design and Control of an Integrally Actuated Composite Panel*, Masters Thesis at the Massachusetts Institute of Technology, 1998.

[Blevins, 1995] Blevins, Robert D., Formulas for Natural Frequencies and Mode Shape, Krieger Publishing Company, Malabar, FL, p. 233-290, 1995.

[Cerat, 2000] Cerat, Mike, Personal Correspondence, Sales Associate at Yarde Aluminum (manufacturer and supplier of Aluminum products), August 2000.

[Char, 1994] Char, K., and S.M. Kuo, "Performance Evaluation of Various Active Noise Control Algorithms," *Noise-Con 94*, May 1994.

[Chaudhuri, 1994] Chaudhuri, Reaz A., Humayun R.H. Kabir, "Static and Dynamic Fourier Analysis of Finite Cross-Ply Doubly Curved Panels Using Classical Shallow Shell Theories," *Composite Structures*, Great Britain, Vol. 28, 1994.

[Cheng, 1995] Cheng, L. and R. Lapointe, "Vibration Attenuation of Panel Structures by Optimally Shaped Viscoelastic Coating with Added Weight Considerations," *Thin-Walled Structures*, Vol. 21, No. 4, 1995.

[Chun, 1995] Chun, Lu, K.Y. Lam, "Dynamic Analysis of Clamped Laminated Curved Panels," *Composite Structures*, Great Britain, Vol. 30, 1995

[Chung, 1997] Chung, Chih-Hung, Glen Steyer and Brian Brassow, "Transmission Side Cover Design Optimization for NVH Part 1 & 2," *Proceedings of the 1997 Noise and Vibration Conference (SAE)*, Vol. 2, Traverse City, MI, 1997.

[Clark, 1993] Clark, R.L., M.R.Flemming, C.R. Fuller, "Piezoceramic Actuators for Distributed Vibration Excitation of Thin Plates: A Comparison between Theory and Experiment," *Transactions of the ASME*, Vol. 115, July 1993.

[Cremer, 1973] Cremer, L., M. Heckl, and E.E. Unger, "Structure-borne Sound," Springer-Verlag, Berlin and New York, 1973

[Crocker, 1993] Crocker, M.J., L.P. Drozdova and N.I. Ivanov, "Noise and Vibration Control in Vehicles," Interpublish, St. Petersburg, 1993.

[Crocker, 1975] Crocker, M.J., Price, A.J., *Noise and Noise Control*, Vol. 1, CRC Press, Cleveland, Ohio, 1975.

[Drozdova, 1997] Drozdova, L.P., N.I. Ivanov, V.Y. Kirpichnikov, B.T. Titov, "Some Features of Noise Control of Circular-Saw Machine Tools," *The 1997 International Congress on Noise Control Engineering*, Vol. 1, Budapest, Hungary, 1997.

[Dym, 1974] Dym, Clive, L., *Introduction to the Theory of Shells*, Pergamon Press, Oxford, 1974.

[Fahy, 1985] Fahy, Frank, "Sound and Structural Vibration: Radiation, Transmission and Response," Academic Press, New York, 1985.

[Gerard, 1989] Gerard, Borello, "Low Frequency Noise Prediction of Internal Acoustic Environment of a Launch Vehicle at Lift-off," *International Conference on Noise Control Engineering*, Newport Beach, CA, Dec. 4-6, 1989.

[Gol'Denveizer, 1961] Gol'Denveizer, A.L., *Theory of Elastic Thin Shells*, Pergamon Press, New York, 1961.

[Gornick, 1997] Gornick, Tina, "The Quest for Quiet," *Appliance: Design, Production, Management*, Vol. 54, No. 12, 1997.

[Hale, 1994] Hale, Layton Carter, *Principles and Techniques for Designing Precision Machines*, Doctoral Thesis at the Massachusetts Institute of Technology, 1999.

[Hansen, 1998] Hansen, Colin H, Scott D. Snyder, Robert L. Clark, "Active Control of Noise and Vibration," *Noise control engineering journal,* Vol. 46, No. 2, 1998.

[Hearmon, 1959] Hearmon, R.F.S., "The Frequency of Flexural Vibration of Rectangular Orthotropic Plates with Clamped or Supported Edges," *Journal of Applied Mechanics*, p. 537, December 1959.

[Hendricx, 1997] Hendricx, Wim, Y.B. Choi, S.W. Ha, and H.K. Lee, "Experimental Body Panel Contribution Analysis for Road Induced Interior Noise of a Passenger Car," *Proceedings of the 1997 Noise and Vibration Conference (SAE)*, Vol. 2, Traverse City, MI, 1997.

[Hu, 1999] Hu, X.X., T. Tsuiji, "Free Vibration Analysis of Curved and Twisted Cylindrical Thin Panels," *Journal of Sound and Vibration*, Vol. 219, No. 1, 1999.

[Iwahara, 1991] Iwahara, M., H. Sakamoto, T. Matsuuki, H. Shibata, Y. Tanaka, and A. Nagamatsu, "A New Method for Car Body Design Optimization," *Proceedings of the 1991 Noise and Vibration Conference (SAE)*, 1991.

[Kabir, 1991] Kabir, H.R.H., and R.A. Chaudhuri, "Free Vibration of Shear-Flexible Anti-Symmetric Angle-Ply Doubly Curved Panels," International Journal of Solid Structures, Vol. 28, No. 1, Great Britain, 1991.

[Kinsler, 1982] Kinsler, L.E., A.R. Frey, A.B. Coppens and J.V. Sanders, *Fundamentals of Acoustics*, Third edition, Wiley, New York, 1982.

[Kryter, 1970] Kryter, K.D., *The Effects of Noise on Man*, Academic, New York, 1970.

[Leheta, 1997] Leheta, Heba W., Alaa E. Mansour, "Reliability-Based Method for Optimal Structural Design of Stiffened Panels," *Marine Structures*, Vol. 10, 1997.

[Leissa, 1973] Leissa, Arthur W., *Vibration of Shells*, NASA, Washington, D.C., 1973.

[Liew, 1996] Liew, K.M., Lim, C.W., "A Higher-Order Theory for Vibration of Doubly Curved Shallow Shells," *Journal of Applied Mechanics*, Vol. 63, September 1996.

[Lord, 1987] Lord, Harold H., William S. Gatley, Harold A. Evensen, *Noise Control for Engineers*, Robert E. Krieger Publishing Co. Inc., Malabar, FL, 1987.

[Marsh, 1994] Marsh, Eric Russel, *An Integrated Approach to Structural Damping*, Doctoral Thesis at the Massachusetts Institute of Technology, 1994.

[Mraz, 1993] Mraz, Stephen, "Zeroing in on Automotive Defects," *Machine Design*, April 1993.

[Macadam, 1976] Macadam, J.A., "The Measurement of Sound Radiation from Room Surfaces in Lightweight Buildings," *Applied Acoustics*, Vol. 9, 1976.

[Maidanik, 1962] Maidanik, G., "Response of Ribbed Panels to Reverberant Acoustic Fields," *The Journal of the Acoustic Society of America*, Vol. 34, No. 6, 1962.

[Mathur, 1993] Mathur, G.P., and B.N. Tran, "Aircraft Cabin Noise Reduction Tests Using Active Structural Acoustic Control," *15th AIAA Aeroacoustics Conference*, Oct. 1993, AIAA Paper No. 93-4437.

[Nachimuthu, 1997] Nachimuthu, Anbarasu, Karen Carnago and Farshid Haste, "Panel Contribution Study: Results, Correlation and Optimal Bead Pattern for Powertrain Noise Reduction," *Proceedings of the 1997 Noise and Vibration Conference (SAE)*, Vol. 2, Traverse City, MI, 1997.

[Nagai, 1991] Nagai, Hiroyuki, Toshiaki Shiota, Takao Taka, and Kiyoyuki Fukui, "The Development of Vibration Damping Steel Sheets for Inner Panels of Automotive Vehicles," *Proceedings of the 1991 Noise and Vibration Conference (SAE)*, 1991.

[Ng, 1995] Ng, C.F., "Close-Fitting Noise Enclosure with Curved Panels and Perforated Absorbers," *The 1995 International Congress on Noise Control Engineering*, Vol. 1, Newport Beach, CA, 1995.

[Oka, 1991] Oka, Yoshio, Hiroyuki Ono and Naoki Hirako, "Panel Vibration Control for Booming Noise Reduction," *Proceedings of the 1991 Noise and Vibration Conference (SAE)*, Vol. 2, 1991.

[Panov, 1994] Panov, S.N., "Identification of Machine Noise Radiators Using Intensity, Holography and Modal Analysis Techniques," *The 1994 International Congress on Noise Control Engineering*, Vol. 3, Yokohama, Japan, 1994.

[Qian, 1997] Qian, Yang, Anuj Aggarwal and Hameed Khan, "Damping Efficiency of Ribbed Panels with Different Damping Materials," *Proceedings of the 1997 Noise and Vibration Conference (SAE)*, Vol. 2, 1997.

[Reza Moheimani, 1998] Reza Moheimani, S.O., H.R. Pota, I.R. Petersen, "Active Control of Noise and Vibration in Acoustic Ducts and Flexible Structures - A Spatial Control Approach," *Proceedings of the American Control Conference*, Vol. 4, 1998.

[Rossetti, 1994] Rossetti, D.J., and M.A. Norris, "A Comparison of Actuation and Sensing Techniques for Aircraft Cabin Noise Control," 1994 AIAA Aeroacoustics Conference, AIAA Paper No. 94-1738.

[Smith, 1965] Smith, P.W. and R.H. Lyon, *Sound and Structural Vibration*, NASA Contractor Report, NASA CR-160, Bolt, Beranek and Newman, Inc., 1965.

[Steyer, 1997] Steyer, Glen, Chih-Hung Chung and Brian Brassow, "Transmission Side Cover Design Optimization for NVH Part 1," *Proceedings of the 1997 Noise and Vibration Conference (SAE)*, Vol. 2, Traverse City, MI, 1997.

[Tanis, 2000] Tanis, Wade, Personal Correspondence, Sales Associate at Plascore (manufacturer and supplier of honeycomb core and panels), August 2000.

[Timoshenko, 1940] Timoshenko, S, *Theory of Plates and Shells*, McGraw-Hill, New York, 1940.

[VanBuskirk, 1993] VanBuskirk, Jeff, "Noise Problems Associated with Geometrically Stiffened Panels," *Proceedings of the 1993 Noise and Vibration Conference (SAE)*, Vol. 3, Traverse City, MI, 1993.

[Wallace, 1972] Wallace, C.E., *Journal of the Acoustic Society of America,* Vol. 51, No. 3, Part 2, 1972.

[Walsh, 2000] Walsh, Ron, Personal Correspondence, Sales Manager at Commercial Plastics and Supply Company (distributor of Plastic products), August 2000.

[Warnaka, 1969] Warnaka, Glenn, "Sound Attenuating Wall for Blocking Transmission of Intelligible Speech," U.S. Patent 3,422,921, assigned to Lord Corporation, Erie, PA, Jan. 21, 1969.

[Watters, 1966] Watters, Bill G., "High Acoustic Transmission Loss Panel," U.S. Patent 3,249,178, assigned to Bolt, Beranek & Newman Inc., Cambridge, MA, April 30, 1963.

[Watters, 1963] Watters, Bill G., "High Acoustic Transmission Loss Panel and the Like," U.S. Patent 3,087,574, assigned to Bolt, Beranek & Newman Inc., Cambridge, MA, May 3, 1966.

[Watters & Kurtze, 1963] Watters, Bill G. and Guenther Kurtze, "Panel and the Like of High Acoustic Transmission Loss," U.S. Patent 3,087,570, assigned to Bolt, Beranek & Newman Inc., Cambridge, MA, April 30, 1963.

[White, 1997] White, John, and Jack Webb, "Air Cleaner Shell Noise Reduction with Finite Element Shape Optimization," *Proceedings of the 1997 Noise and Vibration Conference (SAE)*, Vol. 2, Traverse City, MI, 1997.

[Zhang, 1997] Zhang, Y. Kevin, Jihe Yang, Lung Wu, Walt Mazur, Xiandi Zeng, and Xiaoye Gu, "Acoustic Analysis of Vehicle Ribbed Floor," *Proceedings of the 1997 Noise and Vibration Conference (SAE)*, Vol. 2, Traverse City, MI, 1997.

[Zhang, 1995] Zhang, Y. Kevin, Jihe Yang, Ming-Ran Lee and Jay Prakash, "A New Approach for Noise Reduction of Thin-Shell Structures," *The 1995 International Congress on Noise Control Engineering*, Vol. 1, Newport Beach, CA, 1995.

[Zhang, 1991] Zhang, Y., K. Phaneuf, and W. Hill, "Dynamic Analysis of Rib Patterns," *Proceedings of the 1991 Noise and Vibration Conference (SAE)*, 1991.

AFTERWORD

The earth is not flat...

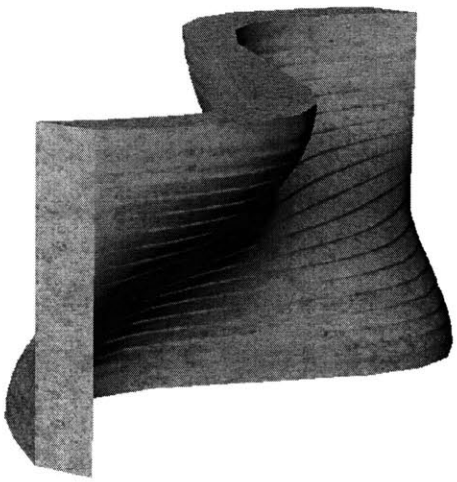

How does one come up with the abstract idea of developing panels with multi-dimensional curvature? It starts with a crazy suggestion, an idea spat forth in a manic lecture by a teacher... *highway barriers could be better, or at least more interesting, if they were sinusoidal.* A student, looking for a new adviser catches the idea and uses the seed, makes it grow, and tries to impress the teacher so he will agree to become the adviser. A simple ploy. A mere transition. A temporary task. The student explores and develops and designs several interesting barrier members...

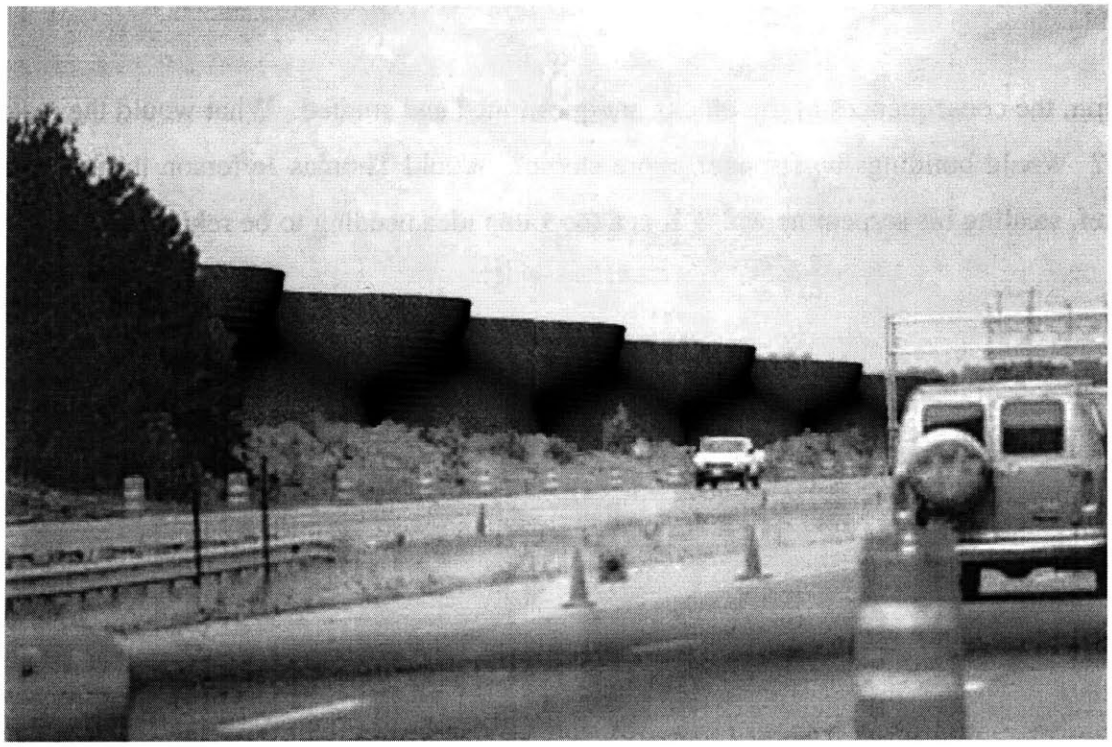

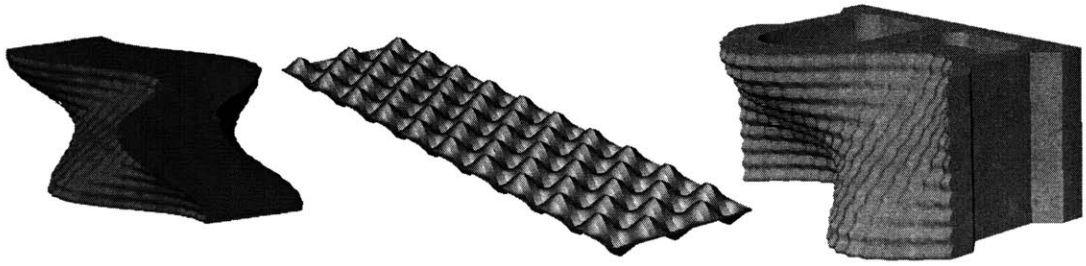

The teacher likes the student's work and agrees to advise the wayward student, encouraging the student to continue the little distraction of playing with curved blocks. The student plays and builds with blocks, developing numerous blocks of all sizes and shapes...

The student even takes the idea of playing with blocks literally and builds some Lego-like blocks...

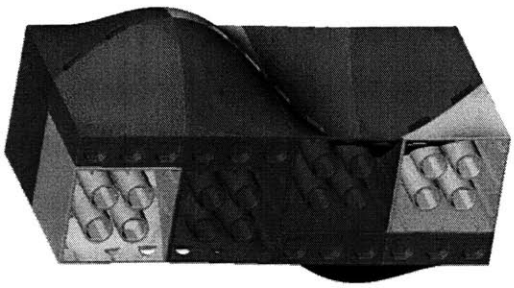

The student uses the simple toys as inspiration for greater projects, and lets the idea gestate inside his head, gurgle and simmer over low heat...

Soon, the consequences of the blocks are questioned and studied. What would the results be? Would buildings be stronger, more stable? Would Thomas Jefferson think I was a thief, stealing his serpentine wall? It is a forgotten idea needing to be rekindled.

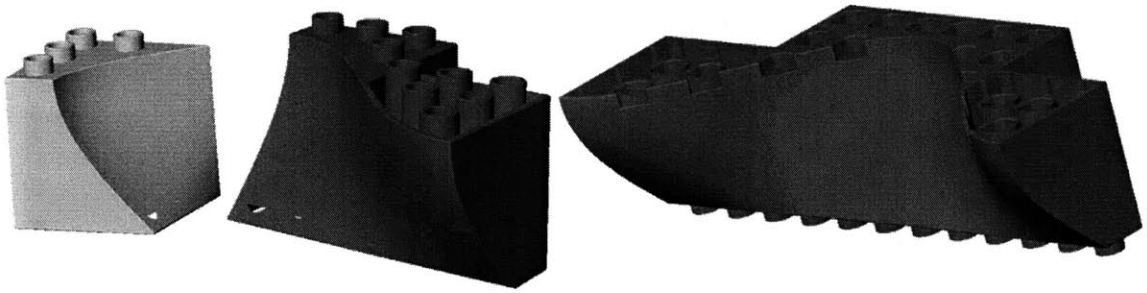

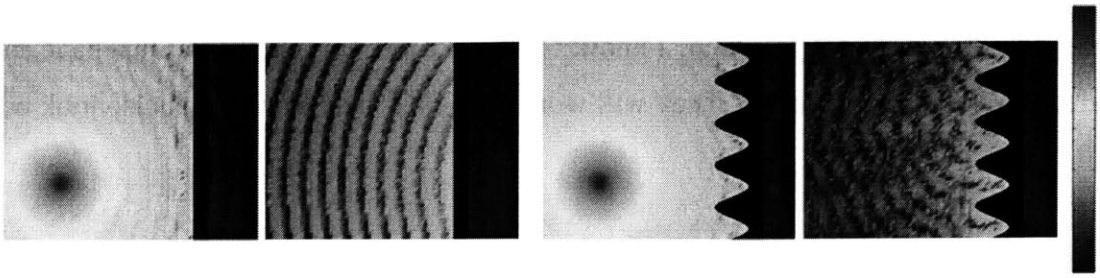

How would the world sound? The diffuse reflections off of the building might make the world sound better, or perhaps just quieter. Can it be modeled? What would the sound *look* like...

Maybe the world can be rebuilt. Rounded buildings on a rounded planet existing in harmony. Delusions of grandeur. Maybe just rebuild campus...

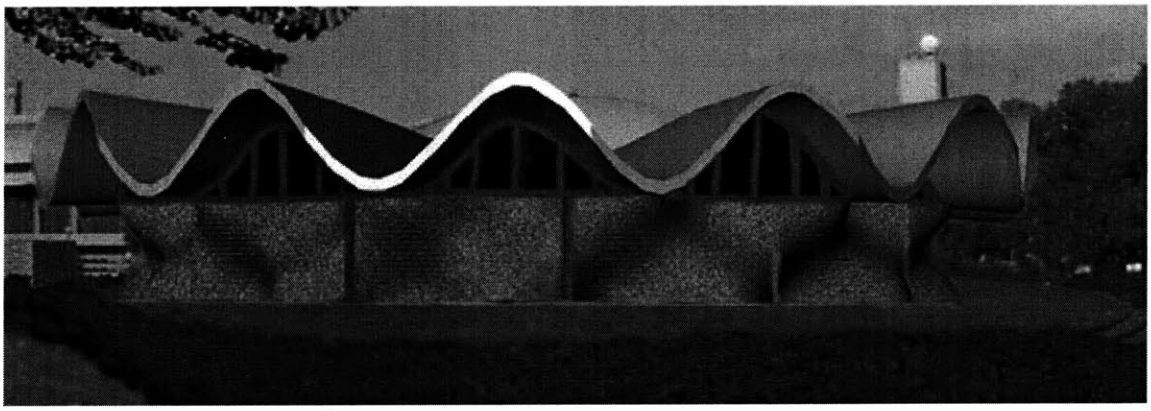

Uh-oh. I have to defend this idea. What do I do? I am not in the architecture department. But I am in a machine design group. I know... I'll make machine enclosures that have curvature. They will sound better. They will work better. Of course they will also look better.

Appendix A

FINITE ELEMENT ANALYSIS OF ISOTROPIC CURVED PANELS

A.1 Overview

The following pages include dynamic information on two of the designs discussed in Chapter 3. For each panel their is a short description of the design and illustrations of the first 8 modes, with their accompanying resonant frequencies. The purpose of this appendix is to allow the reader to visualize some of the dynamic properties of the various designs.

The finite element analysis was performed on Pro\Mechanica. The panels were initially designed and analyzed in Matlab, then their profiles were exported to Pro\Engineer. Only displacement analysis was performed so that the modes could be visualized. The software predicted that all the following results were accurate to within plus or minus 2 percent.

A.2 Results

For comparison, the results of a flat panel are included. The flat panel has the same footprint and thickness as the other panels. All boundaries are clamped.

Panel Design:	**Flat**
Sheet Thickness:	0.064"
Total Thickness:	0.064"
Length:	18.0"
Width:	12.0"
Material:	6061 Aluminum

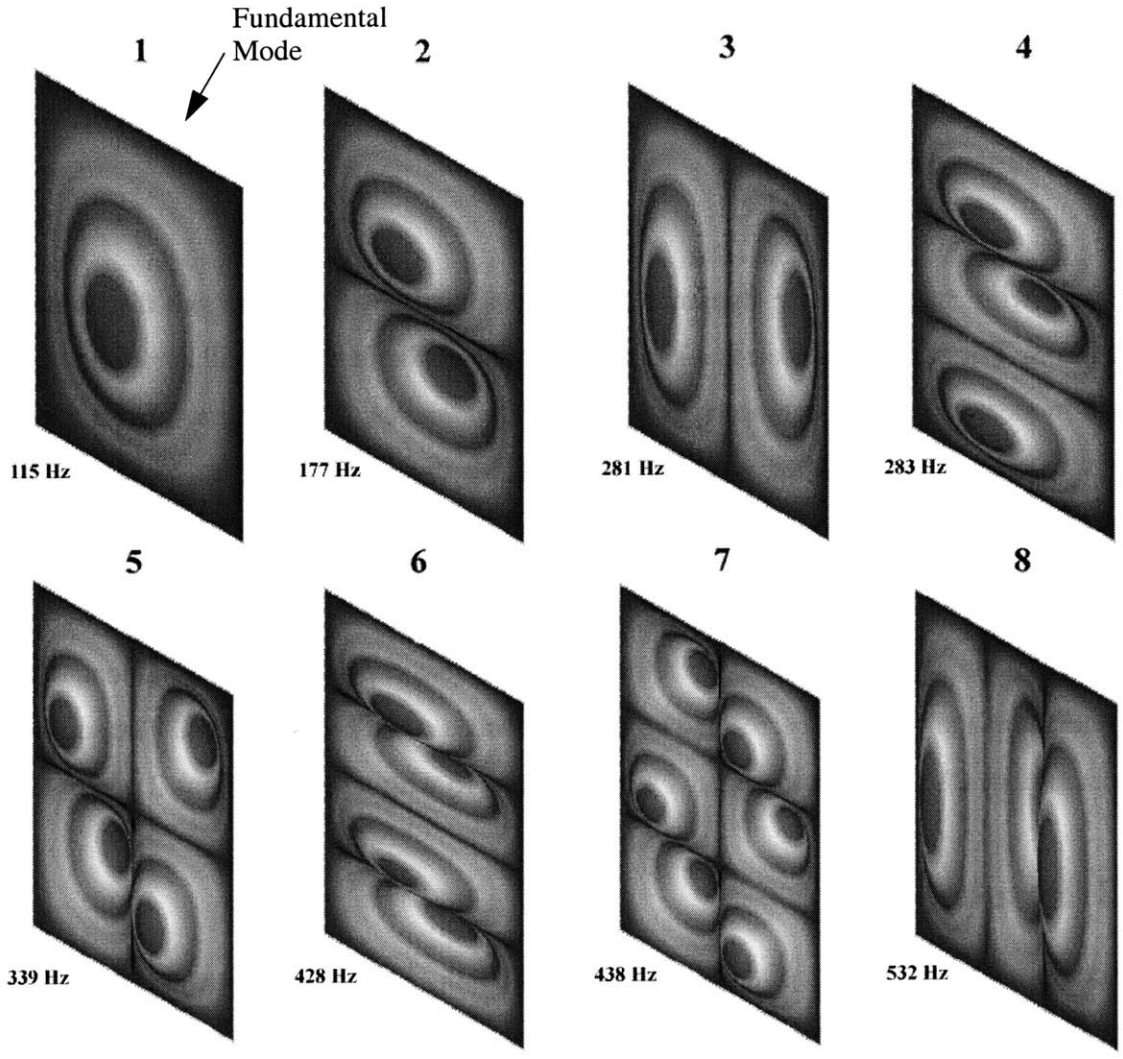

Figure A.1 First 8 modes for a flat panel. *Note: m*odes 1, 4, and 8 are "even" modes, while modes 2, 3, 5, 6, and 7 are "odd" modes. "Even" or "odd" refer to the number of nodal lines parallel to the boundaries. "Even" modes are more detrimental to the acoustics.

Panel Design:	**Fourier** (product and sum of sine waves) see Figure 3.3b
Sheet Thickness:	0.064"
Total Thickness:	0.264"
Length:	18.0"
Width:	12.0"
Material:	6061 Aluminum

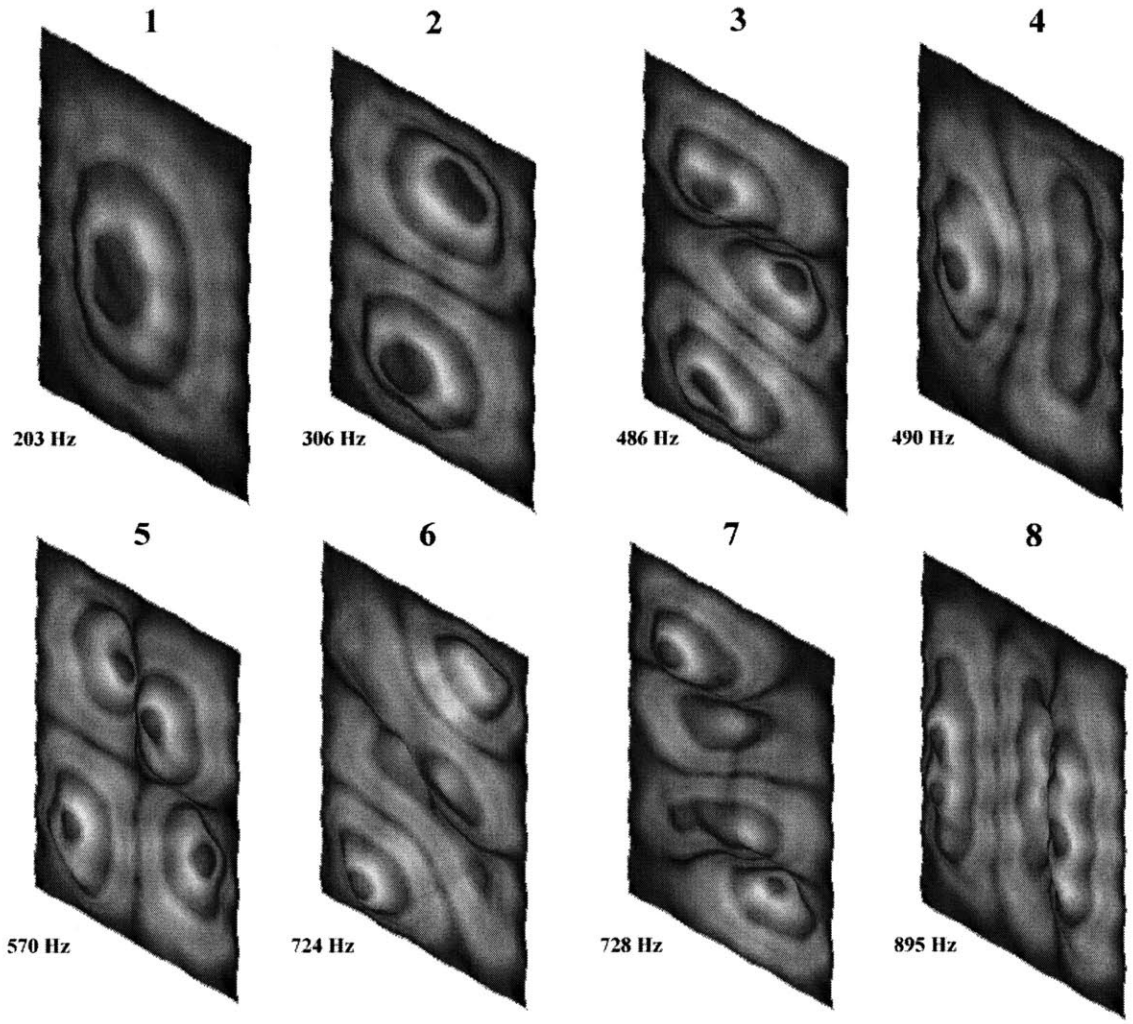

Figure A.2 First 8 modes for a panel design 1 with an amplitude of 0.2".

Panel Design:	**Fourier** (product and sum of sine waves) see Figure 3.3b
Sheet Thickness:	0.064"
Total Thickness:	0.464"
Length:	18.0"
Width:	12.0"
Material:	6061 Aluminum

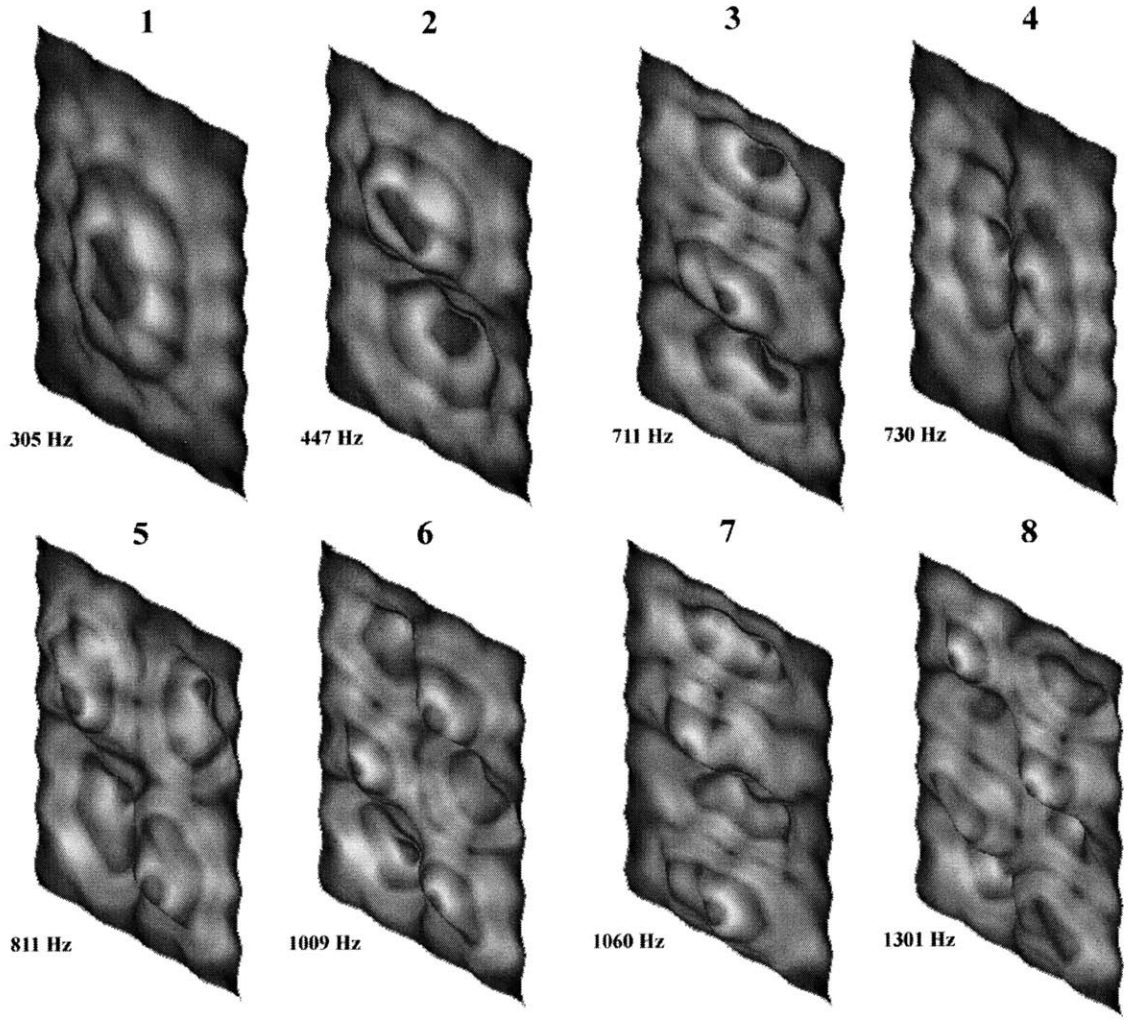

Figure A.3 First 8 modes for a panel design 1 with an amplitude of 0.4".

Panel Design:	**Fourier** (product and sum of sine waves) see Figure 3.3b
Sheet Thickness:	0.064"
Total Thickness:	0.664"
Length:	18.0"
Width:	12.0"
Material:	6061 Aluminum

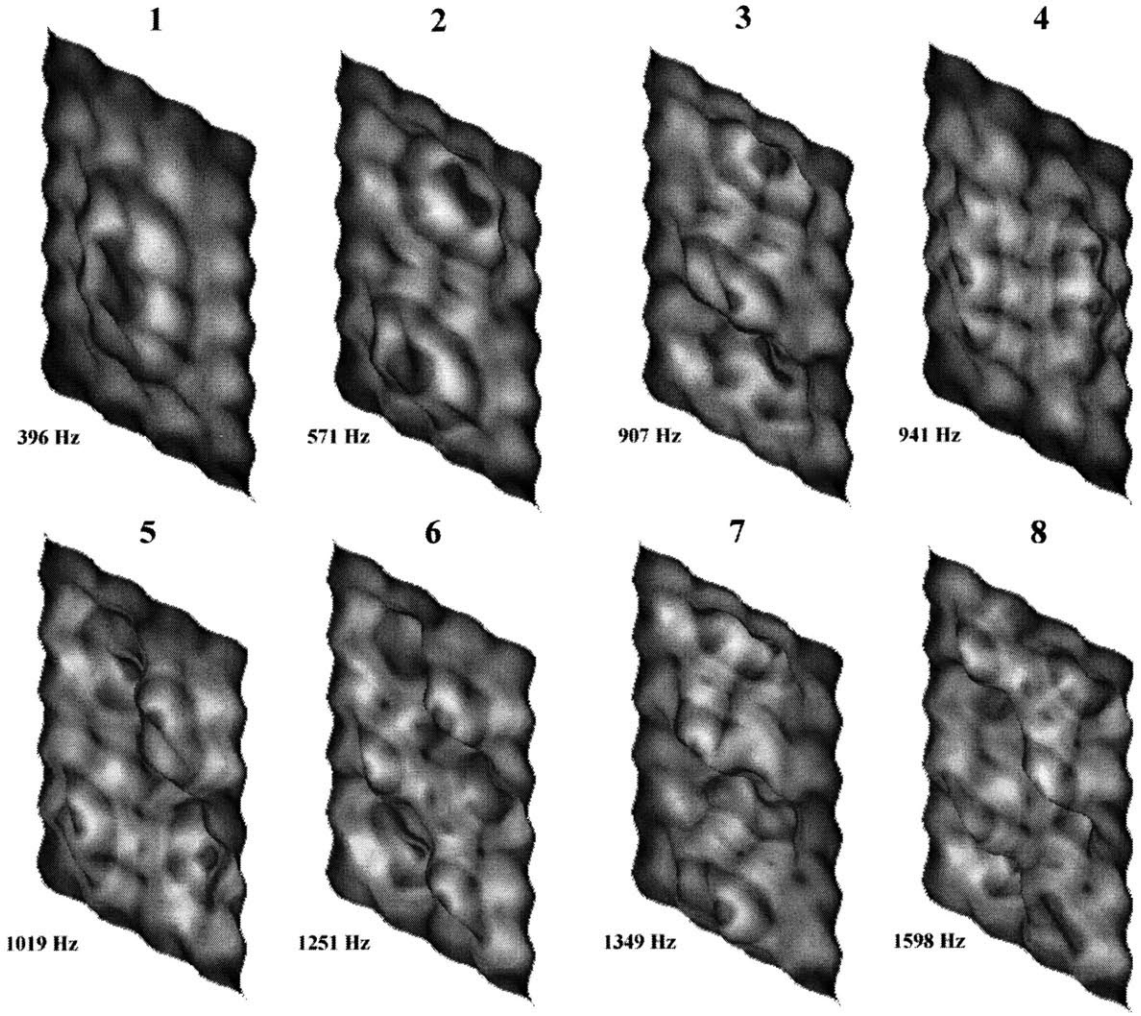

Figure A.4 First 8 modes for a panel design 1 with an amplitude of 0.6".

Panel Design:	**Fourier** (product and sum of sine waves) see Figure 3.3b
Sheet Thickness:	0.064"
Total Thickness:	0.864"
Length:	18.0"
Width:	12.0"
Material:	6061 AluminumP

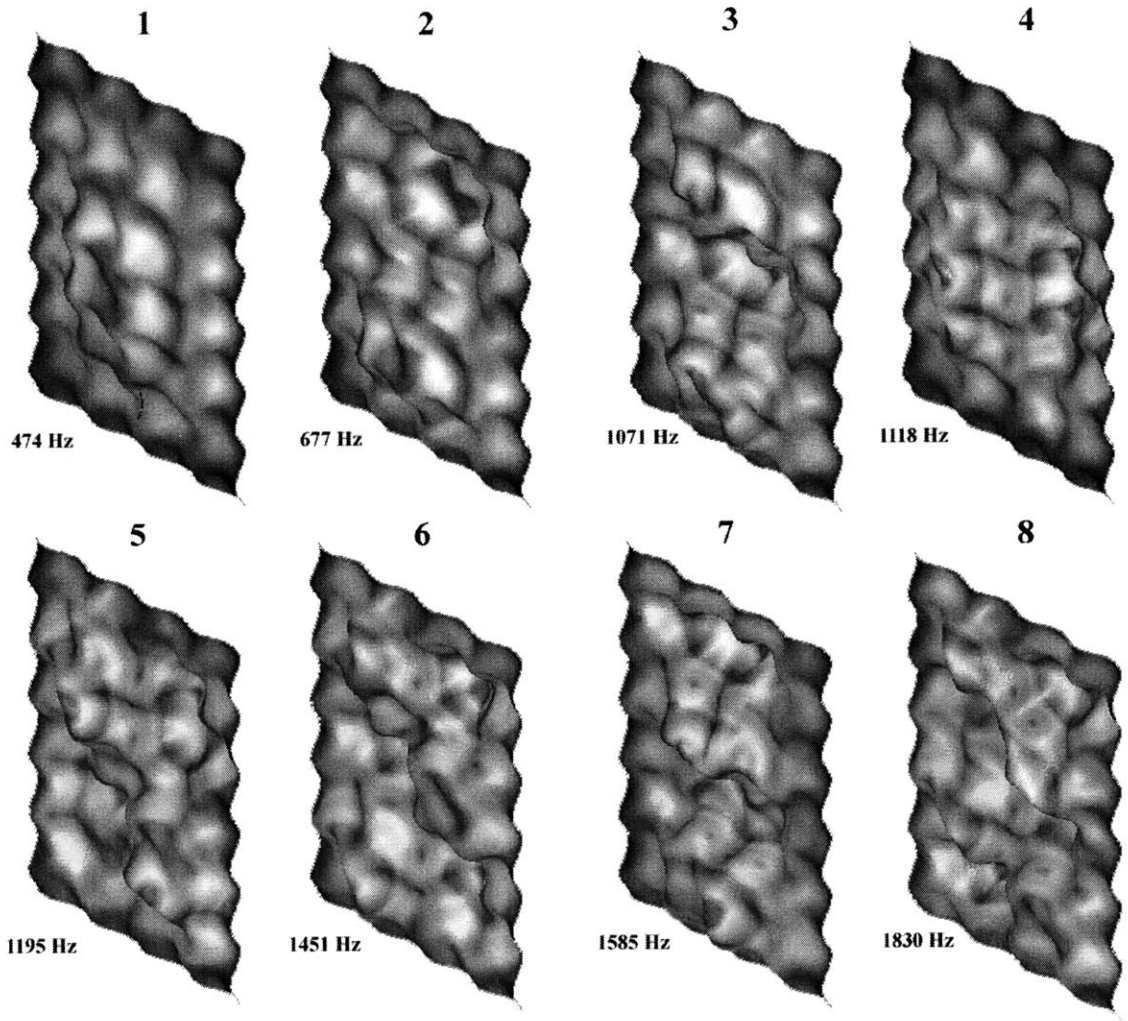

Figure A.5 First 8 modes for a panel design 1 with an amplitude of 0.8".

Panel Design:	**Course Maze Design**, similar to that shown in Figure 3.2d
Sheet Thickness:	0.064"
Total Thickness:	0.664"
Length:	18.0"
Width:	12.0"
Material:	6061 Aluminum

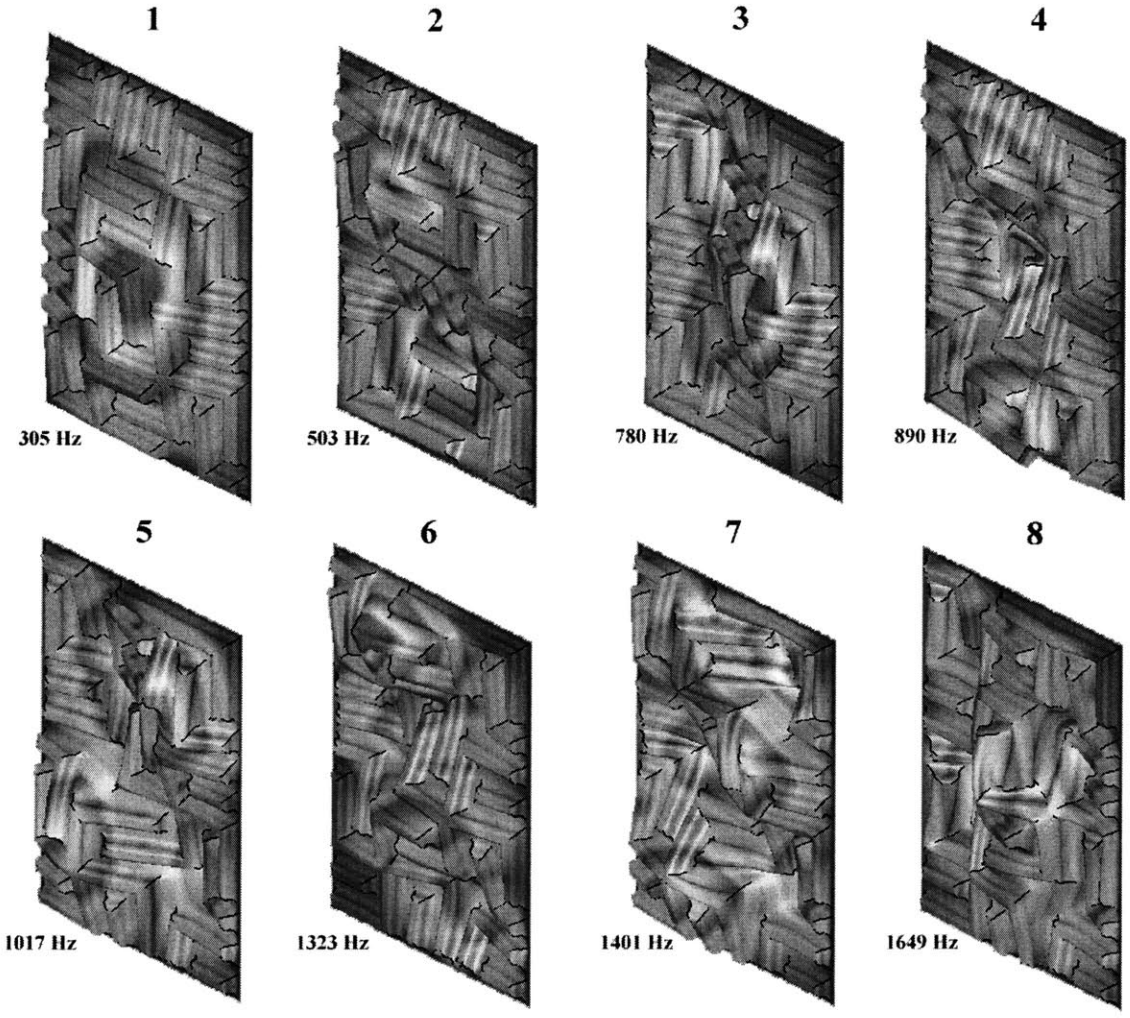

Figure A.6 First 8 modes for a maze shaped panel with an amplitude of 0.6".

Appendix B

FINITE ELEMENT ANALYSIS OF MODE-SHAPED PANELS

B.1 Overview

The following pages include dynamic information on some of the designs discussed in Chapter 4. For each panel their is a short description of the design and illustrations of the first 8 modes, with their accompanying resonant frequencies. The purpose of this appendix is to allow the reader to visualize some of the dynamic properties of the various designs.

The finite element analysis was performed on Pro\Mechanica. The panels were initially designed and analyzed in Matlab, then their profiles were exported to Pro\Engineer. Only displacement analysis was performed so that the modes could be visualized. The software predicted that all the following results were accurate to within plus or minus 2 percent.

B.2 Results

For comparison, the results of a flat panel are included. The flat panel has the same footprint and thickness as the other panels. All boundaries are clamped.

Panel Design:	**Flat**
Sheet Thickness:	0.064"
Total Thickness:	0.064"
Length:	18.0"
Width:	12.0"
Material:	6061 Aluminum

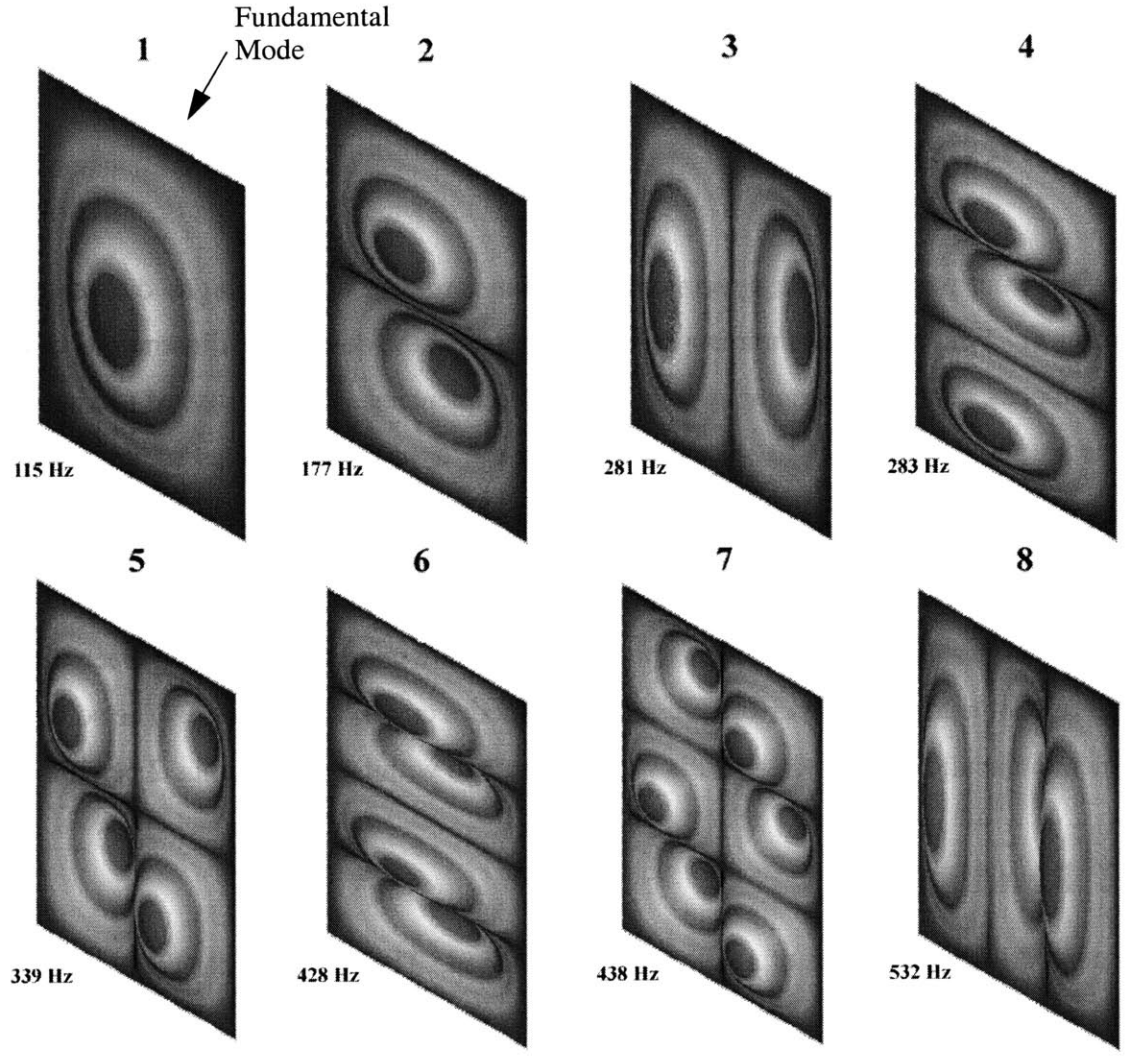

Figure B.1 First 8 modes for a flat panel. *Note: m*odes 1, 4, and 8 are "even" modes, while modes 2, 3, 5, 6, and 7 are "odd" modes. "Even" or "odd" refer to the number of nodal lines parallel to the boundaries. "Even" modes are more detrimental to the acoustics.

Panel Design:	**Mode 0-0**, see Figure 4.1
Sheet Thickness:	0.064"
Total Thickness:	0.164"
Length:	18.0"
Width:	12.0"
Material:	6061 Aluminum

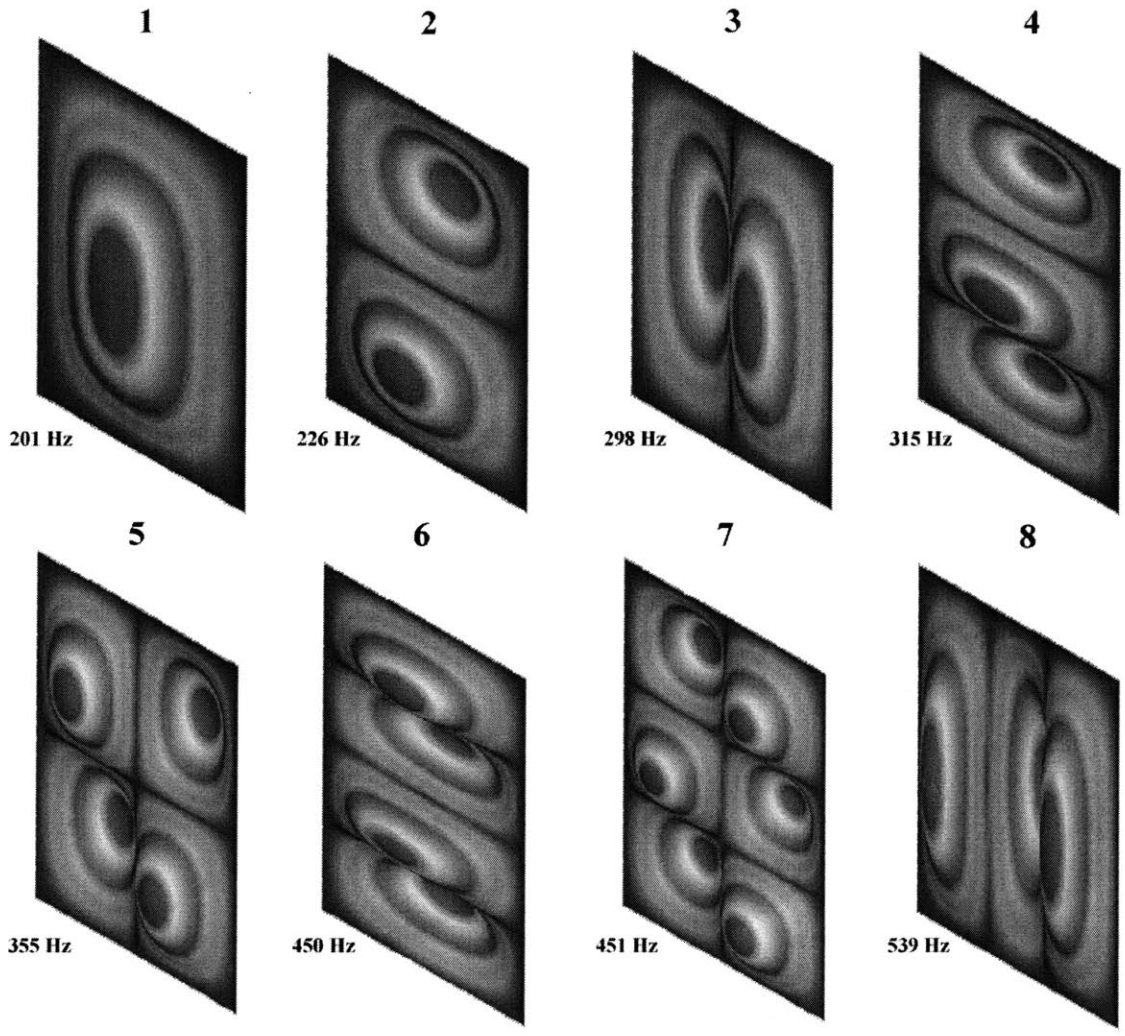

Figure B.2 First 8 modes for a panel shaped as first fundamental mode (of a flat panel) with an amplitude of 0.1".

Panel Design:	**Mode 0-0**, see Figure 4.1
Sheet Thickness:	0.064"
Total Thickness:	0.264"
Length:	18.0"
Width:	12.0"
Material:	6061 Aluminum

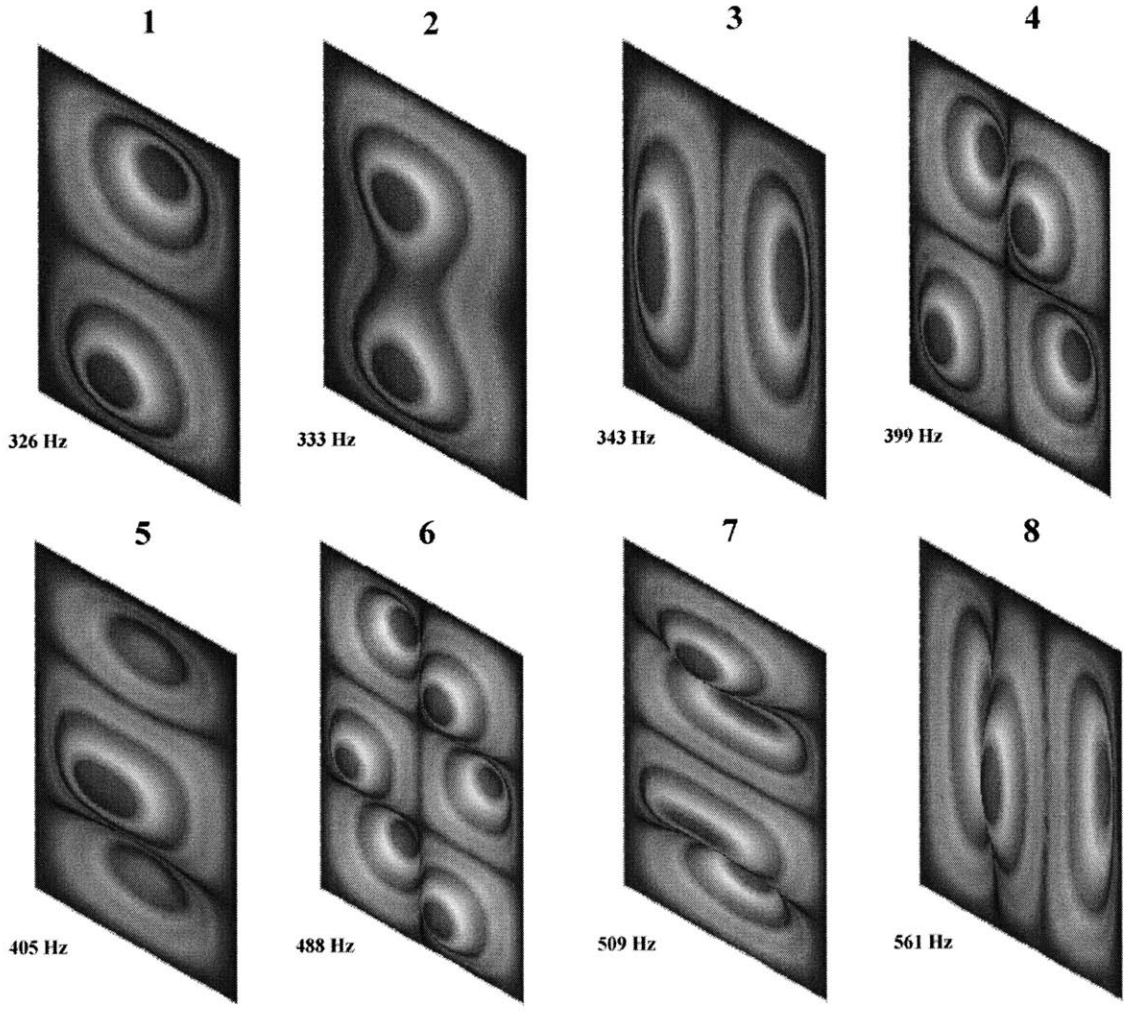

Figure B.3 First 8 modes for a panel shaped as first fundamental mode (of a flat panel) with an amplitude of 0.2".

Panel Design:	**Mode 0-0**, see Figure 4.1
Sheet Thickness:	0.064"
Total Thickness:	0.464"
Length:	18.0"
Width:	12.0"
Material:	6061 Aluminum

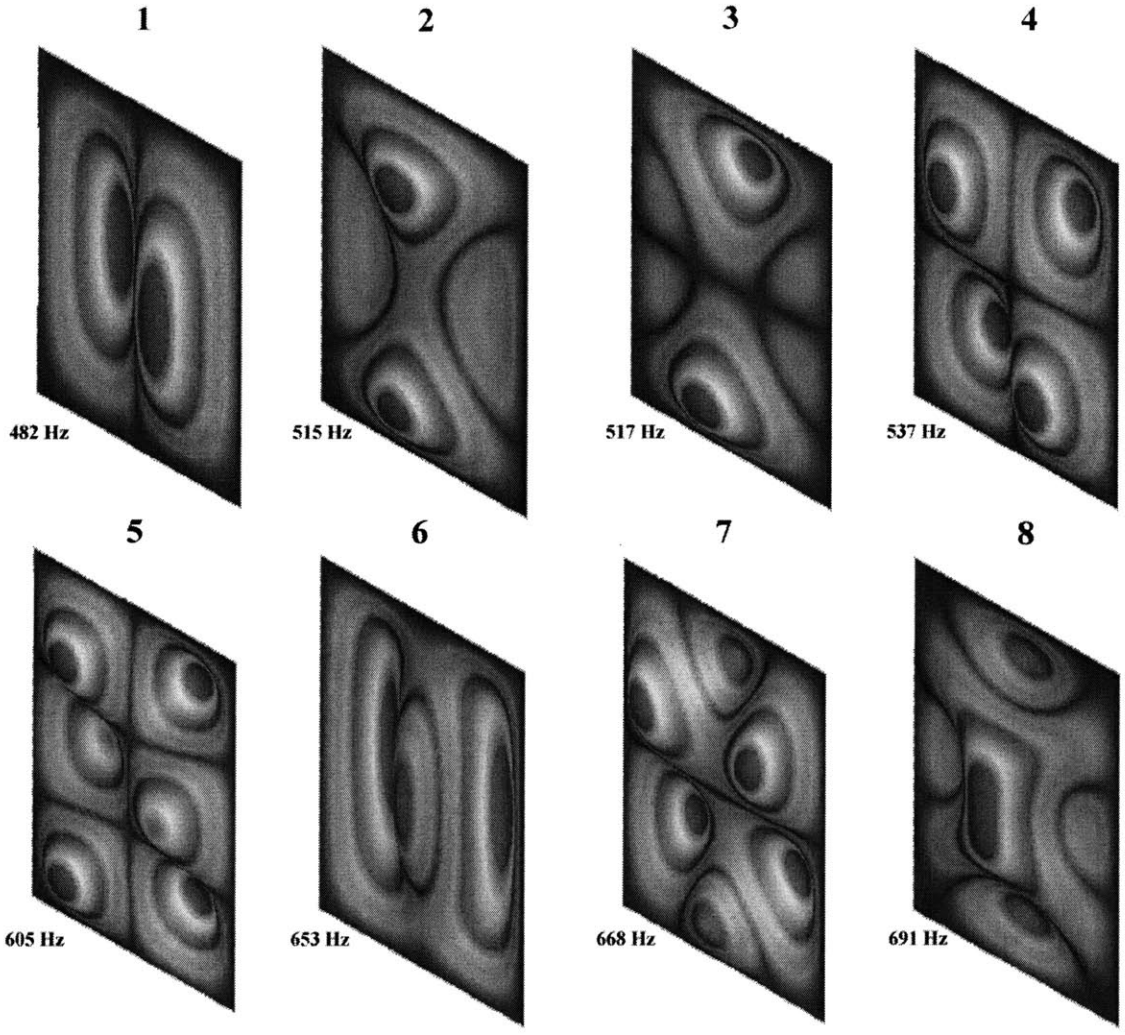

Figure B.4 First 8 modes for a panel shaped as first fundamental mode (of a flat panel) with an amplitude of 0.4".

Panel Design:	**Mode 0-0**, see Figure 4.1
Sheet Thickness:	0.064"
Total Thickness:	0.664"
Length:	18.0"
Width:	12.0"
Material:	6061 Aluminum

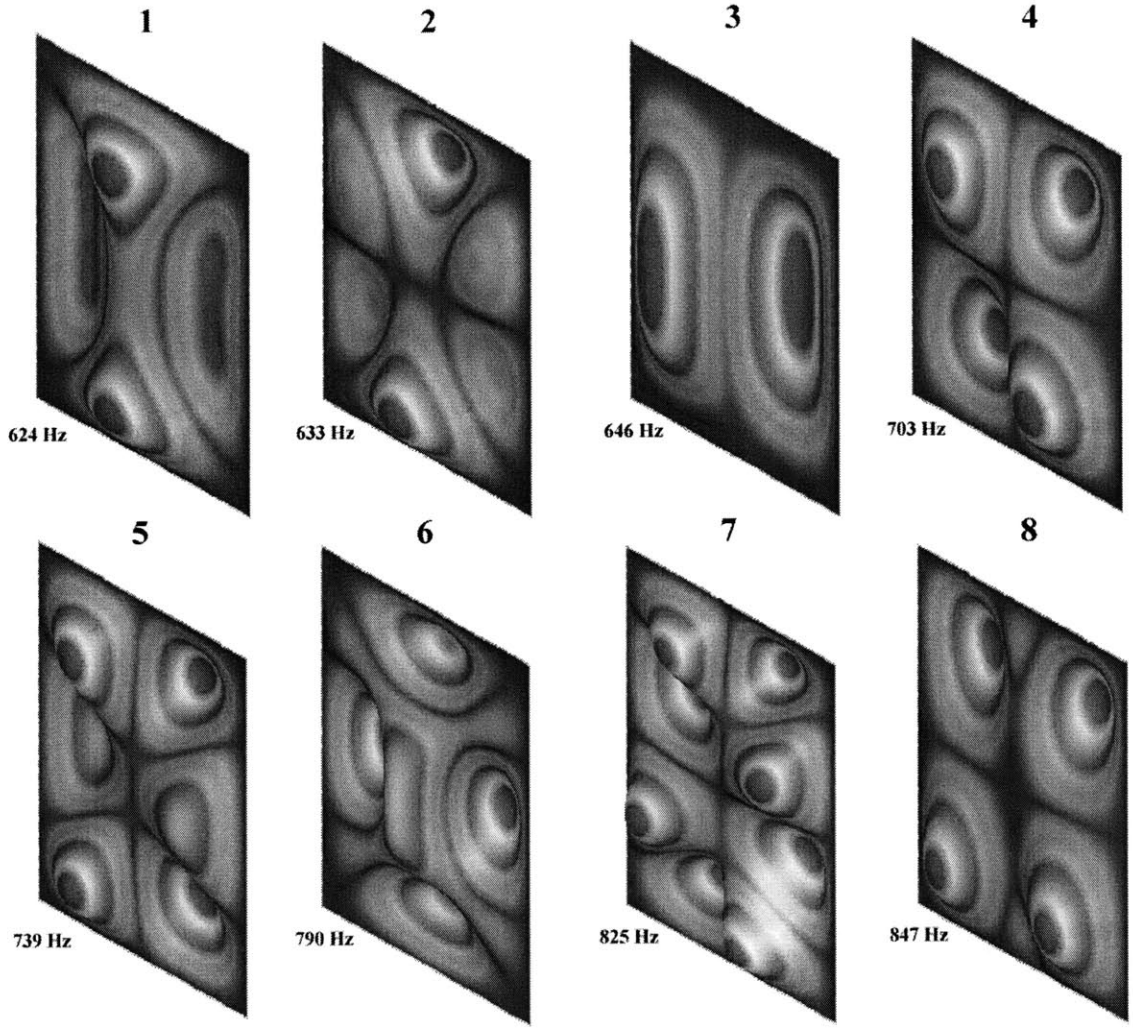

Figure B.5 First 8 modes for a panel shaped as first fundamental mode (of a flat panel) with an amplitude of 0.6".

Panel Design:	**Mode 0-0**, see Figure 4.1
Sheet Thickness:	0.064"
Total Thickness:	0.864"
Length:	18.0"
Width:	12.0"
Material:	6061 Aluminum

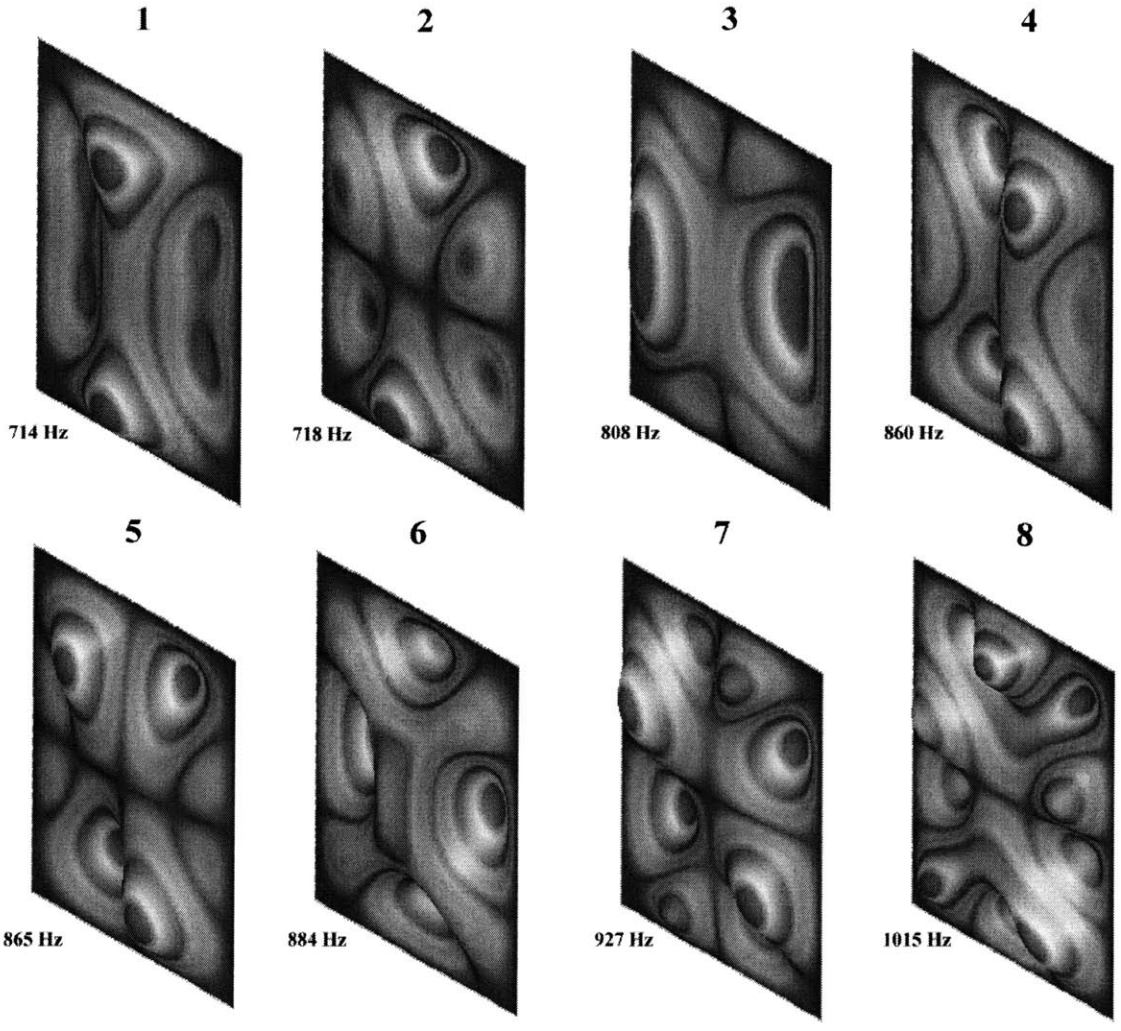

Figure B.6 First 8 modes for a panel shaped as first fundamental mode (of a flat panel) with an amplitude of 0.8".

Panel Design:	**Mode 0-0**, see Figure 4.1
Sheet Thickness:	0.064"
Total Thickness:	1.064"
Length:	18.0"
Width:	12.0"
Material:	6061 Aluminum

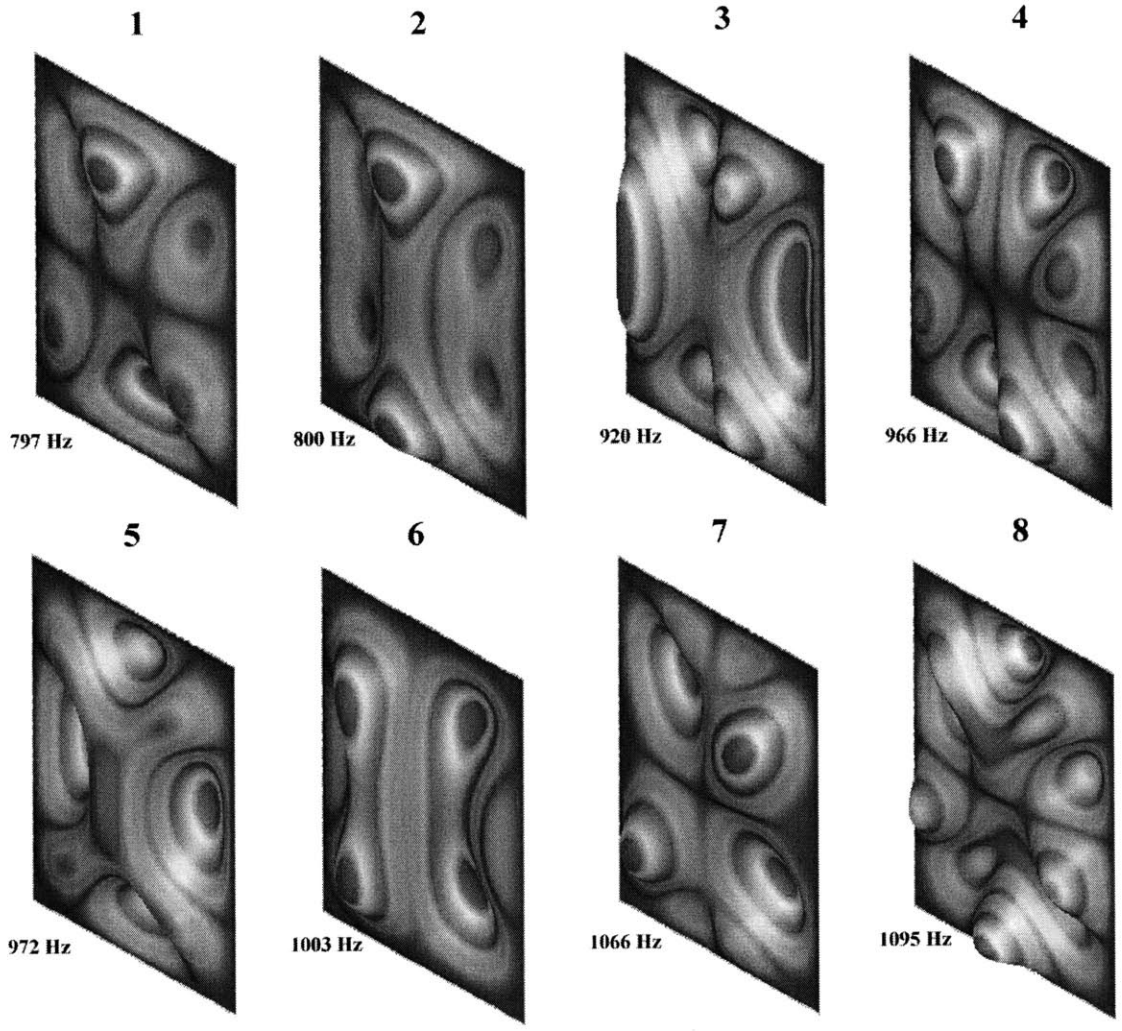

Figure B.7 First 8 modes for a panel shaped as first fundamental mode (of a flat panel) with an amplitude of 1.0".

Panel Design:	**Mode 2-0**, see Figure 4.1
Sheet Thickness:	0.064"
Total Thickness:	0.664"
Length:	18.0"
Width:	12.0"
Material:	6061 Aluminum

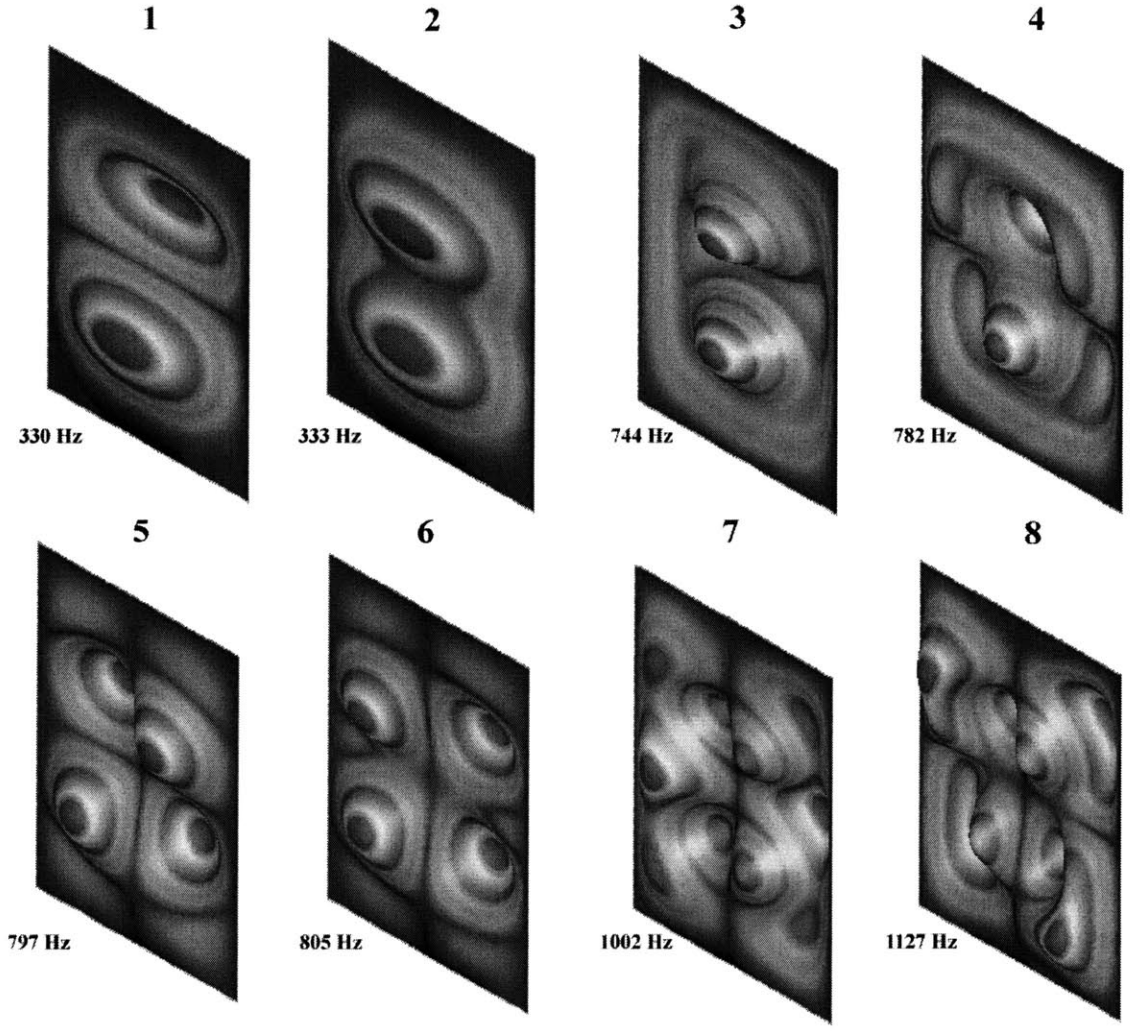

Figure B.8 First 8 modes for a panel shaped as fourth mode (of a flat panel) with an amplitude of 0.6".

Panel Design:	**Mode 0-0 plus Mode 2-0**
Sheet Thickness:	0.064"
Total Thickness:	0.464"
Length:	18.0"
Width:	12.0"
Material:	6061 Aluminum

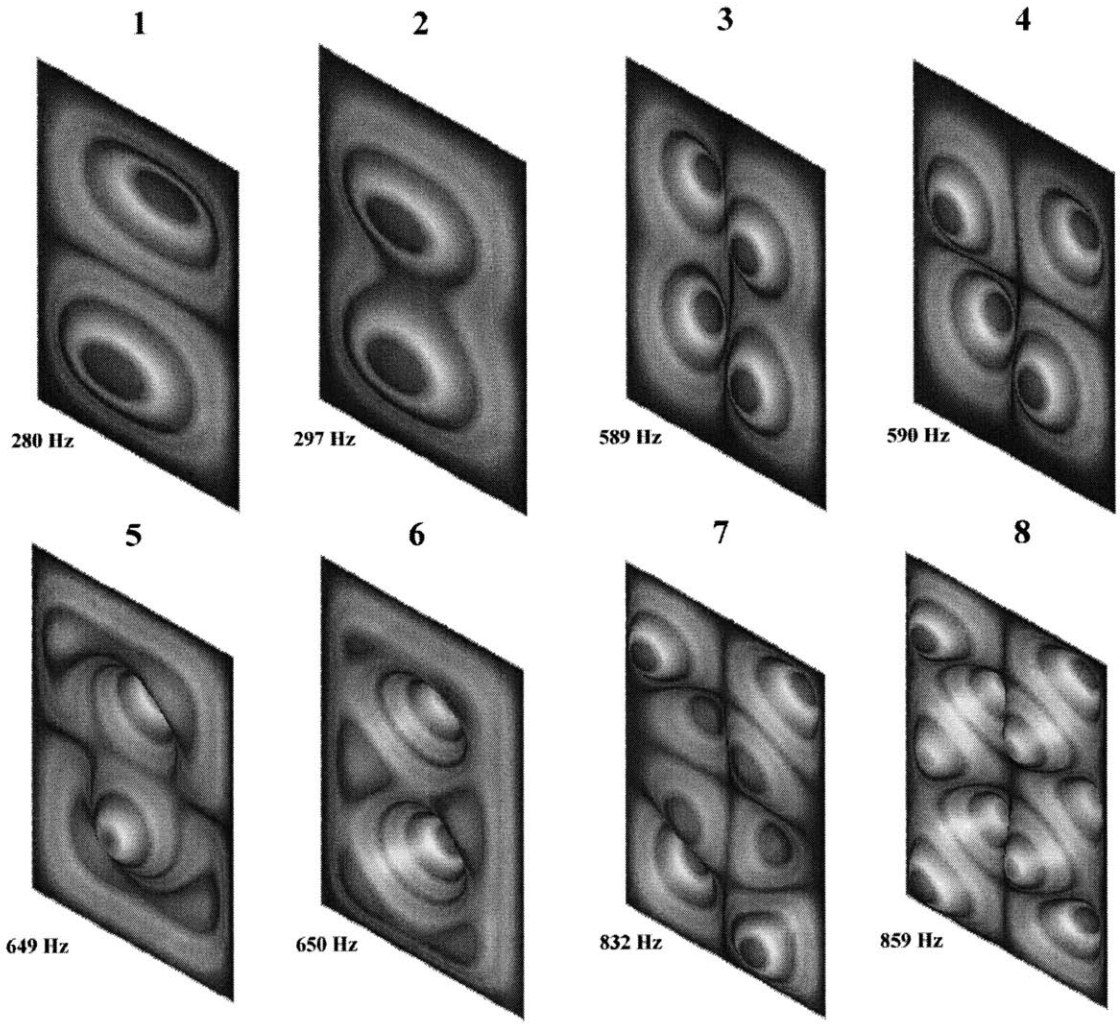

Figure B.9 First 8 modes for a panel shaped as first and fourth modes (of a flat panel) with an amplitude of 0.4".

Panel Design:	**Mode 0-0 plus Mode 2-0,**
Sheet Thickness:	0.064"
Total Thickness:	0.664"
Length:	18.0"
Width:	12.0"
Material:	6061 Aluminum

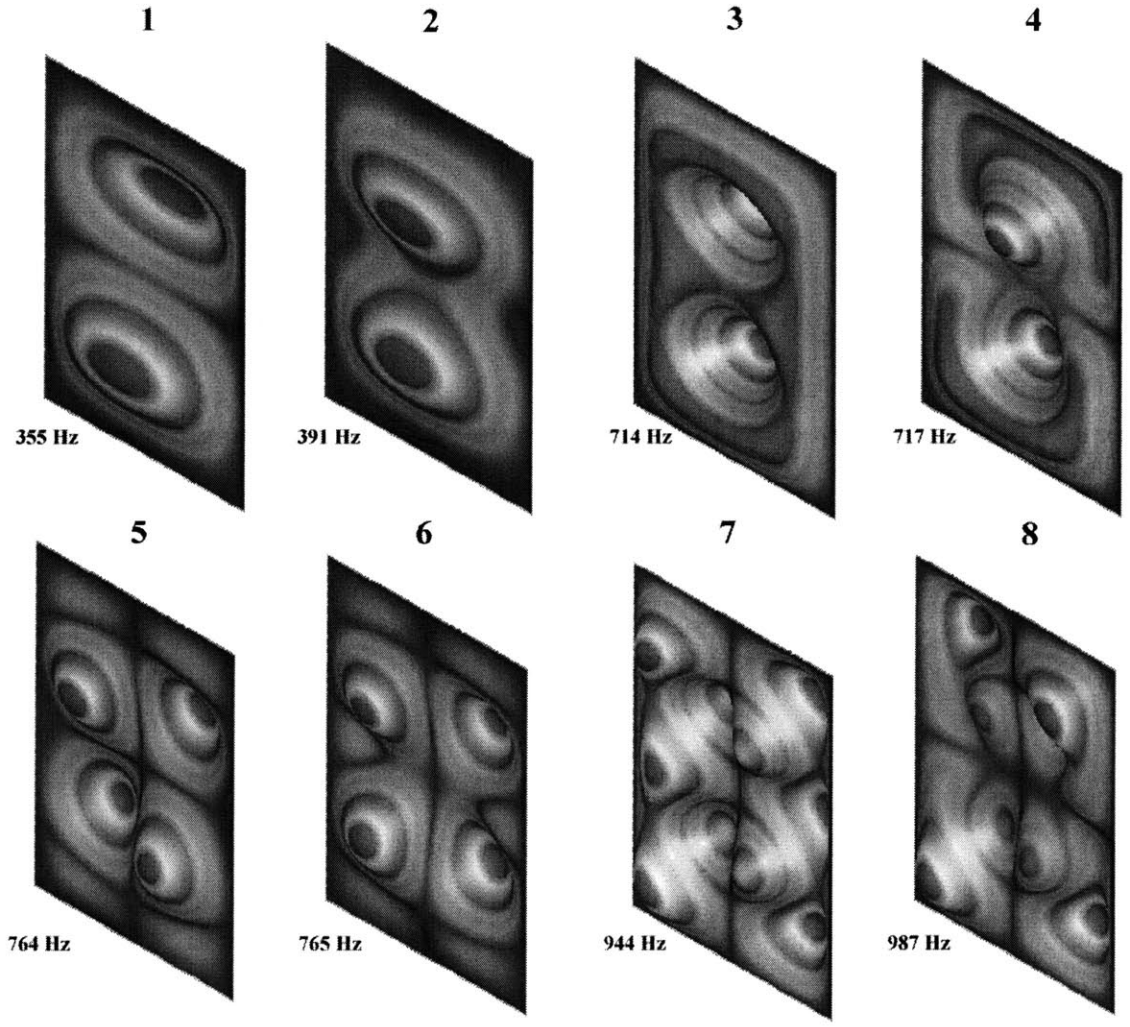

Figure B.10 First 8 modes for a panel shaped as first and fourth modes (of a flat panel) with an amplitude of 0.6".

Panel Design:	**Mode 0-0 plus Mode 2-0**
Sheet Thickness:	0.064"
Total Thickness:	0.864"
Length:	18.0"
Width:	12.0"
Material:	6061 Aluminum

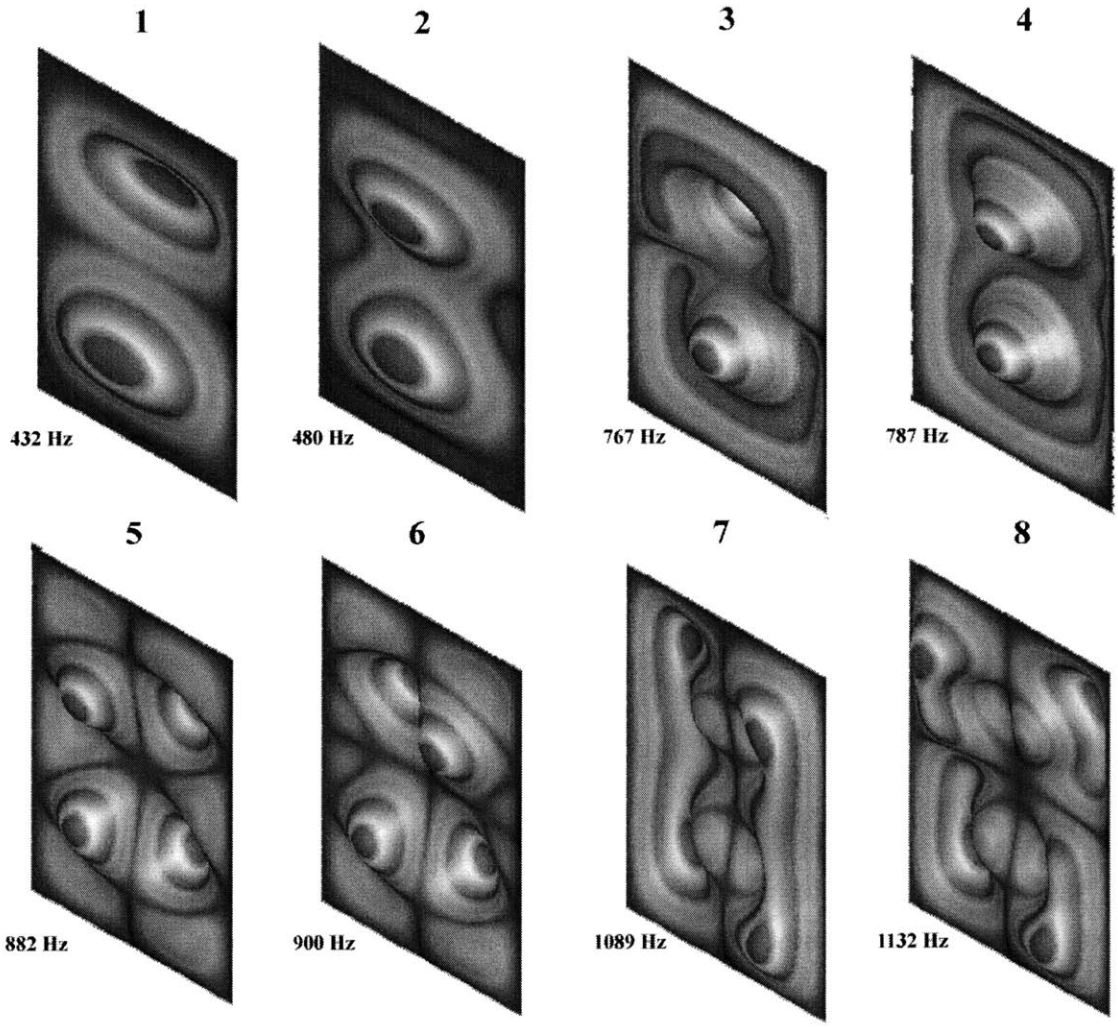

Figure B.11 First 8 modes for a panel shaped as first and fourth modes (of a flat panel) with an amplitude of 0.8".

Appendix C

RAW EXPERIMENTAL RESULTS

All the raw experimental results are contained in this appendix to allow the reader the opportunity to see the data before it was reduced. The raw data is in the form of tables for the static experiments and transfer functions for the dynamic experiments. The transfer functions presented are for individual actuator-sensor pairs instead of averages of pairs, as was presented in Chapter 6. In some cases, data not presented in Chapter 6 is reduced and included in this appendix. This extra data was not seen as central to thesis, but may be of interest to the reader.

C.1 Static Bending Experiment Data

The bending displacement data is presented in the following tables. All data is presented for the 3/8 inch core and 7/8 inch core panels, for both the 4 point and 3 point bending tests.

C.1.1 Four Point Bending Tests on 3/8 inch Core Panels

Bending Along Width

Polypropylene Honeycomb **EI (psi*in.^4) = 25733**

Displacement (mils)	Measured Force (lb)	Idealized Force (lb)	Normalized Force (lb/lb)
0.7	0.50	0.8412	0.4161
1.3	1.10	1.5622	0.9154
2.0	1.70	2.4034	1.4146
2.6	2.20	3.1245	1.8307
3.2	2.75	3.8455	2.2884
3.7	3.20	4.4463	2.6629
4.5	3.90	5.4077	3.2454
5.5	4.85	6.6094	4.0359
6.2	5.35	7.4506	4.4520
7.0	5.95	8.4120	4.9513
7.6	6.35	9.1330	5.2841
8.1	6.80	9.7339	5.6586
8.8	7.60	10.5751	6.3243
9.4	8.05	11.2961	6.6988
SLOPES	**0.8558**	**1.2017**	**0.7122**
R-Squared	**0.9989**		
Deflection due to Shear	**4.56%**		

0.06" Thick Acrylic - Zig-zag Design **EI (psi*in.^4) = 16971**

Displacement (mils)	Measured Force (lb)	Idealized Force (lb)	Normalized Force (lb/lb)
0.6	0.50	0.4850	0.6186
1.1	1.00	0.8892	1.2371
1.8	1.60	1.4550	1.9794
2.4	2.00	1.9400	2.4742
3.0	2.55	2.4250	3.1546
3.6	2.90	2.9100	3.5876
4.2	3.35	3.3950	4.1443
4.8	3.75	3.8800	4.6391
5.5	4.25	4.4459	5.2577
6.0	4.60	4.8500	5.6907
6.6	5.05	5.3350	6.2474
7.2	5.45	5.8200	6.7422
7.9	6.05	6.3859	7.4845
8.5	6.50	6.8709	8.0412
SLOPES	**0.7379**	**0.8083**	**0.9129**
R-Squared	**0.9988**		
Deflection due to Shear	**2.66%**		

0.03" Thick PETG - Zig-zag Design **EI (psi*in.^4) = 13997**

Displacement (mils)	Measured Force (lb)	Idealized Force (lb)	Normalized Force (lb/lb)
0.7	0.40	0.4590	0.6100
1.2	0.75	0.7869	1.1438
1.8	1.25	1.1803	1.9063
2.4	1.70	1.5737	2.5925
2.9	2.00	1.9016	3.0500
3.5	2.50	2.2950	3.8126
4.0	2.80	2.6229	4.2701
4.6	3.25	3.0163	4.9563
5.3	3.65	3.4754	5.5663
6.0	4.05	3.9344	6.1763
6.7	4.40	4.3934	6.7101
7.4	5.00	4.8524	7.6251
8.1	5.40	5.3114	8.2351
8.8	5.95	5.7704	9.0739
SLOPES	**0.67**	**0.6557**	**1.0219**
R-Squared	**0.9979**		
Deflection due to Shear	**4.25%**		

Bending Along Length

Polypropylene Honeycomb **EI (psi*in.^4) = 25733**

Displacement (mils)	Measured Force (lb)	Idealized Force (lb)	Normalized Force (lb/lb)
0.5	1.75	2.9382	0.2978
0.9	3.30	5.2887	0.5616
1.3	4.80	7.6392	0.8168
1.8	7.10	10.5774	1.2082
2.2	8.50	12.9279	1.4465
2.5	10.00	14.6908	1.7017
3.0	11.90	17.6289	2.0251
3.4	13.50	19.9795	2.2974
3.9	15.30	22.9176	2.6037
4.4	17.20	25.8558	2.9270
SLOPES	**4.00**	**5.8763**	**0.6813**
R-Squared	**0.9993**		
Deflection due to Shear	**10.65%**		

0.06" Thick Acrylic - Zig-zag Design **EI (psi*in.^4) = 16971**

Displacement (mils)	Measured Force (lb)	Idealized Force (lb)	Normalized Force (lb/lb)
0.5	3.30	2.1023	0.7849
0.9	4.95	3.7842	1.1773
1.2	7.00	5.0455	1.6648
1.5	8.80	6.3069	2.0929
1.8	10.65	7.5683	2.5329
2.1	12.40	8.8297	2.9491
2.4	14.25	10.0911	3.3891
2.6	15.60	10.9320	3.7102
2.9	17.30	12.1934	4.1145
3.1	18.55	13.0343	4.4118
3.3	19.75	13.8752	4.6972
3.5	20.95	14.7162	4.9826
SLOPES	**6.02**	**4.2046**	**1.4307**
R-Squared	**0.9991**		
Deflection due to Shear	**6.38%**		

0.03" Thick PETG - Zig-zag Design **EI (psi*in.^4) = 13997**

Displacement (mils)	Measured Force (lb)	Idealized Force (lb)	Normalized Force (lb/lb)
0.4	1.25	1.3337	0.3749
1.0	3.75	3.3342	1.1247
1.4	5.40	4.6679	1.6196
1.7	6.30	5.6682	1.8895
2.0	7.55	6.6685	2.2644
2.3	8.80	7.6688	2.6393
2.6	10.00	8.6690	2.9992
2.9	11.20	9.6693	3.3591
3.2	12.40	10.6696	3.7190
3.6	13.95	12.0033	4.1838
4.0	15.50	13.3370	4.6487
4.5	17.55	15.0041	5.2636
SLOPES	**3.96**	**3.3342**	**1.1864**
R-Squared	**0.9998**		
Deflection due to Shear	**9.98%**		

C.1.2 Three Point Bending Tests on 3/8 inch Core Panels

Bending Along Width

Polypropylene Honeycomb **EI (psi*in.^4) = 25733**

Displacement (mils)	Measured Force (lb)	Idealized Force (lb)	Normalized Force (lb/lb)
0.6	0.45	0.5231	0.5162
1.1	0.80	0.9589	0.9177
1.6	1.15	1.3948	1.3192
2.1	1.50	1.8307	1.7207
2.7	1.90	2.3537	2.1795
3.3	2.25	2.8768	2.5810
3.8	2.45	3.3127	2.8104
4.2	2.75	3.6614	3.1546
4.6	3.00	4.0101	3.4413
5.0	3.25	4.3588	3.7281
5.5	3.60	4.7946	4.1296
6.0	3.95	5.2305	4.5311
6.5	4.35	5.6664	4.9899
7.0	4.65	6.1023	5.3341
SLOPES	**0.64**	**0.8718**	**0.7386**
R-Squared	**0.9984**		
Deflection due to Shear	**6.06%**		

0.06" Thick Acrylic - Zig-zag Design **EI (psi*in.^4) = 16971**

Displacement (mils)	Measured Force (lb)	Idealized Force (lb)	Normalized Force (lb/lb)
0.6	0.30	0.3542	0.5082
1.1	0.65	0.6493	1.1012
1.8	1.10	1.0625	1.8636
2.5	1.45	1.4757	2.4565
3.0	1.75	1.7708	2.9648
3.5	1.95	2.0659	3.3036
4.2	2.40	2.4791	4.0660
5.0	2.70	2.9513	4.5742
5.5	3.05	3.2465	5.1672
6.0	3.35	3.5416	5.6754
6.5	3.65	3.8367	6.1836
6.8	3.80	4.0138	6.4378
7.3	4.05	4.3089	6.8613
7.7	4.25	4.5451	7.2001
SLOPES	**0.55**	**0.5903**	**0.9292**
R-Squared	**0.9987**		
Deflection due to Shear	**3.56%**		

Bending Along Length

Polypropylene Honeycomb **EI (psi*in.^4) = 25733**

Displacement (mils)	Measured Force (lb)	Idealized Force (lb)	Normalized Force (lb/lb)
0.4	1.20	1.8199	0.2637
0.9	2.70	4.0949	0.5934
1.4	3.85	6.3698	0.8462
1.8	5.05	8.1898	1.1099
2.2	6.10	10.0097	1.3407
2.5	6.80	11.3747	1.4945
2.9	7.55	13.1946	1.6594
3.2	8.35	14.5596	1.8352
3.6	9.30	16.3795	2.0440
4.0	10.00	18.1995	2.1979
SLOPES	**2.45**	**4.5499**	**0.5384**
R-Squared	**0.9964**		
Deflection due to Shear	**13.74%**		

0.06" Thick Acrylic - Zig-zag Design **EI (psi*in.^4) = 16971**

Displacement (mils)	Measured Force (lb)	Idealized Force (lb)	Normalized Force (lb/lb)
0.4	1.55	1.2577	0.4930
0.8	3.35	2.5153	1.0655
1.1	4.40	3.4585	1.3994
1.4	5.40	4.4018	1.7175
1.7	6.45	5.3450	2.0514
2.0	7.50	6.2883	2.3854
2.3	8.45	7.2315	2.6875
2.6	9.35	8.1747	2.9738
2.9	10.40	9.1180	3.3077
3.2	11.25	10.0612	3.5781
3.4	11.90	10.6901	3.7848
3.6	12.45	11.3189	3.9598
SLOPES	**3.34**	**3.1441**	**1.0630**
R-Squared	**0.9976**		
Deflection due to Shear	**8.35%**		

C.1.3 Four Point Bending Tests on 7/8 inch Core Panels

Bending Along Width

Polypropylene Honeycomb — **EI (psi*in.^4) = 97261**

Displacement (mils)	Measured Force (lb)	Idealized Force (lb)	Normalized Force (lb/lb)
0.5	1.55	2.0937	0.3702
1.0	2.95	4.1875	0.7045
1.4	3.90	5.8625	0.9313
1.8	5.50	7.5375	1.3134
2.2	6.90	9.2125	1.6478
2.6	8.00	10.8875	1.9105
3.0	9.40	12.5624	2.2448
3.4	10.65	14.2374	2.5433
3.8	12.00	15.9124	2.8657
4.2	13.15	17.5874	3.1403
4.6	14.45	19.2624	3.4508
4.9	15.25	20.5187	3.6418
5.3	16.55	22.1937	3.9523
6.0	18.70	25.1249	4.4657
SLOPES	**3.16**	**4.1875**	0.7554
R-Squared	**0.9994**		
Deflection due to Shear	**12.01%**		

0.06" Thick Acrylic - Maze Design — **EI (psi*in.^4) = 80364**

Displacement (mils)	Measured Force (lb)	Idealized Force (lb)	Normalized Force (lb/lb)
0.5	1.50	1.7029	0.4404
1.0	2.85	3.4059	0.8368
1.5	4.00	5.1088	1.1744
2.0	5.20	6.8117	1.5268
2.5	6.50	8.5147	1.9085
3.0	7.50	10.2176	2.2021
3.5	8.70	11.9206	2.5544
4.0	10.00	13.6235	2.9361
4.5	11.20	15.3264	3.2884
5.1	12.50	17.3700	3.6701
5.5	13.35	18.7323	3.9197
6.1	14.60	20.7758	4.2867
6.6	16.00	22.4788	4.6978
7.3	17.80	24.8629	5.2263
SLOPES	**2.36**	**3.4059**	**0.6922**
R-Squared	**0.9995**		
Deflection due to Shear	**13.39%**		

0.06" Thick Acrylic - Fourier Design — **EI (psi*in.^4) = 80364**

Displacement (mils)	Measured Force (lb)	Idealized Force (lb)	Normalized Force (lb/lb)
0.5	2.70	1.7029	0.7927
0.9	4.00	3.0653	1.1744
1.3	4.80	4.4276	1.4093
1.8	6.15	6.1306	1.8057
2.3	7.80	7.8335	2.2902
2.8	8.95	9.5364	2.6278
3.4	10.60	11.5800	3.1123
4.0	12.05	13.6235	3.5380
4.4	13.00	14.9858	3.8169
4.9	14.20	16.6888	4.1693
5.4	15.30	18.3917	4.4922
5.8	16.20	19.7541	4.7565
6.2	17.85	21.1164	5.2409
7.0	20.00	23.8411	5.8722
SLOPES	**2.60**	**3.4059**	0.7629
R-Squared	**0.9985**		
Deflection due to Shear	**13.39%**		

Bending Along Length

Polypropylene Honeycomb **EI (psi*in.^4) = 97261**

Displacement (mils)	Measured Force (lb)	Idealized Force (lb)	Normalized Force (lb/lb)
0.4	2.10	7.7343	0.1086
0.8	4.40	15.4686	0.2276
1.2	7.30	23.2028	0.3775
1.4	9.20	27.0700	0.4758
1.6	11.00	30.9371	0.5689
1.8	12.50	34.8043	0.6465
2.0	13.30	38.6714	0.6878
SLOPES	**7.39**	**19.3357**	**0.3822**
R-Squared	**0.9931**		
Deflection due to Shear	**25.41%**		

0.06" Thick Acrylic - Maze Design **EI (psi*in.^4) = 80364**

Displacement (mils)	Measured Force (lb)	Idealized Force (lb)	Normalized Force (lb/lb)
0.4	2.40	6.1387	0.1564
0.8	4.20	12.2775	0.2737
1.2	5.60	18.4162	0.3649
1.5	8.00	23.0203	0.5213
2.0	10.00	30.6937	0.6516
2.5	13.00	38.3672	0.8471
3.0	15.75	46.0406	1.0263
SLOPES	**5.18**	**15.3469**	**0.3373**
R-Squared	**0.9949**		
Deflection due to Shear	**27.84%**		

0.06" Thick Acrylic - Fourier Design **EI (psi*in.^4) = 80364**

Displacement (mils)	Measured Force (lb)	Idealized Force (lb)	Normalized Force (lb/lb)
0.5	1.15	7.6734	0.0749
1.0	2.45	15.3469	0.1596
1.5	4.60	23.0203	0.2997
1.9	6.20	29.1590	0.4040
2.2	8.10	33.7631	0.5278
2.5	9.90	38.3672	0.6451
3.0	12.30	46.0406	0.8015
SLOPES	**4.58**	**15.3469**	**0.2986**
R-Squared	**0.9849**		
Deflection due to Shear	**27.84%**		

C.2 Vibration Data

The raw vibration data is for a shaker and a speaker to three separate accelerometers. To better understand the location of the actuators and sensors the following key is provided in Figure C.1. The letters in the figure indicate which sensor is which in the transfer function plots (refer to the plot legend).

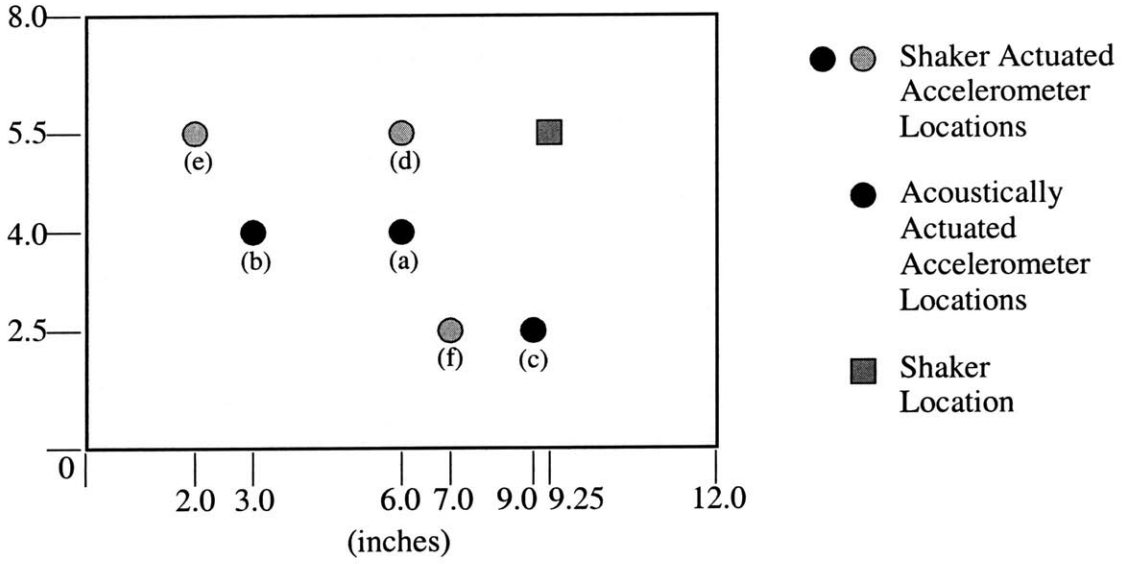

Figure C.1 Illustration showing the locations of the accelerometers and shaker for the vibration and radiation experiments. More accelerometers were required to accurately perform the radiation experiments, and they were performed using a shaker actuator. The letters indicate which transfer function belongs to which sensor on the plot legends.

C.2.1 Shaker Actuated Undamped Panels

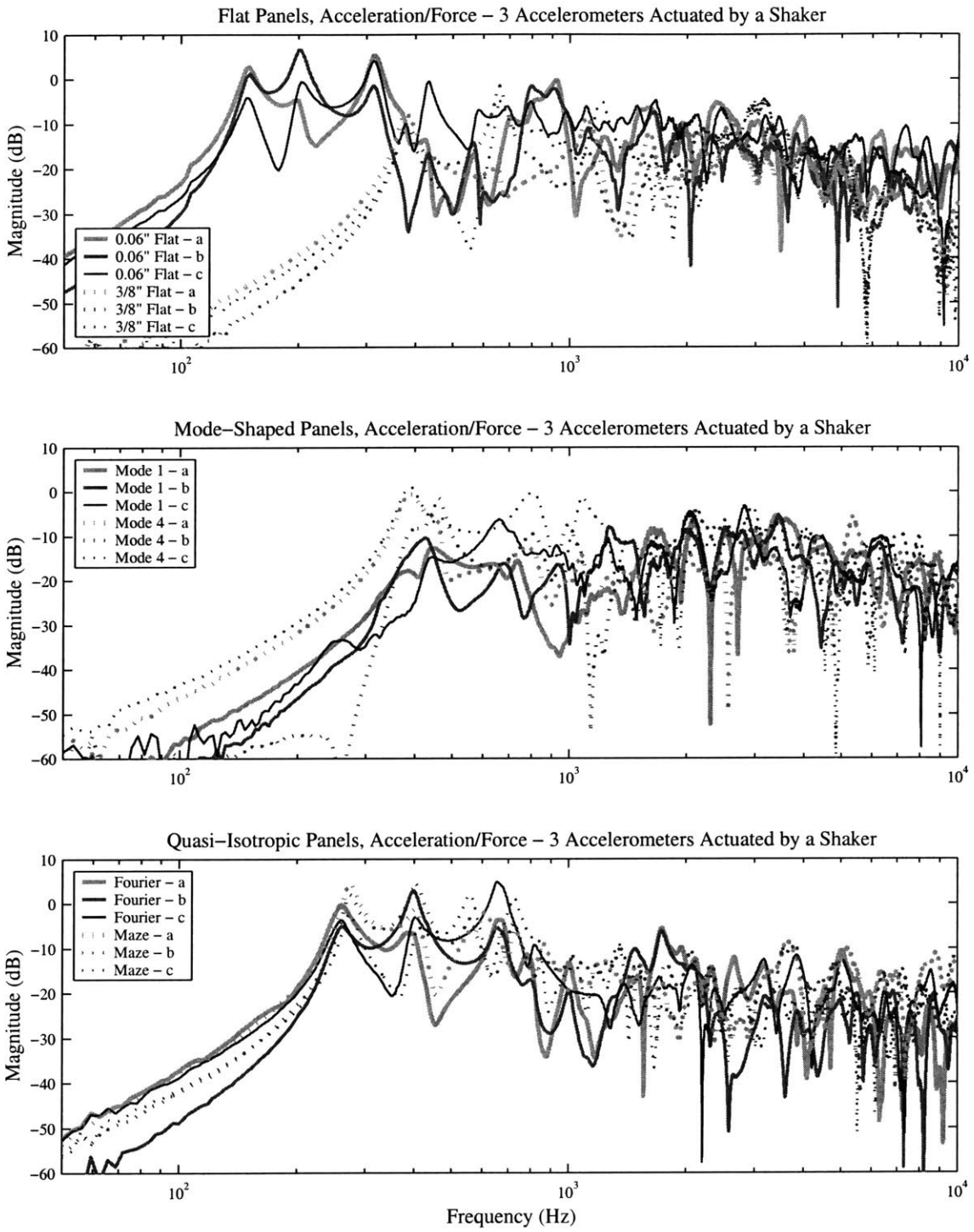

Figure C.2 Raw transfer functions for the sensor actuator pairs in the shaker actuated experiments on the undamped panels.

C.2.2 Shaker Actuated Damped Panels

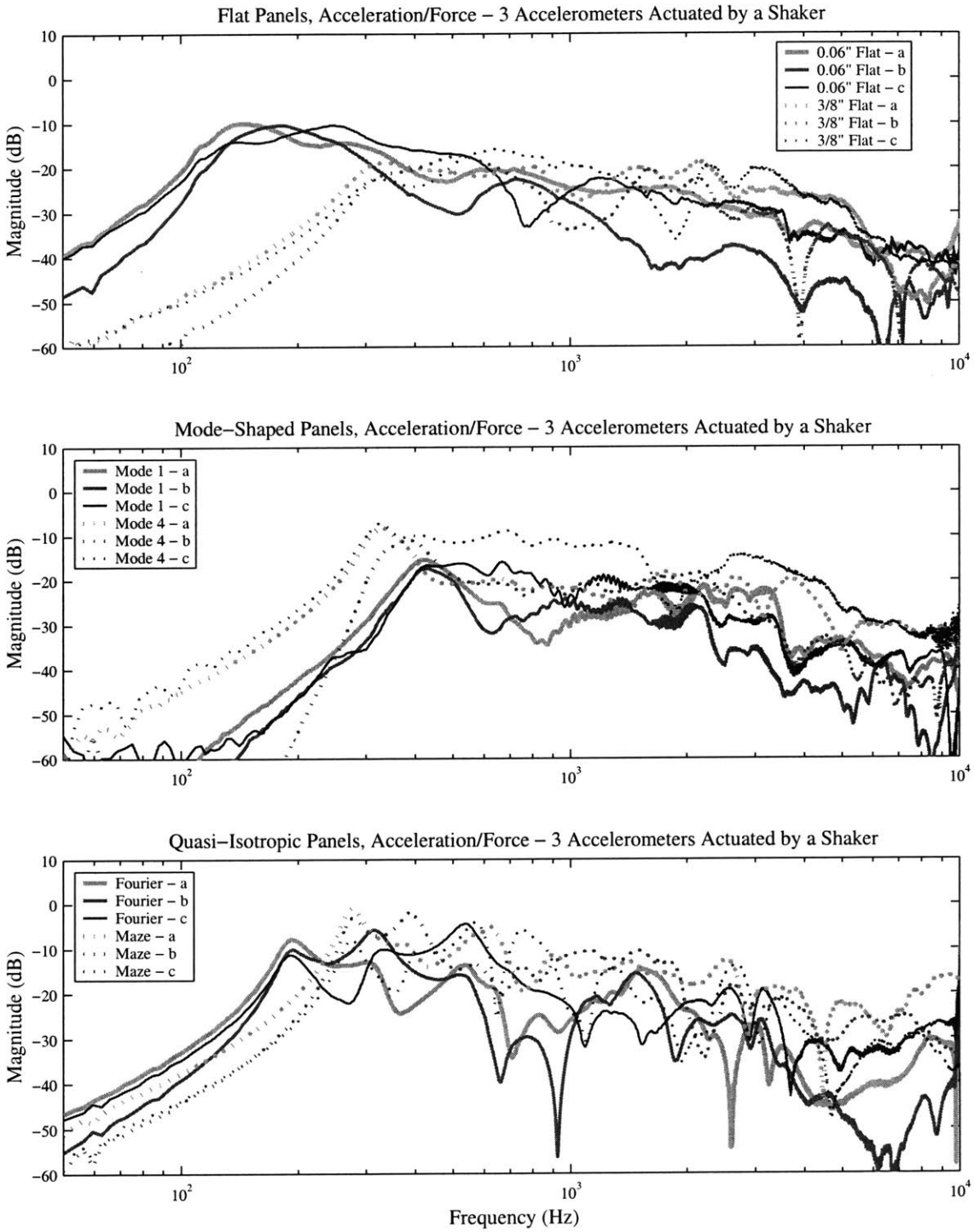

Figure C.3 Raw transfer functions for the sensor actuator pairs in the shaker actuated experiments on the damped panels.

C.2.3 Speaker Actuated Undamped Panels

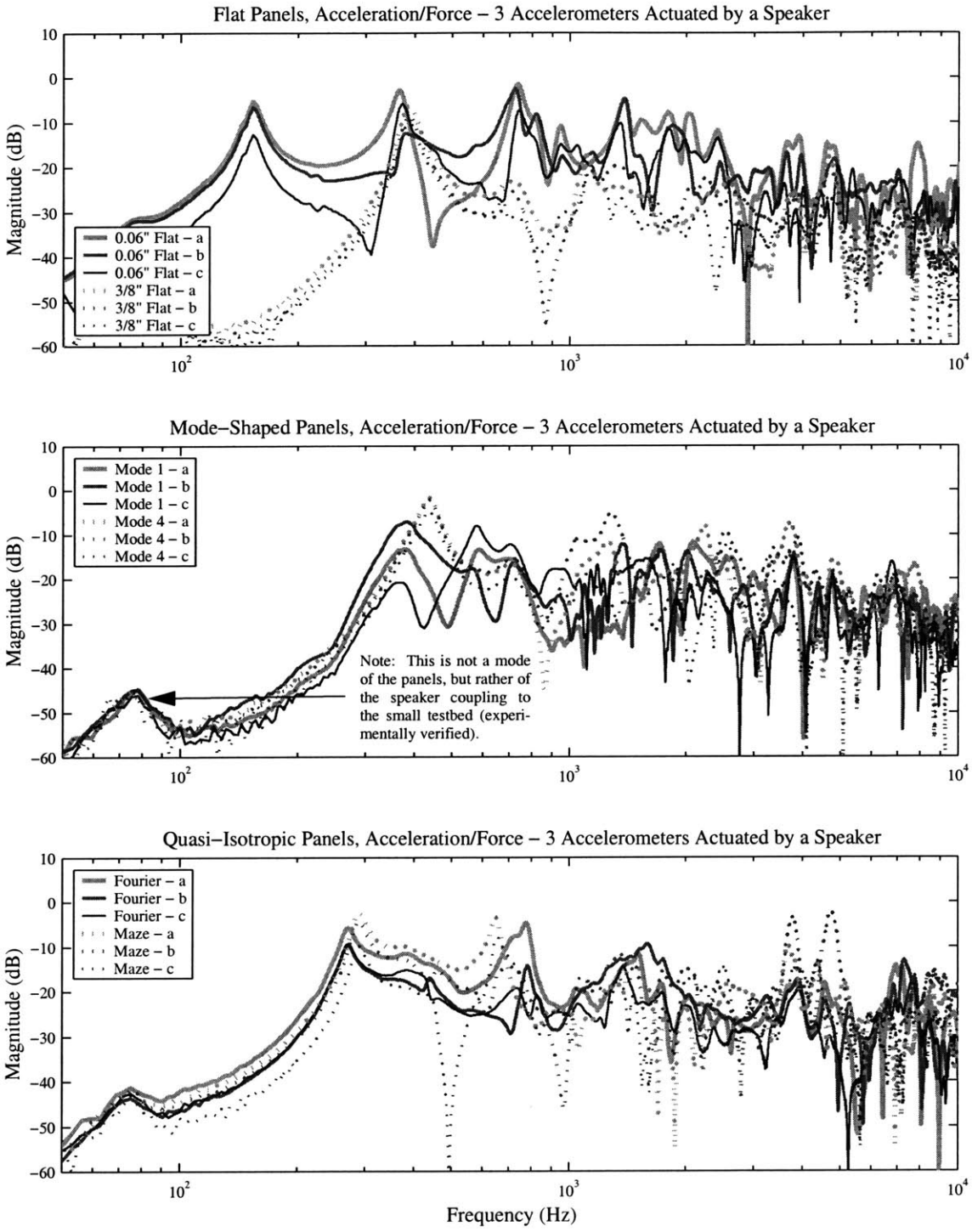

Figure C.4 Raw transfer functions for the sensor actuator pairs in the speaker actuated experiments on the undamped panels.

C.2.4 Speaker Actuated Damped Panels

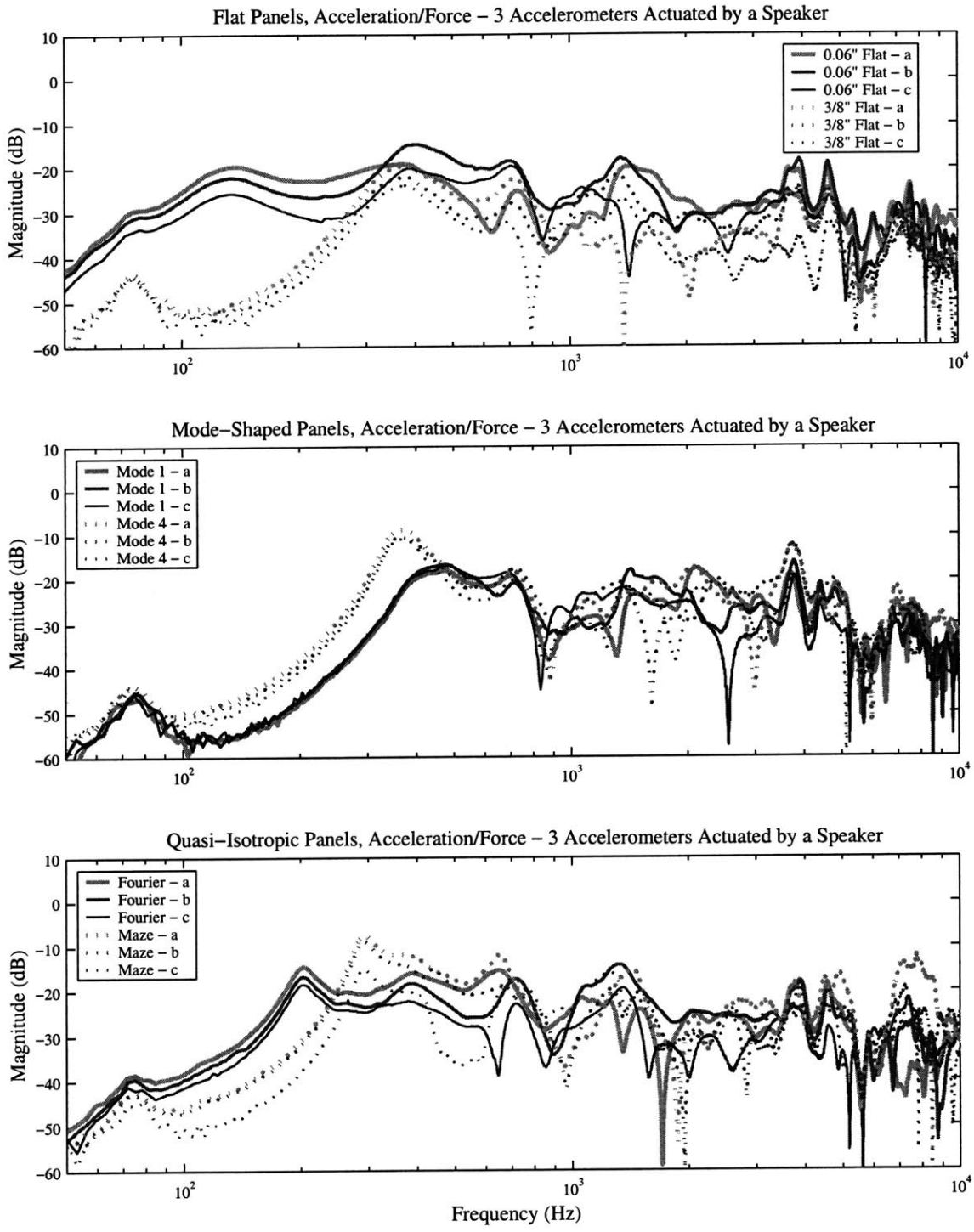

Figure C.5 Raw transfer functions for the sensor actuator pairs in the speaker actuated experiments on the damped panels.

C.2.5 Shaker Actuated Undamped Sandwich Panels

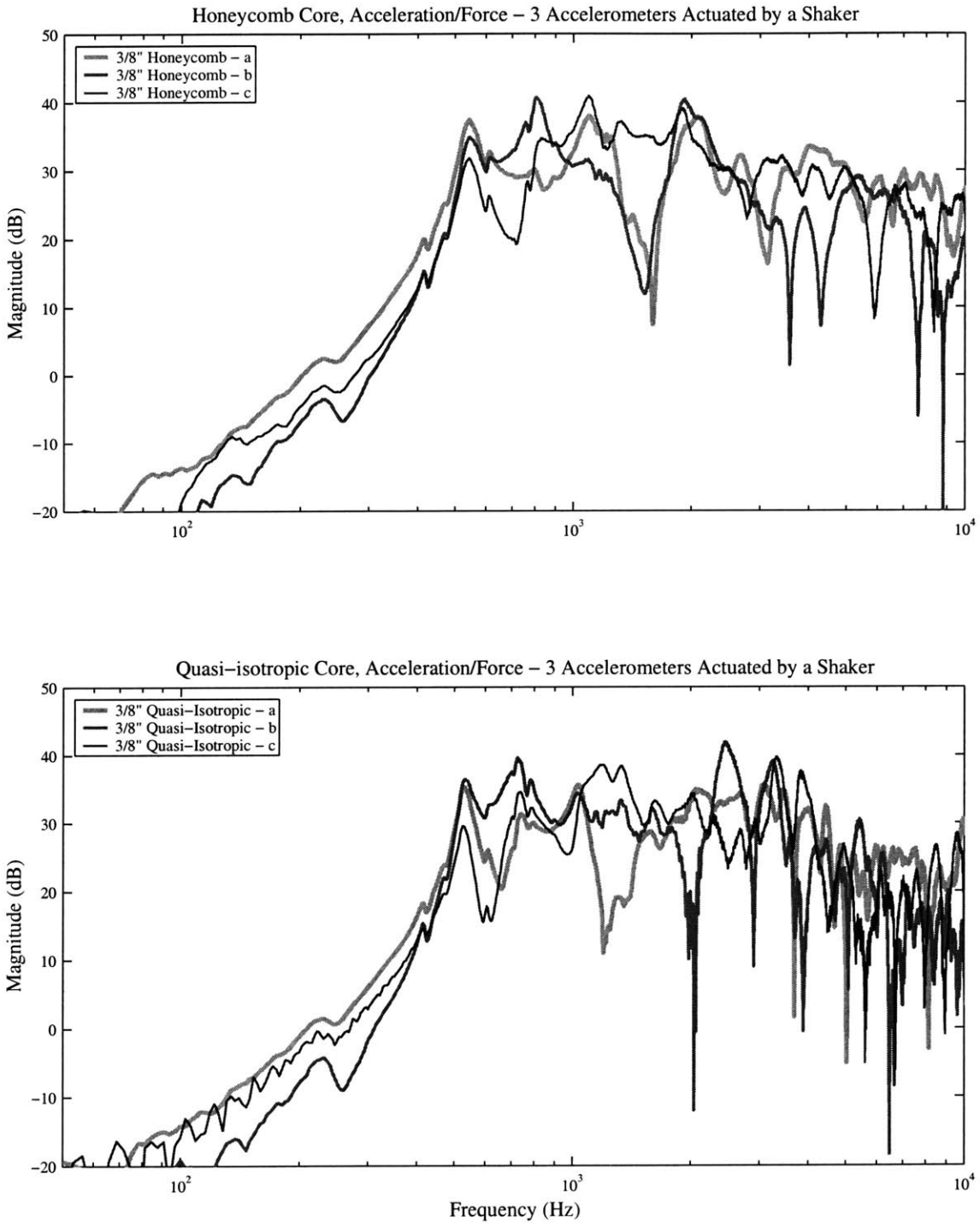

Figure C.6 Raw transfer functions for the sensor actuator pairs in the shaker actuated experiments on the undamped sandwich panels.

C.2.6 Speaker Actuated Undamped Sandwich Panels

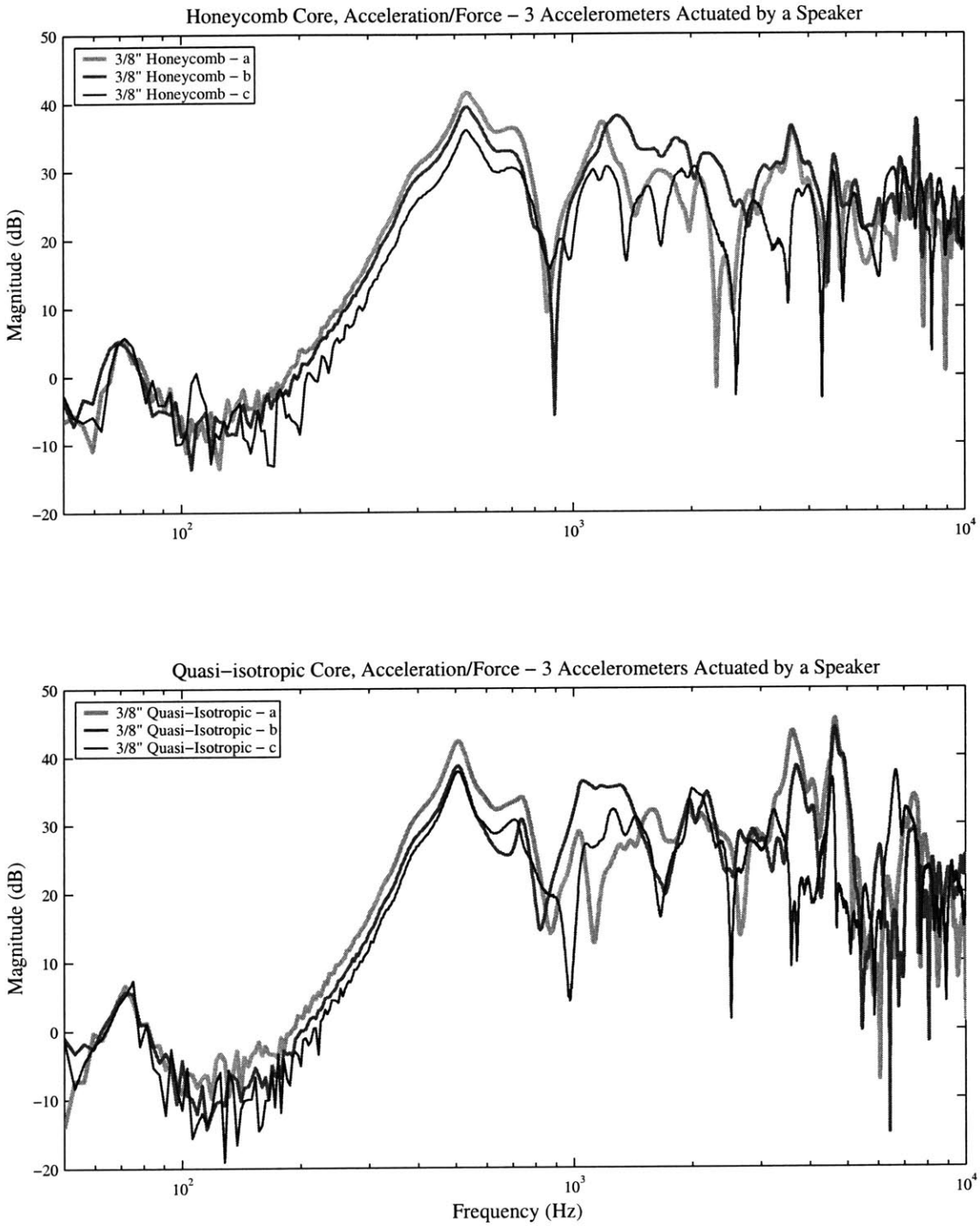

Figure C.7 Raw transfer functions for the sensor actuator pairs in the speaker actuated experiments on the undamped sandwich panels.

C.2.7 Speaker Actuated Damped Sandwich Panels

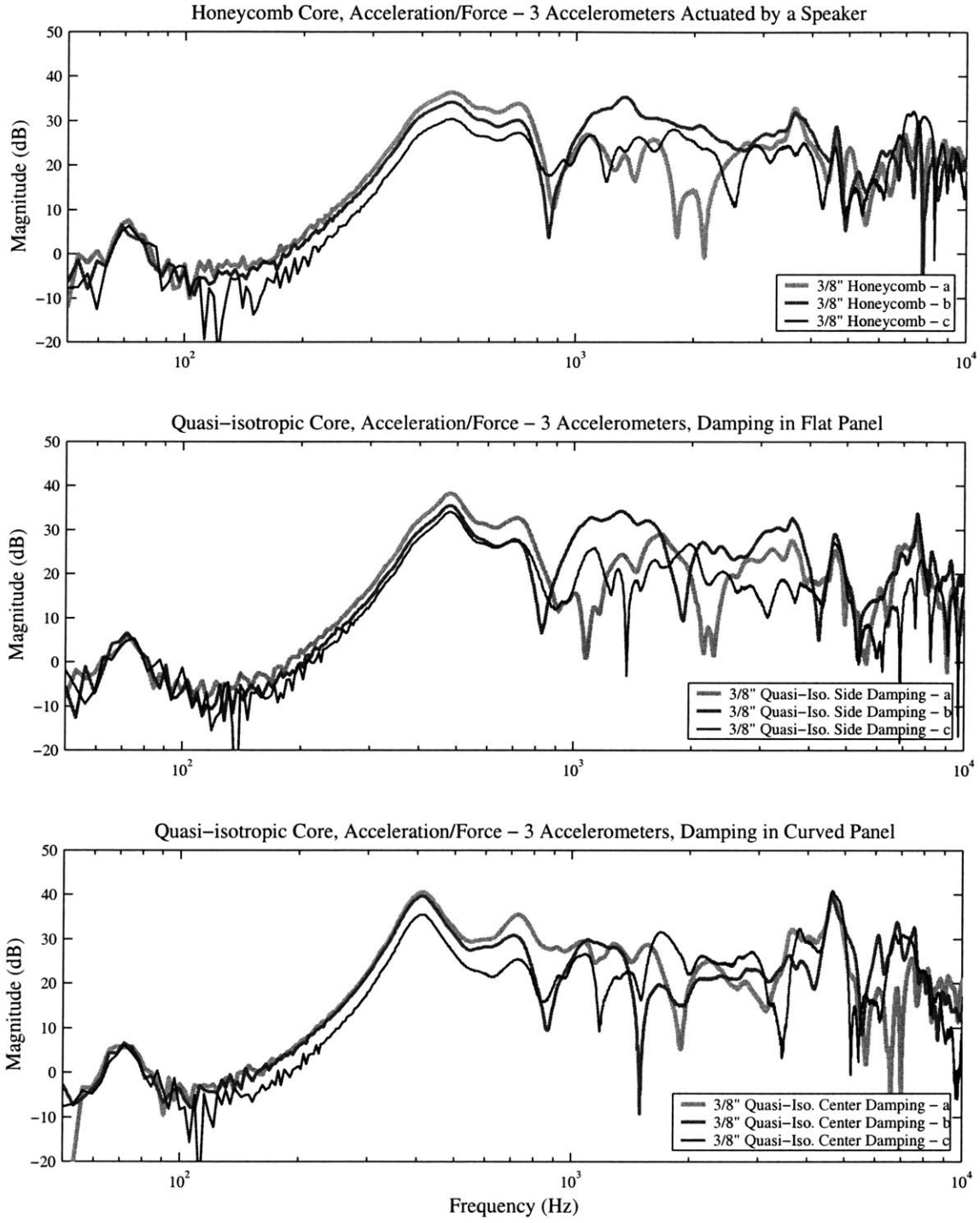

Figure C.8 Raw transfer functions for the sensor actuator pairs in the speaker actuated experiments on the undamped sandwich panels.

C.2.8 Damped Sandwich Panel Comparison - Reduced Data

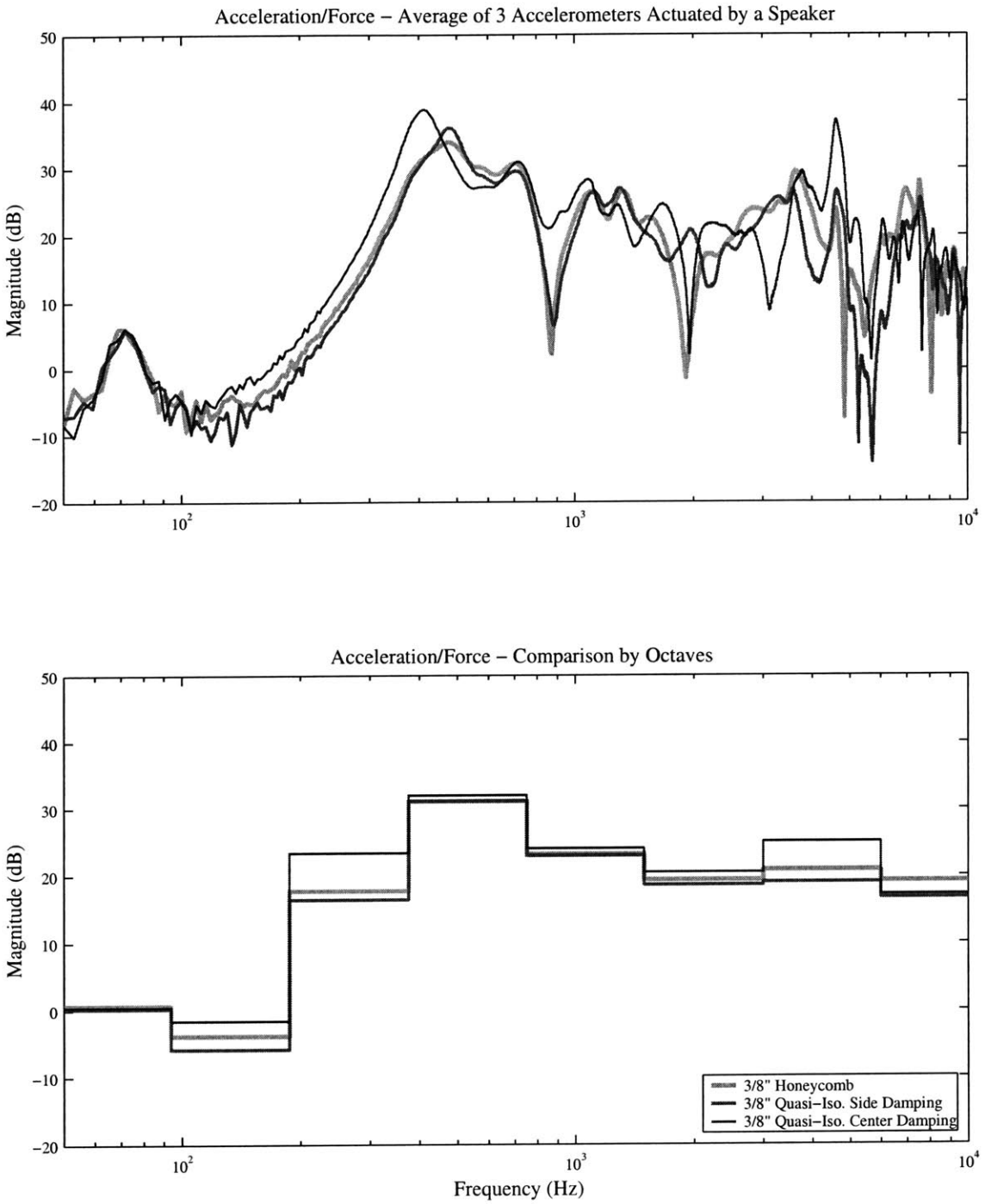

Figure C.9 Comparison of damped sandwich panel configurations. "Side Damping" implies flat constrained damping layer in flat sandwiching layer, while "Center Damping" implies damping within curved panel core. Honeycomb panel is of the "Side Damping" configuration.

C.2.9 Speaker Actuated Fourier Panels - Different Damping Configurations

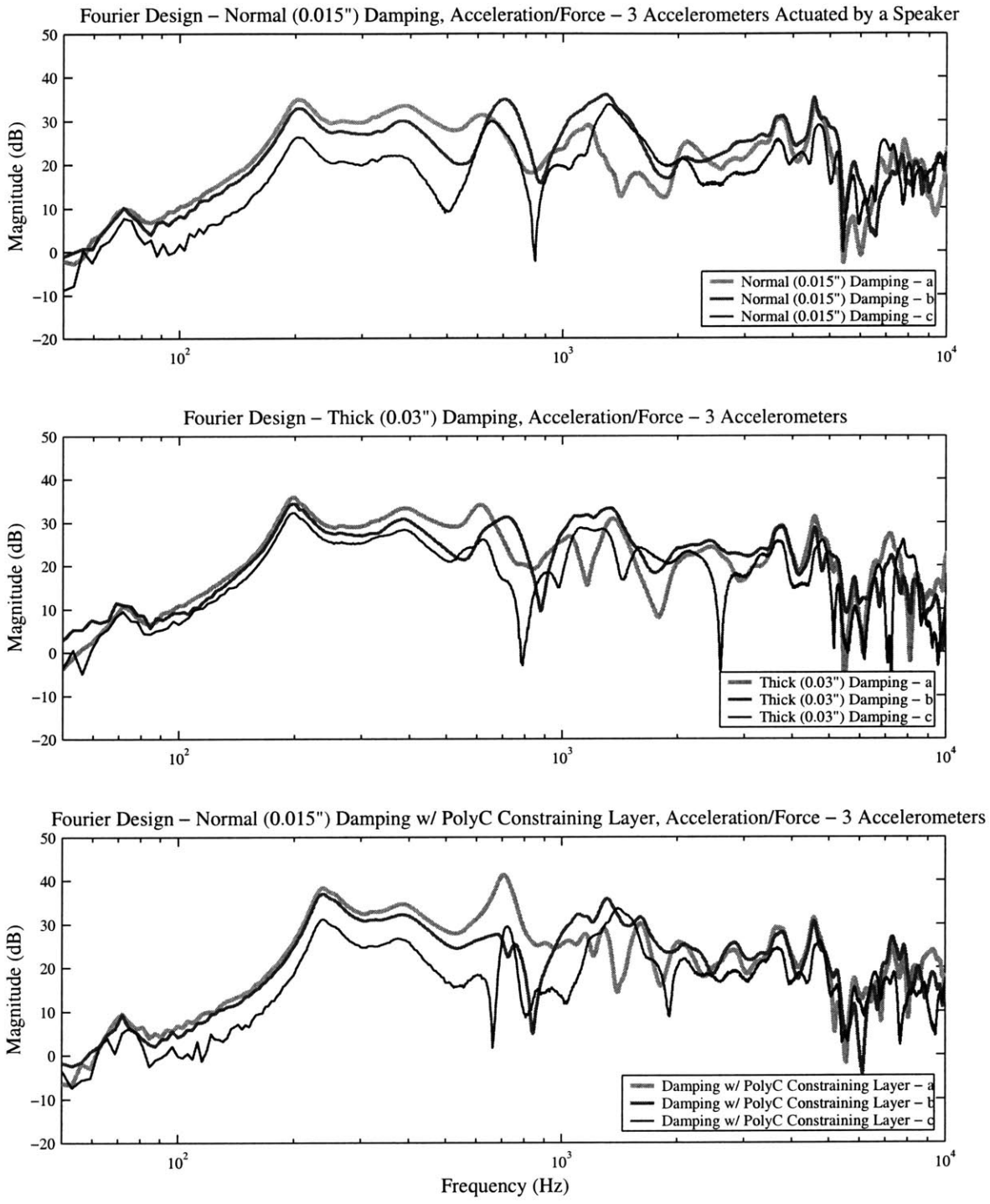

Figure C.10 Raw transfer functions for the sensor actuator pairs in the speaker actuated experiments on the undamped sandwich panels.

C.2.10 Damped Fourier Panel Comparison - Reduced Data

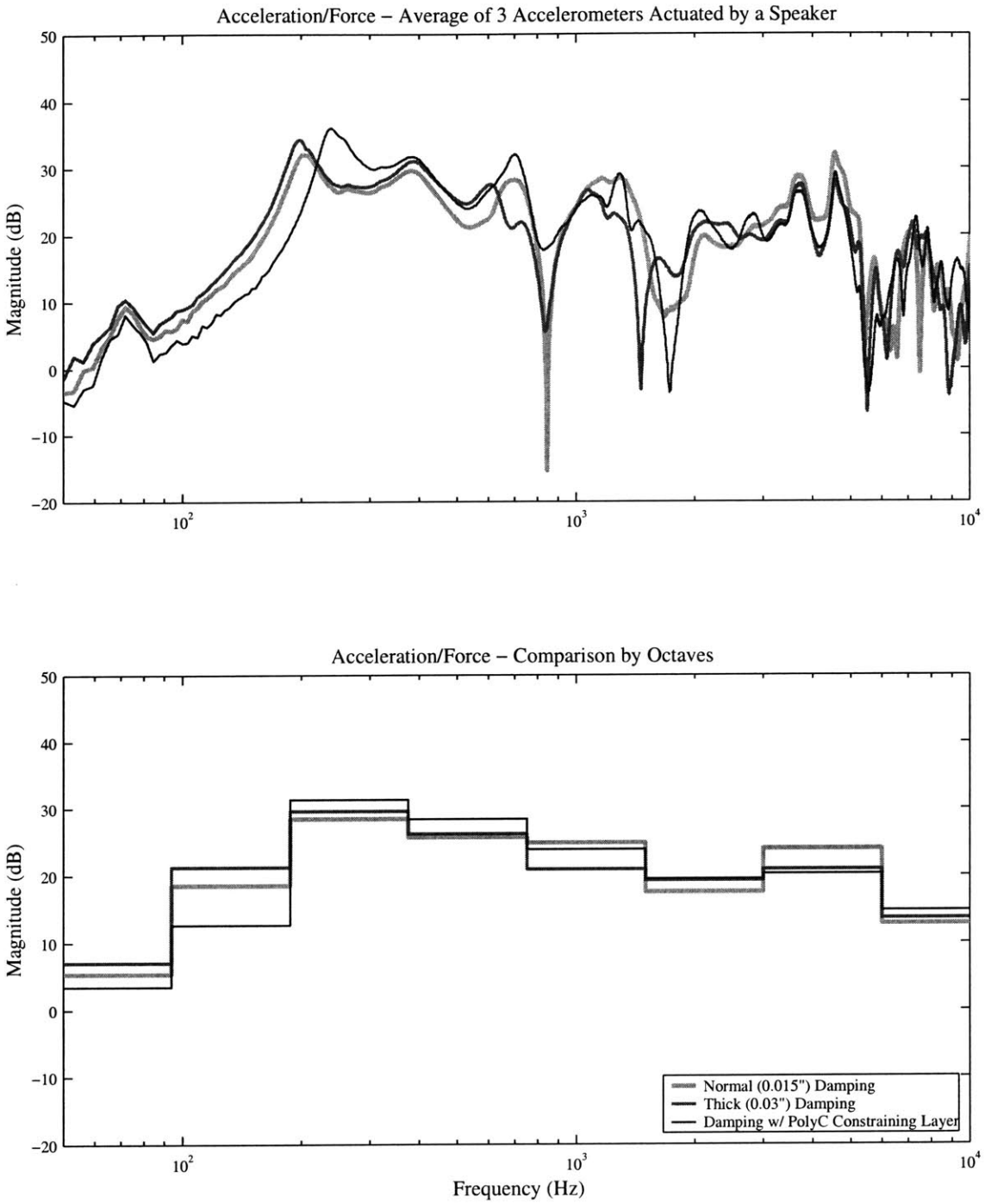

Figure C.11 Comparison of damped Fourier panel configurations. "Normal Damping" implies 0.015" thick constrained damping layer in center of panel design, "Thick Damping" is 0.03" thick constrained damping layer in center of panel design, and "Normal Damping with PolyC" means the damping layer was constrained by a thin layer of polycarbonate away from center.

C.3 Radiation Data

The radiation data includes six accelerometer measurements and three microphone measurements for each panel. Microphone measurements were at three unique locations describing a quarter sphere around the panel at a distance of approximately 3 feet.

C.3.1 Radiation Data - Microphones - Undamped Panels

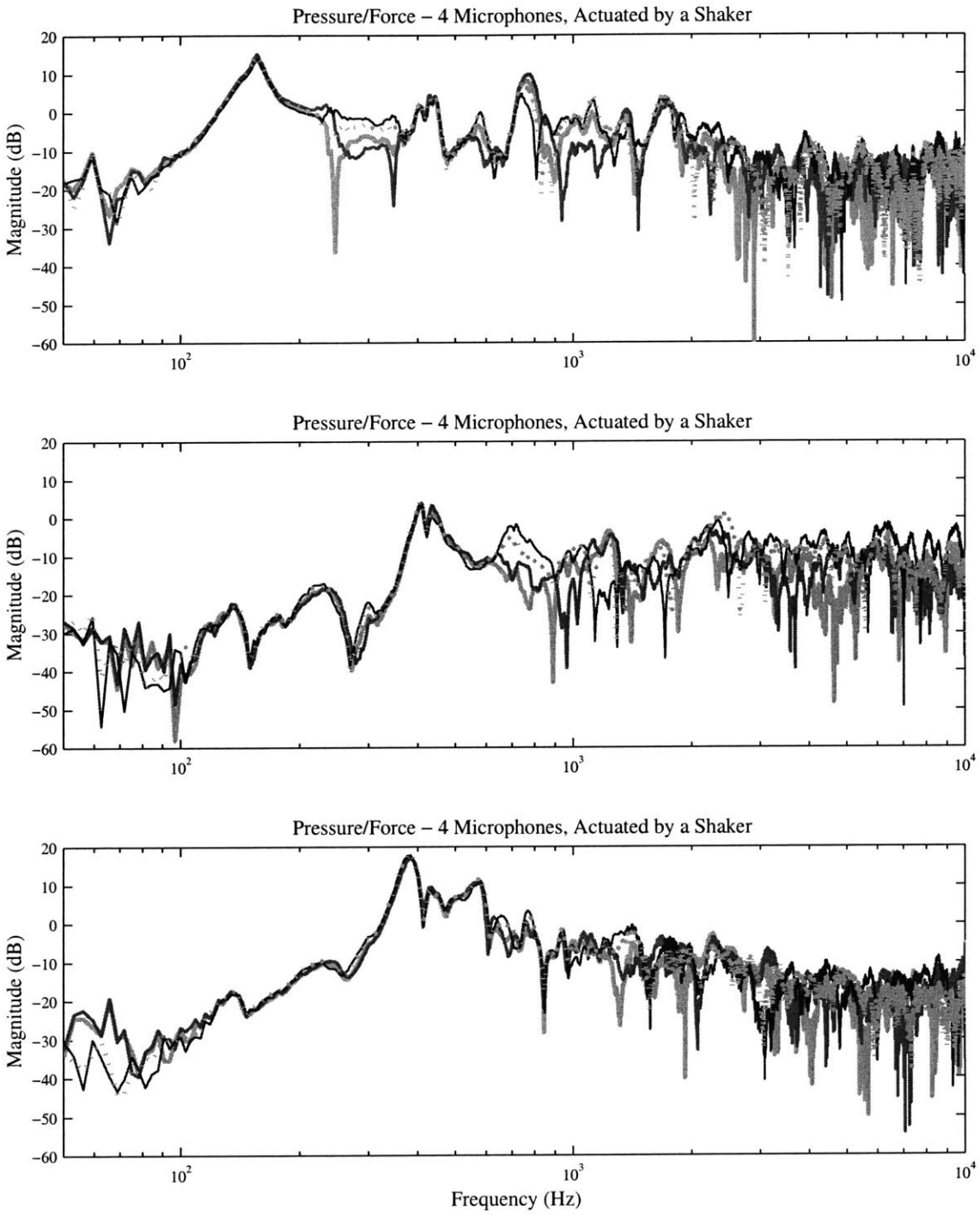

Figure C.12 Raw transfer functions for the microphone sensors for the radiation experiments on the undamped panels.

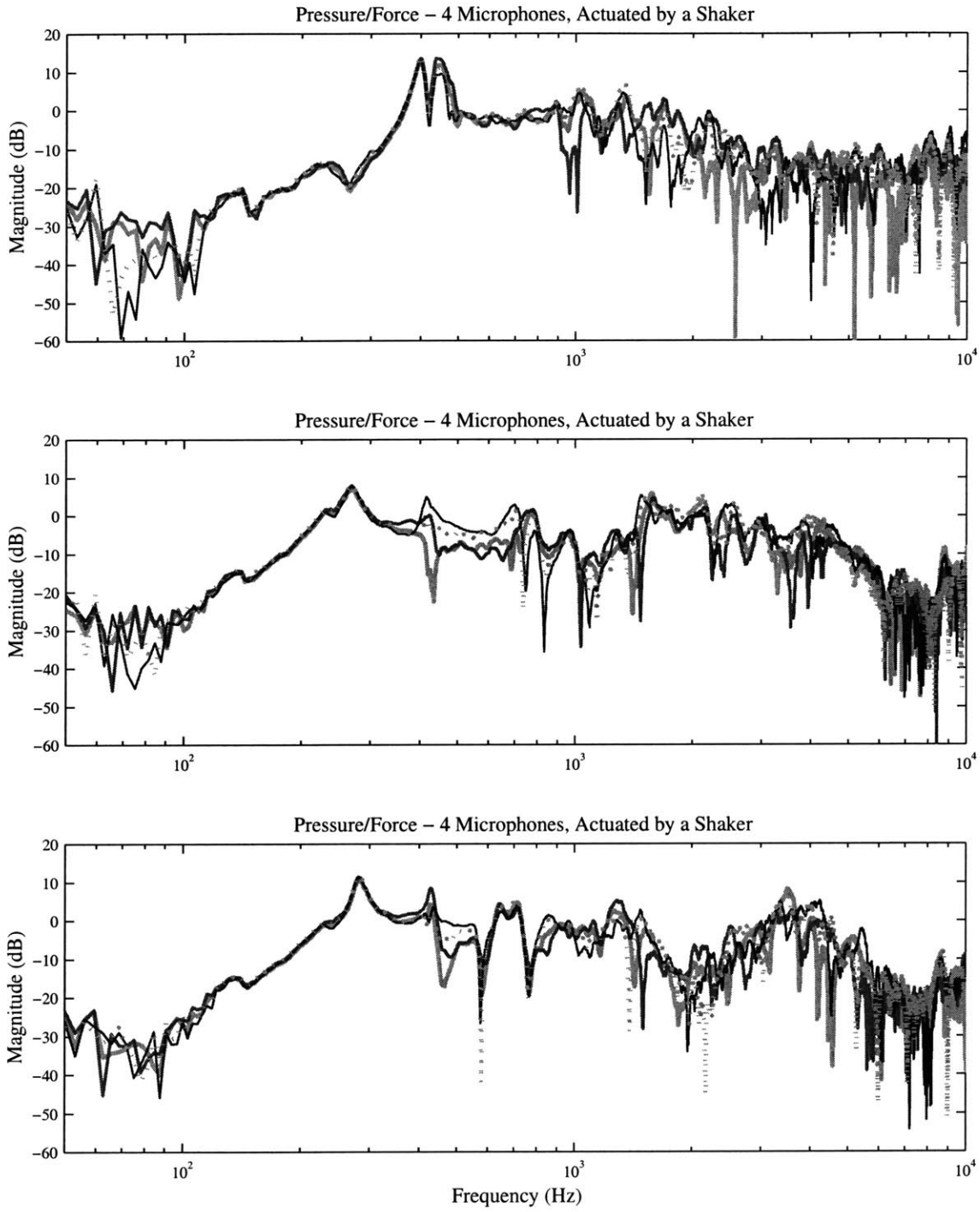

Figure C.13 More raw transfer functions for the microphone sensors for the radiation experiments on the undamped panels.

C.3.2 Radiation Data - Accelerometers - Undamped Panels

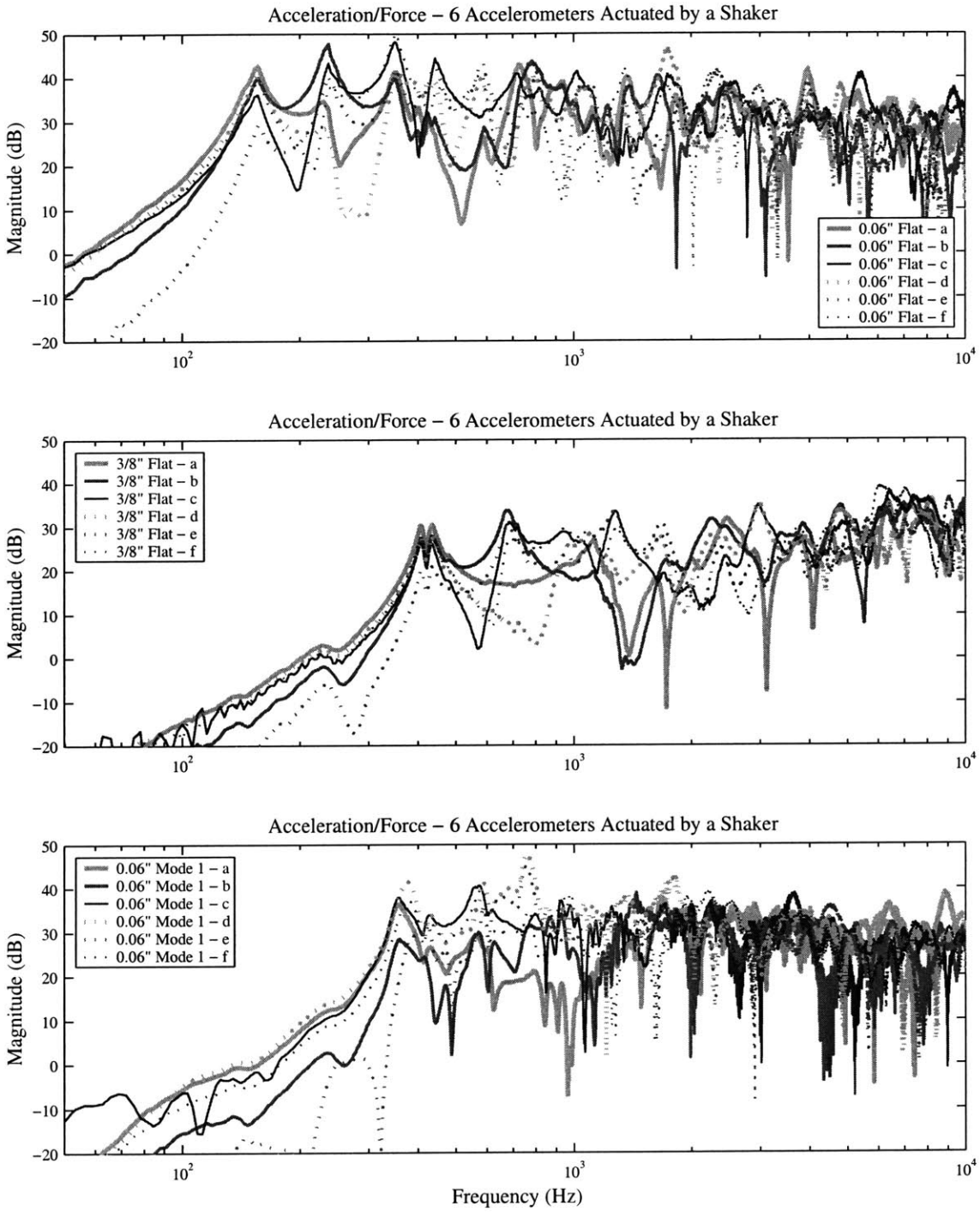

Figure C.14 Raw transfer functions for the accelerometer sensors for the radiation experiments on the undamped panels.

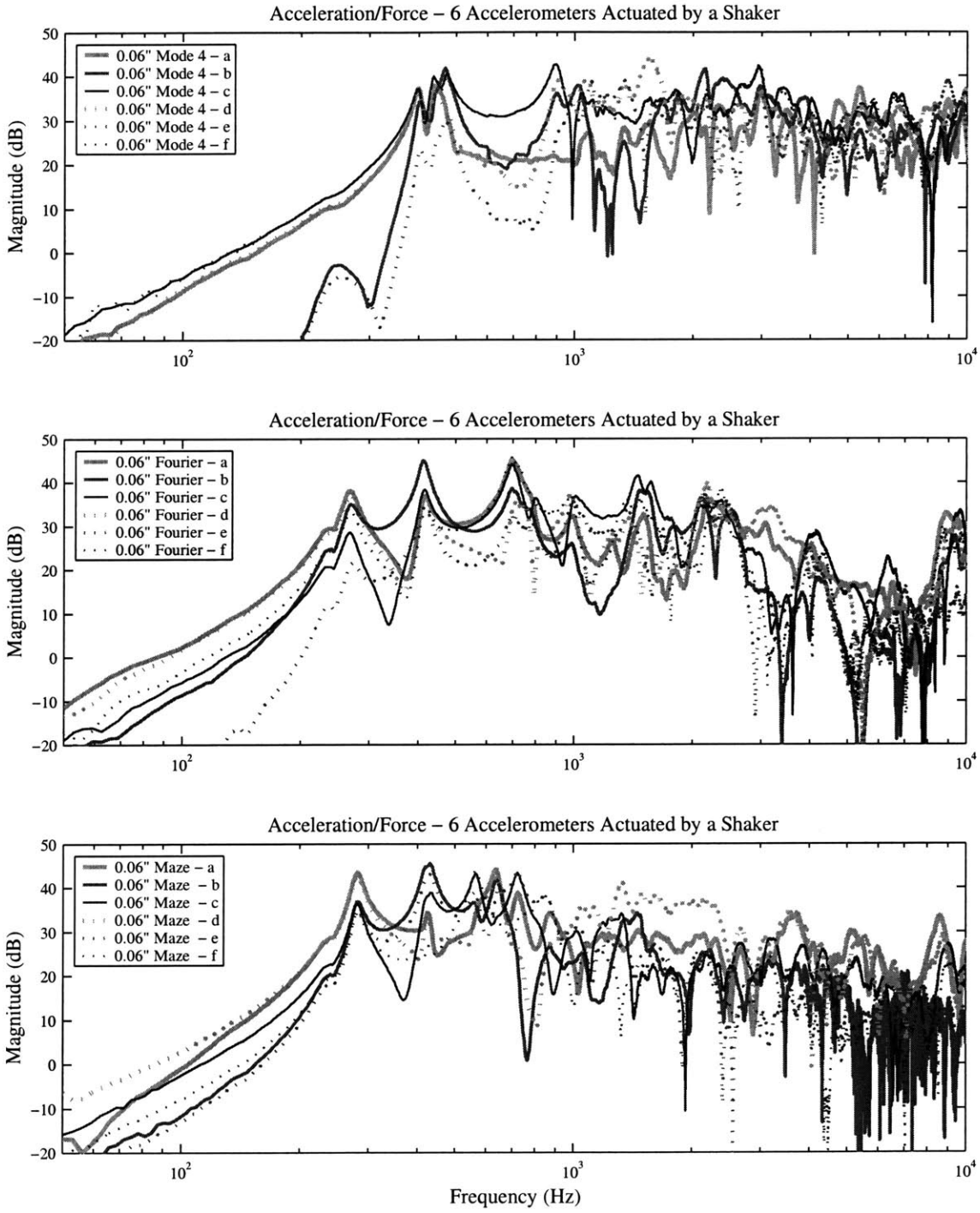

Figure C.15 More raw transfer functions for the accelerometer sensors for the radiation experiments on the undamped panels.

C.3.3 Radiation Data - Microphones - Damped Panels

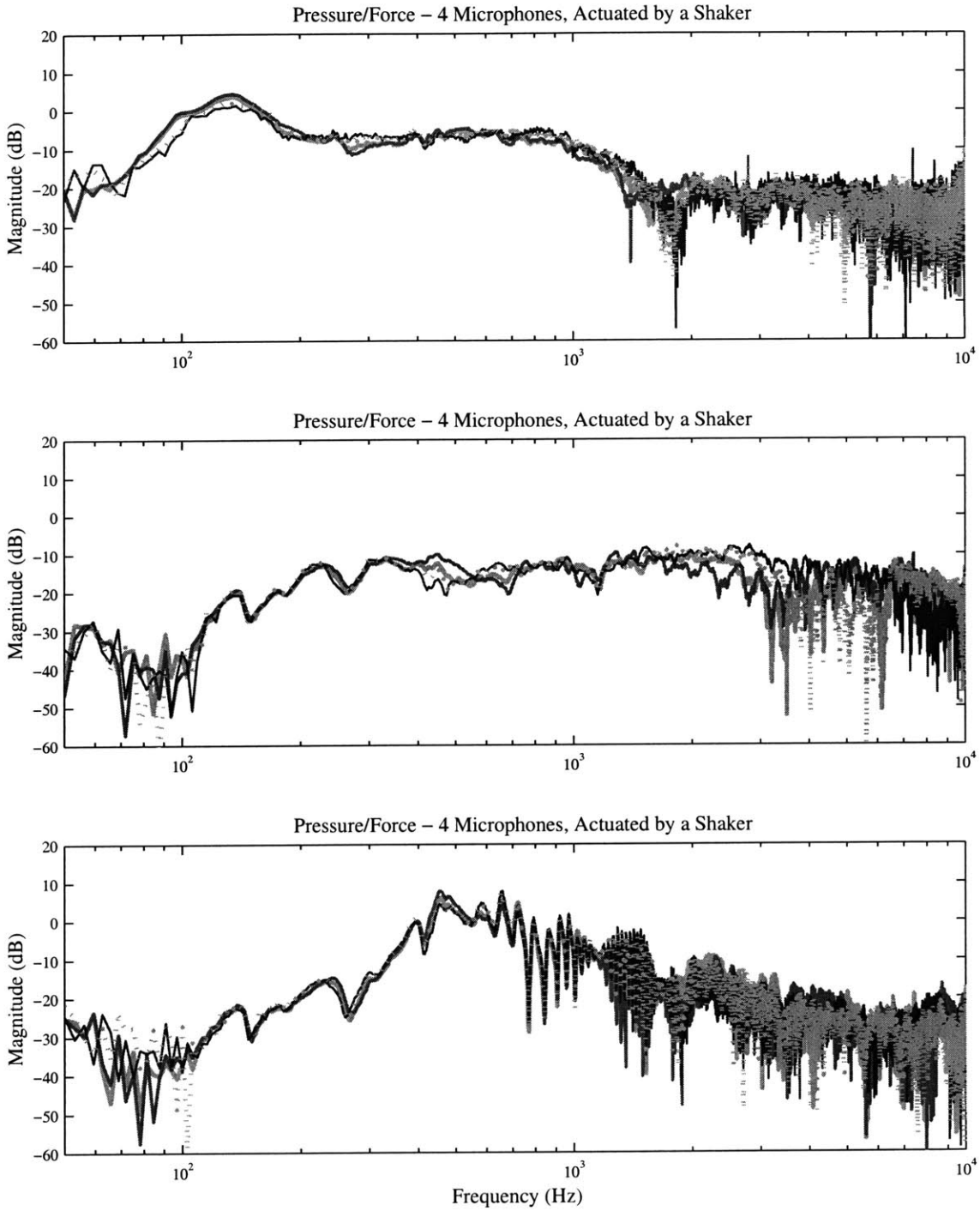

Figure C.16 Raw transfer functions for the microphone sensors for the radiation experiments on the damped panels.

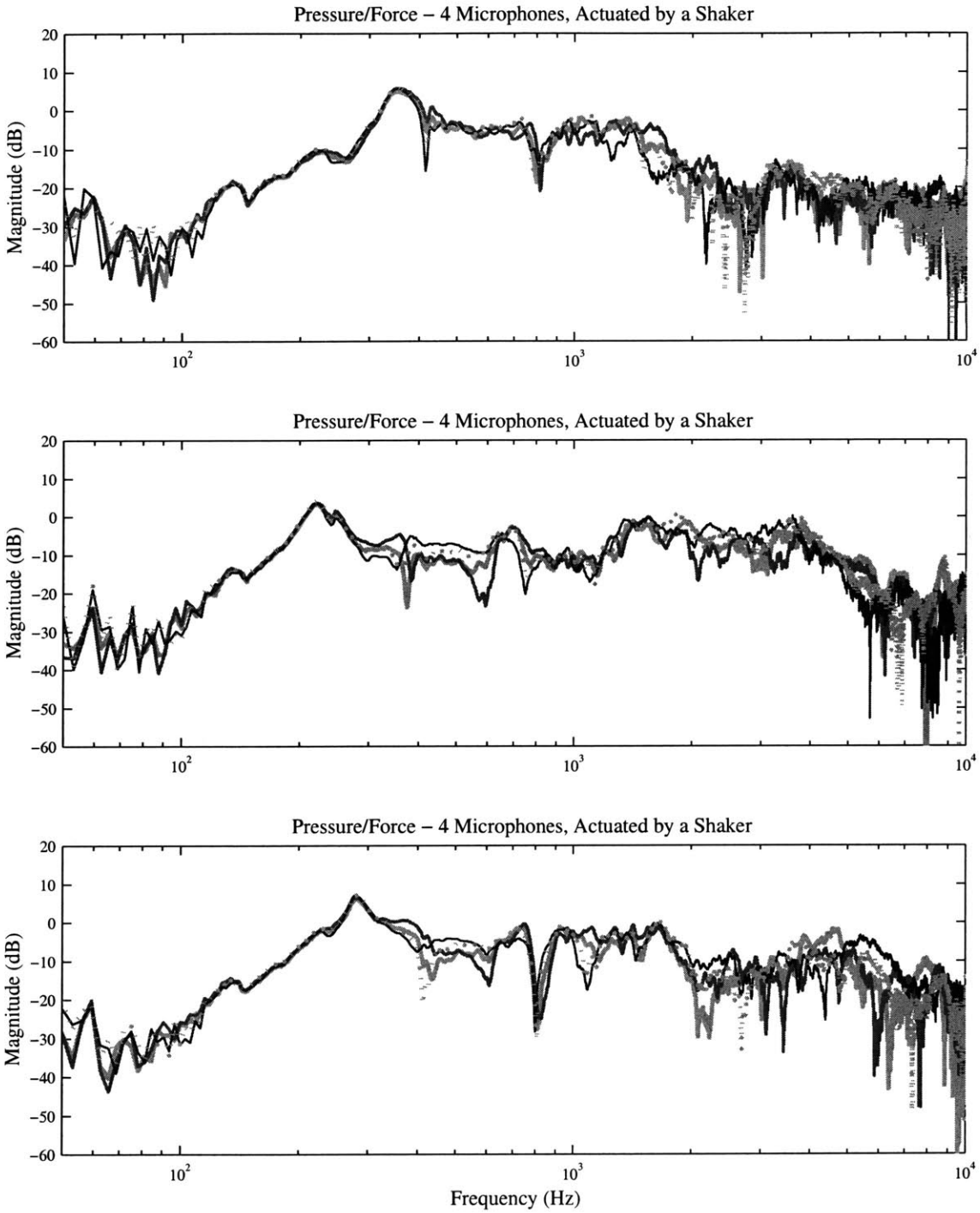

Figure C.17 More raw transfer functions for the microphone sensors for the radiation experiments on the damped panels.

C.3.4 Radiation Data - Accelerometers - Damped Panels

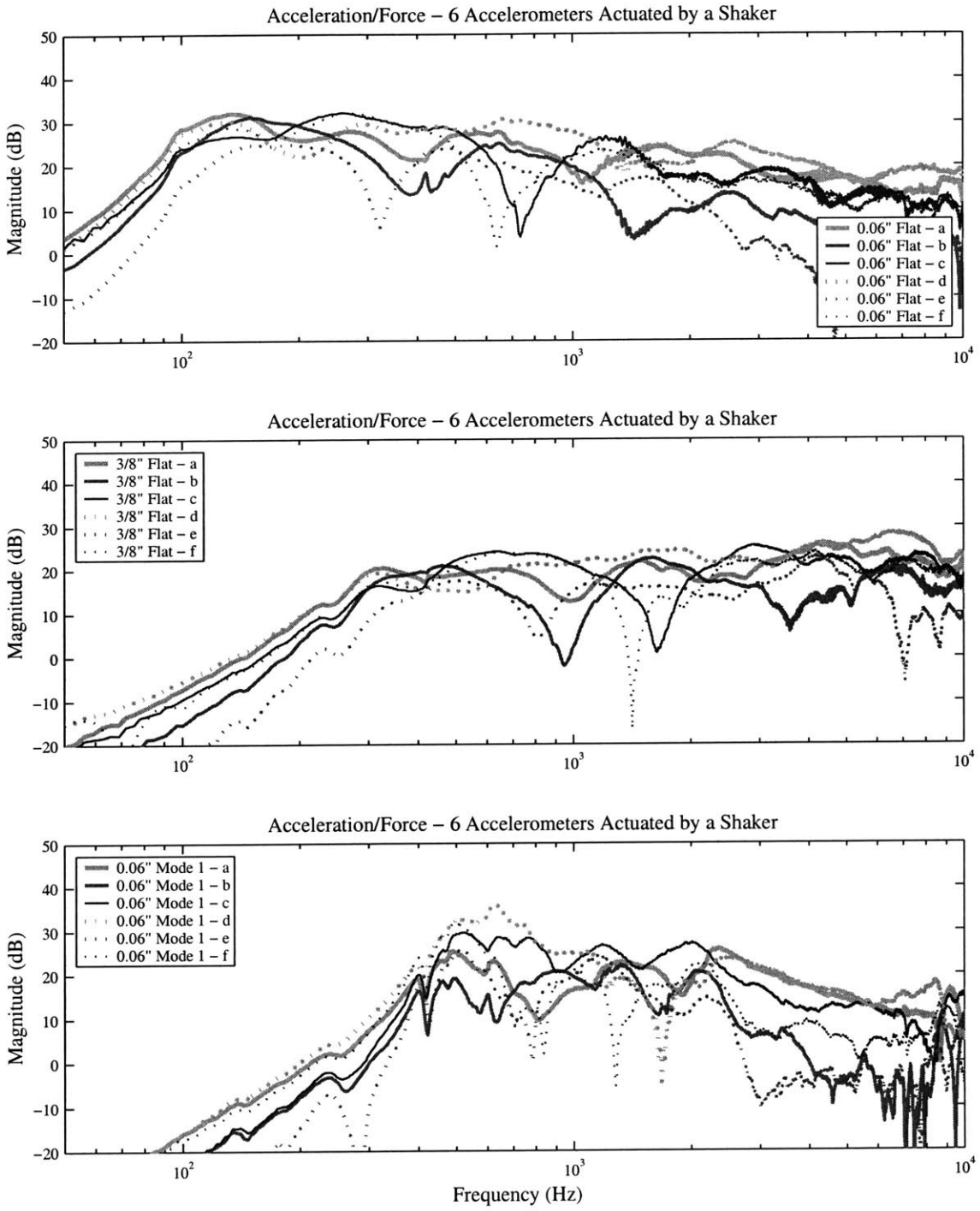

Figure C.18 Raw transfer functions for the accelerometer sensors for the radiation experiments on the damped panels.

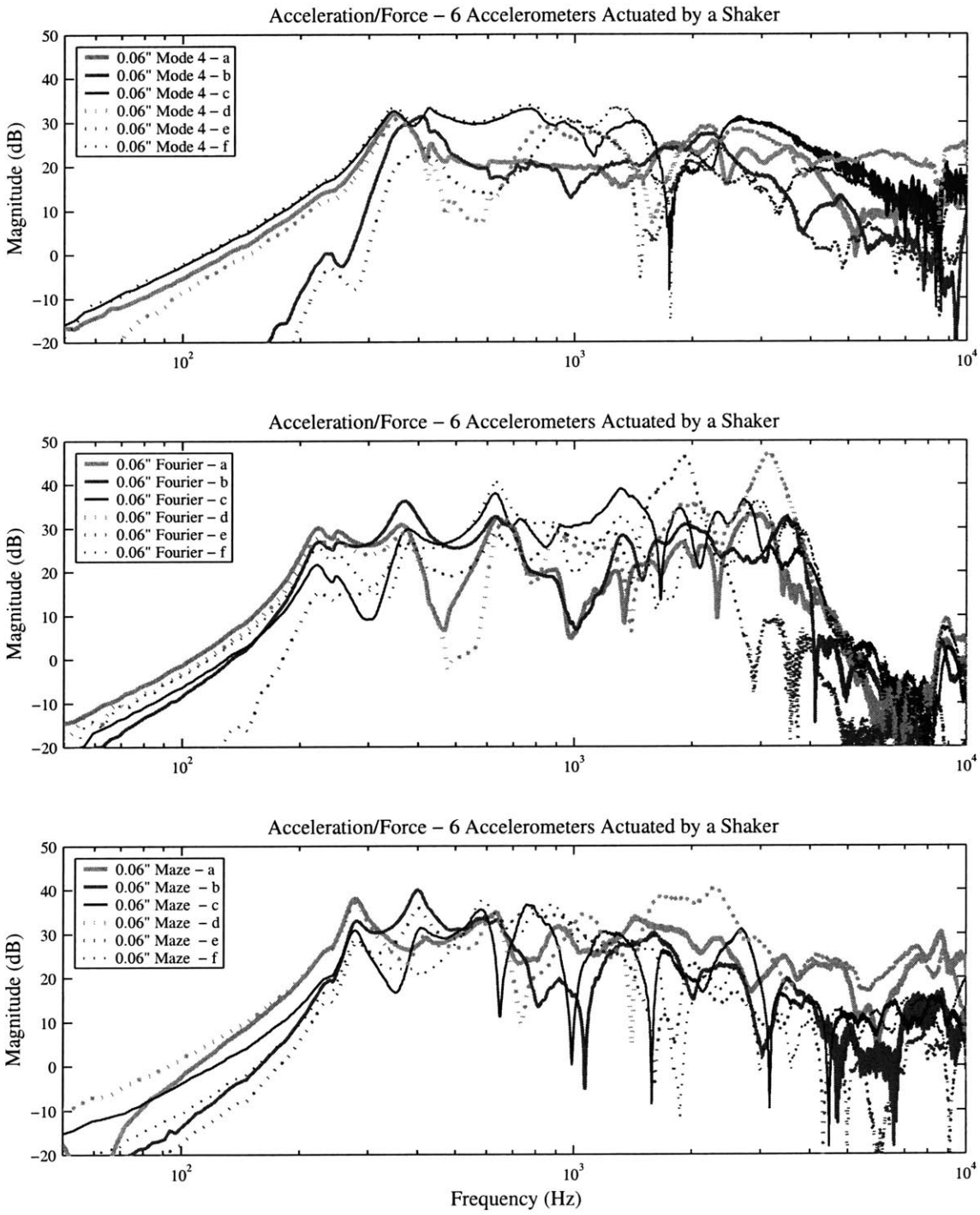

Figure C.19 More raw transfer functions for the accelerometer sensors for the radiation experiments on the damped panels.

C.4 Directional Transmission Data

The directional transmission data includes four microphone measurements for each panel. These experiments were performed on the small testbed. Microphone measurements were made at two locations inside the testbed and two locations outside the testbed at two different distances. The exterior microphones were placed at distance of approximately 1 foot and 6 feet from the panel.

C.4.1 Direction Transmission Data for Undamped Panels

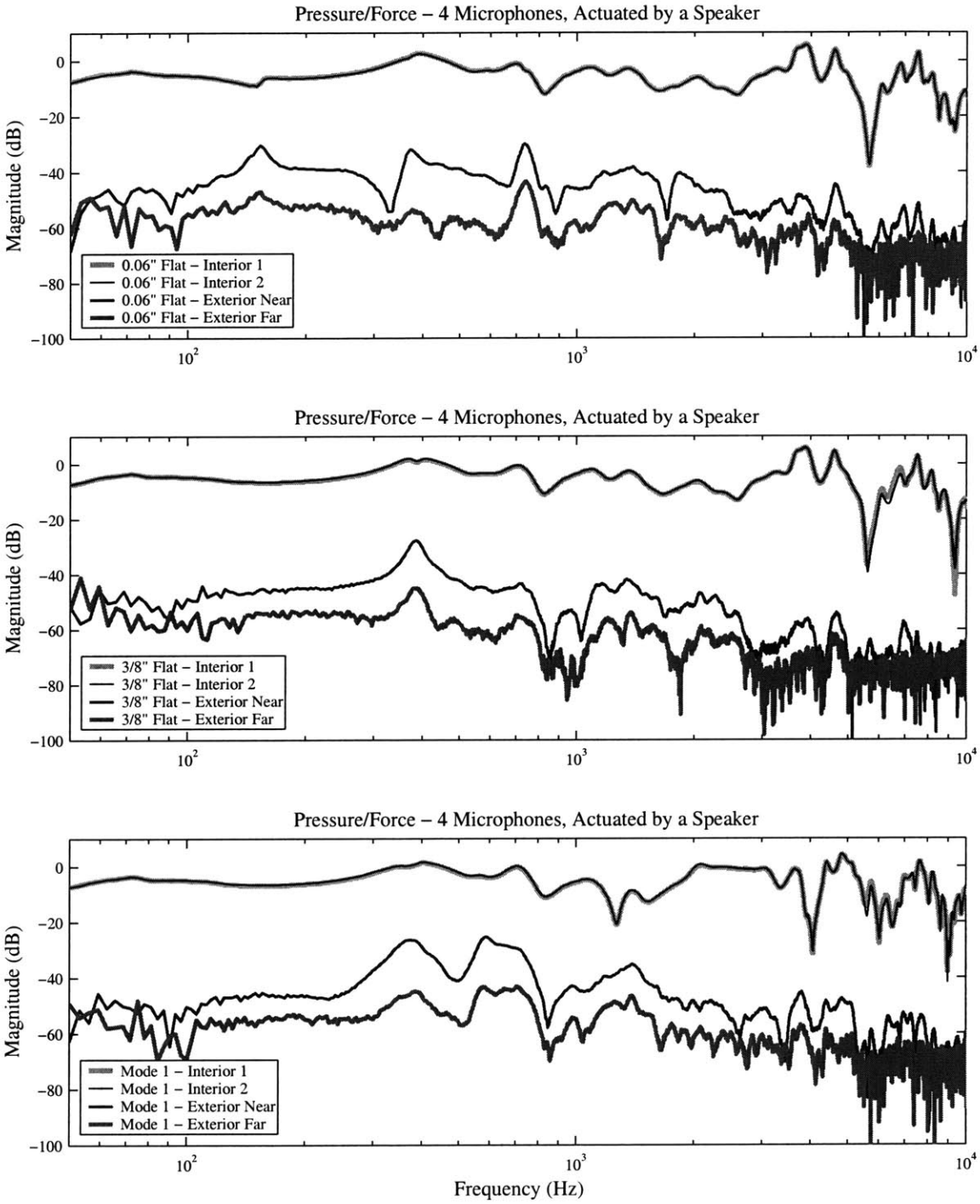

Figure C.20 Raw transfer functions for the microphone sensors for the directional transmission experiments on the undamped panels.

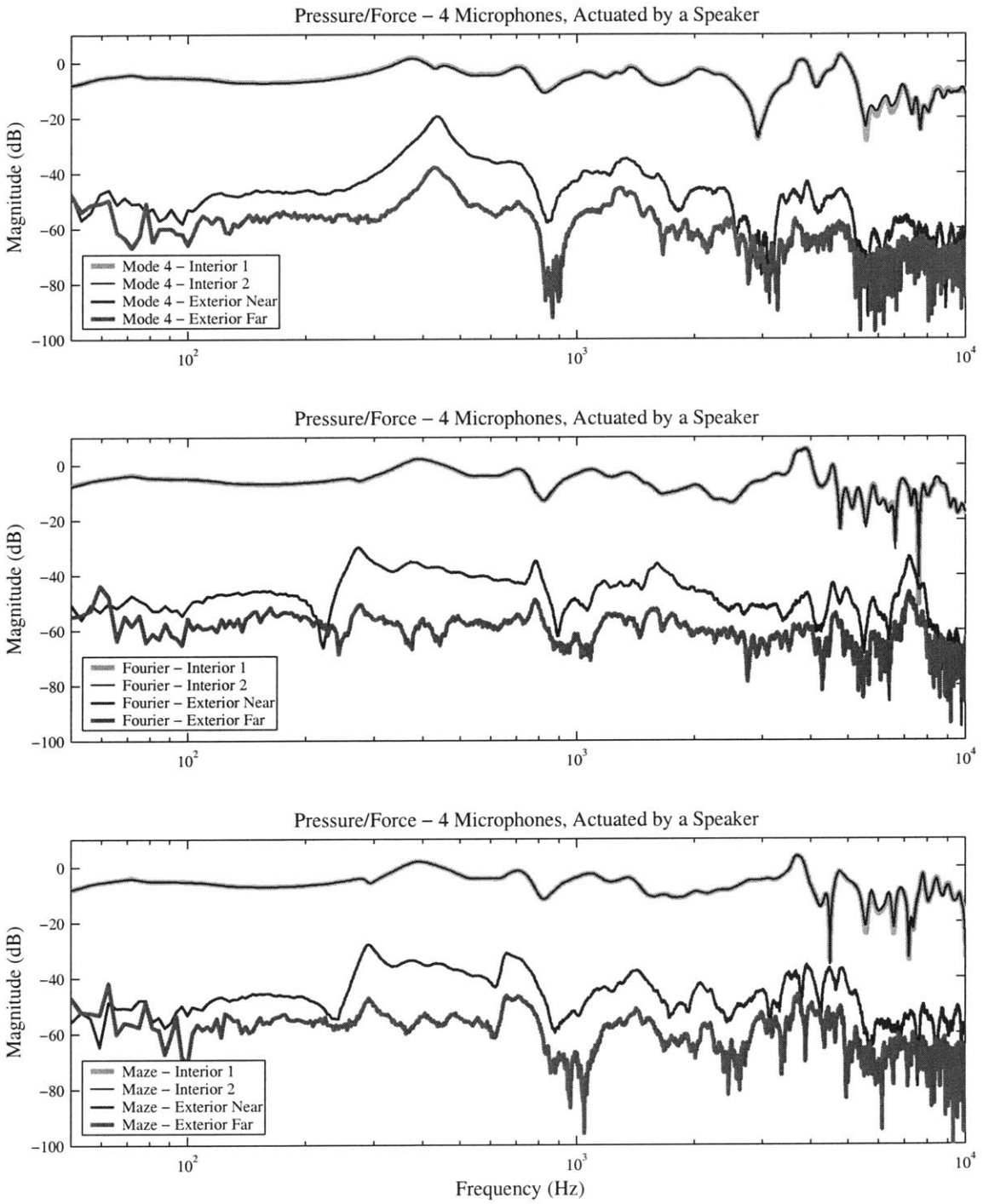

Figure C.21 More raw transfer functions for the microphone sensors for the directional transmission experiments on the undamped panels.

C.4.2 Direction Transmission Data for Damped Panels

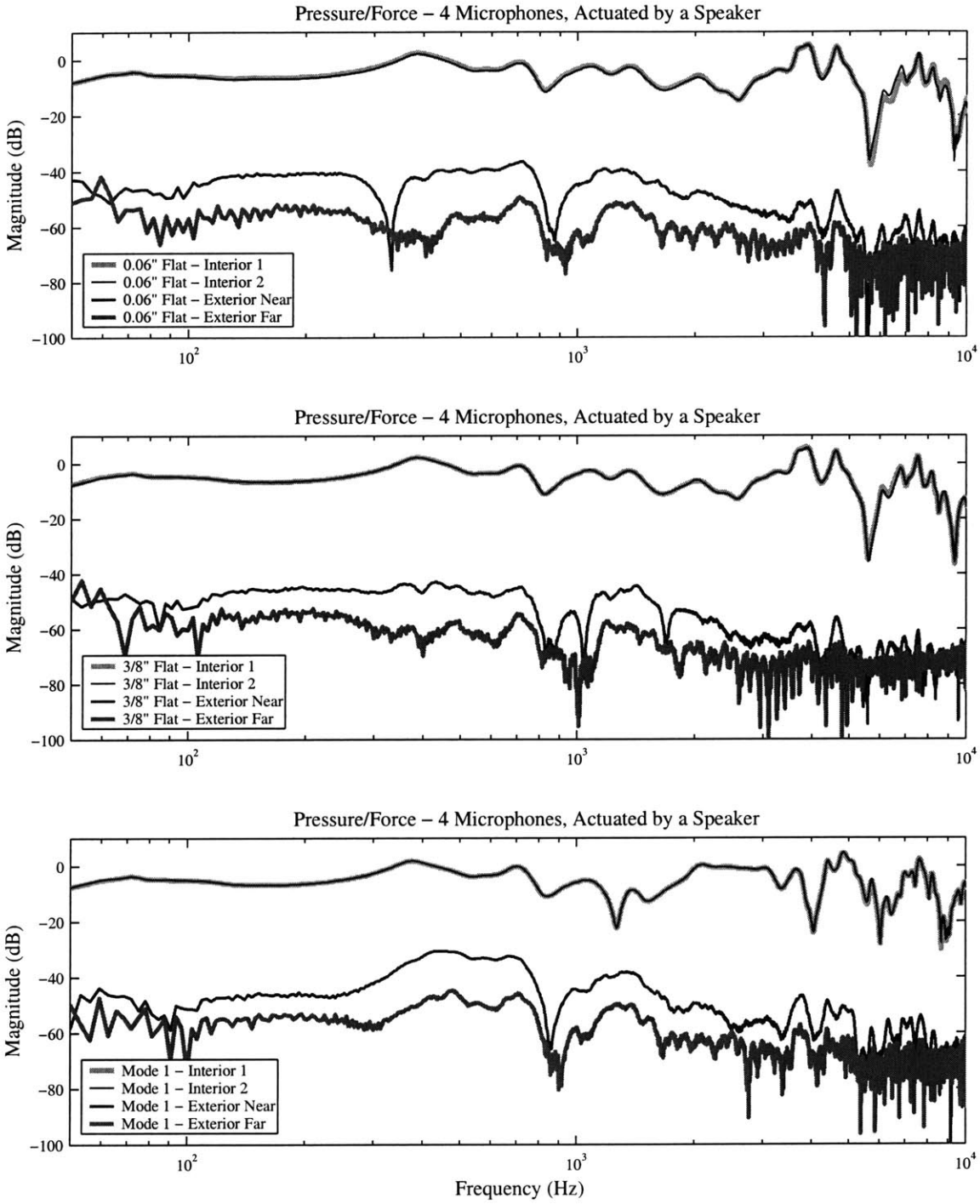

Figure C.22 Raw transfer functions for the microphone sensors for the directional transmission experiments on the damped panels.

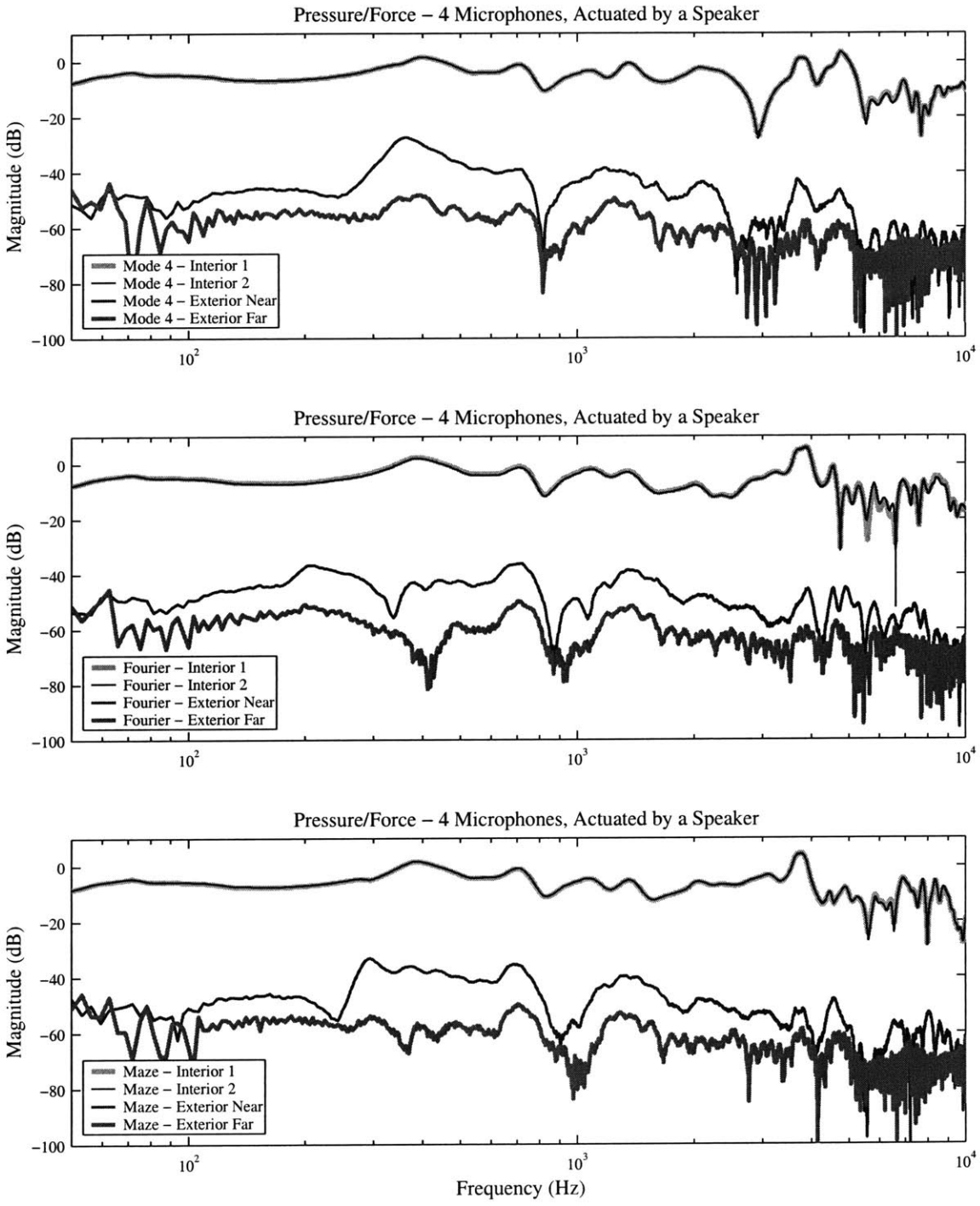

Figure C.23 More raw transfer functions for the microphone sensors for the directional transmission experiments on the damped panels.

C.5 Diffuse Transmission Data

The diffuse transmission data includes six microphone measurements for each panel. These experiments were performed on the large testbed. Microphone measurements were made at three locations inside the testbed and three locations outside the testbed at a single radius of approximately 2.5 feet.

C.5.1 Diffuse Transmission Data for Undamped Panels

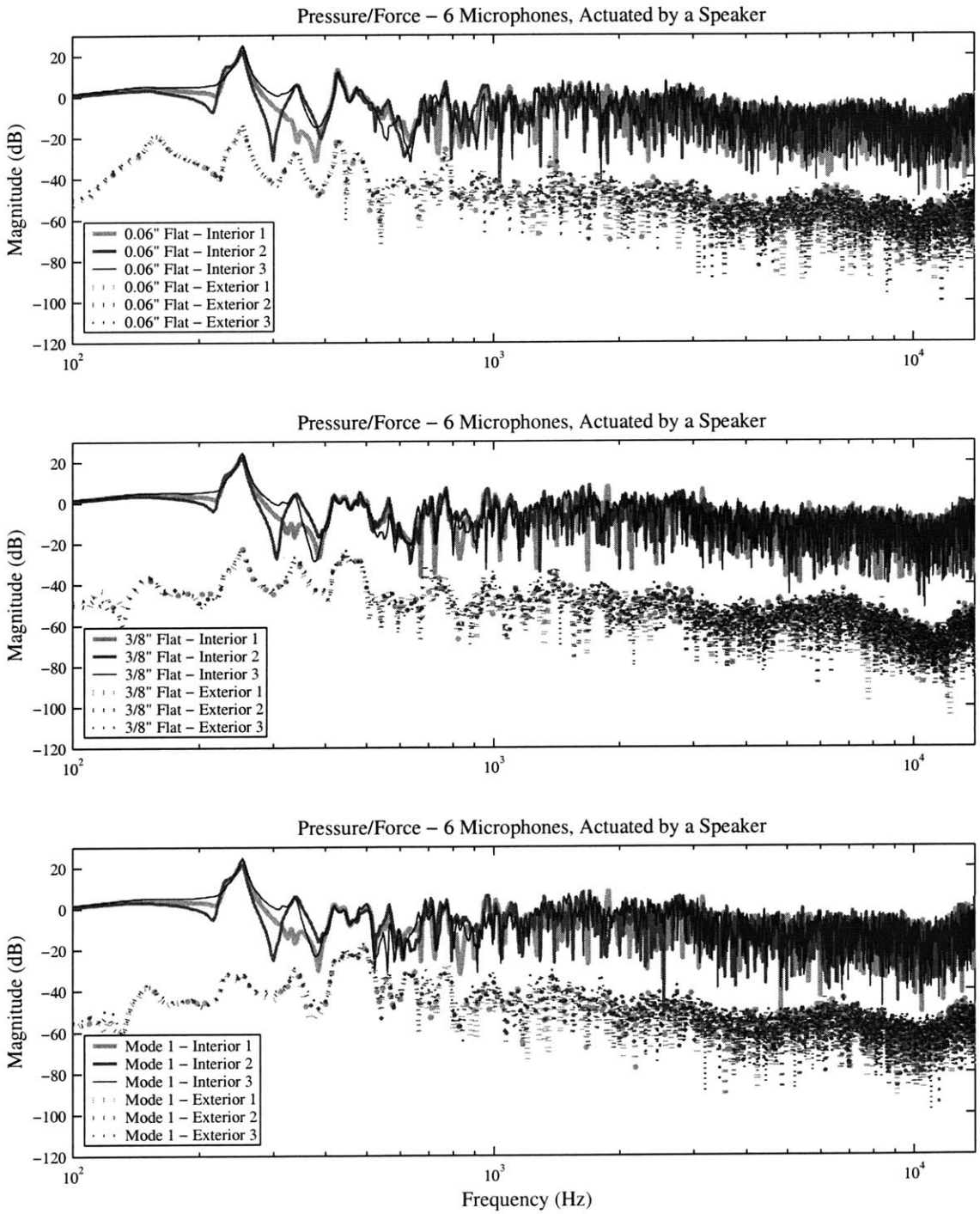

Figure C.24 Raw transfer functions for the microphone sensors for the diffuse transmission experiments on the undamped panels.

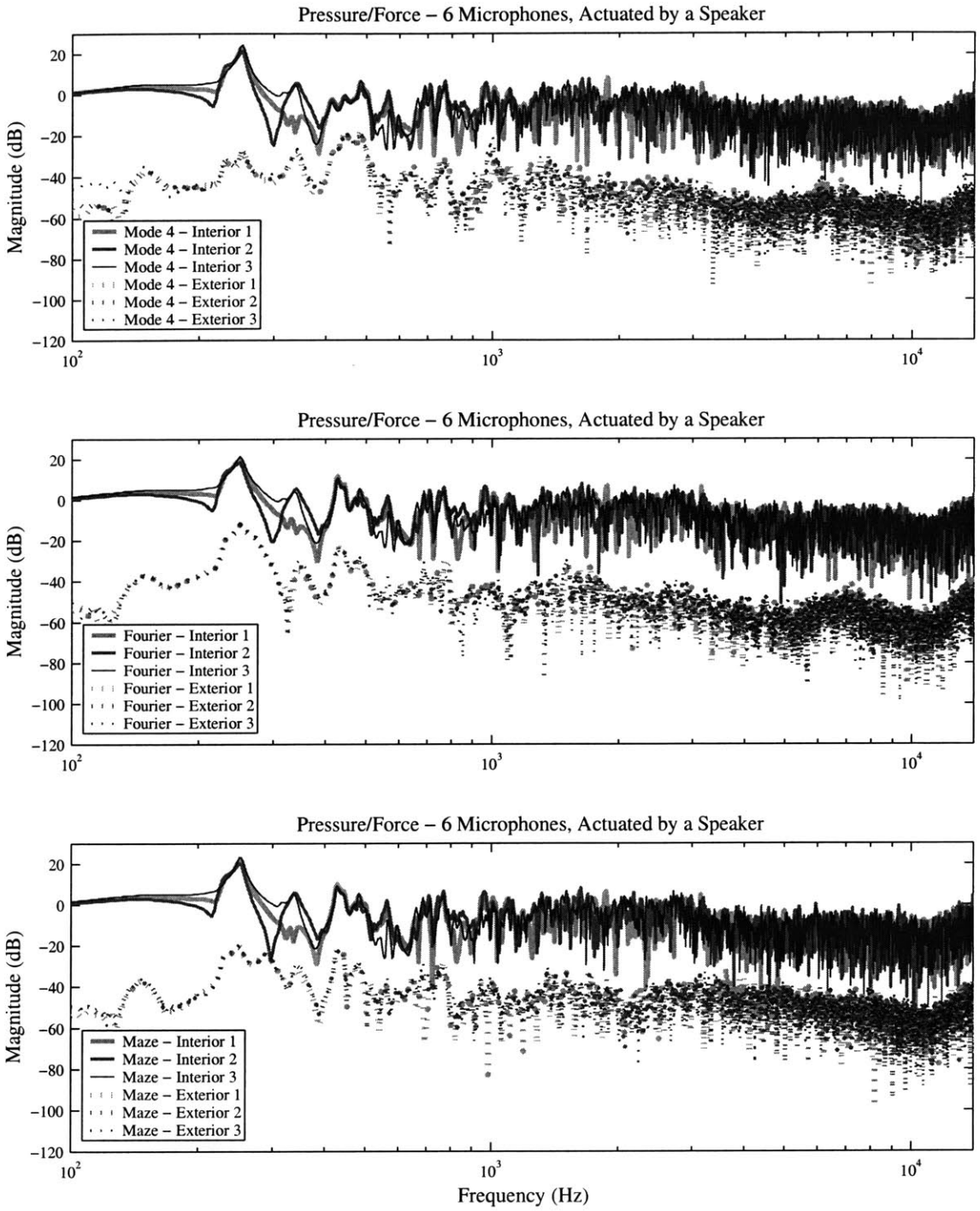

Figure C.25 More raw transfer functions for the microphone sensors for the diffuse transmission experiments on the undamped panels.

C.5.2 Diffuse Transmission Data for Damped Panels

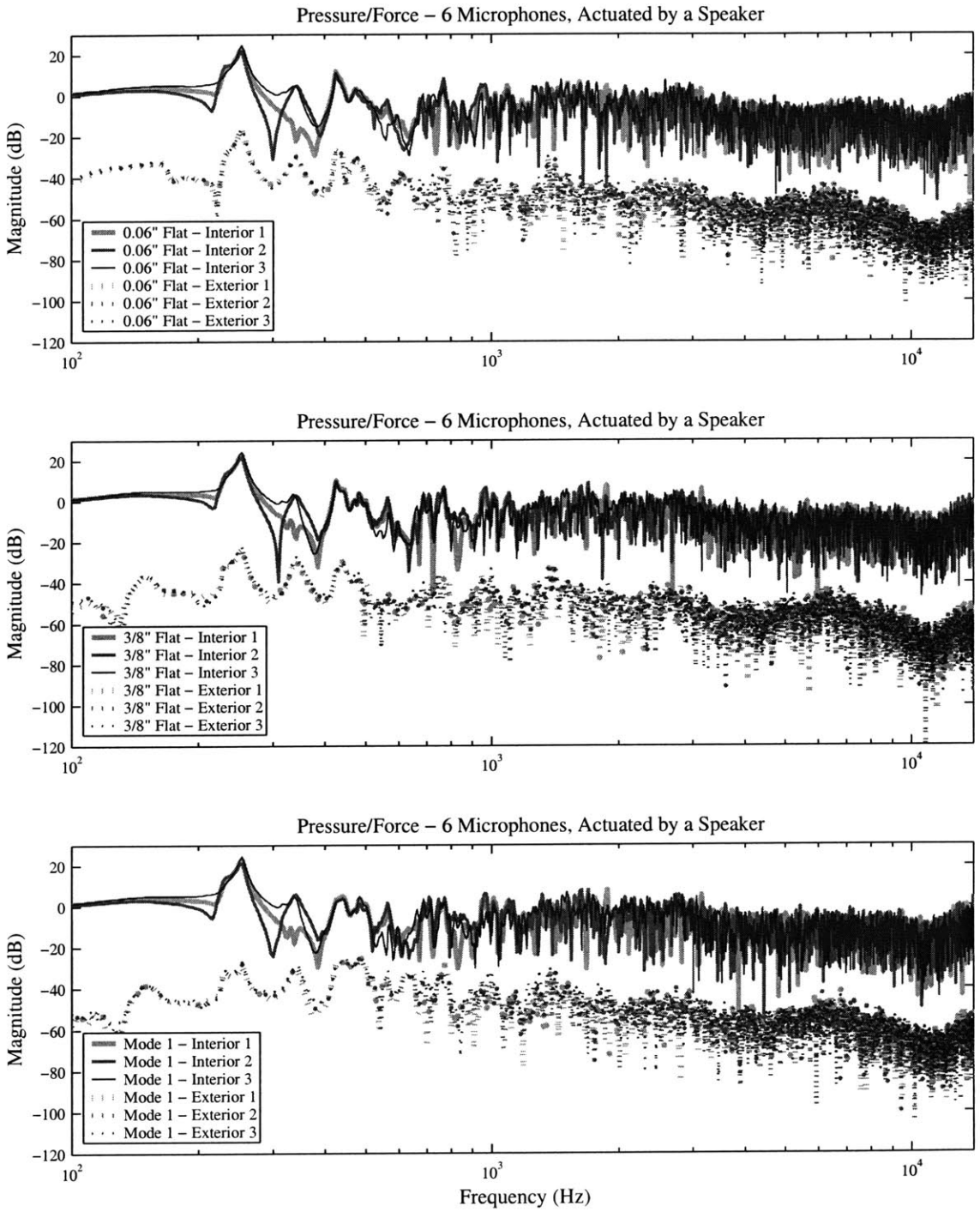

Figure C.26 Raw transfer functions for the microphone sensors for the diffuse transmission experiments on the damped panels.

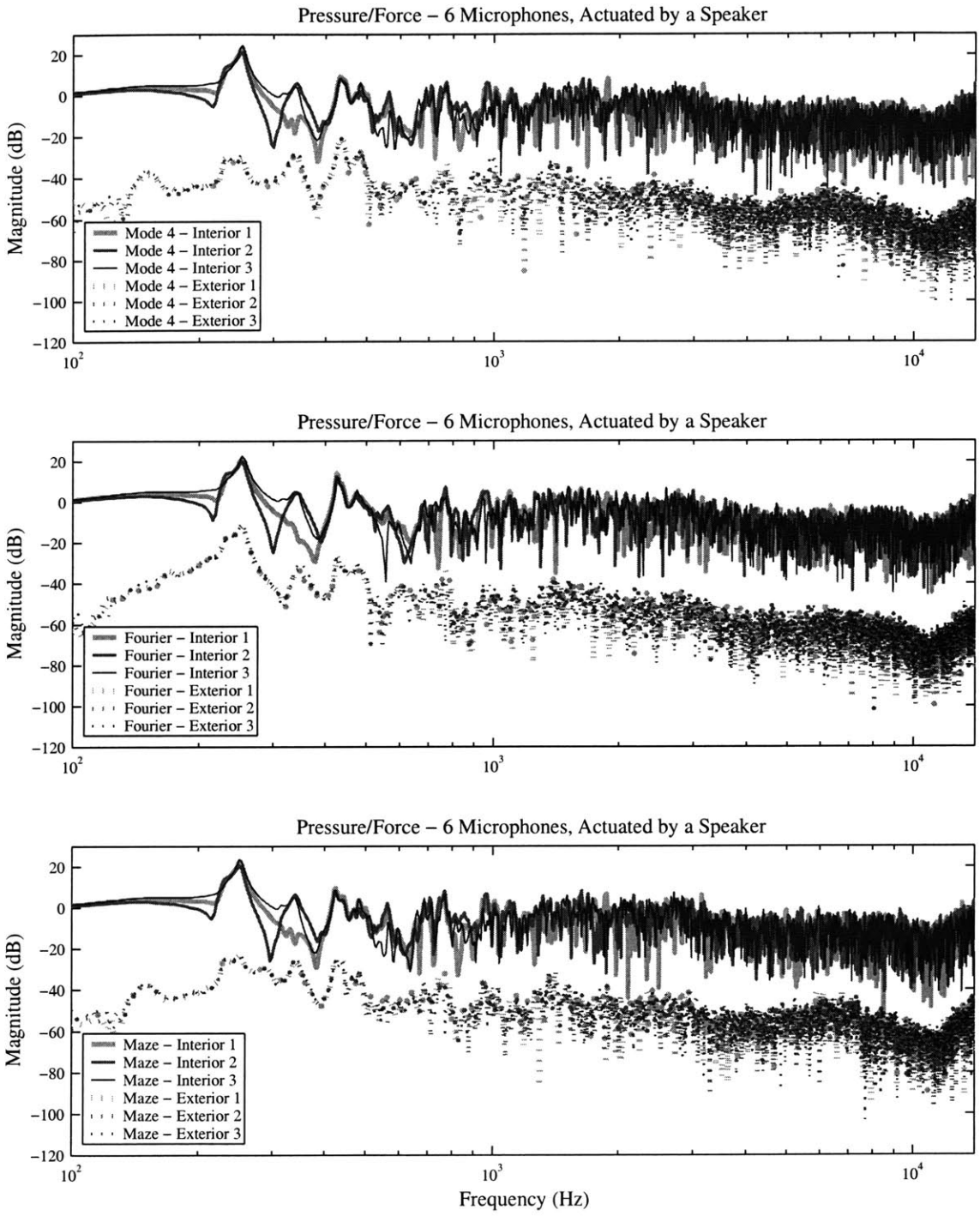

Figure C.27 More raw transfer functions for the microphone sensors for the diffuse transmission experiments on the damped panels.

C.6 FEA and Experimental Transfer Function Comparison

The following data compares the finite element model transfer functions, for the flat and the mode-shaped panels, to that of the experimental results (using the laser vibrometer). The comparison is for the panels without constrained layer damping. The model assumes a single loss factor for all modes.

C.6.1 FEA Model Comparison for the Flat Panel

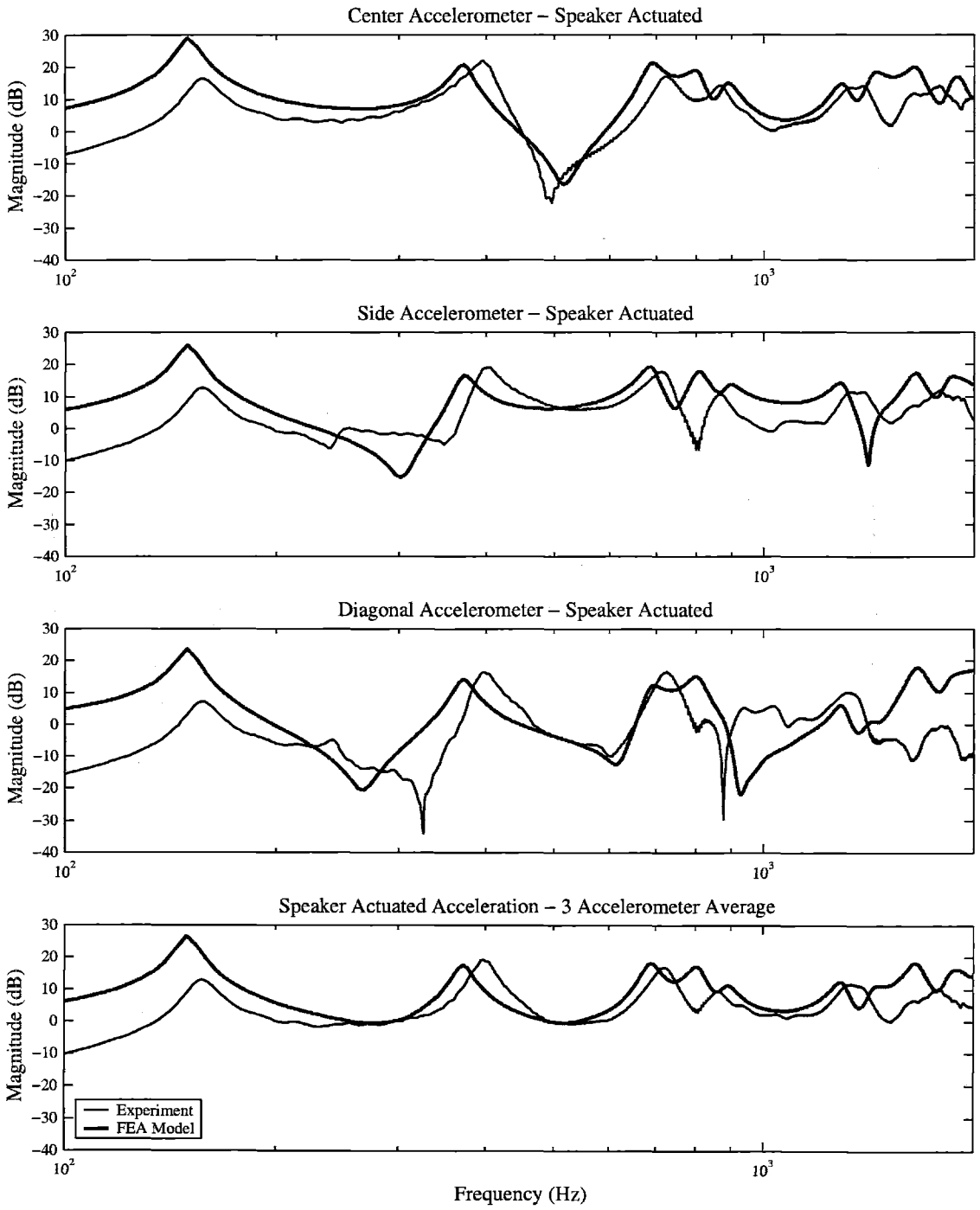

Figure C.28 Transfer functions for the FEA analysis and vibrometer experiments on the undamped flat panel.

C.6.2 FEA Model Comparison for the Flat Panel

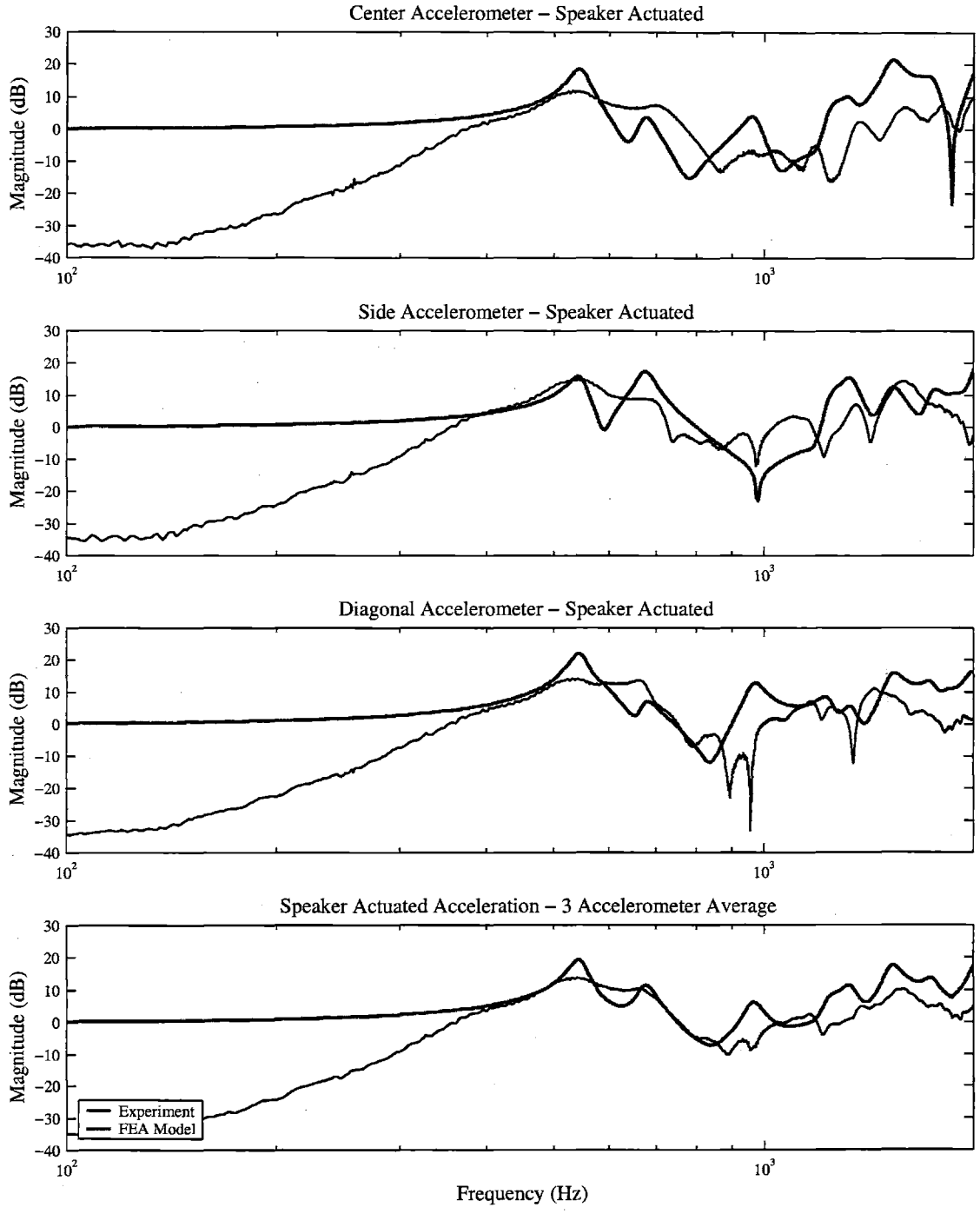

Figure C.29 Transfer functions for the FEA analysis and vibrometer experiments on the undamped mode-shaped panel.